WESTERN SYDNEY
UNIVERSITY

FOAM-FILLED STRUCTURAL PANELS USING PNEUMATIC FABRIC FORMWORK FOR RAPIDLY ASSEMBLED BUILDINGS

Saeed Nemati

A thesis submitted in fulfilment of the requirements for the degree of Doctor of Philosophy

School of Computing, Engineering and Mathematics
Centre for Infrastructure Engineering

Aug 2019

CERTIFICATE OF AUTHORSHIP/ORIGINALITY

I certify that the work in this thesis has not previously been submitted for a degree nor has it been submitted as part of requirements for a degree except as fully acknowledged within the text. I also certify that the thesis has been written by me. Any helps that I have received in my research work and the preparation of the thesis itself has been acknowledged. In addition, I certify that all information sources and literature used are indicated and acknowledged in the thesis.

Saeed Nemati

Aug 2019

To:

My dear family members, Farzaneh and Amir Koorosh, for all of their supports and patience!

Acknowledgment

I want to take this opportunity and express my sincere gratitude to my Principal Supervisor, Professor Bijan Samali, for his encouragement, support, understanding and immense knowledge. Professor Samali brought me into the research world and patiently guided me through my Ph.D. study and helped me with the thesis writing. I would like to also show my highest appreciation to my Co-Supervisor, Dr. Pezhman Sharafi for his tremendous support, guidance and enthusiasm, which helped me through the most challenging period of my research.

TABLE OF CONTENTS

List of Publications

The following journal papers have been published based on the work in this thesis:

1) "Development of an Innovative Modular Foam-Filled Panelised System for Rapidly Assembled Post Disaster Housing". Building, 2018, Special issue on "Modern Prefabricated Buildings", ISSN20755309, 00073725, USA.

2) "Decision Making on the Optimised Choice of Pneumatic Formwork Textile for Foam-Filled Structural Composite Panels". International Journal of GEOMATE, Nov., 2017, Vol.13, Issue 39, pp. 220-228 Geotec., Const. Mat. & Env., ISSN:2186-2990, DOI: https://doi.org/10.21660/2017.39.7350, Japan.

3) "An Experimental Study on the Lateral Pressure in Foam-Filled Wall Panels with Pneumatic Formwork". Case Studies in Construction Materials, ELSEVIER BV, ISSN: 2214-5095, Netherlands.

4) "Feasibility Analysis of the Use of Rigid Polyurethane Foam in Modular Sandwich Panels for Rapid Assembly Structures". International Journal of GEOMATE, Nov., 2018 Vol.15, Issue 51, pp.113-120 Geotec., Const. Mat. & Env., DOI: https: //doi.org/ 10.21660/ 2018.51.06166 ISSN: 2186-2982 (Print), 2186-2990 (Online), Japan.

5) "Edgewise and Flatwise Compressive Behaviour of Foam-Filled Sandwich Panels With 3-D High Density Polyethylene Skins". Engineering Solid Mechanics (ESM), March, 2018 Vol.6, Issue 3, pp. 285-298, DOI: 10.5267/j.esm.2018.3.005, Canada.

6) "Flexural and Shear Performance of an Innovative Foam-Filled Sandwich Panel With 3-D High Density Polyethylene Skins". Engineering Solid Mechanics (ESM), March, 2018 Vol.6, Issue 2, pp. 113-128, DOI: 10.5267/j.esm.2018.3.002, Canada.

7) "Effects of Cold Joints on the Structural Behaviour of Polyurethane Rigid Foam Panels". Engineering Solid Mechanics (ESM), 2018, Canada.

8) "Behaviour of Integrated Connections Between Adjacent Foam Filled Modular Sandwich Panels". Engineering Solid Mechanics (ESM), June, 2018 Vol.6, Issue 4, online, DOI: 10.5267/j.esm.2018.6.001, Volume 6 Issue 4 pp. 361-370 , 2018 Canada.

9) "Non-Reinforced Foam Filled Modules for Rapidly Assembled Post Disaster Housing", International Journal of GEOMATE, May, 2018 Vol.14, Issue 45, pp.151-161, DOI: 10.21660/2018.45.73573, ISSN: 2186-2982 (Print), 2186-2990 (Online), Japan.

10) "Structural Performance of Polyurethane Foam-Filled Building Composite Panels: A State-Of-The-Art". Journal of Composites Science, DOI: 10.3390/jcs3020040, 3(2), 40 (2019).

Conference paper:

11) "Experimental Study of Modular Foam-Filled Panels for Quick Assembly Post-Disaster Housing", 13th International Conference on Steel, Space and Composite Structures (SS18), 31 January - 2 February 2018, Perth, Australia.

List of Figures

Chapter 1:

Chapter 2:

Chapter 3:

Chapter 6:

Chapter 7:

Chapter 10:

List of Tables

Chapter 7:

Chapter 8:

Chapter 9:

Chapter 10:

Executive summary

Crisis management after natural and non-natural disasters is a matter of serious concern for governments. Every year, due to catastrophes worldwide, millions of people have to be accommodated in temporary housing. In the USA alone, such disasters happen over 60 times per year. Rapid assembly building therefore, play a key role in post disaster housing projects. There are several types of rapidly assembled structures. Among them, the use of panelised systems, especially lightweight foam filled sandwich panels, is becoming very popular, because of their improved efficiency, good performance and their ability to reduce construction time and cost. A vast majority of the recent studies in the literature on the performance of structural panels are mainly focused on the panels made by rigid formwork. The structural application of the flexible formwork systems and their capabilities and potentials for rapid assembly building in crises management has not been adequately studies in the literature. In fact, a large portion of the recent research studies regarding the application of the flexible formwork is mainly limited to the architectural concepts. There is a significant gap in the knowledge of application of light weight sandwich panels, and application of flexible formwork systems for rapid assembly housing for crises management.

This research study aims to introduce a novel foam-filled structural panelised system by pneumatic fabric formwork for rapid assembly building and study its structural performance and constructional considerations. For this purpose in this study:

- First essential considerations for construction of these panels are investigated.
- Then, a summary of the development of an innovative panelised system is presented and structural behaviour of them is investigated through numerical and experimental analysis.
- Then, a decision-making method for selection of the most appropriate fabric formwork for foam-filled structural panels in rapidly assembled buildings is introduced.
- Investigation of lateral deformation of panelised flexible formworks is another step of this study.
- Then, a feasibility study on the use of a type of rigid foam with trading name of AUW763 in the sandwich panels is presented.
- Study of real behaviour of foam filled panels with some internal seams and the rigidity of integrated connections between foam filled modular sandwich panels is conducted afterwards.
- Finally, a foam filled 3D module for rapidly assembled post disaster housing is introduced and the compliance with codes is investigated.

The scope of this research covers one storey class 1a of buildings, in accordance with clause A3.2 of Building Code of Australia. Therefore, studying multi-storey structures are beyond the scope of this research. Also, the main service category of the considered system is “temporary housing application”. The results indicate that the 3D modulus made of this system have enough stability and safety as a post disaster housing system even in severe loading conditions such as cyclonic prone areas.

Chapter 1

Introduction

1.1 Introduction

Crisis management after natural and non-natural disasters, such as earthquake, flood, drought, bushfire, refugees' raid and even wars is among significant concerns of governments. In the USA alone, such disasters happen over 60 times per year. In all these cases, fast decision making is an essential element of an effective crisis management system. From the civil engineering point of view, Post Disaster Housing (PDH) is a big challenge in the crisis management field. Every year, due to natural and man-made catastrophes worldwide, millions of people have to be accommodated in temporary housing. Experts estimate that on average, it can take 5 to 10 years for communities to recover from the effects of a major disaster like a destructive seismic event [1], that highlights the importance of Rapidly Assembled Buildings (RAB) as an effective PDH system. In addition to residential accommodation, RAB can be employed in several other applications such as, field hospitals, exhibitions, storehouses and other temporary and semi-permanent facilities. Some rapidly assembled systems have the potential to be used as temporary structures as well as providing long term serviceability.

Mobile and rapidly assembled structures play a major role in post-disaster management through building temporary accommodation and shelters. These types of structures are also of primary importance in many military and civilian service applications and are widely used for rescue and maintenance services. Air-liftable origami-inspired deployable systems (Figure 1.1a), pliable structural systems with rigid couplings for parallel leaf-springs (Figure 1.1b), scissor systems (Figure 1.2), elastic grid shell systems (Figure 1.3), and structural panels (Figure 1.4) are some popular types of mobile and rapidly assembled structures [2]. Wise decision on the selection of RAB systems has an impact on their performance in an effective crisis management system. As an example, big precast structural elements are being used in many existing RAB systems. Yet, as the dimension of precast elements increases, some significant construction problems start to appear in transportation and erection phases. In addition, most of the rapidly assembled structural systems suffer from low tolerance in the making and erection phases, and need skilled labours for installation that will result in an increase in the total construction costs. Use of rapidly assembled panelised systems, especially rapidly assembled lightweight panels, is becoming very popular for cutting the construction time as well as formwork assembling labour and transportation costs that make them suitable options for PDH projects.

(a) (b)

Figure 1.1: Air-liftable origami-inspired deployable systems (a) in comparison with pliable structural systems with rigid couplings for parallel leaf-springs (b)

Figure 1.2: Examples of scissor structural systems

Figure 1.3: Examples of elastic grid shell system [3]

Figure 1.4: Examples of structural panels [3]

All these systems have their own relative advantages and disadvantages. For example, air-liftable origami-inspired deployable systems do not have a reliable architectural form and are not an easily built system. In addition, control of heat exchange in such systems is difficult and sometimes impossible. Pliable structural systems with rigid couplings for parallel leaf-

springs have similar problems in addition to a relatively complex design procedure. The elastic grid shell system, in most cases, is limited to non-residential temporary applications. High rate energy loss and expensive construction equipment are some of other weak points of this system. In addition, most of these rapidly assembled structural systems not only suffer from low tolerance in the making and erection phases, but also need skilled labours for installation that will result in an increase in the total construction costs and time.

1.2 Panelised Systems

In addition to the advantages of other systems, rapidly assembled panelised systems, used commonly in residential buildings as well as industrial structures, offer the following advantages:

- ✓ Panels can be placed on top of each other as plates, and can reduce their transportation cost per unit area.
- ✓ Panels can be made in any sizes and consequently can save construction time.
- ✓ Panels can be connected to each other quickly.
- ✓ Panels can act as structural elements, insulators and partitions at the same time.
- ✓ Panels can provide an integrated structural rapidly assembled system by the use of both dry and wet connections.

Precast flat panel systems, Oriented Strand Board (OSB) panel systems (Figure 1.4), Insulating Concrete Formwork (ICF) panel systems (Figure 1.5) and ordinary/lightweight sandwich panels (Figure 1.6), are some examples of construction panels. Oriented Strand Board is an engineered wood particle board formed by adding adhesives and then compressing layers of wood strands in specific orientations. Insulating Concrete Formwork is a simple construction system using custom made insulating panels or blocks as formwork for in-situ concrete. It consists of twin-walled and expanded polystyrene panels or blocks that are quickly built up to create formwork for the walls of a building. This formwork is then filled with ready-mixed concrete to create a robust structure. The expanded polystyrene blocks remain to provide high levels of thermal insulation and the concrete core provides robustness and good levels of sound insulation. Generally speaking, precast sandwich panels are typically made of an external concrete layer (non-load bearing), an insulation layer and an

internal concrete layer (load bearing) (Figure 1.6). These three layers are then connected using connectors being placed during casting. The sandwich panel can be used as both internal and external wall structure. However, most structural panel systems in the market are suffering from the following drawbacks:

- ✓ Relatively high weight that makes the installation hard (the load bearing part of most of those panel systems is made from concrete, hardwood, or steel frames)
- ✓ Transportation challenges
- ✓ Relatively heavy formwork
- ✓ Need for substantial primary investment and equipment
- ✓ Incompatible with many types of available connections

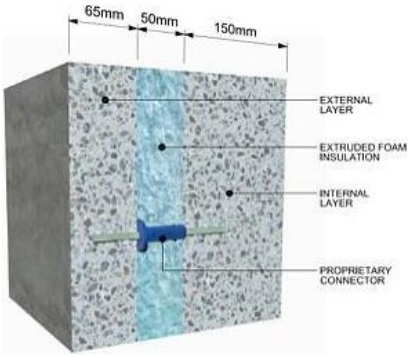

Figure 1.5: Insulating Concrete Formwork (ICF) system [3]

Figure 1.6: Typical sandwich panel wall section [3]

1.3 Formwork Selection

Many of existing panels in the market place are made from conventional construction materials and others are made from new lightweight components. However, in both cases, the

role of formwork and its impact on the mechanical behaviour of structural panels are very important. The formwork systems can be selected based on some construction considerations as follows:

✓ *Easy and economical transportation from factory to construction site*

In some cases, the volume, dimension and/or weight of formworks are so large that result in substantial transportation costs. For example, large panel formworks may encounter some transportation limitations. A major part of this limitation is related to the safety considerations [4].

✓ *Easy and economical assembly and disassembly on construction site*

In some cases, such as when using steel formwork, cranes and/or other heavy equipment have to be provided on site for the assembly and disassembly purposes, which will subsequently result in an increase in the construction cost and time.

✓ *Maximum rate of construction speed to formwork weight*

This rate depends on several parameters such as the formwork material density and surface area of the formwork units. Although increasing the dimensions will increase the efficiency, it increases the formwork's weight too, which will result in higher cost. The opposite trend will lead to lower efficiency, however, lower transportation and installation cost.

✓ *Minimum construction joints and maximum integration*

As an engineering principle, a construction joint is the weak point among integrated components of a structure. Large number of joints would provide the risk of low integration for the structure. Moreover, increasing the number of joints will cause some other problems such as high concrete leakage and low construction speed. Therefore, it is preferred to minimize the construction joints in order to maximize the structural integrity.

✓ *Minimum waste generation in formwork production process*

One of the most critical factors in selecting a formworks system is the life cycle cost, which is in turn influenced by the amount of generated waste in production process.

✓ *Easy and economical storage*

This item includes several parameters such as the allocated storage area, the possibility of pest attack and the fire risk especially after use of releasing oil.

✓ *Applicability to high rise structures*

Utilizing some rigid formworks at height is often very difficult and hence expensive. Therefore, potential to wide applicability of a formwork system to high rise structures can be considered as a significant advantage in construction industry.

✓ *Reasonable potential for prefabrication*

Prefabrication of poured structures is greatly impacted by the type of formwork system. In other words, if a formwork system is not compatible with prefabrication considerations, the percentage of prefabrication activities in the construction process will drop.

✓ *Not reliant on highly-trained and skilled work force*

As illustrated in Figure 1.7, a major part of construction cost is due to the formwork labour cost.

✓ *Compatibility with the core material in order to minimize the environmental effects*

Some formworks may react with the core material. For example, the aluminium formworks may have some chemical reaction with concrete. This issue must be addressed as one of the construction considerations in selecting a formwork system.

✓ *Appropriate specific heat capacity and thermal conductivity*

Safe working with formworks in very cold or very hot weathers depends on the specific heat capacity of their material. Also, inappropriate thermal conductivity of formwork can influence the quality of core material. For instance, using metallic formworks in very hot weather leads to high risk of burn.

✓ *Reusability*

Figure 1.7 shows that the formwork material cost is a major factor in the overall cost of conventional poured structures. Therefore, reusability of formwork is an important parameter, not only from waste management viewpoint, but also from economic point of view.

✓ *Fast connectors applicability*

This parameter has a substantial effect on the labour cost and the project time and is an important construction consideration for selecting formwork.

✓ *The potential to make non-prismatic sections, complex shapes and architectural patterns*

1.4 Fabric Formwork

Most of the above mentioned factors can be addressed by flexible (especially fabric) formwork. For example, the fabric formwork can be conveniently transported from factory to the construction site in an economical way. Therefore, easy transportation and economical storage of the fabric formworks due to their low volume, high flexibility and being free of releasing oil are their significant advantages for construction. Furthermore, fabric formworks, especially double skin fabric formworks, can be successfully used in extreme weather conditions. The fabric formwork system does not require heavy lifting equipment, is simple to install and does not need highly-trained and skilled workforce because it is 100 to 300 times lighter than other conventional formwork systems. Large fabric formwork systems are made at the factory. Therefore, fabric panel formwork systems use the maximum level of prefabrication ability. In addition, they do not have so many connections and do not need fast connectors, so they can reduce the number of construction joints. Furthermore, the amount of waste materials can be reduced to almost zero in this system. High flexibility of fabric formworks prevents any permanent warping and deformation. There is also no chemical reaction between a fabric formwork and most core materials. In addition, fabric formworks improves the strength, durability, sustainability and surface quality [5]. Fabric formwork system has some other distinct advantages over conventional systems such as architectural/structural shape flexibility [6], lower formwork material and subsequently storage costs at approximately $1/10^{th}$ of the cost of traditional formwork per unit area and adaptability to uneven ground conditions [7][8].

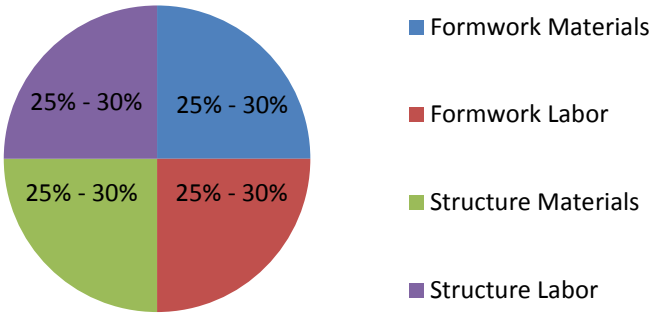

Figure 1.7: Distribution of costs for usually poured structures [8, 9]

Fabric formwork is constructed using textile sheets made of synthetic fibres typically nylon, Polyesters/Polyethylene Terephthalate (PET), Polyolefin, and Polypropylene (PP). They are generally woven, with the "yarns" crossing at right angles [10]. To date, almost all textiles used for fabric formwork have been developed for other uses, such as apparel and most notably, geotextiles. But, the textile industry started developing various types of suitable fabric for applications in construction. Fabric formwork essentially behaves as a membrane under fluid pressure, providing resistance through the generation of pure tension curves in three dimensions. A general principle of structural engineering is that the most efficient means of resisting a force is by axial tension. It makes this system extraordinarily efficient as compared with the rigid frame and panel system of conventional formwork relying on resistance through bending. In this way, the amount of material required to support the pressure of the wet filler is dramatically reduced [7]. In civil engineering applications, fabric formwork has been found to be a practical method of containing concrete, mortar or special grouts, both above ground and under water, and often provided the best way to overcome various difficulties and extra costs [11]. It can also be used in both cast-in-place and precast applications [12]. Using fabric formwork, it is possible to cast architecturally interesting, optimized non-prismatic structures that use up to 40% less concrete (or any filling material) than an equivalent strength prismatic section. It offers potentially significant embodied energy savings in new structures [13] and a striking reduction (1.2%) in CO_2 emissions will be achieved [14]. Fabric formwork can be sewn into any configuration, size, or shape in-situ or in the factory. Some fabric formwork systems use no sewing at all, and rely on standard construction connections [15]. Most fabric formworks consist of simple, flat, rectangular sheets. Besides the shape of the fabric panels used, the variables that affect the final shape of

the fabric are fabric type, boundary conditions, pre-tensioning the fabric, the function of the concrete structure, concreting environment and ballooning phenomenon [16]. In addition, permeability, the viscosity of the in-fill material, the construction details, the required stiffness of the form before filling, the hydrostatic pressure action on the outer skin, the internal restraints on the grout level, the size and shape of flexible formwork and its methods of placing and handling, the effects of buoyancy and currents, the sequence of injection, the position of bleed points or overfill prevention and finally, the provision of overfill compartments to compensate for the settlement of grout resulting from excessive bleed are the major factors to be considered when using fabric formwork.

Concurrent with development of fabric formwork, some advanced ideas have been combined with architectural concepts and the pneumatic formwork is one of them. The main concept of pneumatic formwork application is ramified from membrane behaviour. Membranes may be used for the roof of a building or as a complete exterior enclosure. One way to utilize a membrane for these purposes is to hang it with initial tension between appropriate supports. Another way is to pretension the membrane to enable it to carry compressive loads. A common method of pre-tensioning a membrane is to pressurize the interior with air [17, 18].

Air stabilized structures may be classified, depending on the type of support, as following:

- ✓ Air-inflated system
  - Air-inflated dual wall structures (Figure 1.8a) (*such as pneumatic formworks*)
  - Air-inflated rib structures (Figure 1.9)
- ✓ Air-supported system (Figure 1.8b)
- ✓ Hybrid system

Hybrid structures consist of one of the preceding types of pneumatic construction augmented by light metal framing, such as cables.

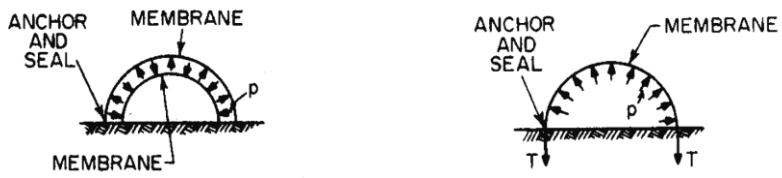

(a) **(b)**

Figure 1.8: Air-inflated dual wall structure (a) and air-supported structure (b) [17, 18]

Figure 1.9: The Fuji Pvilion, an example for structural application of air-inflated rib structures [19]

On the other hand, with regards to the structural performance of panels made of fabric formworks, use of foam materials is a good choice as filler. Many types of foams are on the market. The Polyurethane (PU or PUR) foams are the most popular types that were first introduced into the market in the 1950s. The other popular types of PU foams are: Polyethylene and Polystyrene. Foams are available in three main categories: flexible (the most popular [20]), semi-rigid and rigid foams. Polyether-based PUR foams are used widely for applications such as furniture, bedding, pillows, padding, and carpet underlay. Polyester-based PUR foams are used for textiles, shoulder pads, noise reduction and other applications. Both are used in automotive, aircraft, household, and footwear industries, too. Nevertheless, showing some good level of structural strength and durability, these foams have a great potential to be widely used in structural engineering. For example, foams find many uses in building and construction for sealing and thermal insulation applications, especially recently in sandwich panels. Expansion jointing and use as the support for sporting floors are two other foams' applications. For specific applications, some grades of foams with excellent UV resistance have been made. The foam material can also be used for 'sound deadening' and will significantly reduce impact and airborne noise transfer. In the past years, PU grouting technologies have spread significantly to civil engineering applications. Currently, these technologies are used mainly in mining, underground/geotechnical works, strengthening of subsoil and brick/stone masonry, insulation of structures, sealing of utility entries into constructions and joints, water management works and finally in bridges and roads. Spray-applied Polyurethane Foam (SPF) roof covering is another application of Polyurethane foam. Foams are also used as core materials for a variety of composite panels used in flooring, temporary structures and temporary water defences where it is lightweight, durability and impact-absorbing properties are beneficial.

1.5 Objectives, Scope and Structure of This Thesis

The main objectives of this research are introducing a new foam filled structural panelised system, studying its structural performance and addressing constructional considerations and issues. For this purpose, first essential considerations for construction of these panels will be investigated. After addressing the constructional considerations, structural behaviour of the foam filled composite panels will be investigated through numerical and experimental analysis. The scope of this research covers the following aspects:

- ✓ This study focuses on class 1a of buildings, in accordance with clause A3.2 of Building Code of Australia [21]. Based on this clause, a class 1a building is a single dwelling being a detached house; or one of a group of two or more attached dwellings, each being a building, separated by a fire-resisting wall, including a row house, terrace house, town house or villa unit which are not located above or below another dwelling or another class of building other than a private garage.

- ✓ In this research, the dwellings will be limited to one storey, and therefore, studying multi-storey structures as well as some low-rise buildings, not included in the previous clause, are beyond the scope of this research.

- ✓ The main service category of the considered system is "temporary housing application" for example post disaster sheltering.

- ✓ The applied load, strength factors, safety factors and tolerance limits are in accordance with those suggested for temporary buildings.

Therefore, in Chapter 2 a summary of the innovative panelised system will be presented. Then, in the Chapter 3 an optimised choice of textile for fabric formwork is recommended. This chapter introduces a decision-making method for selection of the most appropriate fabric formwork for foam-filled structural panels in rapidly assembled buildings that will be used in semi-permanent housing such as post disaster sheltering. First, using a questionnaire type survey, the six most effective criteria for a suitable pneumatic fabric formwork; namely, permeability, strength, relative cost, durability, sew-ability, and aesthetics are identified. Some experimental tests were conducted to determine the selection indicators for the criteria like strength for each candidate. Then, a value matrix for these factors has been defined and calculated, and the best formwork candidate for foam-filled structural composite panels is selected from a list of seven potential candidates, using Analytical Hierarchy Process.

Chapter 4 is about the lateral deformation of panelised flexible formworks. In this chapter using polyurethane foam and three types of flexible formworks, some experimental tests were carried out on the foam filled large scale penalised flexible formworks. The formworks had three thicknesses as 100 mm, 200 mm and 300 mm and the density of used polyurethane foam was about 200 kg/m^3. Consequently, the maximum lateral deflection and total raised height were measured. In addition, distribution of lateral deflection was investigated geometrically. Because of the results of this study will be used for design of an innovative foam filled structural panel with a thickness of 100 mm, some finite element studies were carried out on this type of formworks. Finally, suitable arrangement for internal ties is presented for the most critical condition. Chapter 5 is about the feasibility study of the use of rigid foam in sandwich panels. In this chapter, a feasibility study carried out on a commercial type rigid PU foam with trading name AUW763, to be used as the core material of sandwich panels, based on ASTM E1730-15 [22]. Results show that AUW763 meets the standards requirements and specifications for building constructions. Chapter 6 investigates the edgewise and flatwise compressive behaviour of foam-filled sandwich panels. In this chapter, the edgewise and flatwise compressive behaviour of introduced sandwich panel, mainly developed for quick assembly of post-disaster housing as well as load bearing panels for pre-fabricated modular construction and semi-permanent buildings, is investigated experimentally and by finite element modelling. A panel composed of two 3-D high-density polyethylene (HDPE) sheets as the skins, filled with high-density Polyurethane (PU) foam as the core will be studied. Material characterisation tests and flatwise compression and edgewise compression experiments were performed in accordance with ASTM standards to evaluate the compressive strength and the load-carrying behaviour of the sandwich panels. A finite element analysis and validation were also conducted to model the compressive behaviour of sandwich structures. Chapter 7 focuses on the flexural and shear behaviour of the mentioned innovative sandwich panels. An experimental study was carried out to validate the effectiveness of this panel for increasing the ultimate bending strength. Also, a series of experimental tests were performed on medium-scale specimens to characterize their core shear behaviour. Then, some supplementary tests were run to determine the panels' flexural and shear stiffness. Bending behaviour of seamed foam made structural sandwich panels is investigated in Chapter 8. In this chapter, using a unique pneumatic pressure testing rig, bending tests are conducted on two types of rigid polyurethane panels. The panels are categorised based on the existence of construction cold joints (seams) as S (Seamless) type and TS (Transverse Seams) type. The S type panels are tested under monotonic uniform

loading with a maximum nominal pressure of about 1 atm as the control specimens. The TS panels are tested under both monotonic and cyclic uniform loading, and the deflections-pressure behaviour obtained. Integrated connections between foam filled modular sandwich panels is studied in Chapter 9. In this chapter, the structural behaviour of an integrated connection for implementation between adjacent composite sandwich panels in rapid assembly buildings is studied. The integrated connection system consists of 3-D HDPE skin faces, and cores of high-density PU foam integrated into the sandwich panels at the moment of their production. The study included experimental investigations regarding the mechanical and structural response of the connection under actual applied loads, and its bending rigidity, rotational stiffness and behaviour under lateral loading is investigated. Using Finite Element modelling, the stress distribution and the mechanisms of failure are studied. Foam filled 3D modules for rapidly assembled post disaster housing are introduced and then investigated in Chapter 10. This chapter introduces a modular non-reinforced foam-filled system for rapidly assembled buildings and studies its structural performance. A novel structural modular construction system using pneumatic formwork is presented and its structural performance as a post-disaster housing system is studied. To that end, this chapter presents a numerical analysis using finite element modelling on the foam-filled modular units, together with a set of experimental tests on the elements. Finally, the performance of a real size module made of polyurethane foam against snow and wind loads in critical areas is modelled, using the software ROBOT 2016 and ANSYS. It will be checked to see if the systems can meet Standards Australia (AS1170.2) provisions, International Building Code (IBC-2015) and an American standard as Minimum Design Loads for Buildings and Other Structures (ASCE7-10) for cyclonic prone areas. Finally, in Chapter 11 a conclusion to this study and suggested future works are presented. Figure 1.10 illustrates the roadmap of this study.

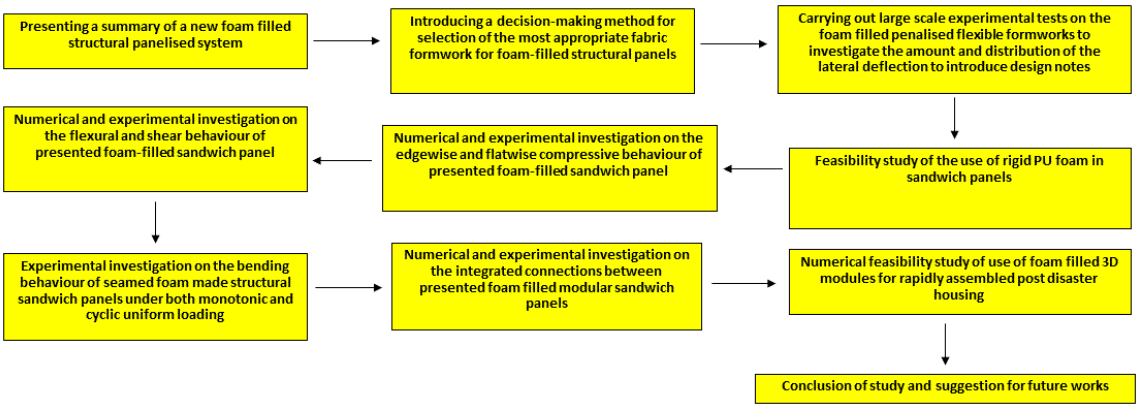

Figure 1.10: Roadmap of this study

Chapter 2

Modular Foam-Filled Panelised System for Rapidly Assembled Post Disaster Housing

The contents of this chapter have been published in the form of a journal paper as follows:

P. Sharafi (Scientific supervision), S. Nemati (Full contribution), B. Samali (Scientific supervision) and M. Ghodratm (English language editing), “Development of an Innovative Modular Foam-Filled Panelised System for Rapidly Assembled Post Disaster Housing”. Building, 2018, Special issue on “Modern Prefabricated Buildings”, ISSN20755309, 00073725, USA.

2.1 Introduction

Natural disasters and emergencies can devastate the communities they hit, and the speed of a response can be crucially important. Crisis management after natural and non-natural disasters such as earthquake, flood, drought, bushfire, refugees, raid and even wars is one of the significant concerns of governments, where, fast decision making is an essential element of an effective crisis management system. When a large number of houses have suffered damages and become unusable, causing a high number of homeless people, rapid housing reconstruction programmes play a decisive role on the disaster recovery and providing temporary housing is a crucial step of these programmes. Experts estimate that on average, it can take 5 to 10 [23, 24] years for communities to recover from the effects of a major seismic event, which highlights the severity of the disaster and the importance of rapidly assembled buildings as an effective post-disaster housing system.

In addition to residential accommodation, rapid assembly buildings can be employed in several other applications such as field hospitals, storehouses and other temporary and semi-permanent facilities. Some rapidly assembled systems have the potential to be used as temporary structures as well as providing long-term serviceability. Scientists defined temporary dwellings as a step toward permanent houses in a disaster recovery and reconstruction plan, and classifies them into two distinct categories: (i) temporary shelter, used to incubate people immediately after a disaster; and (ii) temporary house, allowing the return to normal daily activities, i.e. work, school, cooking at home and shopping [25] .

Mobile and rapidly assembled structures play a major role in post-disaster management through building temporary accommodation and shelters. These types of structures are also of primary importance in many military and civilians service applications and are widely used for rescue and maintenance services. Air-liftable origami-inspired deployable systems, pliable structural systems with rigid couplings for parallel leaf-springs, scissor systems, elastic grid shell system, and structural panels are some popular types of mobile and rapidly assembled structures [26]. Some successful attempts on employing paper tube arches for temporary structures have also been discussed by Preston and Bank [27]. Wise selection of rapid assembly building systems has an impact on their performance in an effective crisis management system. For instance, while use of big precast structural elements is very common for post-disaster housing, as the dimension of precast elements increases, some significant construction problems will be appearing in transportation and erection phases. A temporary accommodation building can be any class of building as defined under the

National Construction Code (NCC) [28]: class 1b (boarding house, guest house, hostel or the like), class 2 (residential units) or class 3 (motel) building, depending on its configuration [29]. Among the existing systems, air-liftable origami-inspired deployable systems, pliable structural systems with rigid couplings for parallel leaf-springs, scissor systems [30], elastic grid shell system [3], and structural panels are some popular types of mobile and rapidly assembled structures [31, 32]. However, most of these rapidly assembled structural systems suffer from low tolerance in the making and erection phases. Also, they need skilled labours for installation that will result in an increase in the total construction costs and lower efficiency. Light-weight structural panels are one of the most popular types of mobile and rapidly assembled structures. Rapidly assembled panels are a form of modular construction, commonly used in residential buildings, as well as industrial structures [33-35].

A wide range of these panels is made from new lightweight components such as foams. Many types of foams are on the market and the Polyurethane (PU) foams are the most popular types [20]. Low self-weight and relatively high stiffness and durability have increased the demand for this type of composite structures [36]. Foam-filled sandwich construction, characterised by two relatively thin and stiff faces and a relatively thick and lightweight foam core, is becoming an interesting solution for prefabricated building wall and floor systems. With regard to the literature, a wide range of studies on the foam-filled composite panels are on those made of polyurethane (PU) foam-core [37].

The results of these studies indicate that the stiffness and strength of a majority of conventional foam-filled sandwich panels hardly meet the structural requirements for use in building floors or walls, at least for standard spans and loads, mainly due to some different failure modes such as delamination of the skins from the core, buckling or wrinkling of the compression skin, flatwise crushing of the core or rupture of the tension skin. The main weaknesses of these panels stem from the low stiffness and strength of the core, and the skin's susceptibility to delamination and buckling, owing to the local mismatch in stiffness and the lack of reinforcements bridging the core and the skins [38]. The use of stitches for connecting the two side skins [39] or use of reinforcing ribs [40] are two popular strengthening techniques being employed for improving the mechanical performance of standard sandwich panels. Despite their very competitive costs, conventional foam-filled sandwich panels are susceptible to some different failure modes. Delamination of the skins from the core, buckling or wrinkling of the compression skin, flatwise crushing of the core and rupture of the tension skin are some of the very common types of failure. In this study, in

order to enhance the properties of the foam-filled sandwich panels with regard to such failure modes for application in semi-temporary housing, a new sandwich system is proposed, in which 3-D high-density Polyethylene (HDPE) sheets with 2 mm thickness are used as the skins, and high-density PU foam is used as the core, as illustrated in Figure 2.1 with a total thickness of 100 mm. The system is cast in a pneumatic fabric formwork, which is used to accelerate the installation and simplifying the transposition process. Using the HDPE sheets, manufactured with approximately 1200 studs per square meter, higher pull-out, and delamination strength, as well as better stress distribution, and buckling performance can be achieved. The studs also improve the resistance of the face sheets and foam-core from debonding and increasing the interface strength between the foam-core and the face sheets.

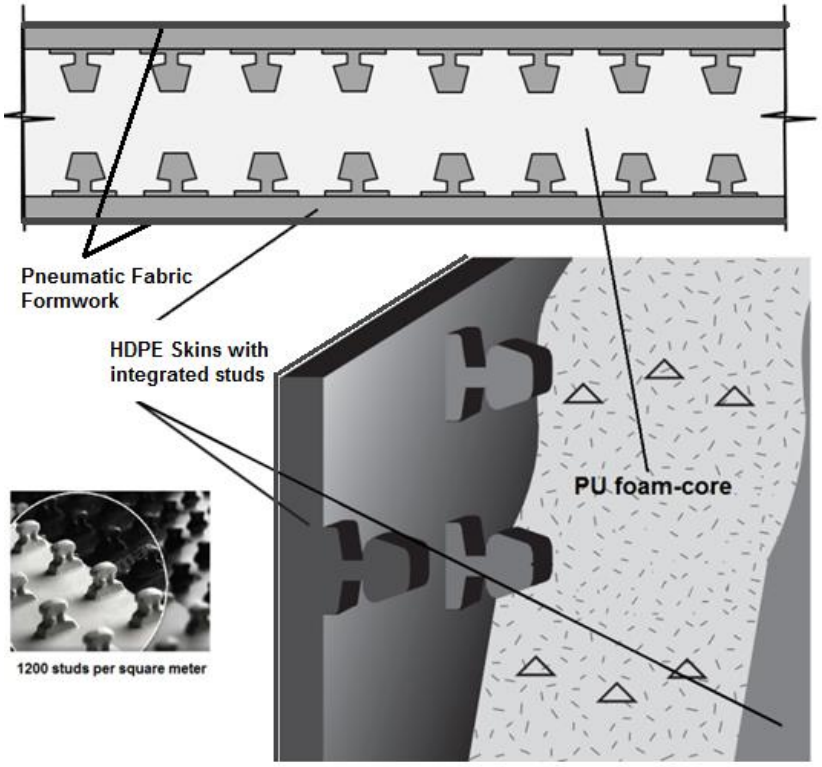

Figure 2.1: Sandwich panel with 3-D HDPE skins, PU foam-core, and pneumatic formwork

The fabrication of these sandwich panels takes place in a single step. Therefore, the face sheets and foam-core are integrated into one construction in the fabric formwork. Rapid assembly, lightweight and easy transportation, durability, and a wide range of applications are some merits of this new design. Given that the introduction of a new design typically brings new challenges to designers to utilize the new properties of the materials and geometry, the main goal of this research work is to investigate some structural properties of the newly developed sandwich system.

2.2 Materials and Methods

To evaluate the basic material properties, in addition to using the manufacturers' data, some experimental tests were performed.

2.2.1 Foam Core

Rigid foam systems are energy efficient, versatile, high-performance systems, where the liquid components are mixed together; and expand and harden on curing. Rigid polyurethane foam is one of the most efficient, high performance insulation materials, enabling very effective energy savings with minimal occupation of space. A 100 mm thick layer of rigid PU provides a U-value of 0.04, which demonstrates high insulation performance of polyurethane foam [41]. U-values measure how effective a material is an insulator. The lower the U-value is, the better the material is as a heat insulator. The popular type of PU foam, being used for thermal insulation, refrigeration and water heater system is made of a 100:100-110 weight ratio mixture of AUSTHANE POLYOL AUW763 and AUSTHANE MDI [42]. This foam is formulated using a zero Ozone Depletion Potential (ODP), zero Global Warming Potential (GWP) and Volatile Organic Compound (VOC) exempt blowing agents. In this study, high-density rigid PU foam with a density of 192 kg/m^3 was selected for the core material, according to the results of the preliminary finite element models. Table 2.1 and Figure 2. show the PU foam's manufacturing and mechanical properties, provided by the manufacturer and validated in the laboratory according to the ASTM E1730 [22] standard specification for rigid foam for use in structural sandwich panel cores. It also meets the thermal conductivity, dimensional stability and flame resistance requirements of ASTM E1730. In Table 2.1, the Cream time is a measure of the beginning of the foam reaction, characterised by a change in the liquids colour as it begins to rise; gel time is the time when the foam has developed enough gel strength to be dimensionally stable; track free time is the time between the beginning of the foam pour and the point at which the outer skin of the foam loses its stickiness; and free rise density is the weight per unit volume of the foam that can be free rise or packed into a mould.

Table 2.1: Mechanical and manufacturing properties of the selected PU rigid foam

Mechanical Properties of the PU foam			
Density (kg/m^3)	Compressive yield strength (MPa)	Tensile yield strength (MPa)	Shear yield strength (MPa)
192	3.51	1.896	1.034
Manufacturing properties of AUW763			
Cream time	Gel time	Track free time	Free rise density
35-40 sec	94 ± 4 sec	115 ± 5 sec	280-300 kg/m^3

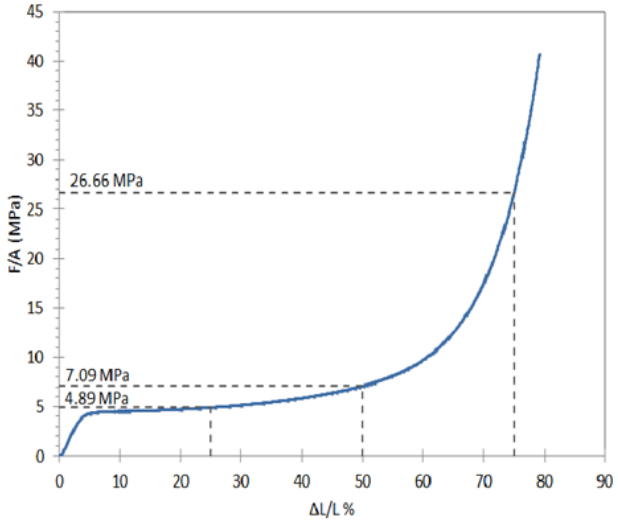

Figure 2.2: Results of the uniaxial load test on PU foam

The yielding behaviour can be explained by the buckling of the foam's internal walls. Scanning Electron Microscopic images (SEM), provided before and after compression test, shown in Figure 7.4, substantiate such behaviour. A long and rather flat plateau was followed. Then, a densification (hardening) region was created by a gradual stress increase when the cell walls were stacked prior to final densification. In this range of loading, no visible signs of failure were observed. Residual displacement of the collapsed foam however, occurs once the unloading stage was complete.

2.2.2 Fabric Formwork

For the selection of formwork system some criteria are usually taken into account: quality (strength, rigidity, position, and dimensions); safety (of both workers and the concrete structure); efficiency (in operation, handling, erection and dismantling, and number of repetitions); and economy (life cycle cost to be consistent with quality and safety). Fabric formworks offer lower weight (approximately 1/300th that of a conventional rigid form),

lower material cost, lower labour cost (no cost of stripping, placing, erection and waterproofing), better constructability (adaptable to uneven ground conditions, easier infill protection, and stakeless system). These make the use of fabric a viable option, especially for rapid assembly construction [7]. Although fabrics have been used as formwork for many years [43], thanks to recent advances in the textile material science, durable and low-cost fabrics are becoming more and more available for construction purposes. Using fabric formwork as a mould in concrete structure, it is possible to cast architecturally interesting, structurally optimised non-prismatic structures that use up to 40% less concrete in comparison with an equivalent prismatic section [7], offering potentially significant embodied energy savings [44] and subsequently, a striking reduction in the CO_2 emissions [45] can be achieved. There are two general types of fabric formworks: slack-sheet mould and energised (tensioned) formwork sheets [46]. Each type of fabric distributes force slightly differently depending on the material it is made of and the nature of its internal structures. This study will focus on the pneumatic fabric formworks, in which pneumatic force is used for the erection of the flexible fabric formwork. The critical aspect of fabric formwork for achieving desirable performance is the selection of the fabric itself. Although a wide range of woven fabrics can be used as formwork for fabric formwork, tensile strengths in both warp and weft directions must be sufficient to hold the infill material (which is polyurethane in this research) and a low creep modulus is desirable to limit formwork deformations during casting and curing/hardening. For the selection of the fabric criteria such as aesthetics, permeability, sew-ability or weldability, relative cost, durability, and strength were considered [47]. Conducting some experimental tests to determine the selection indicators for the criteria like durability and strength for each candidate, Barrateen as the most suitable pneumatic formwork candidate, we selected for foam-filled structural composite panels. Barrateen fabric is an HDPE coated unbalance woven textile. The coating material is low-density polyethylene and well inflatable. In addition, its tensile strengths in the warp and weft directions are not the same. The result of tensile tests on 10 cm wide and 20 cm length specimens according to ASTM D1980-89 showed that the module of elasticity of the principal direction is higher, but, in strain about 270%, it can have a sudden brittle rupture (Figure 2.). A series of weldability tests were also conducted on the fabric. , the tensile bearing capacity of heat-welded connections can reach up to 13% of the average strength of the material. In addition, the maximum strain was measured as 90% at the failure point.

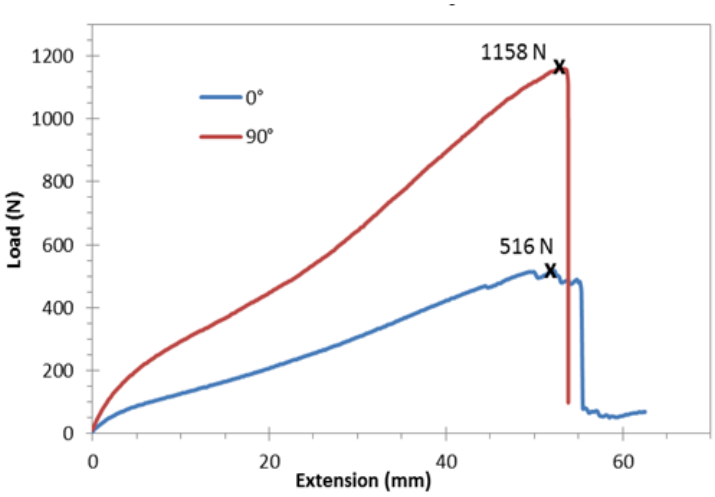

Figure 2.3: Barrateen fabric tensile behaviour in main and transverse directions

With regard to the structural performance of the fabric formwork, some experimental tests were conducted. Formwork should be designed for the ultimate as well as the serviceability limit states. Low yield stress and plastic viscosity of filling material increase the lateral pressure on the forms to a degree as high as the hydrostatic pressure. That is, formwork pressure exists as long as filling material is in a plastic state, and its rate of decay is related to the rate of the stiffening of filling material [48]. Figure 2. depicts the effects of fabric formwork thickness and foam density on the maximum lateral deflection of the fabric formwork. It shows the higher thickness will result in higher effects of density of the maximum lateral deflection.

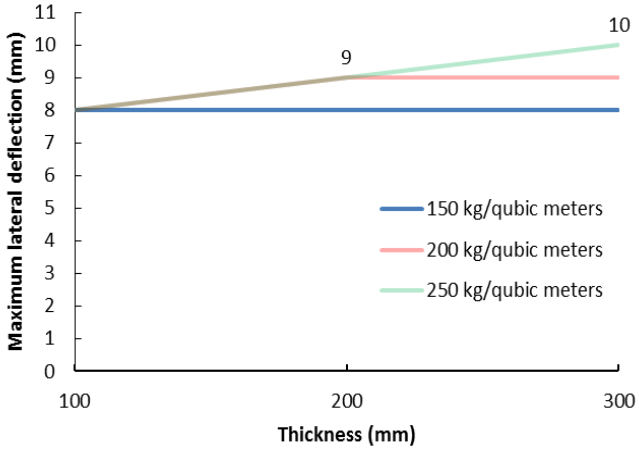

Figure 2.4: Effects of fabric formwork thickness and foam density on the maximum lateral deflection

2.2.3 Skin Sheets

The face sheets of the sandwich panels are made of 3-D HDPE (High-Density Polyethylene) sheets primarily produced as a concrete embedment liner to provide protection from

mechanical damage and a corrosive and erosive environment. In addition to resistance to chemical and environmental threats, its relatively high strength, and in particular its 3-D studded face with approximately 1200 studs per square meter, can effectively contribute to the sandwich composites' structural performance by providing high pull out strength, minimum lateral movement of the skin, and stronger bonding. Four different thicknesses of the sheets were initially investigated (2mm, 3mm, 4mm and 5mm), and at the end, the sheets with 2mm tackiness were selected for the sandwich composite.

In order to identify the structural behaviour of the skin, in-plane tensile tests were conducted on two principal perpendicular directions (lengthwise and crosswise) of the HDPE sheets, using a universal hydraulic testing machine, according to ASTM D6693 standard [49]. Figure 2. shows the coupon test results.

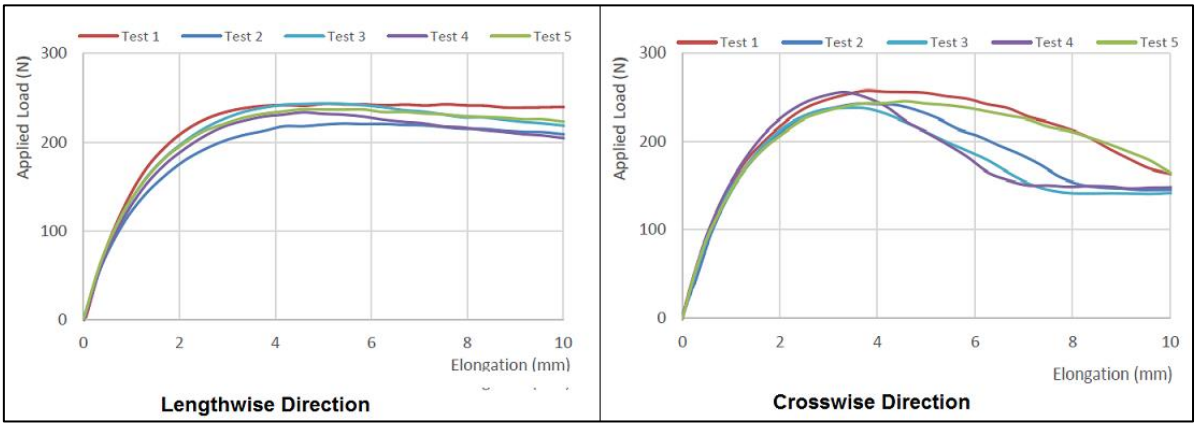

Figure 2.5: The HDPE's tension test results in the lengthwise and crosswise directions

2.3 Edgewise and Flatwise Compressive Behaviour

The edgewise compressive strength of sandwich construction is important as it provides the basis for the assessment of the load-carrying capacity [42]. The compressive properties of the sandwich composite along the direction parallel to the plane of the sandwich face skin were evaluated through edgewise compression tests on 100mm×200mm×300mm samples using a test rig (universal testing machine) in accordance with the ASTM C364 standard [50]. For design purposes, the non-linear behaviour of the stress–strain relationship can be approximated by two linear behaviours with different stiffness. The initial portion can be used to determine the initial elastic modulus using regression analysis of the data up to 2% strain. Due to the significant non-linear behaviour observed beyond the strain level of 2%, the second slope, conservatively representing the reduced elastic modulus can be determined approximately based on the data measured between strains of 4% up to failure strain. These

two calculated slopes are extended between 2% and 4% strain until they intersect each other in order to obtain the full approximation of the compressive edgewise behaviour (Figure 2.).

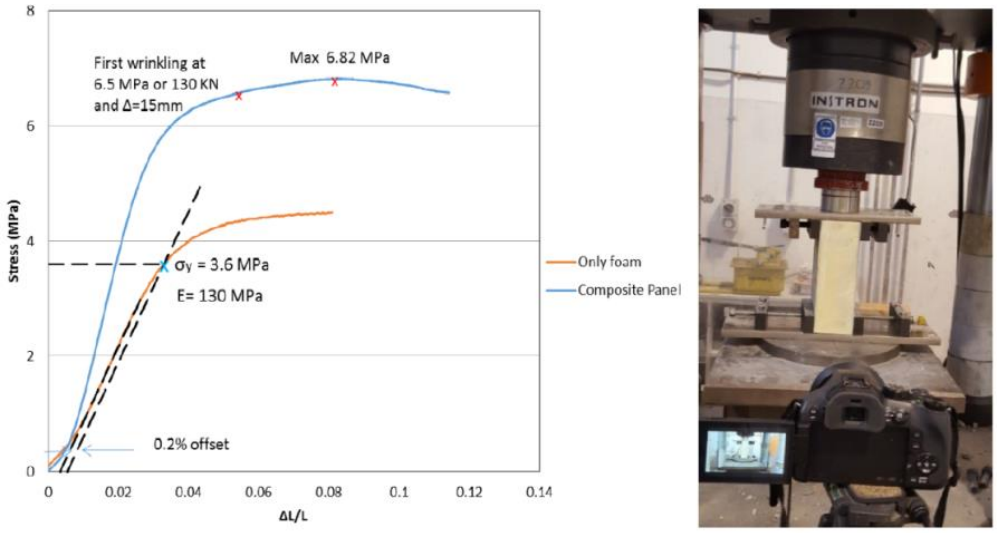

Figure 2.6: Test Setup and design Elasto-Plastic diagram of composite panel under edgewise compression

The compressive strength of the composite was also assessed through the flatwise compressive tests [51, 52] of small sandwich cubes. Four specimens were tested to determine the flatwise compressive strength and elastic modulus for the sandwich core's structural design properties, using a universal testing machine and following the ASTM C365. Flatwise compressive tests were performed until the load–displacement curve indicated a collapsed structure, i.e. with significantly high deformation of specimens.

The results, shown in Figure 2., indicate that the flatwise compressive behaviour of the specimens is governed by the rigid foam behaviour, and the composite specimens show a similar behaviour to the foam specimens. That is, experiment results confirmed that although a separation between the core and the skin is observed at the failure load, the possible local ruptures in the foam, due to the increased stress on the studs' tips, do not influence the flatwise compressive behaviour of the sandwich composite. That is, experiment results confirmed that although a separation between the core and the skin is observed at the failure load, the possible local ruptures in the foam, due to the increased stress on the studs' tips, do not influence the flatwise compressive behaviour of the sandwich composite.

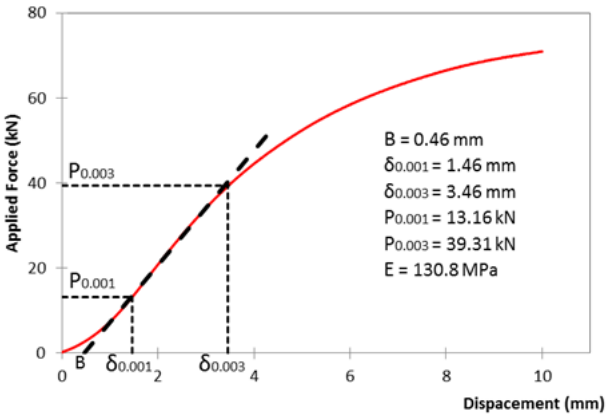

Figure 2.7: Description of flatwise compressive experiments calculation

2.4 Flexural and Shear Behaviour

The flexural stiffness of sandwich beams/panels that can be calculated using First-order Shear Deformation Theory (FSDT) [53-56], is used to estimate the shear stiffness of each sandwich beam type by fitting the results collected from four-point flexural tests. A perfect bond must be assumed to exist between the core and the facings. The bending stiffness can be computed accounting for the deflection components that are associated with bending and shear deformations [57, 58]. This study examined the core shear properties of introduced polyurethane infill-foam composite panels subjected to flexure in such a manner that the applied moments produce curvature of the sandwich facing planes. Also, in this regard, core shear ultimate stress, facing bending stress, transverse shear rigidity and core shear modulus of introduced sandwich panel are calculated based on ASTM C393/C393M [59] and ASTM D7250/D7250M [60] using six medium-scale sandwich specimens with 45 cm length, 20 cm width and 10cm as total thickness of composite section. The applied force versus crosshead displacement and mid-span deflection are shown in Figure 2., and transverse shear rigidity calculated based on ten load-deflection selective steps is shown in Table 2..

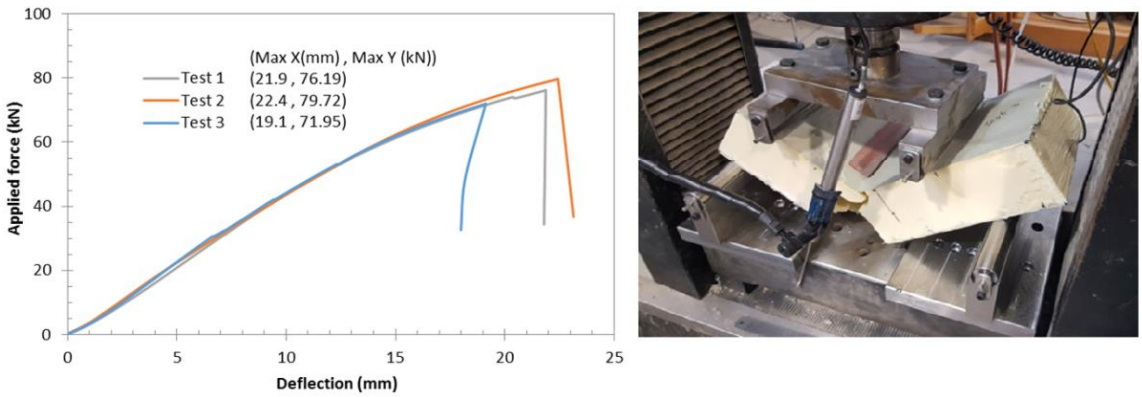

Figure 2.8: Four-point quarter-span loading flexural test results

Table 2.2: The least maximum applied forces and their related mid-span deflections

	4-Point Quarter Span Loading		3-Point Mid Span Loading	
	P_{max} (kN)	$\Delta_{midspan}$ (mm)	P_{max} (kN)	$\Delta_{midspan}$ (mm)
Specimen 1	76.19	21.9	56.23	24.9
Specimen 2	79.72	22.4	52.54 (minimum)	23.8
Specimen 3	71.95 (minimum)	19.1	53.98	24.2
Average	75.95	21.1	54.25	24.3
Standard deviation	3.89	1.8	1.86	0.56
CV (%)	5.12	8.42	3.5	2.3

2.5 Effects of Cold Joints

One of the most important construction problems of foam made panels is cold joints, which is also known as seams. When the placing of foam in the panels is delayed or interrupted for some reasons, the foam that has already been placed starts to condense, producing a kind of construction joint (seam) called a cold joint between it and newly placed foam. A seam is a plane under mixed materials, or a fold that is developed within the rising foam mass, which appears as a line on the foam surface or section . Such joints between new and old portions of foam that are formed when the new foam is placed adjacent to the foam that has hardened or has started to harden, may have negative effects on the strength of rigid foam panel.

Hence, attention must be paid to the position and direction of the joints, and the effects on the structural behaviour. For experimental investigation, three series of bending tests were carried out on two types of panelised specimens. Two types of 1500*1000*100 mm^3 rigid polyurethane panels were used: Type S (seamless) and type TS (with transverse seams) specimens (Figure 2.9). The expansion rate of this type of foam is 3.0, and the average weight of both types of panels is 29.0 kg.

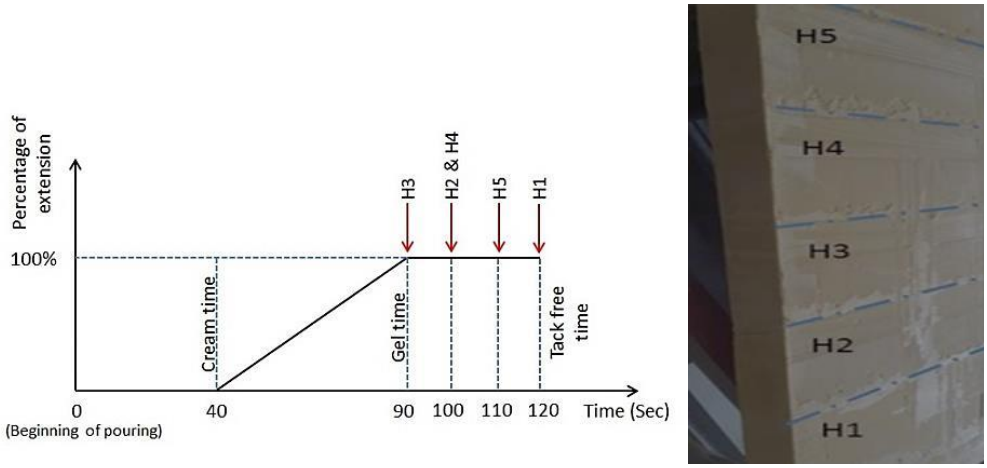

Figure 2.9: Casting schedule of seams at TS specimens Locations of transverse seams

A comparison between the results of the tests shows that casting at the end of gel time instead of the end of tack free time, resulted in 80% increase in the tensile strength of the seams. Also, casting at about 20 sec before of the end of tack free time (120^{th} sec), increased the tensile strength of the seams by 60%. The seamed section exhibited about 33.1% of the maximum tensile strength of an intact section. In addition, the seamless panels showed a larger deflection capacity, as 20% more than that of TS panels.

2.6 Integrated Connections

Connections represent major challenges in the design of composite structures, mainly because they entail discontinuities in the geometry of the structure and material properties, and introduce high local stress concentrations. Despite some constructability complications, integrated connections could be a reliable solution. For the composite sections in this study, the connections between the panels are constructed by continues foam casting to achieve better integrity. The primary function of these connections is to guarantee the transfer of lateral (seismic and wind) loads between the composite panels, as well as between panels and roof in rapid assembly post-disaster buildings. In addition, this connection accounts for restricting the rotation, i.e. the maximum deflections along the span. This is a significant factor because in practice, the maximum allowable deformation is usually the governing factor in the design of lightweight composite sandwich panels. For the experimental investigation, six L shape specimens, representing the connections between adjacent sandwich panels, are tested. In order to better study the composite performance and compare the results with non-composite behaviour, three of the specimens were made of composite sections, while here of them were foam-only sections; all of them were manufactured by one shot casting method in wooden formworks and were cut out of actual adjacent sandwich

panels. The composite connections comprised of 2 mm thick 3-D HDPE face sheets enclosing a 96 mm thick core of rigid PU foam. The test specimens were supported in a cantilever configuration test rig, and a point load was applied at 40 mm of the free edge, as illustrated in Figure 2.10.

Figure 2.10: The ultimate deflection and the mechanism of collapse and dimensions of the connection

As presented in Table , the overall mechanical response, and the stress distributions, and failure modes, moment resistance, initial rotational stiffness and rotational capacity of the connections were studied. The experimental test results indicated that in composite sections the bending ultimate strength increases by 25% compared to foam-only connections. The composite connections also show 2.2% greater rigidity and an increased rotational stiffness of 85%. With regard to the relative ultimate cantilever deflection, i.e. bending stiffness, composite connections presented a better performance by 12% in comparison with foam-only connections.

Table 2.3: Summary of the experimental carried tests for both simple and composite systems

Test Details		Ultimate Load (N)	Ultimate Displacement (mm)	Ultimate Rotation (Degree)
Foam-only Specimens	Specimen 1	7991	42.0	5.0
	Specimen 2	7172	44.0	6.0
	Specimen 3	7870	52.0	8.0
	Average	7678	46.0	6.3
	CV (%)	5.8	11.5	1.8
Composite Specimens	Specimen 1	9299	44.0	4.0
	Specimen 2	9602	41.0	6.0
	Specimen 3	9926	38.0	3.0
	Average	9609	41.0	4.3
	CV (%)	3.3	7.3	1.8

2.7 Concluding Remarks

A new foam-filled sandwich panel and its integrated connections were developed at the Centre for Infrastructure Engineering of Western Sydney University, as a rapid assembly system for post-disaster housing and semi-permanent accommodations. It is composed of 3-D high density Polyethylene (HDPE) sheets, as the skins with a thickness as 2 mm, high-density PU foam core with a total thickness as 100 mm, incorporated into a pneumatic fabric formwork. This paper investigated the structural performance of the panel and integrated connections, with respect to the material properties, edgewise and flatwise compressive behaviour, flexural and shear behaviour and the effect of cold joints (seams). The findings for each criterion indicate that the system fully complies with the relevant standards for semi-permanent and temporary accommodations, and meet their requirements for post-disaster housing. In this regard, the following conclusions are achieved:

- The used rigid foam is accordance with ASTM E1730 Type 4, for which, carrying out thermal conductivity test is not required. A 100 mm thick layer of rigid PU provides a U-value of 0.04, which demonstrates high insulation performance of polyurethane foam
- Barrateen was selected from the mentioned list of seven potential candidates as the best pneumatic formwork candidate for foam-filled structural composite panels. The type of lateral pressure of foam on this fabric formwork with thickness of 100 mm is hydrostatic.
- The failure mode of specimens under the edgewise compression was local buckling (wrinkling) of the HDPE sheets between two edge studs, resulting in a local delamination and de-bonding between the face and core.
- Results indicate that under flexure, the foam core and skins displacement are in sync, which demonstrate well integrated and ductile behaviour of the introduced composite panel.
- Further research on the constructional and architectural aspects, such as the integration of windows and doors, and on-site foam casting methods are in progress.

Chapter 3

Optimised choice of textile for panelised fabric formwork

The contents of this chapter have been published in the form of a journal paper as follows:

Saeed Nemati (Full contribution), Maria Rashidi (contributed in decision making phase) and Bijan Samali (Scientific supervision), "Decision Making on the Optimised Choice of Pneumatic Formwork Textile for Foam-Filled Structural Composite Panels". International Journal of GEOMATE, Nov., 2017, Vol.13, Issue 39, pp. 220-228 Geotec., Const. Mat. & Env., ISSN:2186-2990, DOI: https://doi.org/10.21660/2017.39.7350, Japan.

3.1 Introduction

Fabric formwork is a method for construction of a wide range of architectural and structural components. Fabric formwork is made of textile sheets of synthetic fibres such as nylon, polyesters, polypropylene that are fabricated into containers to contain various type of fillers such as concrete. Fabric formworks can be used to form columns, walls, beams, trusses, slabs, panels, and thin-shell structures in both precast and in-situ construction. Using fabric formwork as a mould in concrete structures, it is possible to cast architecturally interesting, structurally optimised non-prismatic structures that use up to 40% less concrete in comparison with an equivalent prismatic section [7], offering potentially significant embodied energy savings [44] and subsequently, a striking reduction in the CO_2 emissions [45] can be achieved. In a recent ongoing research project at the Centre for Infrastructure Engineering of Western Sydney University, fabric formwork has been used for an innovative foam-filled structural panels in order to be employed for rapidly assembled buildings as a semi-permanent housing system. This study will focus on the pneumatic fabric formworks, in which pneumatic force is used for the erection of the flexible fabric formwork [61]. This system is going to tackle the problems with the existing semi-permanent housing systems' low tolerance in construction, transportation, erection and maintenance phases, as well as their relatively costly materials [62], installation and fabrication methods and labour works. The critical aspect of fabric formwork for achieving desirable performance is the selection of the fabric itself. Although a wide range of woven fabrics can be used as formwork for fabric formwork, tensile strengths in both warp and weft directions must be sufficient to hold the infill material (which is polyurethane [20] in this research) and a low creep modulus is desirable to limit formwork deformations during casting and curing/hardening. In the literature, to date, there is no known study based on systematic decision making methods for fabric formwork selection. This paper identifies the factors influencing the selection of an appropriate fabric, and develops a decision-making system for selecting the best fabric formwork textile for the newly developed foam filled panels, which will be used as a rapidly assembled building system for semi-permanent housing.

3.2 Background of the Study

There are not many studies on the structural applications of fabric formworks. The work of Lamberton in 1968 in the field of Geotextiles led to the first commercial use of fabric

formwork for concrete structures [63]. In the early 1990s, Rob Wheen from the University of Sydney and Asaddoah Redjvani, developed a flexible formwork wall system for both the Persian Gulf and Caspian sea marine and land construction projects using PVC coated polyester fabric internal ties [64]. Ghaib et al. [11] showed that the mechanical characteristics of fabric formwork affect its filled material. Appropriate selection of a formwork system can considerably affect the cost and speed of many construction projects [36, 65-68]. Shin et al. [69] proposed a decision support model to select a formwork system suitable for the construction site conditions. Optimisation and durability in fabric cast double T-beams have been studied by Orr et al. [70]. Proverbs et al. [71] identified nine formwork selection factors including quality of concrete, relative costs, speed of production, availability of plant and equipment, availability of labour, company practice, building form and location, degree of repetition and on-site transport system and ranked them in terms of importance for each international group of contractors. The formwork systems can be selected based on some construction considerations including easy and economical transportation from factory to construction site, easy and economical assembly and disassembly, maximum rate of construction speed to formwork weight, minimum number of construction joints, minimum waste generation in formwork production process, safety, ease of storage, applicability to high rise structures, reasonable potential for preconstruction, the potential to make non-prismatic sections and complex shapes, not reliant on highly-trained and skilled work force, compatibility with the core material in order to minimize the environmental effects, appropriate specific heat capacity and thermal conductivity, reusability and finally fast connectors applicability [72].

3.3 Fabric Formworks

3.3.1 Fabrics Properties

There are two general types of fabric formworks: slack-sheet mould and energised (tensioned) formwork sheets [46]. Fabrics can be categorised as woven/non-woven fabrics, balanced/unbalanced fabrics, knit fabrics, plastic films and coated/uncoated fabrics. There are many different weaving patterns but the basic pattern called a “plain weave” consists of warp threads (running along the long direction of the roll) and weft threads (filling transversely across the width of the roll) [46]. If a woven textile has the same amount of materials in both the wrap and weft directions, it is referred to as a “balanced” weave. An “unbalanced” weave will have more material in one direction that in the other, and so will have unequal strength

and stiffness as well. Because the threads are kept straight, plain woven structures do not allow much stretching at all along the two axes of the weave. Nevertheless, a balanced plain woven fabric will always be slightly less stretchy (i.e. have greater stiffness in tension) in the warp, or machine direction [46]. Non-woven fabric such as felt generally refers to a fabric composed of short fibres, matted and compressed together in what might be described as a structural tangle. Non-woven textiles are not generally used structurally, as they are inherently weaker than woven fabrics, due to their randomised and non-continuous fibres. Knit fabrics are made with a looped thread running in a long meandering course, forming an interlinked mesh. Because the yarns are looped and not straight, a knitted structure allows a good deal of stretch. Plastic films are flexible sheets of plastic, such as a polyethylene vapour barrier film can also be used as a formwork sheet or as a formwork liner. Woven or even knit fabrics can have a waterproof coating applied to one or both sides. Such a coating affects the permeability of the fabric, for example, by making it impervious to water and air. Coating can also inhibit or prevent the threads from fraying at the edges of the cloth, and inhibit or prevent the fabric's fibres from "shearing" on the bias. When a coating is applied to a woven textile, it binds the woven tapes or threads together, fixing the weave's 90° geometry in place. Since the coating prevents, or inhibits, the threads from shearing, the fabric behaves less like a woven structure and more like an isotropic sheet such as a sheet of plastic or a piece of paper [46].

3.3.2 Fabrics for Flexible Formwork

Generally speaking, the viscosity of the fill material, the internal construction details, the hydrostatic pressure action on the outer skin, the internal restraints on the grout level, the size and shape of flexible formwork and its methods of placing and handling, the effects of buoyancy and currents, the sequence of injection, the position of bleed points or overfill prevention and finally, the provision of overfill compartments to compensate for the settlement of grout resulting from excessive bleed are the major factors to be considered when selecting fabric formwork [73]. Current construction practice in this field generally uses woven polyolefin textiles. Polyester, Polyamide, Polypropylene (PP) and Polyethylene (PE), which are not true elastic materials, are the main synthetic polymers used as raw materials to manufacture formwork fabrics [74]. Woven Polyolefin Geotextiles (PP and PE) are a common choice for fabric formwork. PE and PP textiles (that are made from woven high density polyethylene or polypropylene (HDPE or HDPP) threads or tapes) are among the least expensive options, while they are stronger and more robust than the burlap/hessian

fabrics. PP fabrics don't tear easily and are relatively lighter than PE. PE fabrics are resistant to strong acids or strong bases and relatively weaker in strength compared to PP. These materials can be manufactured with varying degrees of quality. Even the lowest quality PP and PE fabrics, such as woven textiles used for sandbags or packaging, will work well as fabric moulds, if used conservatively. There is also a wide range of PE and PP "geotextiles" manufactured for use in landscape construction and road building. These are made of woven high density polyethylene or polypropylene threads or taps and are specifically designed for combinations of strength and permeability to water. PE and PP are so similar in their appearance, handling and performance as formworks, that user will not be able to tell them apart. One weakness of PP and PP fabrics is that they will eventually degrade from exposure to ultraviolet radiation (sunlight), although they can be manufactured with anti-UV stabilizers that do a good job of resisting this degradation. The woven PE and PP fabrics are quite strong and will usually have plenty of reserve strength. Their behaviour is non-linear, with a rough service strain of above 2%. Linear, elastic behaviour may be maintained to 5% strain, or more. PP or PE woven fabrics will not propagate a tear, which makes them safe to use, and allows them to be connected using staples, screws or nails. PP and PE are also thermoplastics.

3.3.3 Studied Fabrics

The textile industry is developing various types of suitable fabrics for applications in construction [75]. In order to be used as a fabric formwork for structural panels, the most important properties of fabrics are strength, stiffness, failure mode (slow/plastic failure are more desirable than sudden/elastic failure), permeability, weldability (coated PE or PP fabric can be heat-welded together and uncoated fabrics cannot), reusability, easy sewing , and stress distribution ability. Accordingly, in this study seven types of fabrics that meet the abovementioned criteria, and are widely used for similar purposes have been selected and then evaluated as potential options for fabric formwork of foam filled panels. The selected fabrics were: Lockram, Hydrophobic Polyester Fabric, Laminated Chamois, Vinyl Crystal Clear, Rubber fabric, Herculon Fabric, and Barrateen (left to right in Figure 3.1).

Lockram is made from a semi-industrial type of cotton, and produced in 145 cm wide rolls. The common applications are household applications. This fabric is a balanced woven fabric, and has the identical tensile strength in both the warp and weft directions and is well inflatable too. The result of tensile tests according to ASTM D1980-89 in warp direction is shown in Figure 3.2. The applied width of specimens is 10cm and mechanism of failure is sudden/brittle rupture. The failure strain has been measured as 15%.

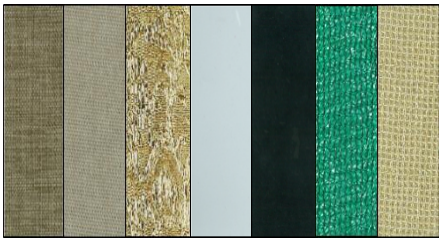

Figure 3.1: Studied fabrics

Hydrophobic Polyester Fabric is made from pure polyester and is 100% washable and mould resistant, and produced in 260 cm wide rolls. Its common applications are household applications such as curtains.

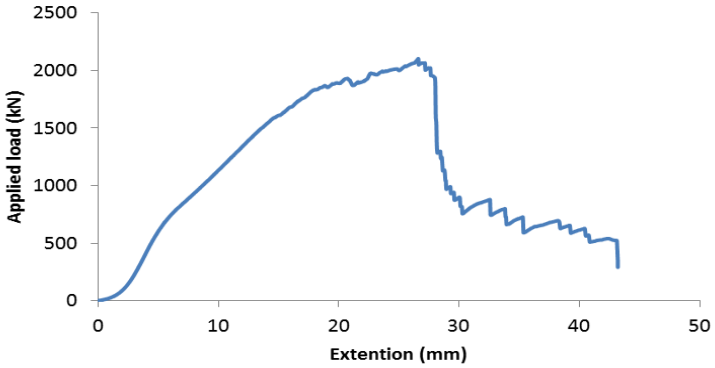

Figure 3.2: Lockram tensile behaviour

This fabric is a balanced woven fabric. It has the same tensile strength in both the warp and weft directions, and is well inflatable. The result of tensile tests on 10 cm wide specimens according to ASTM D1980-89 in warp direction is shown in Figure 3.3. The failure strain has been measured as 17%, and the mechanism of failure is a sudden/brittle rupture. Laminated Chamois is composed of a plastic film and a layer of non-woven compressed to each other. It is used for household applications and produced in 135 cm wide rolls. By using as internal fabric formwork layer, the cost of finishing and maybe painting can be reduced. The result of tensile tests on 10 cm wide specimens according to ASTM D1980-89 is shown in Figure 3.4, which shows that its failure strain is about 110%. Laminated Chamois is crimped during the tensile test, but at rupture point, only its plastic layer was ruptured and its un-woven layer kept deforming. The mechanism of failure is a ductile rupture. Vinyl Crystal Clear is an un-dyed polymeric fabric, used for household and produced in 135 cm wide rolls. Because of its tensile behaviour and high failure strain (350%) and good stress distribution ability, as shown in Figure 3.5, it can be suitable for mechanical connections. Rubber fabric does not display any plastic behaviour during tensile tests. Its fracture mode is very brittle (Figure 3.6) but, the

failure strain has been measured as 90%. This brittle behaviour can create some structural problems when used for mechanical connections. It is produced in 100 cm wide rolls. Herculon fabric is a woven polyolefin textile, used as window shades, children's sandbox cover, pergola; veranda and patio cover, and produced in 185 cm wide rolls. It possesses relatively high strength and durability, and as a lead-free material has 100% UV-stabilised yarn and can reduce the UV flow by 90%. It is classified as mould and mildew resistant and non-shrink heat fabric and is not inflatable.

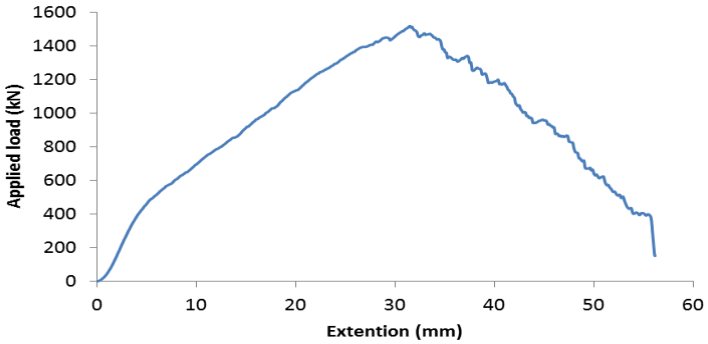

Figure 3.3: Tearing of hydrophobic polyester fabric and its tensile behaviour

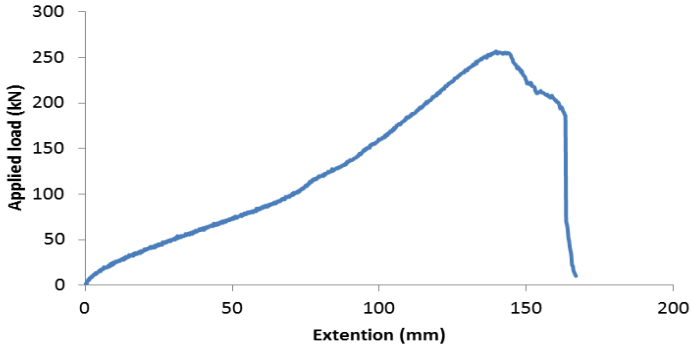

Figure 3.4: Laminated Chamois tensile behaviour

This fabric is an unbalance plain woven fabric. Therefore, its tensile strengths in two directions perpendicular to each other (the warp and weft directions) are not the same. The result of tensile tests according to ASTM D1980-89, is shown in Figure 3.7. As shown in Figure 3.9, before strain reaches 75%, Herculon fabric has similar behaviour in the two directions. Then, before reaching 225% strain, it has elastic behaviour in both directions. Under strains between 75% and 225%, the modulus of elasticity of the principal direction is higher, but, under the strain of 225% the harder specimen had a sudden rupture, whiles the softer specimen continues its deformation to about 250% strain.

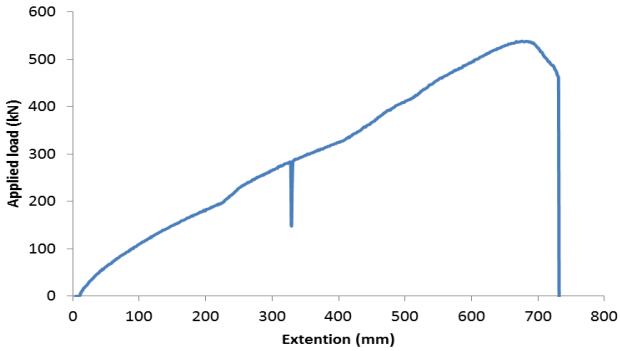

Figure 3.5: Vinyl Crystal clear tensile behaviour

Barrateen is a HDPE coated unbalance woven textile. It is produced in 184 cm wide rolls. The coating material is low density polyethylene and well inflatable. In addition, its tensile strengths in the warp and weft directions are not the same. The result of tensile tests according to ASTM D1980-89 is shown in Figure 3.8. As can be seen in Figure 3.8, the modulus of elasticity of the principal direction is higher, but, under the strain of about 270%, both specimens had a sudden brittle rupture. As maintained before, weldability is one of the main benefits of the coated fabric. A series of weldability tests was also conducted on the fabrics (Figure 3.9).

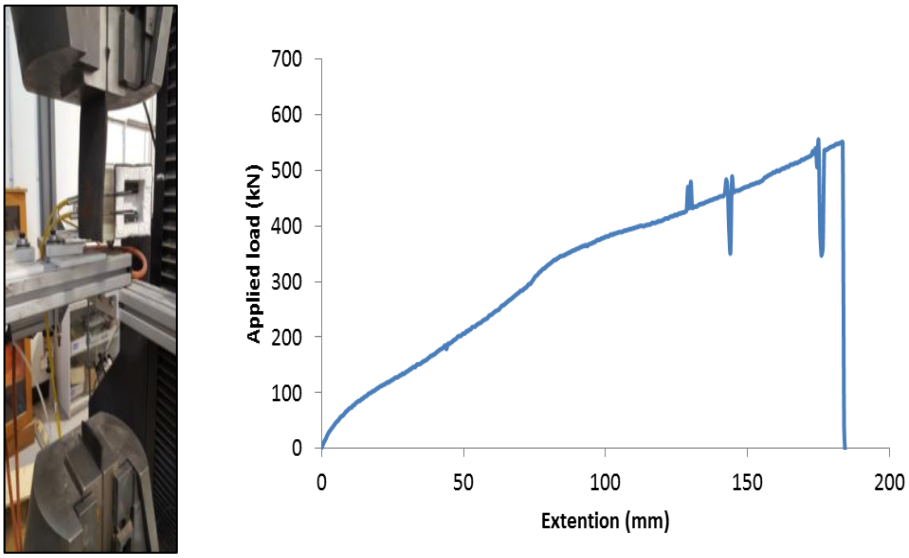

Figure 3.6: Brittle behaviour of Rubber fabric specimens

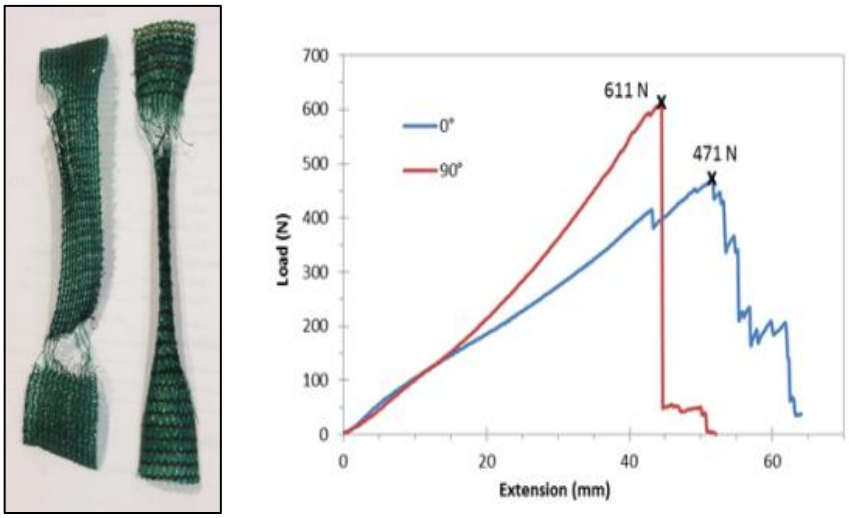

Figure 3.7: Herculon fabric tensile behaviour in main (90º) and transverse (0º) directions

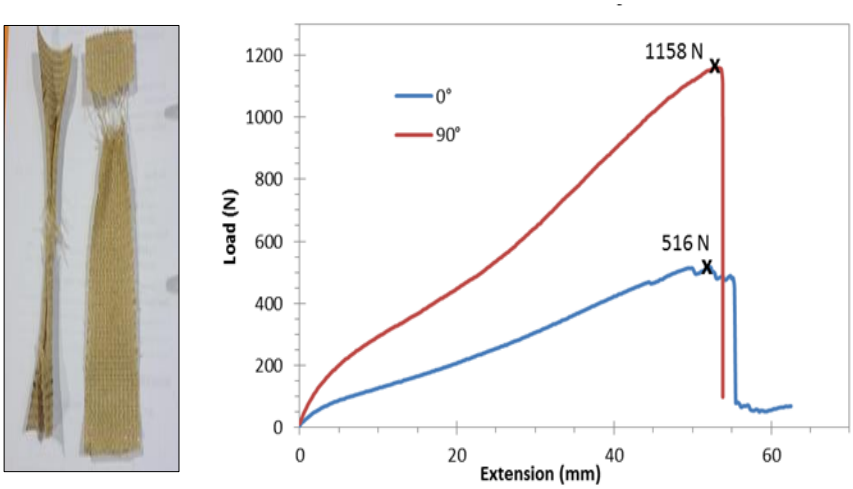

Figure 3.8: Barrateen fabric tensile behaviour in main (90º) and transverse (0º) directions

The results of tensile tests of heat-welded parts showed that this kind of connections has no reliable structural performance (Figure 3.10). According to the results, the tensile bearing capacity of heat-welded connections can reach up to 13% of the average strength of the material. In addition, the maximum strain was measured as 90% at the failure point.

Figure 3.9: Heat-welded specimens of Barrateen fabric

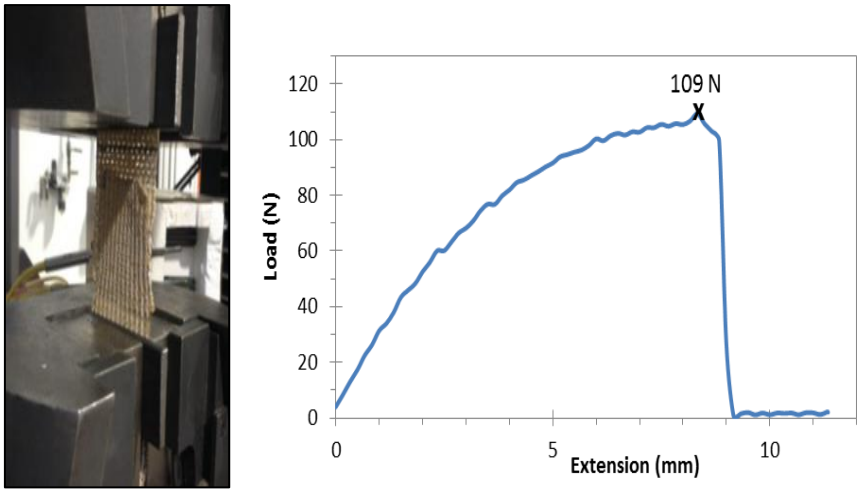

Figure 3.10: Tensile behaviour of heat-welded Barrateen fabric specimens

3.4 Decision Making

Most real-world decisions are not limited to unique and single solutions. The decisions are typically less than optimal and are drawn from a set of reasonable alternatives that have been known as 'satisficing' solutions [55, 56, 76]. Therefore, the potential range of rational alternatives should be identified and classified [77]. In this case, selection of the most suitable fabric involves a case-by-case assessment to determine the potential risks associated with any given alternative. Potential users and decision makers have various criteria and constraints that must be coped with when endeavouring to suggest the best possible alternative. The main idea of using criteria is to quantify the performance of alternatives in relation to the objectives of the decision maker based on a numerical scale [78, 79].

3.4.1 Decision Criteria

The selection of an appropriate formwork system is mainly dependent on the intuitive and subjective opinion of practitioners with limited experience. In this study a survey and semi-structured interview with 30 potential users and specialists have been conducted. Based on this survey, the following six constraints/criteria for a suitable pneumatic fabric formwork are selected: permeability, strength, relative cost, durability, sew-ability, and finally aesthetics (Table 3.1). For scoring of durability, fabrics' resistance was examined against freezing and thawing. Three samples have been tested for different weather conditions. The process has been conducted three times within the interval of two days. At the next step, tensile strength tests were conducted on the specimens and the ratio of rupture force to tensile strength of the fabrics were measured. The average of the above-mentioned ratios was used as an indicator of the overall durability (Table 3.2).

3.4.2 Application of Analytical Hierarchy Process (AHP) for Decision Making

AHP is a multi-attribute decision making method which belongs to a broader class, known as "additive weighting methods". The AHP was proposed by Saaty [80] and uses an objective function to aggregate the different features of a decision problem [79, 81] where the main aim is to select the action item that has the highest value of the objective function. The AHP is based on four axioms [82].

Table 3.1: Rating of the decision alternatives against the major criteria (7 = best rank)

	Lockram	Hydrophobic Polyester	Laminated Chamois	Vinyl Crystal Clear	Rubber Fabric	Herculon	Barrateen
Aesthetics	5	6	7	2	1	3	4
Permeability	2	3	5	6	6	1	4
Sew-Ability	6	7	5	2	1	3	4
Relative Cost	1	1	1	1	1	2	2
Durability	2	3	1	4	4	4	4
Strength	6	5	1	2	2	3	4

Table 3.2: The ratio of after freezing-thawing tensile strength to natural tensile strength (F_f/F_n)

FABRIC	(%) F_f/F_n*
Lockram	٩٠
Hydrophobic Polyester	94
Laminated Chamois	86
Vinyl Crystal Clear	99
Rubber fabric	99
Herculon	99
Barrateen	99

Similar to MAU/VT and SMART, the AHP is classified as a compensatory method, where criteria with low scores are compensated by higher scores in other criteria, but contrasting the utilitarian systems, the AHP uses pairwise comparisons of criteria rather than value functions or utility where all individual criteria are paired with all other constraints and the end results accumulated into a decision matrix [83]. The process of AHP includes three phases: decomposition, comparative judgments, and synthesis of priority. Through the AHP process,

decision problems are decomposed into a hierarchical structure, and both qualitative and quantitative data can be used to derive ratio scales between the decision elements at each hierarchical level by means of pair wise comparisons. The top level of hierarchy characterises overall objectives and the lower levels correspond to criteria, sub-criteria, and alternatives. With comparative judgments, decision makers are requested to set up a comparison matrix at each hierarchy by pairwise comparison of criteria or sub-criteria. A scale of values, ranging from 1 (indifference) to 9 (extreme preference) is employed to express the users' priority. Finally, in the synthesis of priority stage, each matrix is then solved by an eigenvector method for defining the criteria importance and alternative performance [81]. The comparisons are normally documented in a comparative matrix A, which must be both transitive such that if, i > j and j > k then i > k where i, j, and k are alternatives; for all j > k > i and reciprocal, $a_{ij}=1/a_{ji}$. Priorities are then estimated from the comparison matrix by normalising each column of the matrix, to develop the normalised primary right eigenvector, the priority vector, by $A.W=\lambda_{max}.W$; where A is the comparison matrix; W is the principal Eigen vector and λmax is the maximal Eigen value of matrix A [83, 84]. Through the AHP process, decision-makers' inconsistency can be estimated via consistency index (CI) which is employed to determine whether decisions break the transitivity rule, and to what extent. A threshold value of 0.10 is acceptable, but if it is more than that then the CI is calculated by using the consistency ratio CR= CI/RI where RI is the ratio index. CI is further defined as $CI=((\lambda_{max}-n)) \diagup ((n-1))$; where λ_{max} is as above; n is the dimension [83]. The average consistencies of RI from random matrices are shown in Table 3.3. The advantages of the AHP method are that it has a systematic approach (through a hierarchy) and presents an objectivity and reliability for quantifying weighting factors for criteria [85]. It can also deliver a well-tested method which allows analysts to include multiple, conflicting, non-monetary features of alternatives into their decision making [86]. On the other hand, the disadvantages are that the estimation of a pair-wise comparison matrix for each attribute is complicated and as the number of criteria and/or alternatives increases, the complexity of the estimations increases considerably. Moreover if a new alternative is added after finishing an evaluation, it is very difficult because all the calculation processes have to be restarted again [85]. The shortcomings of AHP are of a more theoretical nature, and have been the subject of some debate in the technical literature. Many analysts have pointed out that, the attribute weighting questions must be answered considering the average performance levels of the alternatives. Others have noted the possibility for ranking reversal among remaining action items after one is deleted from consideration. Finally, some theorists go so far as to state that

as currently practiced, “the rankings of AHP are arbitrary”. Defenders of AHP, such as Saaty himself, justified that rank reversal is not a fault because real-world decision-making shows this characteristic as well [87].

Table 3.3: Random Inconsistency Index, Adapted from[88]

N	1	2	3	4	5	6	7	8	9	10
RI	0	0	0.58	0.9	1.12	1.24	1.32	1.41	1.45	1.49

3.4.3 Strategy Selection Using AHP

Through the AHP process, the problem under consideration is broken down into a hierarchy, including at least three major levels: goal, criteria (objectives) and alternatives. The criteria might be general and are required to be broken down into more specific sub-criteria introduced as attributes in another level of hierarchy. AHP deals with identifying the overall goal and proceeding downward until the measure of value is included. Figure 3.11 shows a four-level hierarchy structure considering the general features of the problem. The first level of the structure is the overall goal of the ranking (Fabric Selection). The second level contains the identified objectives (criteria) to achieve the main goal. The third level holds the sub criteria to be used for assessing the objectives. The final level is added for the alternatives [86]. Each criterion/constraint has a weighting indicating its significance and reflecting the organisational policy. These weightings are defined by the users/decision makers employing the pair wise comparison approach embedded in the AHP and will vary for different problems with different decision makers. The AHP has the major advantage of allowing the decision makers to conduct a consistency check for the developed judgment in regard to its relative importance among the decision making components. Therefore, the decision maker(s) can modify their evaluations to improve the consistency and to supply more informed judgments under consideration.

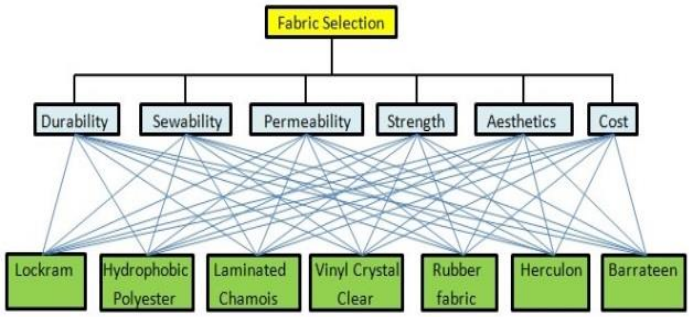

Figure 3.11: Multi Criteria Decision Hierarchy for Fabric Selection

The procedure is also able to provide flexibility in selecting the criteria to evaluate the alternatives (different types of fabric) and even increasing or decreasing the number of levels (associated with the criteria) in the hierarchy. The overall ranking value of each alternative for a four level hierarchy (as shown in Equation 1) Xj is expressed as follows:

$$\boldsymbol{X_j = \sum_{i=1}^{n} W_k W_{ki} a_{ij}} \qquad (1)$$

-W_k is the weighting of criterion k

-W_{ki} is the weighting of the i^{th} sub-criterion in the category of criterion k

-a_{ij} is the importance level of j^{th} alternative with respect to the i^{th} sub criterion and kth criterion.

Table 3.4 presents the developed comparison matrix for the criteria identified for fabric selection. Vector of priorities (the Eigen vector of the developed matrix) addressing the weight of criteria has been identified and presented in Equation (2):

$$\text{VOP}=\begin{bmatrix}\mathbf{0.1376}\\ \mathbf{0.4581}\\ \mathbf{0.2627}\\ \mathbf{0.0453}\\ \mathbf{0.0663}\\ \mathbf{0.0299}\end{bmatrix}=\begin{bmatrix}\textbf{Durability}\\ \textbf{Cost}\\ \textbf{Permeability}\\ \textbf{Sewability}\\ \textbf{Tesnsile Strength}\\ \textbf{Aesthetic}\end{bmatrix} \qquad (2)$$

Since the decision makers may be unable to deliver perfectly consistent pairwise comparisons, it is demanded that the comparison matrix should have an adequate consistency, which can be checked by the following consistency ratio (CR):

$$\text{CR}=\frac{\boldsymbol{(\lambda max - n)/(n-1)}}{\textbf{RI}} \qquad (3)$$

where, λ_{max} = 9.73(0.1376) + 1.9(0.4581) + 4.79(0.2627) + 25.33(0.0453) + 16.83(0.0663) + 29(0.0299) = 6.59

In calculating λmax, the values in front of brackets are the summations in AHP matrix in Table 3.4, and the values inside the brackets are the corresponding VOPs. Random inconsistency index (RI) for 6 criteria is extracted from Table 3.3 provided by Saaty [84]. The Consistency Ratio (CR) has been calculated based on Equation 3. Since the value of CR is less than 0.1, it can be concluded that the accomplished judgement has consistency.

$$\text{CR}=\frac{\boldsymbol{(\lambda max - n)/(n-1)}}{\textbf{RI}} = 0.095 < 0.1$$

Then the experts were asked to compare the main alternatives with respect to each criterion. Finally, global priorities of the different major options were estimated by multiplying the weightings of the alternative associated with each constraint by the criterion weighting and

finding the overall sum. As shown in Table 3.5, 'Barrateen' has got the highest score in this analysis; hence it has been selected as the most suitable fabric for pneumatic formwork.

Table 3.4: AHP Matrix- Pairwise comparison of criteria

	Cost	Permeability	Strength	Sewability	Durability	Aesthetic
Cost	1	1/5	1/3	5	3	5
Permeability	5	1	3	9	7	9
Strength	3	1/3	1	7	5	9
Sewability	1/5	1/9	1/7	1	1/3	3
Durability	1/3	1/7	1/5	3	1	2
Aesthetic	15	1/9	1/9	1/3	1/2	1

Table 3.5: Fabric Selection using AHP method

									Alternatives						
		Rubber fabric (3mm)		Vinyl Crystal 0.75 mm		Herculon		Lockram		Laminated	Chamois	Hydrophobic	Polyester	Barrateen	
Criteria	Weight of the Criteria	Rating of the alternatives	Overal importance	Rating of the alternatives	Overal importance	Rating of the alternatives	Overal importance	Rating of the alternatives	Overal importance	Rating of the alternatives	Overal importance	Rating of the alternatives	Overal importance	Rating of the alternatives	Overal importance
Durability	0.07	4	0.27	4	0.27	4	0.27	2	0.13	1	0.07	3	0.2	4	0.27
Sewability	0.05	1	0.05	2	0.09	3	0.14	5	0.23	6	0.27	7	0.32	4	0.18
Permeability	0.46	1	0.46	2	0.92	3	1.37	4	1.83	6	2.75	5	2.29	7	3.21
Strength	0.27	4	1.05	3	0.79	2	0.53	7	1.84	1	0.26	6	1.58	5	1.31
Aesthetic	0.03	1	0.03	3	0.09	5	0.15	2	0.06	7	0.21	4	0.12	6	0.18
Cost	0.1	1	0.14	2	0.28	7	0.96	4	0.55	5	0.69	3	0.41	6	0.83
Total Score			1.99		2.4		3.41		4.64		4.25		4.92		5.97

3.5 Conclusions

Innovations in formwork solutions and introduction of flexible fabric in place of stiff traditional formwork elements have created new possibilities for a wide range of construction components. Combined with textile formwork, the production of a new range of structural foam-filled panelised systems has become possible without intensive labour for traditional formwork installation. The objective of this study was to select the most appropriate fabric for a pneumatic formwork, which will be used for the newly developed structural foam-filled panels. First, based on the results of a survey, six criteria for a suitable pneumatic fabric formwork were selected; namely: permeability, strength, relative cost, durability, sew-ability, and aesthetics. Some experimental tests were conducted to determine the selection indicators for the criteria like durability and strength for each candidate. Then, an analytical hierarchy process was employed for decision making on the best pneumatic formwork candidate for foam-filled structural composite panels. The model can be applied on any potential decision alternatives considering the identified constraints and the associated determined weightings.

Chapter 4

Lateral deformation of panelised flexible formworks

The contents of this chapter have been published in the form of a journal paper as follows:

Bijan Samali (Scientific supervision), Saeed Nemati (Full contribution), Phezhman Sharafi (Scientific supervision), Babak Abtahi (English language editing), Yahya Aliabadizadeh (contributed in numerical phase), "An Experimental Study on the Lateral Pressure in Foam-Filled Wall Panels with Pneumatic Formwork". Case Studies in Construction Materials, ELSEVIER BV, ISSN: 2214-5095, Netherlands.

4.1 Introduction

In construction industry, formwork is a temporary or permanent mould into which concrete or other similar materials are poured. It is used to form concrete into structural shapes such as beams, columns, slabs and shells in a structure. Construction using cast-in-situ structural elements relies on various formwork systems offering the opportunity to create economic structures with almost any geometry. Yet, formwork is one of the critical elements impacting construction efficiency and planning, and its costs account for a significant part of the total construction time and cost [89]. This cost significantly varies bases on the type of formwork [90]. A large percentage of structural wall panels, used in building construction, are filled with concrete or concrete foams and casted in rigid formworks. The design methods for such formwork systems are established in the literature. There are several parameters playing a role in formwork selection process such as accessibility, fabrication cost, assembling and dismantling cost, total and special weight, mechanical properties, and geometric formability. On the other hand, many of the traditional formwork systems suffer disadvantages, such as low productivity, labour intensiveness, and long cycle times. As an alternative, flexible formwork made of specific fabrics (also known as fabric formwork) is a sustainable construction system for optimised cast-in-situ geometries with lower cost, higher durability, and potential for a variety of architectural designs [33-35, 91]. Therefore, there has been increasing interest in the use of fabric formwork as an alternative for the conventional steel, aluminium or timber formworks [12]. Fabric formwork is made of textile sheets of synthetic fibres such as nylon, polyesters, polypropylene that are fabricated into containers to contain various type of fillers such as concrete during its placement and curing. As flexible moulds, they offer further flexibility in design and construction. Using fabric formwork as a mould in cast-in-situ structures elements such as concrete structures, it is possible to cast architecturally interesting, structurally optimised non-prismatic structures that use up to 40% less concrete in comparison with an equivalent prismatic section [7], offering potentially significant embodied energy savings [44] and subsequently, a striking reduction in the CO_2 emissions [45] can be achieved [36, 55, 56]. Formwork must support all loads (dead, imposed, environmental and other loads), which may be applied until these loads can be carried by the cast-in-situ structure itself. Although fabric formwork enables creating iconic and revolutionary forms based on natural laws of the catenary, when it comes to structural applications some obstacles limits their practical applications. From the structural engineering point of view, formworks should be designed for different ultimate and

serviceability loads including the lateral pressure of filling materials [92]. Most codes determine the lateral formwork pressure resulting from casting of fresh concrete to be equal to a full water head of concrete. This hydrostatic model is the most conservative as it considers the cast-in-situ material to be a fluid, establishing that the lateral pressure on the formwork follows a hydrostatic distribution, with that material's density. Such specifications are seen to be undoubtedly safe, but it is too conservative and therefore uneconomical. Cast-in-situ or a filled mould exerts a hydrostatic pressure on the formwork. The flexible formwork assumes the geometry required to resist this load, which is dictated by both this fluid pressure and internal stresses in the formwork material. In this way, the final shape of the casting can be controlled by pre-stressing the formwork or selecting the desired formwork stiffness characteristics. The lateral pressure of concrete on different formwork materials has been widely studied in the literature and models and formulae have been suggested in design standards [93, 94], and some reviews and discussion have been presented in this regard [8, 43, 95]. McCarthy et al. [48] have shown low plastic viscosity of filling material increases the lateral pressure, and enhancing workability increases the formwork pressure. Khayat et al. [96] showed formwork pressure exists as long as filling material is in a plastic state and its rate of decay is related to the rate of the stiffening of filling material. On the other hand, they shew the placement rate and method are critical to formwork pressure; i.e. the higher rate of placing, the higher lateral pressure. They showed that pumping into the formwork from the bottom of the form exhibits higher pressures than that placing from top. Their research revealed that rigid and smooth formwork materials result in higher lateral pressure and lower rate of pressure drop after placement. Hanna [93] studied the functions of tie rods to resist the tensile forces resulting from the pressure of fresh filling material. Teixeira et al. [97] analysed the effect of casting rate on the maximum lateral pressure exerted by self-compacting concrete on vertical formworks. Zhang et al. [98] showed that slump, casting speed, and vibration mode can greatly influence the formwork pressure. Wolfgang et al. [99] showed a lower rate of placement can result in lower lateral pressure. Assaad et al. [100] found the lowering the casting rate has no significant effect on the rate of pressure drop in time. There is not much data pertaining to the effects of formwork dimensions on lateral pressure [101]. For instance, the influence of formwork dimensions on lateral pressure was evaluated using experimental test by Khayat et al. [102]. Test results show that the scale effect has an influence on the rate of drop in lateral pressure with time. Rodin [103] reported that the maximum pressure appears to be lower in formwork systems of smaller cross-sections. Gardner [104] demonstrated that the larger dimension of the formwork, the larger lateral

pressure from conventional vibrated concrete. Omran et al. [105] presented the influence of formwork width, shape and surface material of formwork on lateral pressure characteristics. The results showed that the increase in formwork width can increase the initial lateral pressure and delay the time needed for the formwork removal. Although the density is the most important factor in lateral pressure on formwork, in foam-filled structures, parameters like the gel time and expansion rate affect the foam pressure distribution. Considering expansion ratio of PU foams is the ratio between the volumes of a given amount of the components in liquid form compared to the volume of the same amount of substance in solid form, one could have expected that the density controls structure and related properties. Any increase in core density results in improvement in compressive test results [106]. Goods et al. [107] also reported the mechanical properties dependency to density by following a power-law relationship. This dependency and relationship between density and mechanical, morphological, insulation, and dimensional stability of polyurethane foams have been investigated by various research groups [108-110]. As the blowing agent increases, the pore sizes decreases and because they act as a nucleating agent, it induces narrow size distribution. Gelation time also controls pore size distribution and reflected final mechanical properties [111]. Despite a relatively large amount of literature on the lateral pressure of traditional materials such as fresh concrete on conventional formwork systems, when it comes to such information about foam filled panels, the literature is almost silent. On the other hand, the hydrostatic model is the too conservative as it considers the foam to be a fluid, establishing that the lateral pressure on the formwork follows a hydrostatic distribution, with the foam density. This is the focus of this study where the lateral pressure of foam on the flexible formwork of different sizes will be investigated. Then, the intermediate ties for securing the formwork against lateral pressure are designed accordingly.

4.2 Material Properties

In this research study, fabric pneumatic formwork and polyurethane (PU) foam are the used for the wall system. This foam-filled structural wall panel with fabric formwork (which can be stiffened by high density Polyethylene (HDPE) sheets and erected by pneumatic force) is developed at the Centre for Infrastructure Engineering of western Sydney University, as a rapidly assembled construction system. Rapid assembly, low maintenance, high structural quality, and ease of transportation are some key aspects of this system that make it a suitable construction system for temporary and semi-permanent housing.

4.2.1 Fabric Formworks

Fabric formwork systems are mostly made of textile sheets of synthetic fibres such as nylon, polyesters, polypropylene being fabricated to contain various types of filling martials. A critical aspect of fabric formwork for achieving desirable performance is the selection of fabric itself. The textile industry is developing various types of suitable fabrics for applications in construction. Findings of a study [47] for identifying the best pneumatic formwork showed the Barrateen (Figure 4.1) is the best candidate for being used as fabric formwork. Barrateen is a high density polyethylene or polypropylene (HDPE) coated by unbalance woven textile. The coating material is low density polyethylene and well inflatable, whose tensile strengths in the warp and weft directions are not the same. The result of tensile tests according to ASTM D5039 [112] demonstrated adequate strength for high walls.

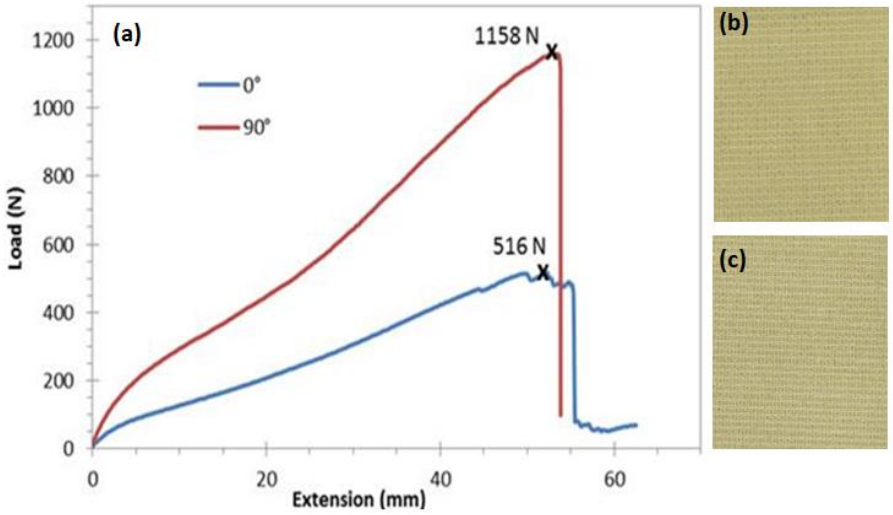

Figure 4.1: (a) Barrateen fabric tensile behaviour in main and transverse directions; Barrateen fabric's (b) smooth coated side, and (c) rough uncoated side

4.2.2 Filling Material

Polyurethane rigid foam with density of 192 kg/m^3 was used for the core material. PU foam is made 100:110 weight ratio mixture of AUSTHANE POLYOL AUW763 and AUSTHANE MDI ISOCYANATE [42]. The current ratio was found to induce gas bubble nucleation resulting in smaller cells with a narrower size distribution and the mechanical properties were found to be the best. These foams meets ASTM 1730 [22] standard requirements for use in structural panel [113]. Table 4.1 shows the PU foam's manufacturing and mechanical properties, provided by the manufacturer, and validated in the laboratory according to the ASTM 1730 [22].

Table 4.1. Mechanical and manufacturing properties of the selected PU rigid foam

Mechanical properties			
Density (kg/m^3)	Compressive yield strength (MPa)	Tensile strength (MPa)	Shear strength (MPa)
192	2.81	1.896	1.034
Manufacturing Properties			
Cream time	Gel time	Tack free time	Free rise cup density
35-40 sec	94 ± 4 sec	115 ± 5 sec	280 – 300 kg/m^3

4.2.3 Formwork Stiffeners

In order to enhance the properties of the foam-filled wall panels with respect to composite action, and better stiffen the fabric formwork for ease of fabrication, 3-D high density Polyethylene (HDPE) sheets with 2 mm thickness are used as the skins, attaching to the interior sides of the fabric formwork. HDPE sheets, manufactured with approximately 1200 studs per square meter, are used for stiffening the fabric formwork and restraining its lateral deformation. The HDPE studs also contribute to the resistance, prevent the face sheets and foam-core from debonding and increasing the interface strength between the foam-core and the formwork. The mechanical properties of the HDPE sheet, provided by the manufacturer and validated by experimental tests in the laboratory, in accordance with the ASTM D5199 [114], ASTM D1505 [115] and ASTM D6693 [49] at a loading rate of 5 mm/min. The HDPE sheets possess a density of 940 kg/m3 and an average module of elasticity of 159 MPa.

4.3 Test Setup and Specimens Specifications

In order to study the lateral pressure of PU foam on the formwork, the lateral deformation of fabric formwork while casting is first studied. At this stage no HDPE stiffener is used. Three types of large scale panelised fabric formworks with three thicknesses of 100, 200 and 300 mm (S100, S200 and S300) were investigated. Three specimens of 550 mm width and 1700 mm height for each type were tested (Figure 4.2). To be in the conservative side and have a larger deflection [96], the coated side of fabric was used for the inside of formwork (in contact with foam). Also, the initial prestressing tension of fabric was about zero. Given that the expansion rate of the PU foam used for this study was about 4, one fifth of the specimens

height (340mm) were filled by polyurethane foams with casting rate of 25 m/h u sing bucket placement method, as per ASTM 1730 [22]. Once the liquid foam had been poured to a height of 340 mm, the changes in the lateral deformation, environmental temperature, gel time, and other parameter values were recorded.

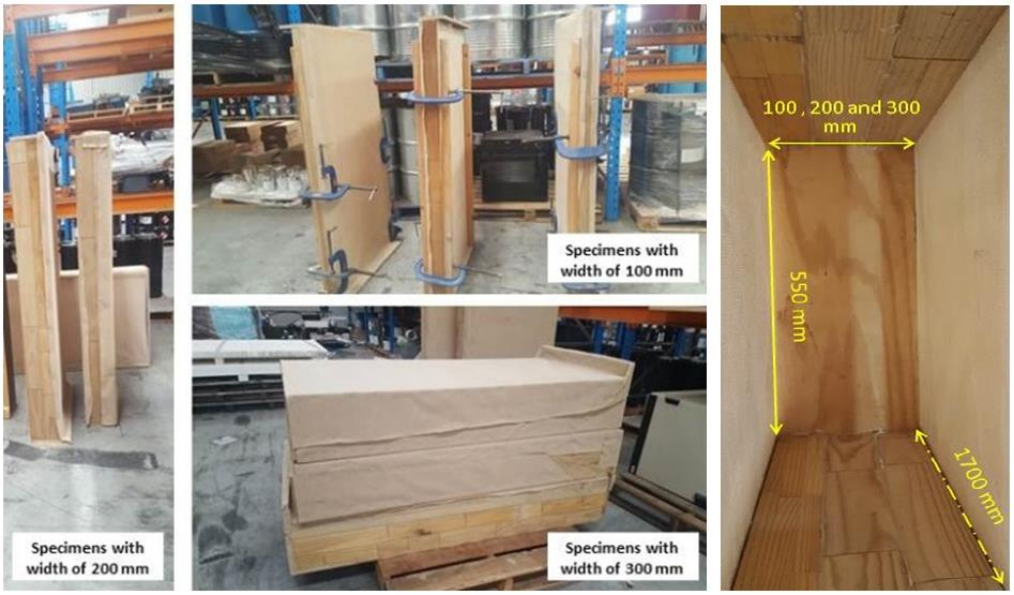

Figure 4.2: Fabric formwork specimens and dimensions

4.4 Results and Discussion

As per the observations, similar to concrete, when placed in a vertical form, PU foam liquid exerts a lateral pressure on the formwork. Due to the mechanical properties, density and gel time of the foam, it was expected that the pressure exerted on formwork to be less than a liquid head. Therefore, it is a function of elevation. Initially, the pressure is hydrostatic from the top downward, then increases at a lower rate until it reaches a maximum lateral pressure, at which point the pressure remains relatively constant, but finally gradually decreases somewhat near the bottom of the form. For the 100 mm thick specimens, the locations of maximum lateral deformation, which was 80 mm were at 340 mm from the bottom of formworks, which is exactly the point of primary level of liquid foam. The average height of raised foam was measured as 1150 mm. The lateral deformation of this point was zero in all specimens. Therefore, hydrostatic pressure is the dominant type of lateral pressure of foam in the S100 specimens. In addition, as shown in Figures 4.3 and 4.4 the final transverse profiles of these specimens were symmetric. The variations of lateral deflection between minimum and maximum points were nonlinear. Graphs in Figures 4.3 and 4.4 show the mathematical equations of vertical and horizontal deformation obtained from polynomial curve fitting.

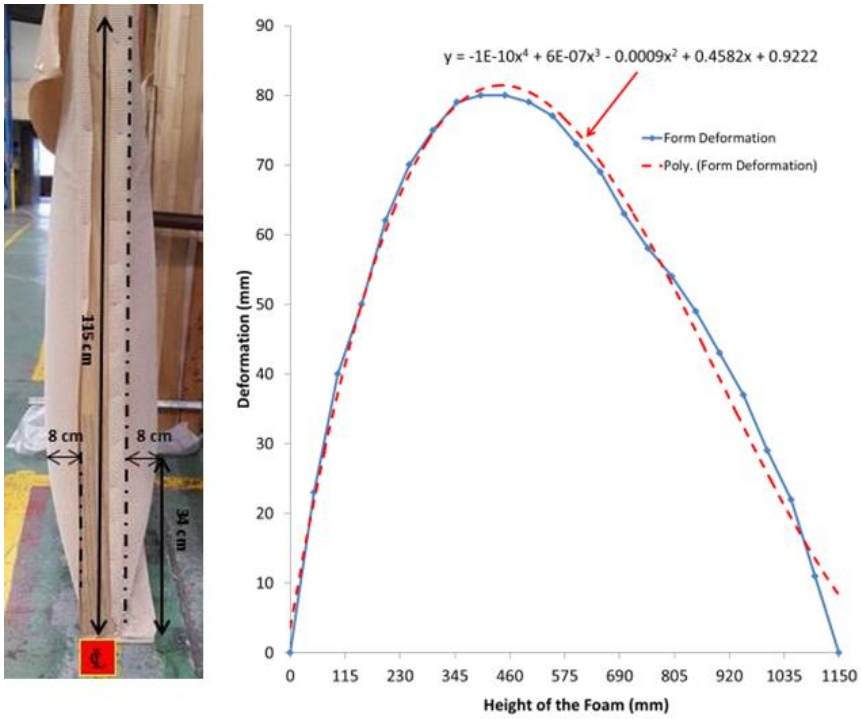

Figure 4.3: Deformation profile in vertical direction (height) for S100 specimens

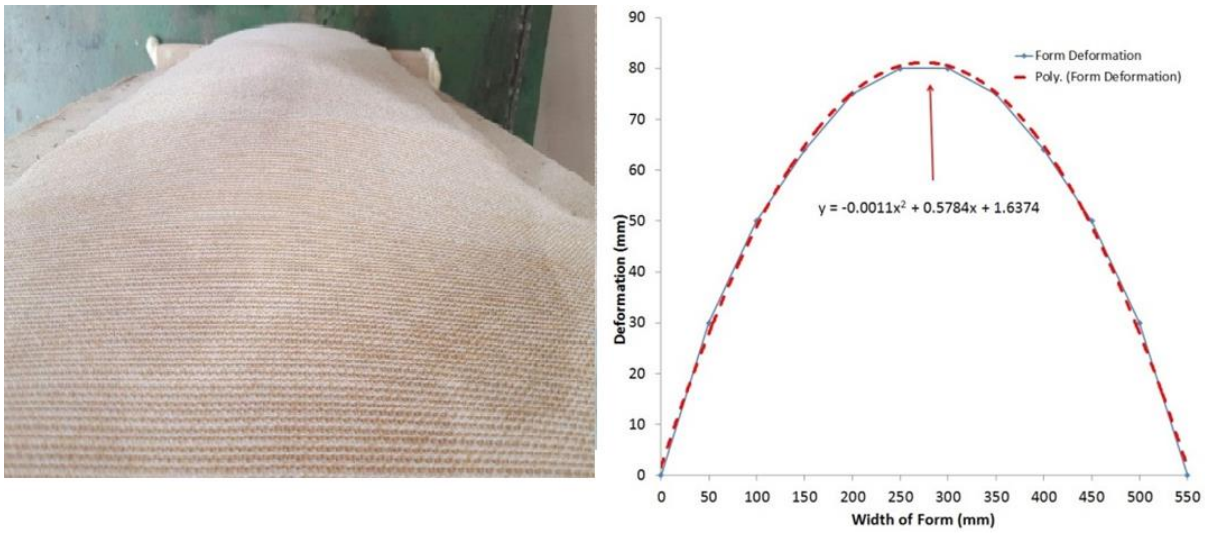

Figure 4.4: Deformation profile in horizontal direction (width) for S100 specimens

Polynomial curves were fit to the data achieved from the experiments for the specimens with 100mm thickness. Equations (1) and (2) shows the polynomial functions for curves.

$$y = -0.0011x^2 + 0.578x + 1.6374 \quad (1)$$

$$y = -0.0009x^2 + 0.4582x + 0.922 \quad (2)$$

For the 200 mm thick specimens, the locations of maximum lateral deformation, which was 87 mm were at an average of 340 mm from the bottom of formworks, which is exactly the

point of primary level of liquid foam. The average height of raised foam was measured as 957 mm. The lateral deformation of this point was 20 mm in all specimens. In addition, as shown in Figure 4.5, the final transverse profiles of these specimens were symmetric. The variations of lateral deflection between minimum and maximum points were nonlinear. Lateral distribution graphs were similar to those for S100 specimens.

Figure 4.5: Deformations for S200 specimens

For 300 mm thick specimens, the locations of maximum lateral deformation, which was 90 mm were at 340 mm from the bottom of formworks, which is exactly the point of primary level of liquid foam. The average height of raised foam was measured as 797 mm. The lateral deformation of this point was 30 mm in all specimens. The final transverse profiles of these specimens were symmetric, but with a softer distribution compared that for previous tests. Figure 4.6 shows the deformation of fabric formwork for S300 specimens. Figure 4.7 compares the maximum deflections for each type of panels. In fact, the results indicate that the lateral pressure of foam on the fabric formwork with thickness of 100 mm is a hydrostatic pressure, in which the thickness of fabric formworks has no effect on the location of maximum deflection. The lateral deformation increases by 8.75% and 3.45%, when the formwork thickness varies from 100 to 200, and then 200 to 300, respectively, with a relatively linear relationship.

Figure 4.6: Deformations for S300 specimens

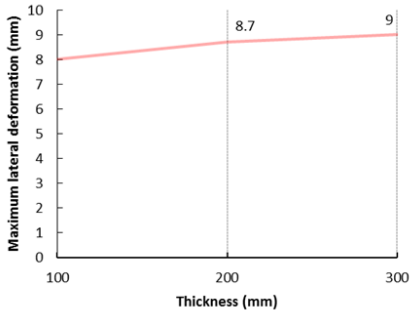

Figure 4.7: Variation of thickness of fabric formwork vs the maximum lateral deformation

4.5 Design of Form Ties

The results of other studies [42, 58] on the mechanical properties and structural behaviour of the panels demonstrated that S100 panels can fully meet the ASTM requirements for semi-permanent housing and shelters. Therefore, in this part the ties, connecting two HDPE sheets together, and being required for holding the formwork securely in place will be designed for S100. To that end, knowing the lateral deformation curves for fabric formwork filled with PU foam, the lateral pressure distribution, and then the required strength for intermediate ties spacing between two sides of the formwork can be calculated. The pressure distribution will be used to find the tensions in ties, and then the appropriate size and distribution of ties. The ties are designed in a way that restrains the lateral deformation of the fabric formwork. Test results demonstrated that for S100 specimens, hydrostatic pressure is the dominant behaviour of lateral pressure. Figure 4.8 shows the lateral pressure, lateral deformation and maximum principal stresses of fabric of S100 specimens form the FEM model, in which foam was meshed using Hexahedral dominant, Quadrilateral and Triangular meshing. The HDPE sheets were meshed using multi-zone hexahedral/prism with quadrilateral and triangular elements and the studs meshed using hexahedral elements.

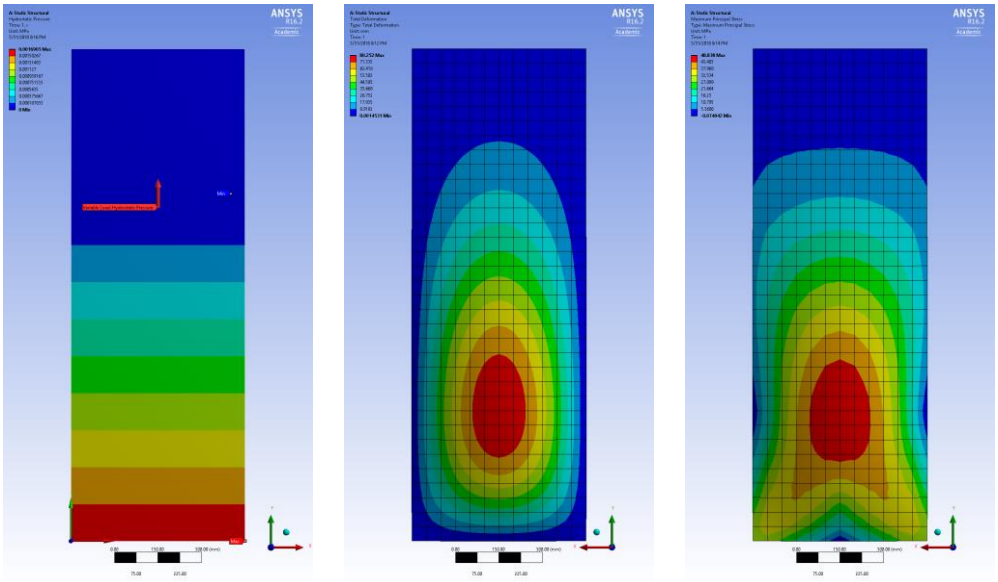

Figure 4.8: Hydrostatic pressure (left), lateral deformation (middle) and maximum principal stresses (right) of S100

Figure 4.9 shows the distribution of lateral deformation and maximum principal stresses of the reinforced fabric formworks. The results show that employing facing sheets and internal ties spacing at 20 cm vertical and 20 cm horizontal intervals, the maximum deformation of fabric formwork has been decreased to almost zero (0.082 mm). In addition, the maximum principal stress has been decreased to 17.08 MPa which is considerably less than yielding point of HDPE (20.2 MPa). Based on FE analysis the maximum tensile force of internal ties is 53.8 N. Therefore, the minimum diameter of needed steel strand is calculated as 0.7mm.

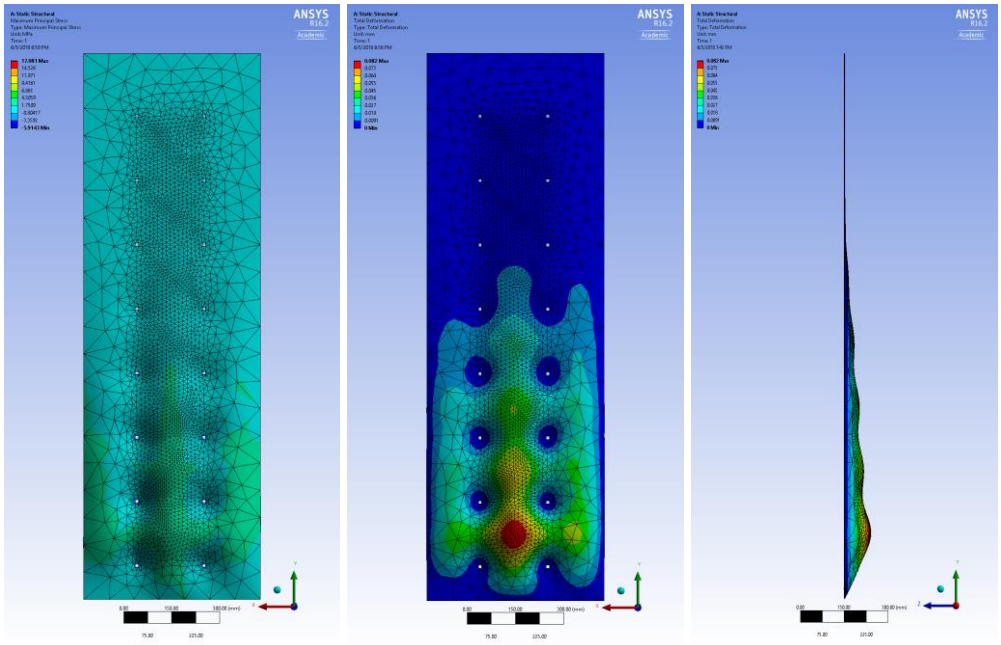

Figure 4.9: FEM of HDPE sheets and distribution of lateral deformation, maximum principal stresses

4.6 Conclusion

The focus of this study was on the lateral pressure of foam on the flexible formwork of different sizes. Based on the experimental results, the intermediate ties for securing the formwork against lateral pressure were designed for the formwork.

- The type of lateral pressure of foam on the panelised fabric formwork with thickness of 100 mm is hydrostatic.
- The thickness of panelised fabric formworks has not any effect on the location of maximum deflection.
- The location of maximum deflection lies at the intersection of primary level of the liquid foam and the vertical centre line of fabric formwork.
- Increasing the foam filled fabric formwork thickness from 100 mm to 200 mm will increase the lateral deformation by 8.75%.
- Increasing the foam filled fabric formwork thickness from 200 mm to 300 mm will increase the lateral deformation only by 3.45%.
- Increasing the foam filled fabric formwork thickness from 100 mm to 300 will decrease the total raised height of foam by 16.7%.
- Increasing in the foam filled fabric formwork thickness shows a relatively linear relationship with the decrease in the total raised height of foam.
- Using facing HDPE sheets and internal ties of 0.7 mm diameter spacing at 20 cm vertical and 20 cm horizontal intervals, the lateral deformation will be reduced to almost zero; i.e. fully prevented.
- The horizontal and vertical deformation curves of panelised fabric formwork with thickness of 100 mm follow second-order and quadratic equations, respectively

Chapter 5

Feasibility study of the use of rigid foam in sandwich panels

The contents of this chapter have been published in the form of a journal paper as follows:

Bijan Samali (Scientific supervision), Saeed Nemati (Full contribution), Phezhman Sharafi (Scientific supervision), Farzad Yaghmaei (contributed in literature review), Alireza Farrokhi (Contributed in typing editing phase), "Feasibility Analysis of the Use of Rigid Polyurethane Foam in Modular Sandwich Panels for Rapid Assembly Structures". International Journal of GEOMATE, Nov., 2018 Vol.15, Issue 51, pp.113-120 Geotec., Const. Mat. & Env., DOI: https: //doi.org/ 10.21660/ 2018.51.06166 ISSN: 2186-2982 (Print), 2186-2990 (Online), Japan.

5.1 Introduction

In building construction, polyurethane (PU) foams are used to make high-performance products that are relatively strong but lightweight, durable and versatile. PU products also can help enhance the aesthetic design of homes and buildings. In the last decade, the structural behaviour of rigid PU foam filled sandwich panels is investigated worldwide. Yan et al. studied the Quasi-static and dynamic mechanical responses of hybrid laminated composites based on high-density flexible PU foam [116]. Wu et al. studied the energy absorption capacity of a simple and innovative foam-filled lattice composite panel using PU foams with various densities [117]. Nasirzadeh et al. investigated the effect of foam density variations in sandwich structure under high velocity impact loadings [118]. Sharma et al. studied all vibration modes of sandwich panels in order to ensure that debonding between facings and PU core with variation in density [119]. He et al. studied on the dynamic response of composite sandwich plates which are fabricated with carbon fiber-reinforced plastic (CFRP) skins and rigid PU foam cores, subjected to low-velocity impact [120]. Wang et al. performed experimental studies on the low-velocity impact behaviour of PUR foam-core sandwich panels with plain weave carbon fabric laminated face-sheets [121]. Feli et al. studied the low-velocity impact on sandwich panels with hybrid nanocomposite face sheets and rigid PU foams [122]. In a research undertaken by Mirzapour et al., an experimental study to investigate and optimize the processing conditions in the fabrication of the sandwich structures designed for flexural load bearing applications was carried out. Sandwich beams with two glass/epoxy faces and a rigid PU foam core were constructed under four different processing conditions [123]. Sharaf et al. studied the flexural behaviour of a new sandwich panel proposed for cladding of buildings. The panel was fabricated by laminating two glass fiber reinforced polymer skins to a prefabricated PU foam core with two different densities 32 kg/m^3, referred to herein as ‘soft’ foam, and 65 kg/m^3, referred to as ‘hard’ foam [124]. Sharaf et al. also addressed the flexural performance of sandwich panels composed of a rigid PU foam core and glass fiber-reinforced polymer (GFRP) skins in their studies [125-127]. Mostafa et al. studied on behaviour of PU-foam/glass-fiber composite sandwich panels under flexural static load using closed cell semi-rigid PU with a density of 62 kg/m^3 [128]. Berggreen et al. studied the skin delamination of FRP sandwich with low and high core density [129]. Tuwair et al. evaluated mechanical behaviour of three core alternatives for GFRP foam-core sandwich panels. The used foams were low density and high density closed PU [130]. Kakroodi et al. investigated the strengthening effects of soy-based rigid PU foam

cores, neat and composite foams containing wood fiber, on the performance of small-scale wooden wall panels under monotonic and static cyclic shear loads [131]. Garrido et al. presented experimental and analytical investigations about the effects of elevated temperature on the shear response of Polyethylene Terephthalate and semi rigid PU foams used in sandwich panels [132]. In addition, Garrido et al. presented the experimental assessment and the analytical modelling of the viscoelastic response of two types of sandwich panels, with and without reinforcement ribs using) GFRP faces, cores of rigid PU foam, and longitudinal GFRP ribs are considered [133]. Also, Garrido et al. presented an experimental and analytical study about the effect of temperature on the shear creep response of a rigid PU foam within the scope of sandwich panel [134]. George et al. studied on sandwich panels fabricated using a fixed carbon fiber reinforced polymer truss and a variety of closed cell polymer and syntactic foams with density variations [135]. Also, the behaviour of foam core sandwich and polymer in-reinforced rigid foam core sandwich panels (PRFCS) was experimentally explored for flatwise compression and flexural loadings by Abdi et al. [51]. Yanes-Armas et al. studied the structural creep behaviour of rigid GFRP-PU web-core sandwich structures subjected to sustained loading was investigated [23]. Mohamed et al. studied the stiffness, load-carrying capacity and compressive strength of three designs of glass reinforced composite sandwich structures using PU rigid foam [136]. Mostafa et al. presented a semi-circular shear keys inserting between the skin and the foam core to improve the shear performance and skin–core debonding resistance for sandwich panels with Polyvinylchloride (PVC) and semi rigid PU foam core [137]. In a recent study, Sharafi et al. [33, 42, 58] and Nemati et al [42, 47]. In this study, a feasibility study is carried out on a commercial type of rigid PU foam with trading name AUW763 in order to use as core material of sandwich panels, based on ASTM E1730-15. This PU foam is widely available in the market at a reasonable price that can be widely employed for the construction of modular sandwich panels [35, 36, 138].

5.2 AUW 763 Rigid Foam

Rigid foam systems are energy efficient, versatile, high performance systems, where the liquid components are mixed together; and expand and harden on curing. The common applications of this foam, which is made of a 100:100-110 weight ratio mixture of AUSTHANE POLYOL AUW763 and AUSTHANE MDI, are thermal insulation and refrigeration, water heater system, continuous and discontinuous panel line systems, marine

buoyancy, cavity filling of rotary moulded parts, pipe injection and Vessel insulation, packaging foam, moulding and structural systems. This foam is formulated using a zero Ozone Depletion Potential (ODP), zero Global Warming Potential (GWP) and Volatile Organic Compound (VOC) exempt blowing agent. Table 5.1 shows the manufacturing properties of AUW 763.

Table 5.1 Manufacturing properties of AUW763

Cream time	Gel time	Tack free time	Free rise cup density
35-40 sec	94 ± 4 sec	115 ± 5 sec	280 – 300 kg/m3

5.3 Specification Check, Based on ASTM E1730-15

This specification covers rigid PU thermal insulation for sandwich panels used in shelter construction for exposure to ambient temperatures of -32 °C to 71 °C. Painted surfaces of shelters in actual field use reach temperatures of 93 °C.

5.3.1 Density

In this study the density of used foam has been controlled in accordance with the test method D1622/D1622M. In this regard, three cylindrical specimens (Figure 5.1) were tested at 24 °C and 51 % relative humidity.. The results are shown in table 5.2.

Figure 5.1: Obtained cylindrical specimens for density test

Table 5.2 Dimensions and weights of cylindrical specimens for density test

	First measurment	Second measurment	Third measurment	Average
Diameter (mm)	40.1	40	40	40
Height (mm)	80.1	80.1	8	80.1
Volume (mm^3)				100605.6
Weight (gr)	19.3	19.6	18.8	19.3

Based on D1622/D1622M the density will be calculated as: $D = W_s / V$, where: W_s is the weight of specimen (kg), and V is the volume of specimen (m^3). Therefore, the average density of foam is 191.8 kg/m^3, which meets the ASTM E1730's criteria for all types, shown in Table 5.3.

Table 5.3 Standard types of foams based on ASTM E1730

Requirement Procedure	Type 1	Type 2	Type 3	Type 4
Density (kg/m^3), max	41.6	55.7	72	192

5.3.2 Thermal Conductivity

Thermal conductivity shall be determined at mean temperatures of 5 °C, 24 °C and 52 °C after conditioning for 7±1 days at 24±2°C, and less than 60% relative humidity from the time of manufacture. The heat flow is to be measured parallel to the rise of the foam. But, based on ASTM E1730, and because of type of used foam (Type 4), carrying out this test is not required, as shown in Table 5.4.

Table 5.4 Thermal conductivity requirements based on ASTM E1730

Thermal conductivity, W/m·K, max	Type 1	Type 2	Type 3	Type 4
at approximately 5°C mean	0.25	0.257	0.257	not required
at approximately 24°C mean	0.25	0.257	0.257	not required
at approximately 52°C mean	0.25	0.257	0.257	not required

5.3.3 Dimensional Stability

Dimensional changes measured by this test method can be used to compare the performance of materials in a particular environment, to assess the relative stability of two or more cellular plastics, or to specify an acceptance criterion for a particular material [139]. Accordingly, ASTM E1730 provides some limitation on linear and volumetric stabilities of rigid foams, which are shown in Table 5.5.

Table 5.5 Dimensional stability requirements based on ASTM E1730

Dimensional stability	Type 1	Type 2	Type 3	Type 4
Linear Δ%	±1.5	±1.5	±1.5	±1.5
Volumetric Δ%	±2.5	±2.5	±2.5	±2.5

In this study dimensional stability was determined in accordance with ASTM test method D2126 [139], at 72 °C and ambient humidity. The test duration was 836 h (two weeks). In this regard, five 100mm × 100mm × 100mm cubic specimens were tested (Figure 5.2). The

faces of specimens were finished using # 0 sandpaper. Dust has been blown off the specimens with compressed air. Prior the tests, specimens were conditioned to constant mass at the temperature of 23 °C and relative humidity of 52%. After exposure, allow the specimens to come to room temperature for 2h before measuring and testing.

Figure 5.2: Empty cubic formworks (bottom) and foam filled ones (top) before been machined (mild)

The changes in dimensions are expressed as a percentage of the original measurement, as $[(m_f - m_o) / m_o] \times 100$, where mf is the final measurement, and m_o is original measurement. Table 5.6 shows the results of tests and related calculations. In addition, some visual examination carried out on the specimens, whose results are shown in Table 5.7 and Figure 5.3.

Table 5.6 Dimensional stability measurement test results

	Original Measurment					Final Measurement					Change (%)				
Specimens No.	1	2	3	4	5	1	2	3	4	5	1	2	3	4	5
X dimention (mm)	100.23	100	100.24	100.22	100.2	98.99	98.98	99.07	99.51	99.81	-1.24	-1.02	-1.17	-0.71	-0.39
Y dimention (mm)	100.12	100.11	100.19	100.11	100.14	99.69	98.98	99.99	99.49	99.57	-0.43	-1.14	-0.2	-0.62	-0.56
Z dimention (mm)	100.19	100.38	100.33	100.16	100.1	99.38	99.99	99.13	99.07	98.92	-0.81	-0.39	-1.2	-1.09	-1.18
Volume (mm^3)	1005409.42	1004904.18	1007618.765	1004907.7	1004406.2	980712.956	979606.07	981982.7019	980817.758	983075.04	-2.46	-2.52	-2.54	-2.4	-2.1

Table 5.7 Dimensional stability visual test results

			Visual Change (%)		
Specimens No.	1	2	3	4	5
General appearance	Minor darkening	Nothing	Minor darkening	Nothing	Nothing

Figure 5.3: Minor darkening of specimens at 72 °C after 836 hours

5.3.4 Flame Resistance and Energy-Dispersive X-Ray Spectroscopy

The flame resistance of foam can be evaluated through tests according to the ASTM E1730. To that end, low-cost additive fire retardants can be used in PU foam. Nowadays a wide range of fire retardants are being used particularly for rigid foams. In contrast, it is difficult to impart fire retardants to flexible foams because of several factors such as open their cell structure, low degree of crosslinking, and chemical structure impair. Flame resistance test as well as heat and smoke release rate, are carried out by manufacturer for all types of produced foams. Based on the required flame resistance, a variety of resistance is achievable without any considerable change in the physical or mechanical properties, by using such fire retardant additives. A major disadvantage is that they frequently cause shrinkage, which is mainly the case in flexible foams, not the rigid ones.

In this regard, Tris Chloroisopropyl Phosphate (TCPP) is a commonly used retardant used by many manufacturers. TCPP is a colorless or light yellow transparent liquid, whose molecular formula is C9H18Cl3O4P. TCPP is used as a low-cost flame inhibitor and usually is used as a flame retardant in rigid and flexible PU foam. Past studies shows that by using TCPP any degree of fire resistant foam (even full fireproof rigid foams) are achievable [134]. In order to further study the feasibility of using PU foam in structural members, an energy-dispersive X-ray spectroscopy investigation was carried out on AUW763 using a JSM-6510LV (Low Vacuum with EDS microanalysis) machine at western Sydney university (Figure 5.4).

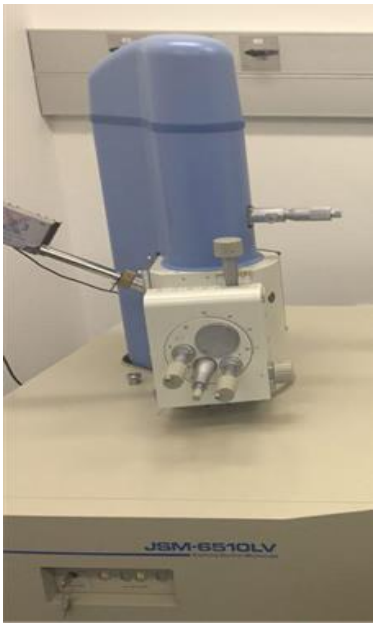

Figure 5.4: JSM-6510LV machine

Energy-dispersive X-ray spectroscopy (EDS, EDX, EDXS or XEDS), or energy dispersive X-ray analysis (EDXA) or energy dispersive X-ray microanalysis (EDXMA), are analytical techniques used for the elemental analysis or chemical characterization of a sample. As the energies of the X-rays are characteristic of the difference in energy between the two shells and of the atomic structure of the emitting element, EDS allows the elemental composition of the specimen to be measured. The accuracy of the measured composition is also affected by the nature of the sample [139]. Figures 5.5 and 5.6 shows the results of EDS analysis on the PU foam. No toxic components can be observed in investigated foam subsequently in its burned oxides.

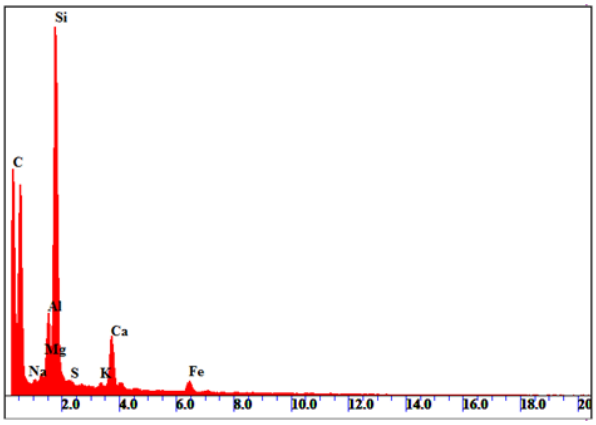

Figure 5.5: Results of EDS analysis of presented foam

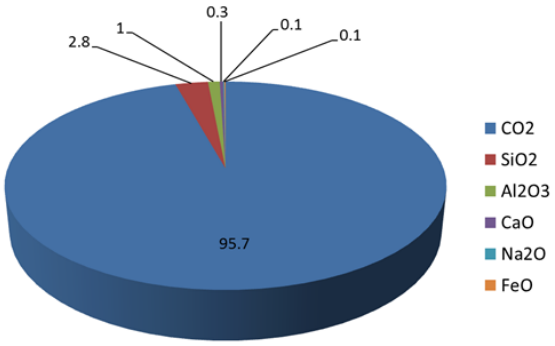

Figure 5.6: List of oxides (weight %)

5.3.5 Impact Resistance

Materials such as masonry and concrete are robust and can generally be expected to resist normal impacts such as windborne debris or hailstone. However, many materials used in facades are more susceptible to damage and require testing to assess their performance. To examine the effect of transverse impact, a quasi-static impact test was used to simulate a low velocity impact. The specimen of rigid PU foam (610 mm long, 610 mm wide and 50 mm thick) was used, as shown in Figures 5.7. The face of the foam specimen is bonded to a 0.8 mm thick aluminium sheet. For determining the impact resistance a 31.7 kg steel hemispherical cylinder of 80 mm diameter was dropped vertically from 762 mm distance, so that the hemispherical end of the weight strikes the centre of the outer skin of the specimen on a horizontal plane. The cylinder was not permitted to re-impact the specimen after the first impact. Specimens were supported along their four edges by a framework backed by concrete. The frame was made of four pieces of lumber, rigidly connected together to form a 610 mm square on a side, as illustrated in Figure 5.8. The panel specimens had their four surfaces bound with a channel frame of skin material attached through flanges. Impact did not result in rupture to either skin. No crushing of core is allowed outside a 3 in. radius from the centre of the impact [22]. Figure 5.9 shows the crushing areas of skin and core foam respectively. The maximum crushing radius was measured as 21 mm. Therefore, result shows an acceptable impact resistance for the specimens.

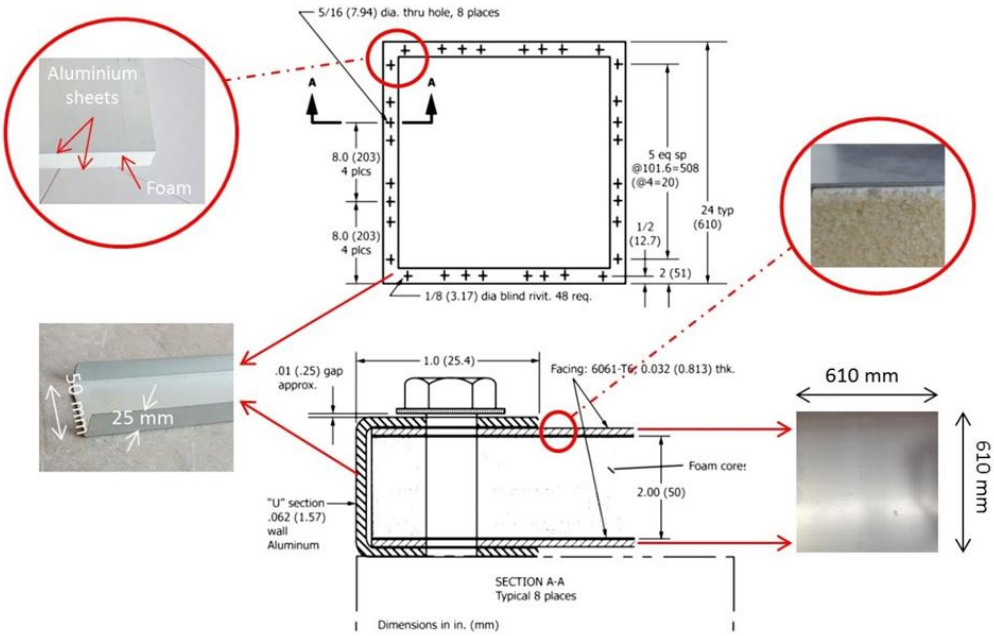

Figure 5.7: Details and components of specimen

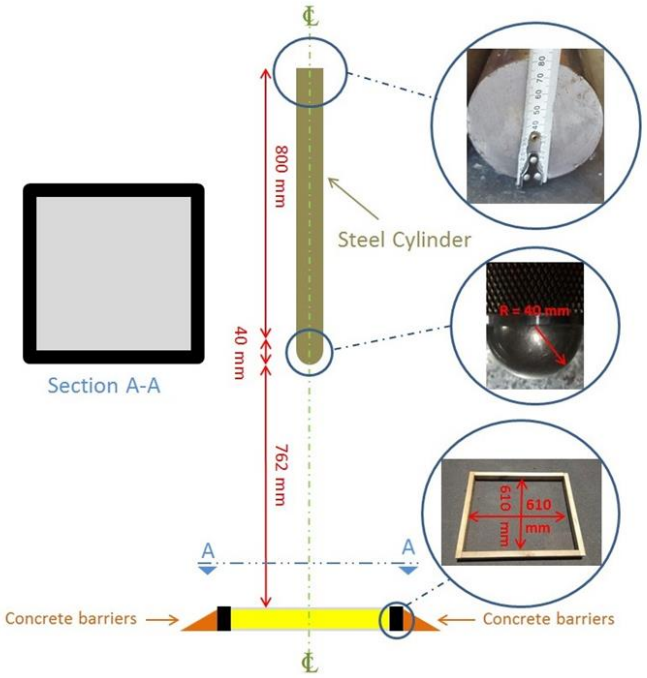

Figure 5.8: Configuration of impact resistance test rig

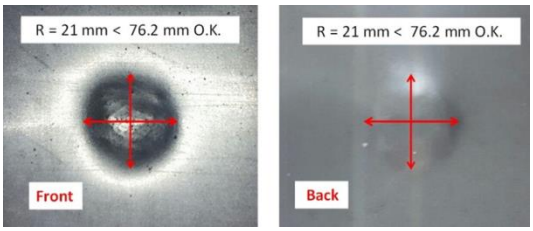

Figure 5.9: Crushing areas of skin at impact resistance test

5.4 Conclusion

Results of carried out tests on AUW763, based on ASTM E1730-15 show it meets the ASTM requirements and needed specifications as following:

- The used rigid foam is accordance with ASTM E1730 Type 4.
- Because of the used foam is accordance with ASTM E1730 Type 4, carrying out thermal conductivity test is not required.
- Dimensional stability visual test results show minor darkening of specimens at 72 °C after 836 hours.
- Dimensional stability test results show that the average of maximum linear change in specimens was only -0.81% which is less than the allowed amount as +/-1.5%.
- Dimensional stability test results show that the average of maximum volumetric change in specimens was only -2.4% which is less than the allowed amount as +/-2.5%.
- The results of carried out flame resistance test as well as heat and smoke release rate show the accordance of AUW763 with ASTM E1730-15.
- Based on energy-dispersive X-ray spectroscopy, no toxic components can be observed in investigated foam subsequently in burned oxides.
- The results of impact resistance test show the maximum crushing areas of skin was 21mm which is less than the allowed amount as 76.2 mm.

Therefore, the investigated foam is absolutely suitable for use in structural sandwich panel cores.

Chapter 6

Edgewise and flatwise compressive behaviour of foam-filled sandwich panels

The contents of this chapter have been published in the form of a journal paper as follows:

P. Sharafi (Scientific supervision), S. Nemati (Full contribution), B. Samali (Scientific supervision), A. Mousavi (Contributed in typing editing phase), S. Khakpour (General advising), and Y. Aliabadizadeh (General advising), "Edgewise and Flatwise Compressive Behaviour of Foam-Filled Sandwich Panels With 3-D High Density Polyethylene Skins". Engineering Solid Mechanics (ESM), March, 2018 Vol.6, Issue 3, pp. 285-298, DOI: 10.5267/j.esm.2018.3.005, Canada.

6.1 Introduction

Sandwich composite structures have attracted the attention of construction professionals because of many advantages such as lightweight, high strength, corrosion resistance, durability and speedy construction. Various forms of sandwich construction are being produced by combining different skin and core materials, with various geometries. Foam-filled sandwich panels, as efficient building elements, are becoming a major player in modular construction with a variety of applications in residential and commercial buildings worldwide. These products are popular because they are light, easy to install and have good thermal and acoustic properties. In addition to their applications as non-structural building elements, sandwich panels with polyurethane foam-core and exterior and interior facing materials such as gypsum [36], engineered wood or some composite materials can be parts of the structure of a building [140]. Alongside the foam-filled composite panels, in recent years, considerable research efforts have been continuously looking for new construction materials and efficient designs for sandwich structures. Fang et al. [141] developed innovative GFRP-bamboo-wood sandwich beams and investigated their mechanical performance experimentally and by finite element modelling. Hou et al. [142] described the manufacturing and testing of graded conventional/auxetic honeycomb cores, manufactured using Kevlar woven fabric epoxy employing Kirigami techniques, consisting of a combination of Origami and ply-cut processes.

Reis and Rizkalla [143] presented an innovative 3-D glass fibre reinforced polymer (GFRP) panels with foam-core designed to overcome delamination problems, typically encountered in traditional sandwich panels. Lameiras et al. [144, 145] developed an innovative and thermally efficient sandwich panel for the structural walls of a pre-fabricated modular housing system, comprising GFRP connectors and two thin layers of Steel Fibre Reinforced Self-Compacting Concrete. Compared to the other innovative structural composite panels, different designs of foam-filled sandwich panels are among the most widely investigated types of composite structures [145], and a large number of research studies regarding the behaviour of foam-filled sandwich composites have been published in the literature [146]. A wide range of studies on the foam-filled composite panels are on those made of GFRP skins and rigid polyurethane (PU) foam-core [37, 146]. Recently, Codyre and Fam [147] studied the effect of density of a Polyisocyanurate foam-core on the behaviour of axially loaded sandwich panels with GFRP skins, for different panel heights. Mohamed et al. [136] proposed new designs of foam-filled glass reinforced composite sandwich structures, using two-part

thermoset polyurethane resin systems as matrix materials, with vacuum assisted resin transfer moulding process. Fam and Sharaf [148] explored the feasibility of fabrication and flexural performance of panels composed of low-density polyurethane foam-core sandwiched between two GFRP skins. The shear response of the composite sandwich panels with Polyvinylchloride foam-core between GFRP skins using epoxy resin was investigated by Mostafa et al. [137] . Despite their very competitive costs, the stiffness and strength of a majority of these conventional foam-filled sandwich panels hardly meet the structural requirements for use in building floors or walls, at least for standard spans and loads. Conventional sandwich panels are susceptible to some different failure modes. Delamination of the skins from the core, buckling or wrinkling of the compression skin, flatwise crushing of the core and rupture of the tension skin are some of the very common types of failure. The main weaknesses of these panels stem from the low stiffness and strength of the core, and the skin's susceptibility to delamination and buckling, owing to the local mismatch in stiffness and the lack of reinforcements bridging the core and the skins [38]. In this study, in order to enhance the properties of the foam-filled sandwich panels with regard to such failure modes, a new sandwich panel is proposed, in which 3-D high density Polyethylene (HDPE) sheets with 2 mm thickness are used as the skins, and high-density PU foam is used as the core, as illustrated in Figure 6.1 with a total thickness as 100 mm. Using the HDPE sheets, manufactured with approximately 1200 studs per square meter, higher pull-out and delamination strength, as well as better stress distribution, and buckling performance can be achieved. The studs also improve the resistance of the face sheets and foam-core from debonding and increasing the interface strength between the foam-core and the face sheets. The fabrication of these sandwich panels takes place in a single step. Therefore, the face sheets and foam-core are integrated into one construction. This innovative sandwich panel was developed to be used as modular walls and floors in rapid assembly buildings, in a recent research project on the semi-permanent post disaster housing at the Centre for Infrastructure Engineering at Western Sydney University. Rapid assembly, lightweight and easy transportation, durability, and wide range of applications are some merits of this new design. Given that the introduction of a new design typically brings new challenges to designers to utilize the new properties of the materials and geometry, the main goal of this research work is to investigate some structural properties of the newly developed sandwich panel.

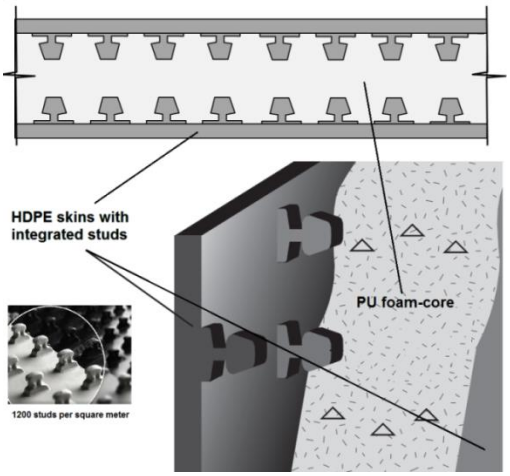

Figure 6.1: Schematic illustration of the sandwich panel with 3-D HDPE skins and PU foam-core

6.2 Characteristics of the Materials

The detailed descriptions of the tests carried out on material characterization of the constituent materials i.e. PU rigid foam and 3-D HDPE skin sheets are presented here. In addition to use the manufacturers' data, some experimental tests were performed, in order to evaluate the basic material properties. High density PU high-density rigid foam was chosen for the core material, according to some preliminary finite element investigations. Table 6.1 shows the basic mechanical properties of the PU, provided by the manufacturer, and validated in the laboratory. The detailed mechanical behaviour and stress-strain curves are presented by Nemati and et al. [42]. Using uniaxial load machine, three cubic specimens (dimensions: 50mm×50mm×50mm) were tested based on the ASTM E1730 and ASTM D1621 [149] at a loading rate of 5 mm/min in order to identify the structural properties. This type of PU foam, which is made of a 100:110 weight ratio mixture of AUSTHANE POLYOL AUW763 and AUSTHANE MDI, can undertake considerable deformation before the failure. The results showed that the foam has an average yield stress of 3.51 MPa, and the elastic modulus of 135.5 MPa.

Table 6.1 Mechanical and manufacturing properties of the selected PU rigid foam

Mechanical Properties of the PU foam			
Density (kg/m^3)	Compressive yield strength (MPa)	Tensile yield strength (MPa)	Shear yield strength (MPa)
192	3.51	1.896	1.034

The face skins of the sandwich panels are made of 3-D HDPE sheets primarily produced as a concrete embedment liner to provide protection from mechanical damage and a corrosive and erosive environment. In addition to resistance to chemical and environmental threats, its relatively high strength, and in particular its 3-D studded face can effectively contribute to the sandwich composites' structural performance by providing high pull out strength, minimum lateral movement of the skin, and stronger bonding through the shear keys on their surface (Figure 6.2).

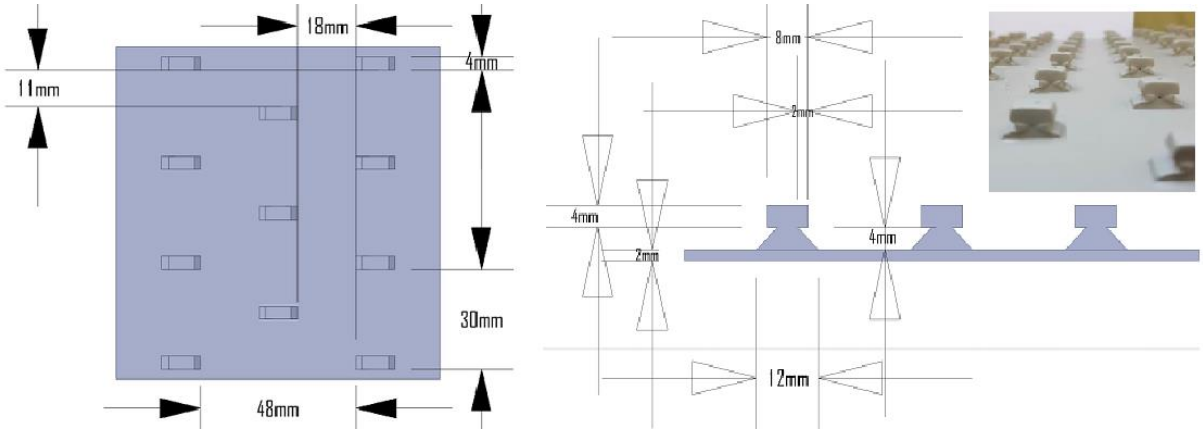

Figure 6.2: 3-D studded facing sheet

Table 6.2 shows some mechanical properties of the 3-D HDPE sheet, provided by the manufacturer and validated by experimental tests in the laboratory, in accordance with the ASTM D5199, ASTM D1505 and ASTM D6693 at a loading rate of 5 mm/min. In order to identify the structural behaviour of the skin, in-plane tensile tests were conducted on two principal perpendicular directions (lengthwise and crosswise) of the HDPE sheets, using a universal hydraulic testing machine. Five identical specimens were tested for each direction of the HDPE face sheet.

Table 6.2 Mechanical properties of the HDPE sheets

Density (g/cm^3)	Tensile strength at yield (MPa)	Shear strength at yield (MPa)	Elongation at break (%)	Stud pull-out strength (kN/m^2)	Average module of elasticity (MPa)
0.94	20.2	5.2	500	670	159

6.3 Experimental investigation of composite specimens

For sample preparation, the specimens were prepared by pouring the PU foam liquid into the temporary moulds containing two layers of HDPE sheets, attached to the sides, as shown in

Figure 6.3. The dimensions of each sample were set based on the corresponding standard test. No glue bond was used to allow the entire composite action to be burdened with the mechanical attachment between the studded surface and the foam.

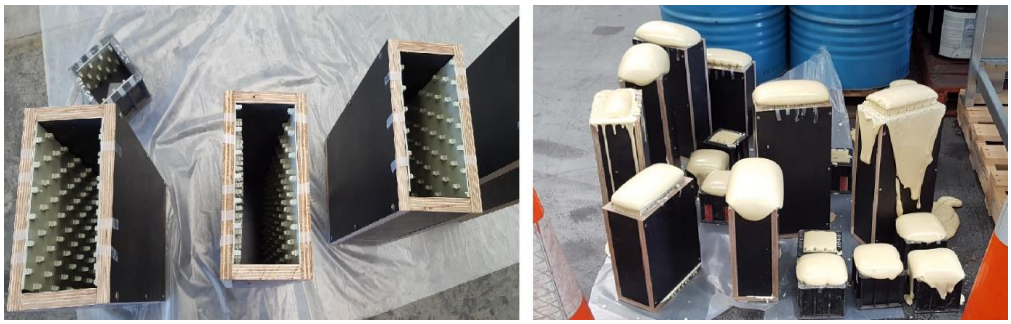

Figure 6.3: Specimens' preparation

6.3.1 Edgewise Compressive Strength

The edgewise compressive strength of sandwich construction is important as it provides the basis for the assessment of the load-carrying capacity [136]. The compressive properties of the sandwich composite along the direction parallel to the plane of the sandwich face skin were evaluated through edgewise compression tests on 100mm×200mm×300mm samples using a test rig (universal testing machine) in accordance with the ASTM C364 standard [50]. The specific machine configuration setup is shown in Figure 6.8, with the bottom plate fixed and the top plate moving downwards at a constant velocity of 0.5 mm/min using an edgewise compression test fixture. The use of such quasi-static tests implies that the loading force has sufficient time to be transmitted throughout the entire graded sandwich structure before the specimen fails. Attention was paid to make sure the ends of the specimen are flat to prevent localised end failures. Figure 6.4 shows the test setup and the stress-strain curve.

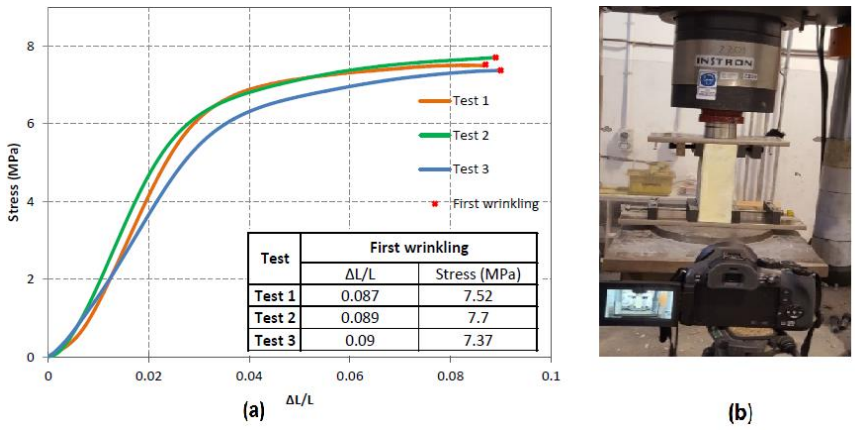

Test	First wrinkling	
	ΔL/L	Stress (MPa)
Test 1	0.087	7.52
Test 2	0.089	7.7
Test 3	0.09	7.37

Figure 6.4: Edgewise compression experiments (a) results (b) test set up

Figure 6.4 shows a good agreement between edgewise compressive behaviour of composite panel and foam compressive behaviour at linear phase. Composite panel can bear 3.51 MPa of compressive stress at a strain of 0.016. Then, at 4 MPa (strain 0.02) the slop of diagram changes approximately to a strain of 0.04 in composite panel. After this point, the behaviour is nonlinear until a stress of 7.53 MPa (strain of 0.09). At this point, the first wrinkling happened at HDPE sheets. Therefore, the failure mode of the specimens under edgewise compression, as shown in Figure 6.5, was local buckling (wrinkling) of the HDPE sheets between two edge studs, resulting in a local delamination and debonding between the face and core. Despite the specimens' rather considerable bulge under pressure, no global delamination was observed. Although the post-buckling strength of the HDPE sheets could resist more compression, the load associated with such wrinkling failure mode was considered as the edgewise strength of the specimens. By applying more pressure to the specimens and after about 118 sec, an edge crush and large deformation will occur on the edges of HDPE sheets (at a stress of 16.71 MPa), shown in Figure 6.6.

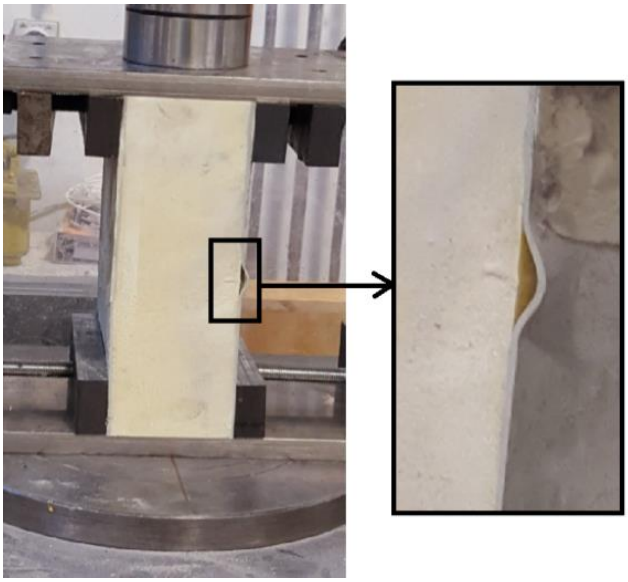

Figure 6.5: Local buckling (wrinkling) in the compression edgewise test

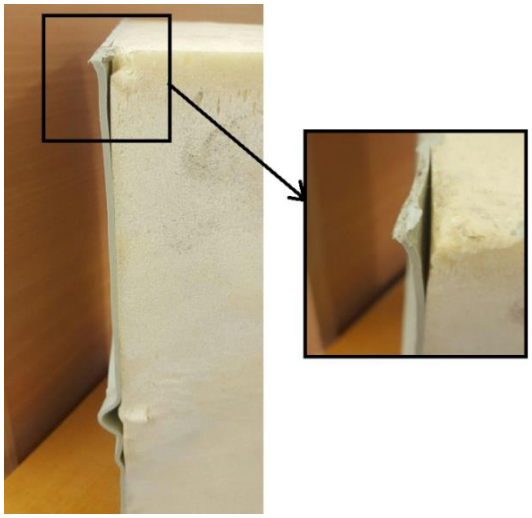

Figure 6.6: HDPE edge crush in the compression edgewise test

For design purposes, the non-linear behaviour of the stress–strain relationship can be approximated by two linear behaviours with different stiffness. The initial portion can be used to determine the initial elastic modulus using regression analysis of the data up to 2% strain. Due to the significant non-linear behaviour observed beyond the strain level of 2%, the second slope, conservatively representing the reduced elastic modulus can be determined approximately based on the data measured between strains of 4% up to failure strain. These two calculated slopes are extended between 2% and 4% strain until they intersect each other in order to obtain the full approximation of the compressive edgewise behaviour (Figure 6.7).

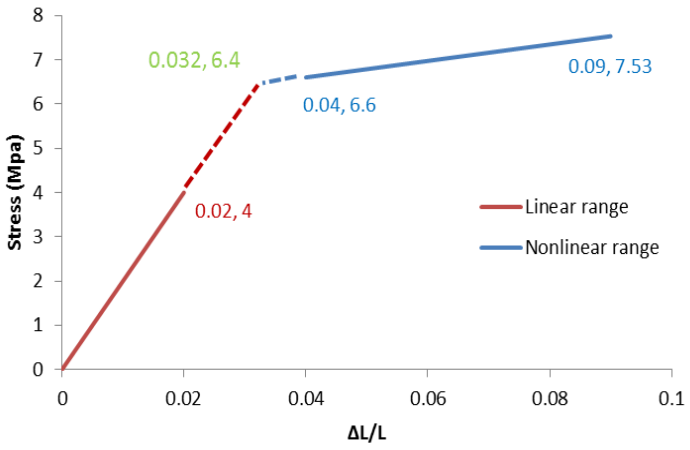

Figure 6.7: Design Elasto-Plastic diagram of composite panel under edgewise compression

6.3.2 Flatwise Compressive Strength

The compressive strength of the composite was also assessed through the flatwise compressive tests of small sandwich cubes [51, 52]. Four specimens were tested to determine the flatwise compressive strength and elastic modulus for the sandwich core's structural

design properties, using a universal testing machine and following the ASTM C365. The test rig was setup accordingly. Specimens had 100 mm thickness and a constant square cross-section of 100 mm × 100 mm corresponding to a cross-sectional area of 10,000 mm^2, which was smaller than the 10,323 mm^2 area recommended by the ASTM C365. Each specimen was cantered under the loading plate to ensure a uniform load distribution. All specimens were tested under displacement control with the bottom plate being fixed and the top plate moving downwards at a constant velocity of 0.5 mm/min. Flatwise compressive tests were performed until the load–displacement curve indicated a collapsed structure, i.e. with significantly high deformation of specimens. Figure 6.8 and Table 6.3 show the results. In addition, Figure 6.9 illustrates the results of Table 6.4 for one of the specimens.

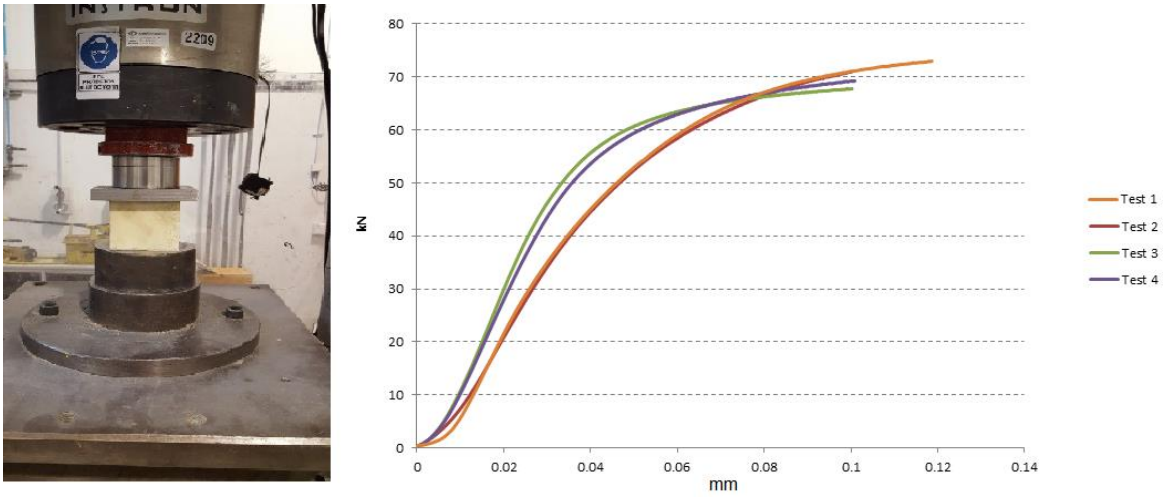

Figure 6.8: Flatwise compressive experiments results

The first part of the curve was relatively linear in the elastic region, followed by the plateau region where the stress was almost constant under increasing deformation, and was produced by the development of localised buckling within the foam cell walls. Then, there was a sharply increasing loading region at a large strain corresponding to solidification. Some minor variations were observed among the specimens, and the average compressive elastic modulus of the sandwich panels was 147.55 MPa. The yield region occurred at an average stress of 4.3 MPa, attributed to buckling of the foam's internal cell walls, with over 22% improvement compared to bare foam. As the deformation increased, the cell walls stacked on top of each other resulting in the closure of most of the voids. Therefore, the foam-core became densified and displayed higher strength.

Table 6.3 Results of the flatwise compressive experiments on the specimens

Test No.	$б_{0.001}$ (mm)	$б_{0.003}$ (mm)	$P_{0.001}$ (kN)	$P_{0.003}$ (kN)	Compressive Chord Modulus, E (MPa)
1	1.51	3.51	13.47	40.47	135
2	1.46	3.46	13.16	39.31	130.8
3	1.33	3.33	16.67	49.94	166.4
4	1.34	3.34	16.04	47.65	158
Average					147.55
Standard Deviation					17.35
CV%					11.8

$б_{fc0.02}=P_{0.02}$ / A = flatwise compressive stress at 2% deflection, MPa
$P_{0.02}$ = applied force corresponding to $б_{0.02}$, N
$б_{0.02}$ = recorded deflection value such that б/t is closed to 0.02
t = measured thickness of core specimen prior to loading , mm

$E_{fc} = ((P_{0.003} - P_{0.001}).t)/((б_{0.003} - б_{0.001}).A)$= core flatwise compressive chord modulus, MPa
$P_{0.003}$ = applied force corresponding to $б_{0.003}$, N
$P_{0.001}$ = applied force corresponding to $б_{0.001}$, N
$б_{0.003}$ =recorded deflection value such that б/t is closed to 0.003
$б_{0.001}$ = recorded deflection value such that б/t is closed to 0.001

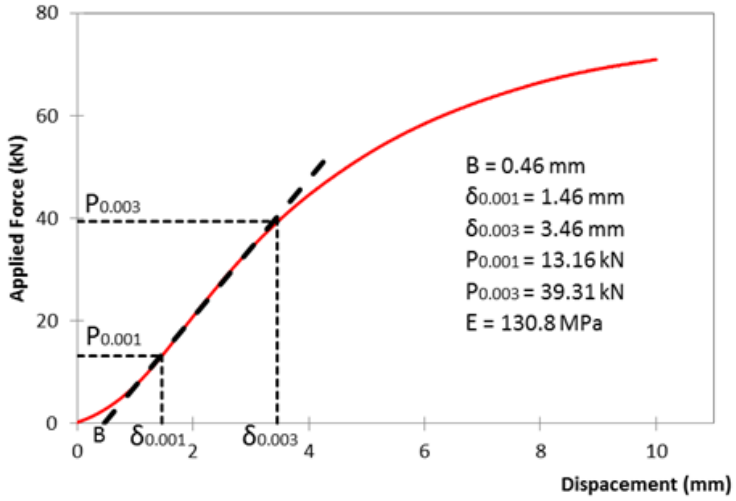

Figure 6.9: Description of flatwise compressive experiments calculation for test no. 2 (for example)

The results indicate that the flatwise compressive behaviour of the specimens is governed by the rigid foam behaviour, and the composite specimens show a similar behaviour to the foam specimens. That is, experiment results confirmed that although a separation between the core and the skin is observed at the failure load, the possible local ruptures in the foam, due to the increased stress on the studs' tips, do not influence the flatwise compressive behaviour of the sandwich composite.

6.4 Finite Element Modelling

The FE modelling was performed using ANSYS 16.2 where a quasi-static three-dimensional model has been developed to simulate and predict the mechanical performance of the

composite sandwich panel under compression. For FE modelling, the same dimensions, and the same loading rate were considered as for the experimental program. The PU foam was meshed using Hexahedral dominant, Quadrilateral and Triangular meshing. The HDPE sheets were meshed using Multizone Hexahedral/prism with Quadrilateral and Triangular elements while the studs meshed using hexahedral elements (Figure 6.10 and 6.11). The mechanical properties of the PU foam and the HDPE sheets, obtained from experiments, were used for calibrating the inputs.

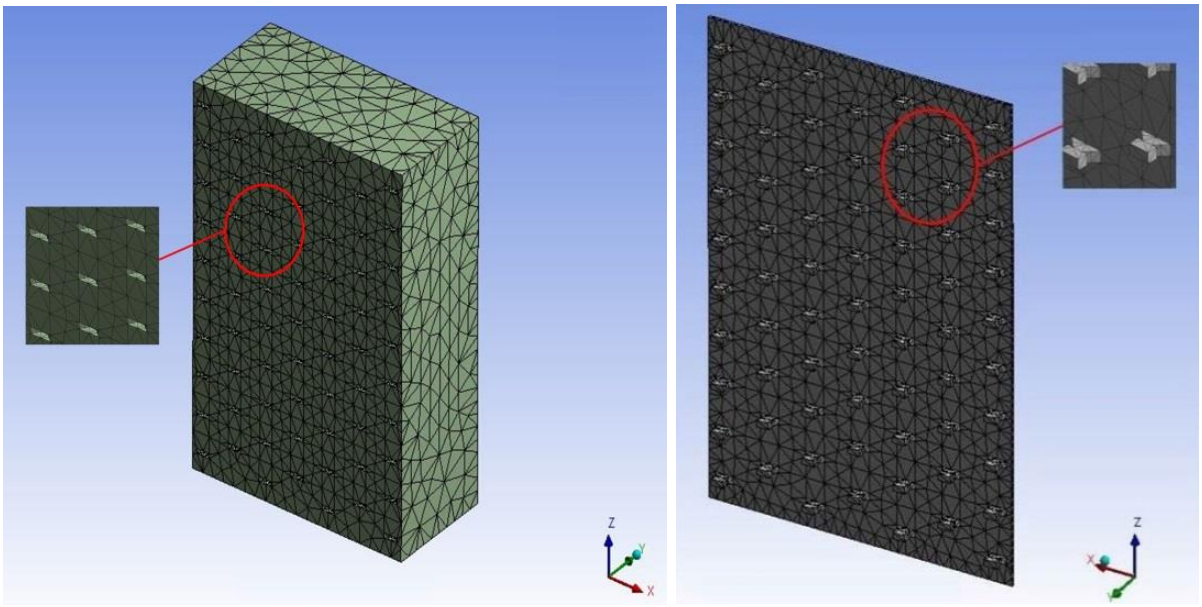

Figure 6.10: Finite element meshes at foam core (left) and HDPE sheets (right)

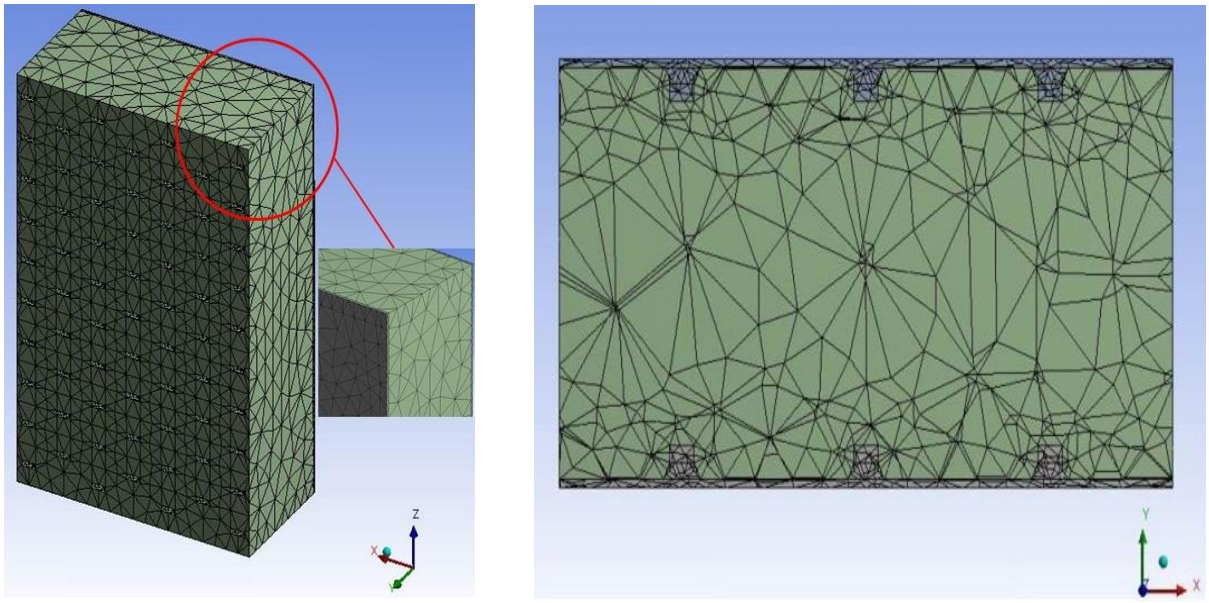

Figure 6.11: Composite panel finite element meshes (left) and section at studs position (right)

6.4.1 FEM Results for Edgewise Compression

As presented in Table 6.2, the modulus of elasticity of the PU foam in this study is E_{PU} = 135.5 MPa, which is not so much different from the HDPE material (159 MPa). On the other hand, the HDPE is relatively a thin sheet of material with not considerable resistance against compression. Therefore, it could be expected to observe relatively similar stress and strain in both PU foam and HDPE, especially in linear range. Hence, the HDPE will not significantly changes in the edgewise load-bearing capacity of specimens (Figure 6.12).

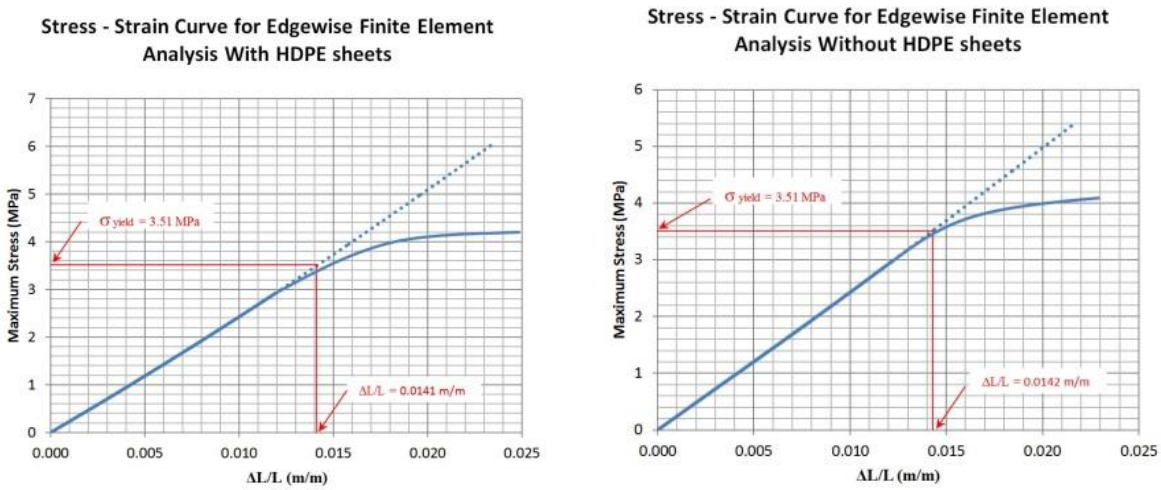

Figure 6.12: FE analysis results for edgewise model with (left) and without (right) HDPE sheets

The results shows a very good agreement between numerical analysis and experimentals. As can be seen in Figure 6.17, PU foam reaches to its yield point (3.51 MPa) at bottom edge with a maximum strain of 0.014 mm/mm which is very close to experimental result as 0.016 mm/mm. In this situation, the HDPE sheets remain in elastic range yet. In addition, there is not any notable compressive or shear stress concentration at studs at the end of foam yielding range (Figure 6.13). However, these researchers in another article have showed the critical role of studs in bending behaviour. By applying more pressure, the HDPE reaches to its compressive yielding point (15.956 MPa) at top edge (Figure 6.14) as similar as the experimental test as 16.71 MPa (Figure 6.10).

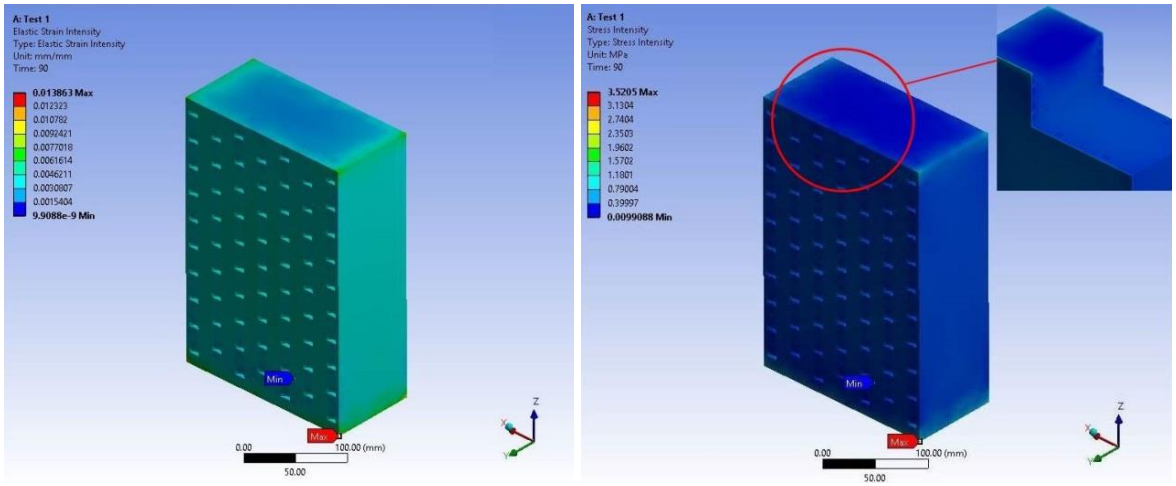

Figure 6.13: Stress and strain of PU core at foam yielding point

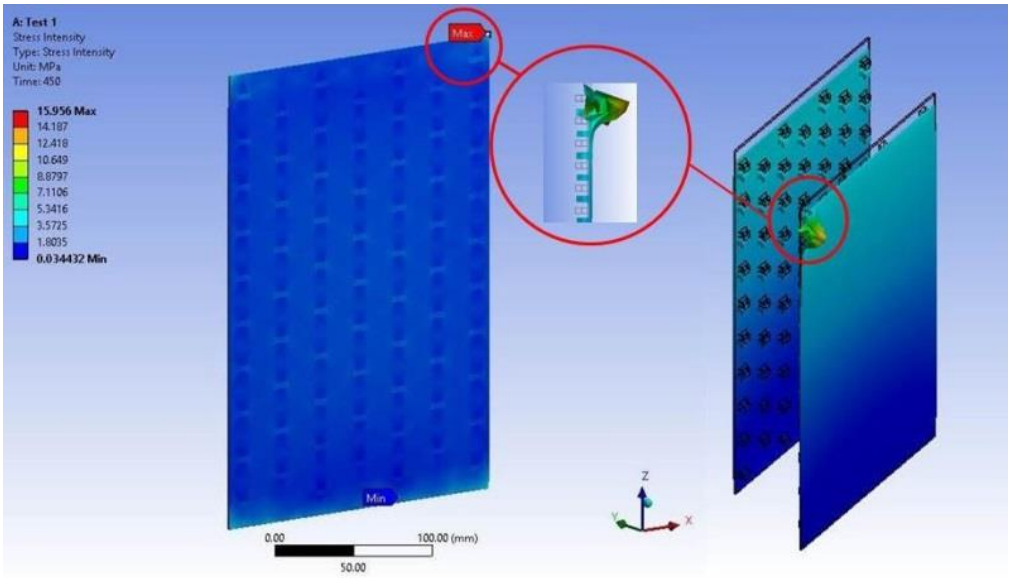

Figure 6.14: Ultimate deformation diagrams under edgewise compression

The FE model shows the stress is evenly distributed along the sample. This confirms the fact that the load is evenly applied at the top using the distributing plate. The evenly distributed load will eliminate the possibility of stress concentration. This amount of stress (15.956 MPa) is very close to experimental result (16.71 MPa) and shows a good agreement between experimental tests and numerical analysis at the collapse point. In addition, the FEM model confirmed that relative deformation for HDPE sheets and the PU foam is negligible; meaning that they work well as a composite section (Figure 6.15). Figures 6.16 and 6.17 illustrate the maximum shear stress diagrams for xy, zx, and yz-planes. The composite exhibits fairly linear shear behaviour in the xy-plane for strains below 0.01, while linear behaviour in yz-plane and zx-plane can be seen in higher ranges of strain.

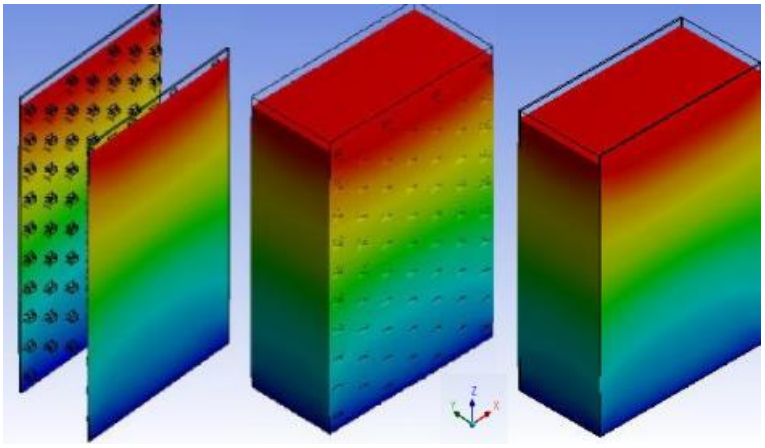

Figure 6.15. The typical relative deformation of PU and HDPE under edgewise compression

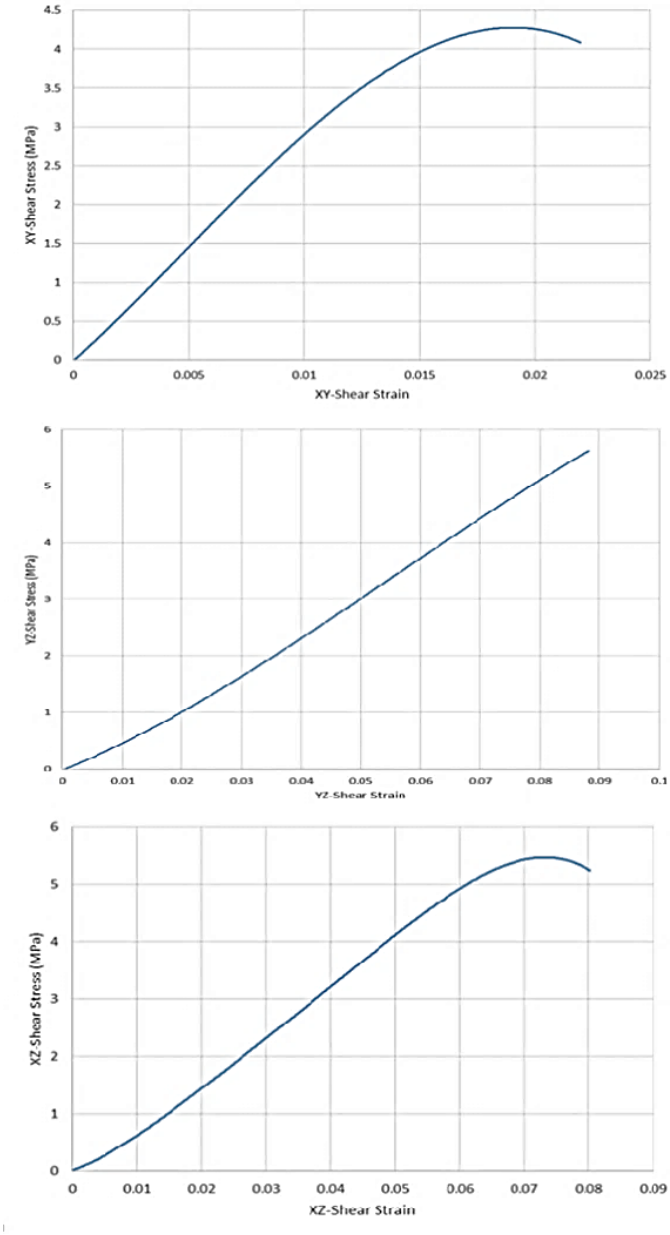

Figure 6.16: Maximum shear stress under edgewise compression in the principal directions

It is worth mentioning that at experimental tests, the first shear yielding occurs at the corners of foam, approximately at the same time with the first wrinkling (Figure 6.17). This fact can be a reason for the local wrinkling accrued by the lateral pressure on the Studliner at yielding point (Figure 6.18). Figure 6.19 shows a comparison between the FEM model and experimental results for von Mises stress of the composite sample under the edgewise compression. Although FE model predicts the composite strength for lower strains accurately, for higher strains (over 0.04) it underestimates the edgewise strength.

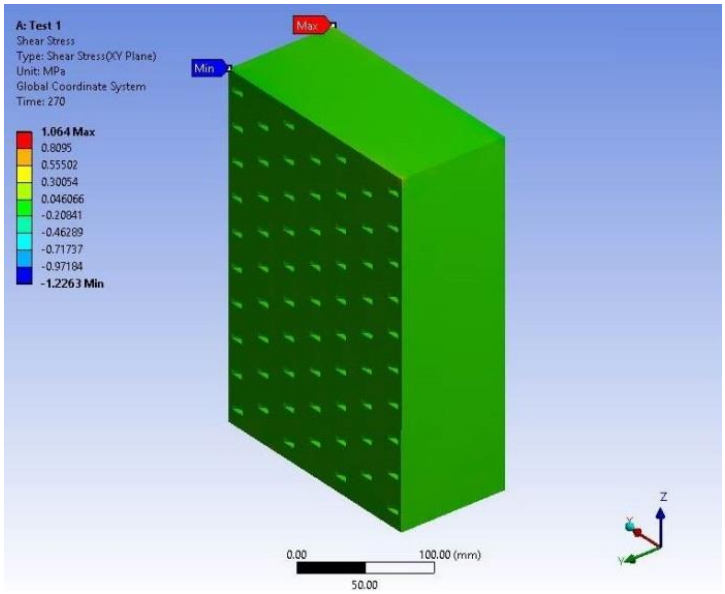

Figure 6.17: Stress distribution counter of X-Y shear stress of PU at shear yielding point

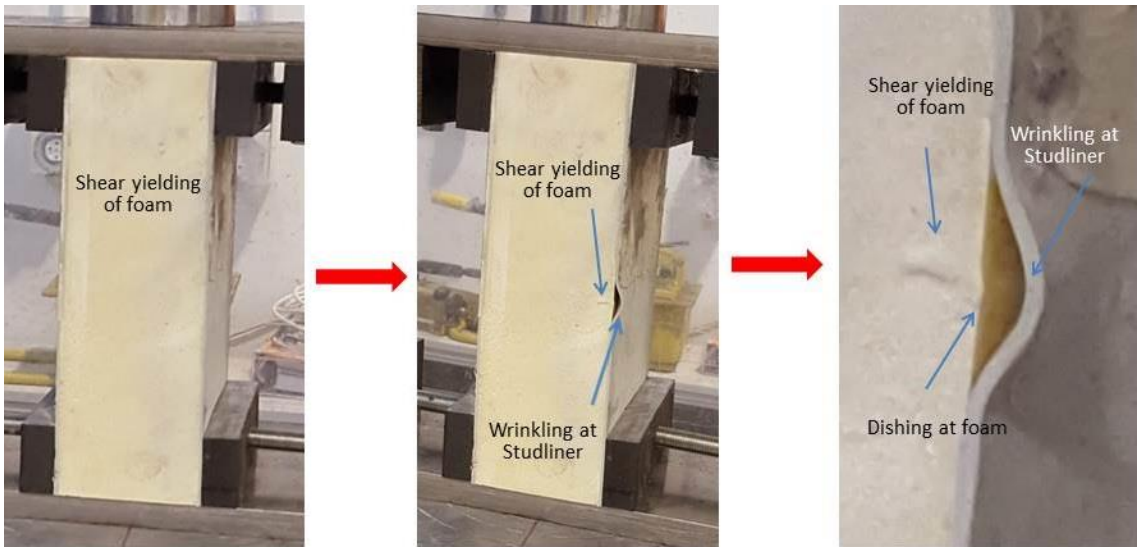

Figure 6.18: Wrinkling at studliner due to shear yielding of foam (also see Figure 10)

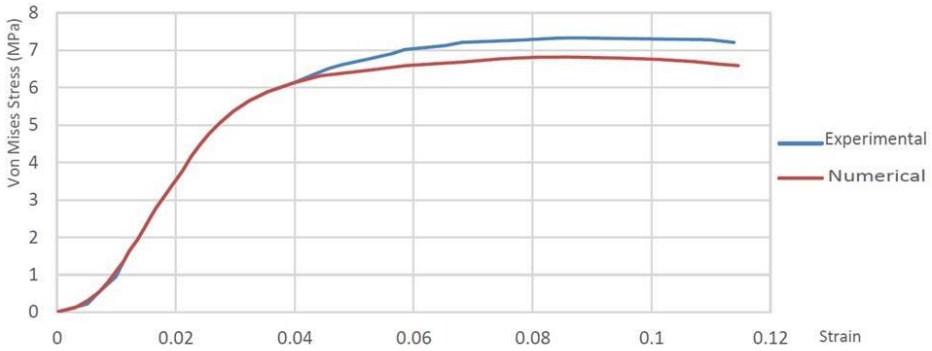

Figure 6.19: Comparing FEM and experimental results for von Mises edgewise compressive stress

6.4.2 FEM Results For Flatwise Compression

The FE modelling results of flatwise compression model are shown in Figures 6.20, 6.21 and 6.22. High deformation values are localised in the foam-cores. Although the flatwise compression behaviour of the composite is mostly governed by the behaviour of the foam-core, the failure is due to the local separations between the skin and core at the ultimate stage. Confirming the experimental results, the deformation of the skin was negligible compared with that of the core. With regard to the shear behaviour, there was a uniform distribution of shear stress in the xy and yz-planes with the exception of areas around the edges. As shown in Figure 6.21, in lower ranges of strain (up to 0.02), the composite shows a relatively linear shear behaviour in both the xy and yz-planes. In the zx-plane however, the composite exhibits non-linear shear behaviour with considerably lower shear resistance compared to those of xy and yz planes; meaning that the composite undertakes lower shear stress before it fails in zx-plane.

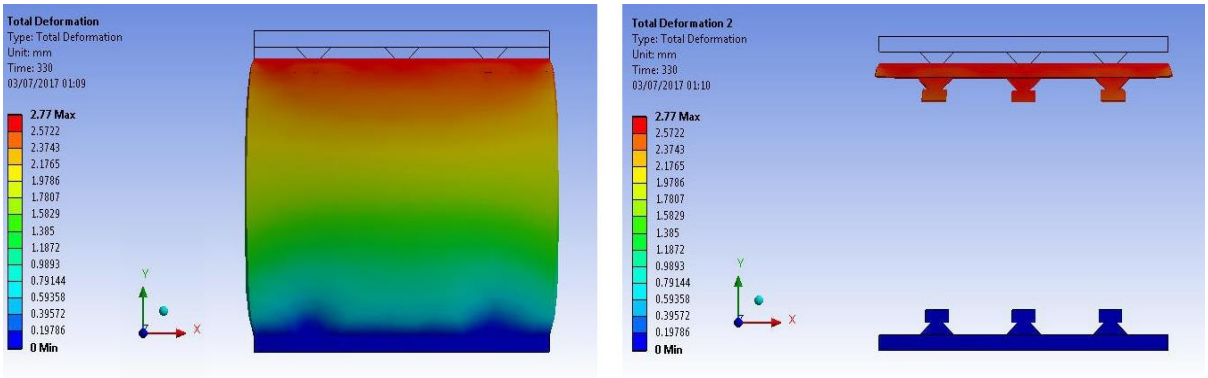

Figure 6.20. The relative deformation diagrams under edgewise compression

Figure 6.22 shows a comparison between the FEM model and experimental results for von Mises stress of the composite sample under the flatwise compression, which shows a good agreement between the results.

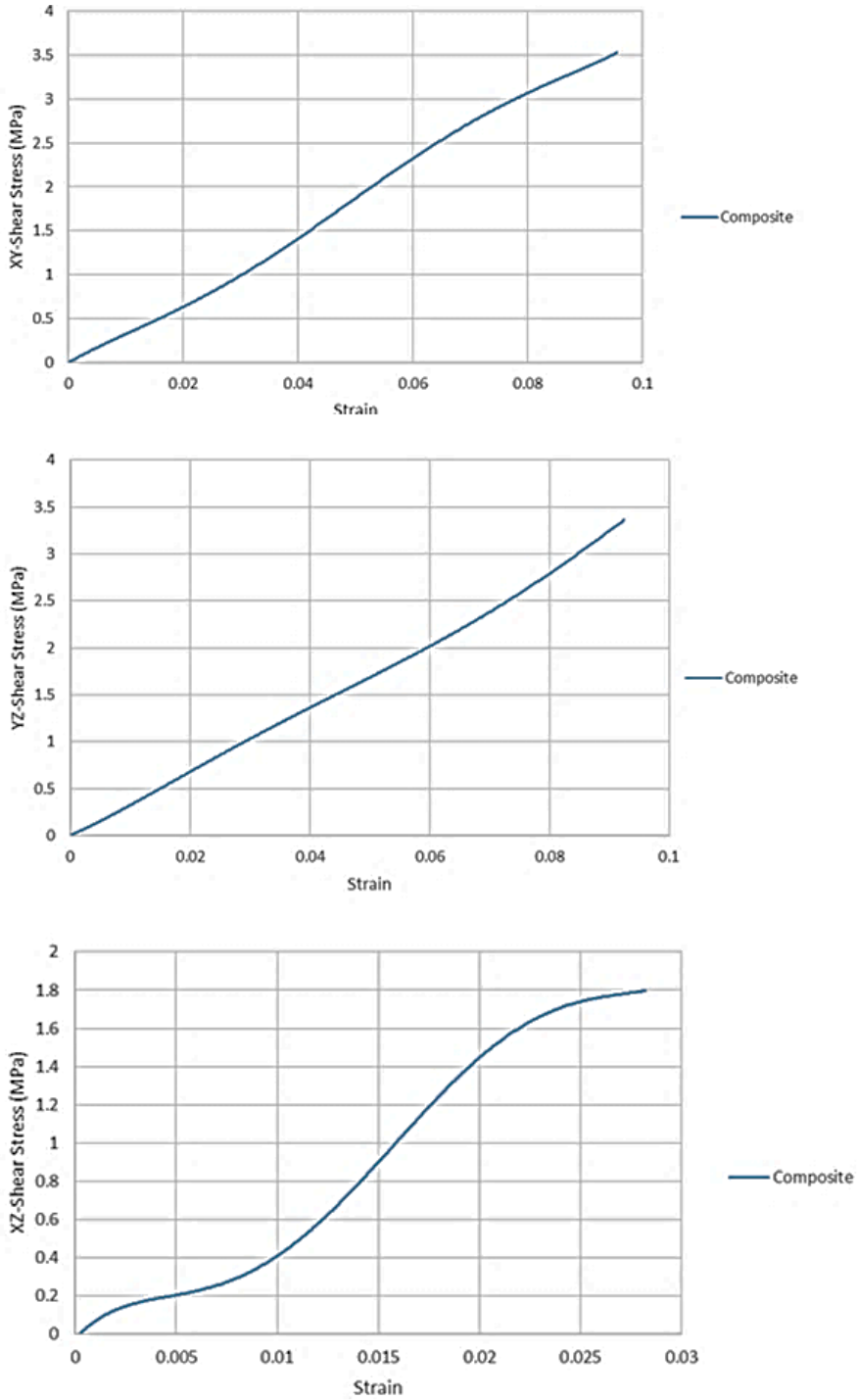

Figure 6.21: Maximum shear stress under flatwise compression in the principal directions

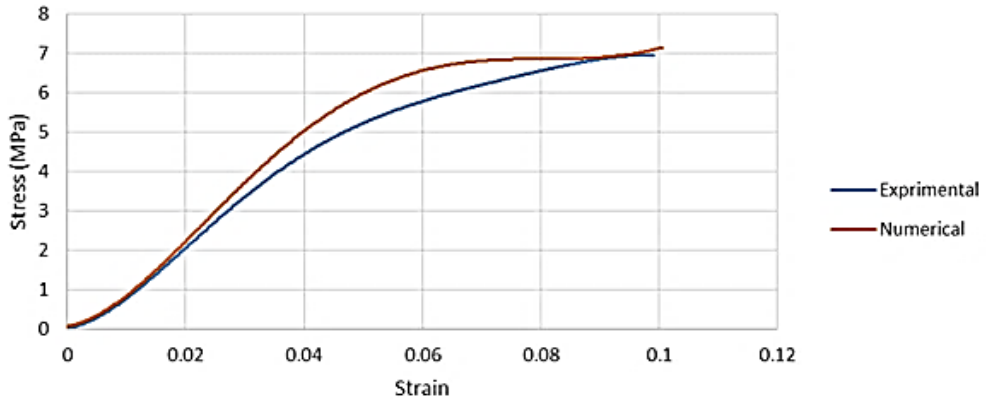

Figure 6.22: Comparing FEM and experimental results for von Mises flatwise compressive stress

6.5 Conclusion

The compressive behaviour of a newly developed sandwich panel proposed for post-disaster rapid assembly buildings is studied. The panel is fabricated by filling high-density polyurethane foam-core between two 3-D high density polyethylene skins. The compressive performance of the panel was investigated through material characterisation tests and flatwise compression and edgewise compression experiments, and validated and modelled by the finite element method. The failure behaviour, the test values and the FE modelling results suggest a very good bond strength between PU foam-core and the 3-D HDPE skins in compression that offers interesting capabilities in terms of flatwise compression and edgewise loading. The failure mode of specimens under the edgewise compression was local buckling (wrinkling) of the HDPE sheets between two edge studs, resulting in a local delamination and debonding between the face and core. The results of the flatwise compression test, on the other hand indicated that the flatwise compressive behaviour of the specimens is governed by the rigid foam behaviour. Despite some minor discrepancy between the FE model and experimental tests, the results suggest that the FE model well agrees with the experimental test results, and could be used as a design tool to evaluate the compression performance of the sandwich panels.

Chapter 7

Flexural and shear performance of foam-filled sandwich panel

The contents of this chapter have been published in the form of a journal paper as follows:

P. Sharafi (Scientific supervision), S. Nemati (Full contribution), B. Samali (Scientific supervision), A. Bahmani (General advising), S. Khakpour (contributed in numerical phase) and Y. Aliabadizadeh (General advising), "Flexural and Shear Performance of an Innovative Foam-Filled Sandwich Panel With 3-D High Density Polyethylene Skins". Engineering Solid Mechanics (ESM), March, 2018 Vol.6, Issue 2, pp. 113-128, DOI: 10.5267/j.esm.2018.3.002, Canada.

7.1 Introduction

Innovative foam-filled sandwich composite structures have attracted attention in the past decade, mainly because of their great comparative advantages such as light weight, high strength, corrosion resistance, durability and speedy construction. These types of sandwich panels are becoming a major role player in modular and rapid assembly construction with a variety of applications in residential and commercial buildings worldwide [140]. These products are popular because they are light, easy to install and have good thermal and acoustic properties. In recent years, considerable research efforts have been continuously looking for new construction materials and efficient designs for such sandwich panels. Various forms of sandwich construction are being produced by combining different skin and core materials, with various geometries and configuration. In addition to their applications as non-structural building elements, sandwich panels with polyurethane (PU) foam-core and exterior and interior facing materials such as gypsum, engineered wood or some composite materials are being used as structural members in building construction [140].

With regard to the literature, a wide range of studies on the foam-filled composite panels are on those made of polyurethane (PU) foam-core [150]. Fam et al. [148] explored the feasibility of fabrication and flexural performance of panels composed of low-density polyurethane foam core sandwiched between two GFRP skins. Reis and Rizkalla [143] presented an innovative 3-D glass fibre reinforced polymer (GFRP) panels with foam-core designed to overcome delamination problems, typically encountered in traditional sandwich panels. Sharaf et al. [125] studied the flexural behaviour of sandwich panels fabricated by laminating two glass fibre reinforced polymer skins to a prefabricated polyurethane foam core. They showed that flexural strength and stiffness increased substantially, as the core density was doubled. Manalo investigated the structural behaviour of an emerging prefabricated wall system made up of glass fibre reinforced rigid polyurethane foam and Magnesium Oxide board [151]. Their results indicated that the behaviour of the composite walls is governed by the strength of the board. Wang et al. focused on the bending behaviour of an innovative sandwich panels with GFRP face sheets and a foam-web core (GFFW) panels, where their experimental study demonstrated that the ultimate bending strength and initial bending stiffness can be significantly enhanced by increasing web thickness [152]. Kumar and Soragaon [153] studied on the effect of change thickness of fiber reinforced polymer (FRP) facing sheets and inserts on the flexural behaviour of sandwich panels with a

constant total thickness. Tuwar et al. [154] evaluated three different polyurethane foam configurations for (GFRP) foam-core sandwich panels. Lv et al. [154] studied on bending properties of 3-D honeycomb sandwich structure composites with three different cross section shapes. Sharaf [125] and Sharaf and Fam addressed the flexural performance of sandwich panels composed of a polyurethane foam core and GFRP skins [126]. They also presented numerical modelling of the flexural behaviour of sandwich panels composed of woven glass fibre reinforced polymer skins and polyurethane foam core, including various patterns of glass fibre reinforced polymer ribs, as well as different densities of cores [127]. In a similar study, Dawood et al. evaluated the two-way bending behaviour of 3-D GFRP sandwich panels consisting of GFRP skins with a foam core and through-thickness fibre insertions [40]. In a comprehensive study, Mostafa et al. [137] studied composite sandwich panels composed of GFRP skin with polyvinylchloride and polyurethane foam core, reinforced with shear keys under static bending load, while the semicircular shear keys inserts were made of chopped strand glass fibre impregnated with epoxy resin. They conducted series of quasi-static tests, while the flexural response of the sandwich panel with and without shear keys has been evaluated under four-point bending test. A significant improvement in the flexural stiffness and strength of the panel incorporated with shear keys accompanied with a good correlation with the analytical results were observed. They also tested light weight sandwich structures through four-point bending tests to characterize their flexural behaviour [128] and tried to extend the knowledge of mechanical properties of the sandwich structures, by studying the effects induced by inserting semi-circular shear keys between the skin and the foam core [155].

The results of these studies indicate that the stiffness and strength of a majority of conventional foam-filled sandwich panels hardly meet the structural requirements for use in building floors or walls, at least for standard spans and loads, mainly due to some different failure modes such as delamination of the skins from the core, buckling or wrinkling of the compression skin, flatwise crushing of the core or rupture of the tension skin. The main weaknesses of these panels stem from the low stiffness and strength of the core, and the skin's susceptibility to delamination and buckling, owing to the local mismatch in stiffness and the lack of reinforcements bridging the core and the skins [38]. This study proposes a new geometry design and material to enhance the properties of the foam-filled sandwich panels with regard to such failure modes. A 3-D high density Polyethylene (HDPE) sheets are used as the skins with a thickness as 2 mm, and high-density PU foam is used as the core with

a total thickness as 100 mm, as illustrated in Figure 7.1. Using the HDPE sheets, manufactured with approximately 1200 studs per square meter, higher pull-out and delamination strength, as well as better stress distribution, and buckling performance can be achieved. The studs also improve the resistance of the face sheets and foam-core from debonding and increasing the interface strength between the foam-core and the face sheets. This innovative sandwich panel was developed at the centre for infrastructure engineering (CIE) in the Western Sydney University to be used as modular walls and floors in rapid assembly buildings for semi-permanent post disaster housing.

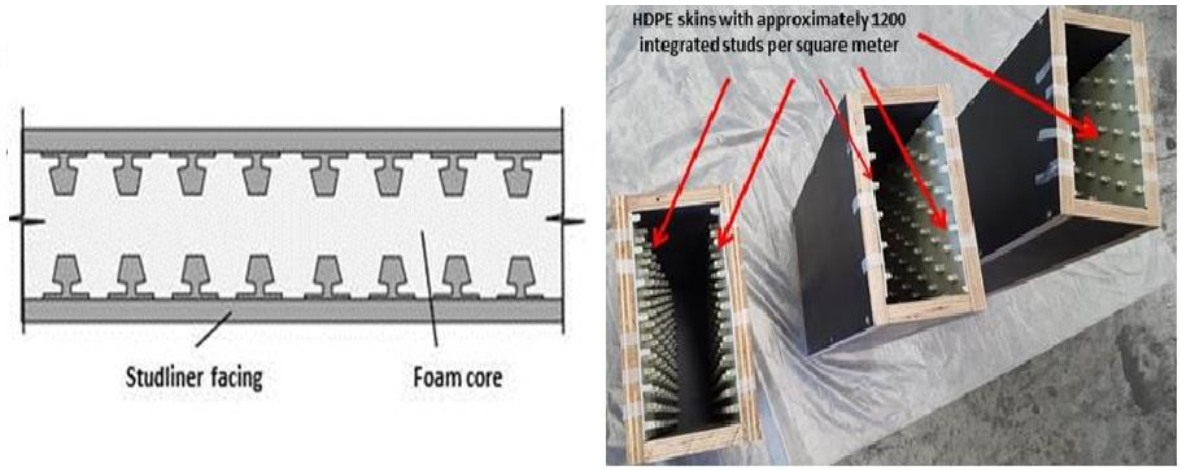

Figure 7.1: Introduced sandwich panel with HDPE skins and PU foam-core

7.2 Material Characterisation

This section reports the detailed descriptions of the tests carried out for material characterization of the constituent materials i.e. PU rigid foam and 3-D HDPE skin sheets. To evaluate the basic material properties, in addition to using the manufacturers' data, some experimental tests were performed.

7.2.1 Polyurethane Foam Used in the Sandwich Panel

Polyurethane high-density rigid foam with a density of 192 kg/m^3 was selected for the core material, according to the results the preliminary finite element models. Table 7.1 shows the PU foam's manufacturing and mechanical properties, provided by the manufacturer, and validated in the laboratory according to the ASTM 1730 standard specification for rigid foam for use in structural sandwich panel cores [22].

Table 7.1 Mechanical and manufacturing properties of the selected PU rigid foam

Mechanical Properties of the PU foam			
Density (kg/m^3)	Compressive yield strength (MPa)	Tensile yield strength (MPa)	Shear yield strength (MPa)
192	3.51	1.896	1.034
Manufacturing Properties			
Cream time	Gel time	Tack free time	Free rise cup density
35-40 sec	94 ± 4 sec	115 ± 5 sec	280 – 300 kg/m^3

Using a uniaxial load machine (Figure 7.2), three cubic specimens (dimensions: 50mm×50mm×50mm) were tested based on the ASTM E1730 and ASTM D1621 (ASTM-D1621, 2010) standards at a loading rate of 5 mm/min in order to identify the structural properties of the rigid PU foam.

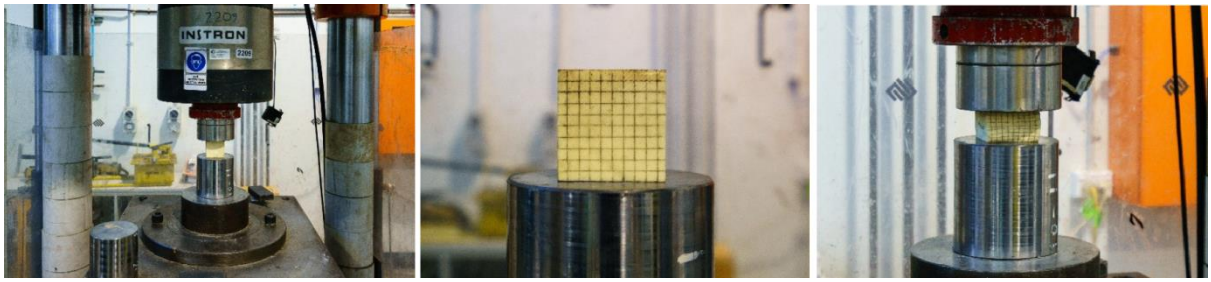

Figure 7.2: Uniaxial load test for determining the compressive behaviour of PU foam

Table 7.2 shows the yield stress and elastic modulus for each specimen, and Figure 7.3 illustrates the stress-strain curves in the elastic region and failure graph, respectively. The curves show that this type of PU foam, which is made of a 100:110 weight ratio mixture of AUSTHANE POLYOL AUW763 and AUSTHANE MDI, can undertake considerable deformation before the failure. These stress-strain curves are relatively linear in the elastic region, with a yield region at an average stress of 3.51 MPa, and an average elastic modulus of 135.5 MPa.

Table 7.2 Yield stress and elastic modulus of PU specimens

	σ_y (MPa)	E (MPa)
Test 1	3.6	130
Test 2	3.52	137.9
Test 3	3.45	132.9
Test 4	3.5	141.3
Test 5	3.48	136.7
Average	3.51	135.5
Standard Deviation	0.056	5.05

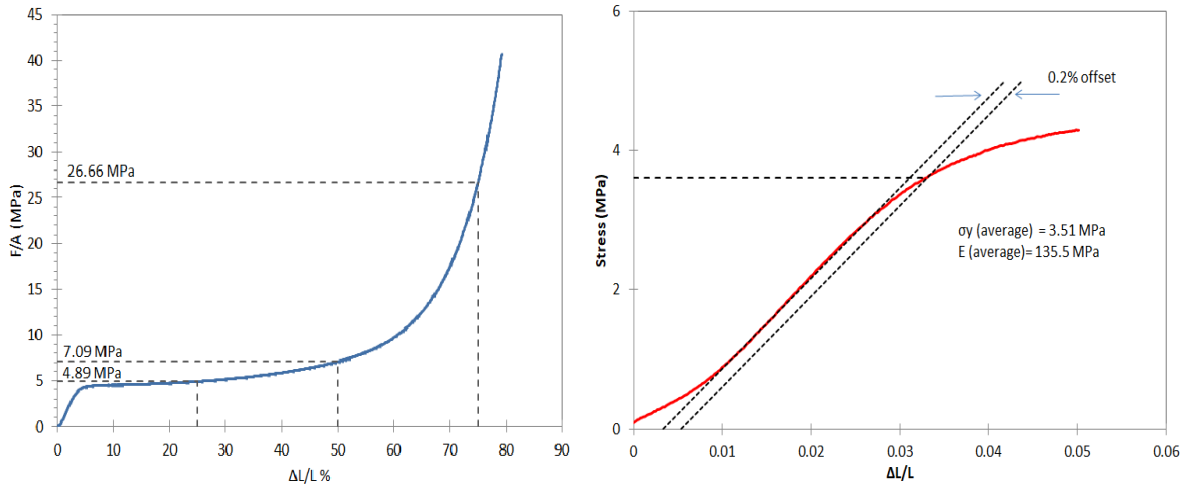

Figure 7.3: Results of the uniaxial load test on PU foam, left: total behaviour and right: elastic range

The yield behaviour can be explained by the buckling of the foam's internal walls. Scanning Electron Microscopic images (SEM), provided before and after compression test, shown in Figure 7.4, substantiate such behaviour. A long and rather flat plateau was followed. Then, a densification (hardening) region was created by a gradual stress increase when the cell walls were stacked prior to final densification. In this range of loading, no visible signs of failure were observed. Residual displacement of the collapsed foam however, occurs once the unloading stage was complete.

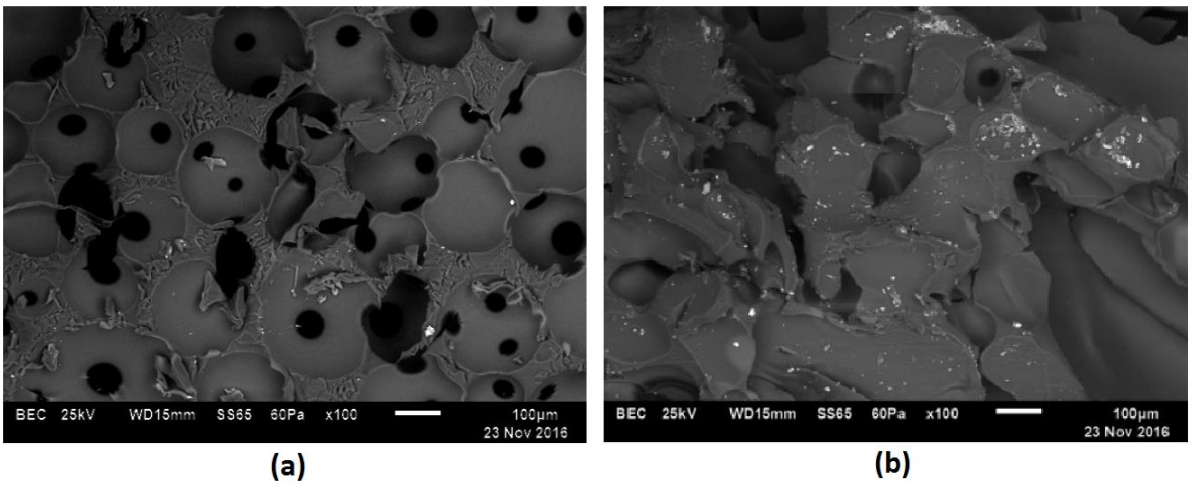

Figure 7.4: Images from the scanning electron microscope on the PU specimens (a) before and (b) after the compression test

7.2.2 High Density Polyethylene Sheets

The face sheets of the sandwich panels are made of 3-D HDPE (High Density Polyethylene) sheets primarily produced as a concrete embedment liner to provide protection from

mechanical damage and a corrosive and erosive environment. In addition to resistance to chemical and environmental threats, its relatively high strength, and in particular its 3-D studded face with approximately 1200 studs per square meter, can effectively contribute to the sandwich composites' structural performance by providing high pull out strength, minimum lateral movement of the skin, and stronger bonding. Four different thicknesses of the sheets were initially investigated (2 mm, 3 mm, 4 mm and 5 mm), and at the end the sheets with 2 mm tackiness were selected for the sandwich composite. Table 7.3 shows some mechanical properties of the selected sheet, provided by the manufacturer and validated by experimental tests in the laboratory, in accordance with the ASTM D5199, ASTM D1505 and ASTM D6693 provisions at a loading rate of 5 mm/min.

Table 7.3 Specifications of the HDPE sheets

Tested Property	Test Method	Nominal Value
Thickness (mm)	ASTM D 5199	2
Density (g/mm^2)	ASTM D 1505	0.94
Sher strength at yield (MPa)		5.2
Elongation at Break (%)		500
Stud pull-out strength (kN/m^2)		>670
Notched Constant Tensile Load, hours	ASTM D 5397	400
Coefficient of Linear Thermal Expansion, per °C	ASTM D 696	1 .20E-04
Low Temperature Brittleness, °C	ASTM D 746	-77
Dimensional Stability, % (each direction)	ASTM D 1204	1
Water Absorption, %	ASTM D 570	0.1

In order to identify the structural behaviour of the skin, in-plane tensile tests were conducted on two principal perpendicular directions (lengthwise and crosswise) of the HDPE sheets, using a universal hydraulic testing machine. Five repeated specimens for each direction of the HDPE face sheet were tested as shown in Figure 7.5. Typical tension specimens consisted of flat strips with a total width of 19 mm and a total length of 115 mm, according to ASTM D6693 standard (ASTM-D6693, 2015). Figure 7.6 shows the coupon test results. The 3-D HDPE sheets exhibited a relatively linear elastic response up to a strain of 0.15 mm/mm at the yield stress of 19.7 MPa in the lengthwise direction; and to a strain of 0.11 mm/mm at the yield stress of 20.6 MPa in the transverse (crosswise) direction, indicating relatively similar behaviour in the elastic range. Since the coupon specimens were cut from 3-D panels, the minor differences in behaviour could be due to the combination of the presence of the studs in different directions, or manufacturing homogeneity of the sheets. A non-linear plastic stress–strain relationship was observed in the higher ranges of strain. Results show the HDPE modulus of elasticity in lengthwise direction is E_L=19.7/0.15 = 131.33 MPa, and in crosswise direction is E_C = 20.6/0.11 = 187 MPa. In the computer model average value of E_{STUD} = 159 MPa is used to model the HDPE as isotropic material.

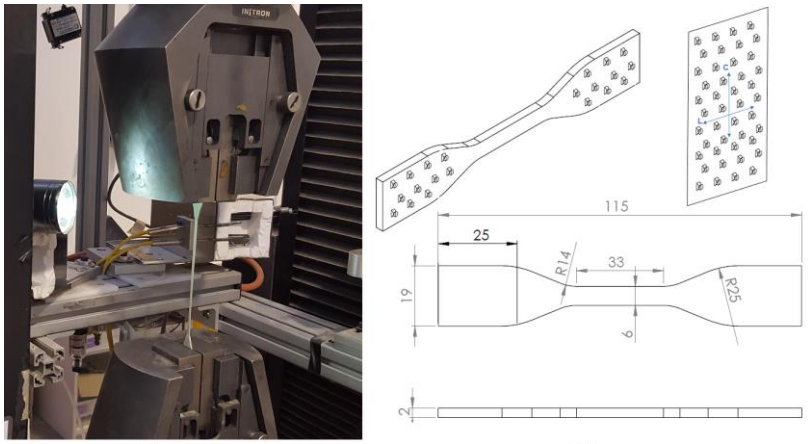

Figure 7.5: HDPE coupon test and specimens' dimensions

Test No.	Applied Load at Yield Point (N)	Yeild Stress (Mpa)	Yeild Elongation (%)
1	243	20.3	15
2	221	18.4	16
3	243	20.3	15
4	234	19.5	14
5	237	19.8	14
Avrage	236	19.7	15
Standard Deviation	9	0.75	1.1

Test No.	Applied Load at Yield Point (N)	Yeild Stress (Mpa)	Yeild Elongation (%)
1	258	21.5	11
2	243	20.1	11
3	238	19.8	10
4	256	21.3	10
5	246	20.5	14
Avrage	248	20.6	11
Standard Deviation	8.6	0.72	1.6

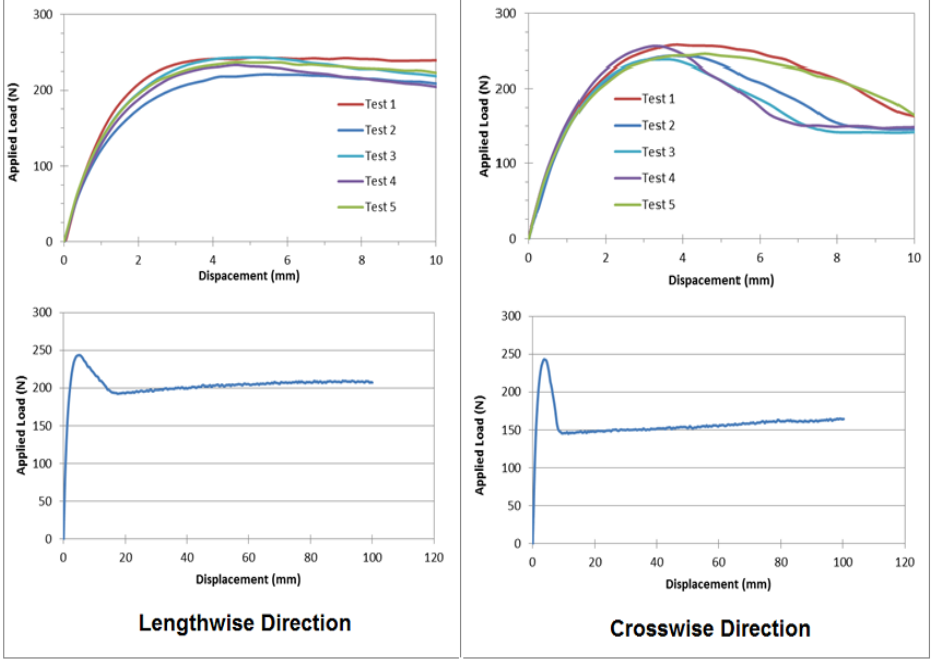

Figure 7.6: HDPE coupon tests results for the lengthwise and crosswise directions

7.3 Experimental Program

General speaking, the flexural stiffness of sandwich beams/panels can be calculated using First-order Shear Deformation Theory (FSDT). The FSDT can also be used to estimate the

shear stiffness of each sandwich beam type by fitting the results collected from four-point flexural tests. In this regard, a perfect bond must be assumed to exist between the core and the facings. The bending stiffness can be computed accounting for the deflection components that are associated with bending and shear deformations (Hayes, 2003). This study examined the core shear properties of introduced polyurethane infill-foam composite panels subjected to flexure in such a manner that the applied moments produce curvature of the sandwich facing planes. Also, in this regard, core shear ultimate stress (F_s^{ult}), facing bending stress (σ), transverse shear rigidity (U) and core shear modulus (G) of introduced sandwich panel are calculated based on ASTM C393/C393M and ASTM D7250/D7250M (ASTM-D7250/D7250M, 2011) using six medium-scale sandwich specimens with 45cm length, 20cm width and 10cm as total thickness of composite section. The detailed descriptions of the tests carried out on specimens which are four-point quarter-span loading and three-point mid-span loading flexural tests (Figure 7.7) are discussed in this section.

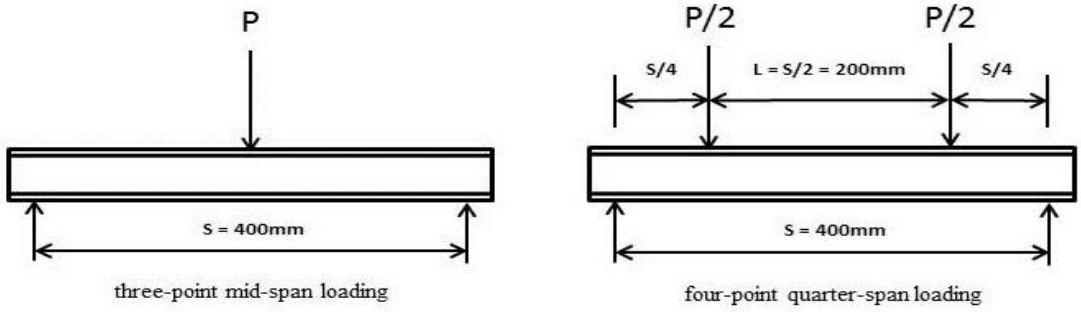

Figure 7.7: Four-point quarter loading and three-point mid span loading configurations

The four-point bending test in accordance with ASTM C393/C393M under quarter point loading configuration is performed for core shear ultimate stress (F_s^{ult}) and facing bending stress (σ) calculations. This test method is limited to obtaining the core shear strength or core-to-facing shear strength, and to obtaining load-deflection data for use in calculating sandwich beam flexural and shear stiffness using practice D7250/D7250M. The test setup is illustrated in Figure 7.8(a). An INSTRON test machine (model no. 5500R) was used. High resistance rubber pads (with a Shore A durometer hardness of 60, a nominal width of 25 mm and a nominal thickness of 3 mm) were inserted at the loading and supporting points to distribute the load uniformly and reduce the stress concentrations. Three specimens were investigated, where they were tested in one-way bending with the span of 400 mm, under two equal point loads, applied at 100 mm from each support. The specimens have been inserted into the test fixture and then were aligned so that the longitudinal axis of the specimen was perpendicular

(within 1°) to the longitudinal axes of the loading bars, and the bars were parallel (within 1°) to the plane of the specimen facings. The specimens were loaded to failure at a displacement rate of 6 mm/min. The bottom deflection at mid-span was recorded using a Linear Potentiometer (LP) having a minimum accuracy of +/-1%. A data acquisition system was used to record the load, displacement, and deflection during testing. In this study applied force versus crosshead displacement, and applied force versus deflection data were recorded continuously. In addition, the visual method was used to determine any initial failure (Figure 7.8(b)).

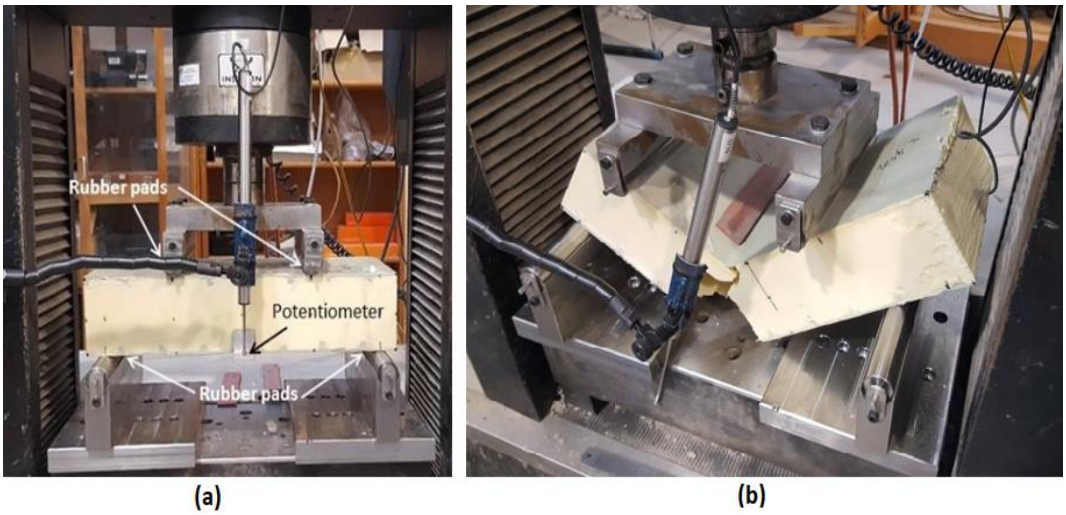

Figure 7.8: (a) Four-point quarter-span loading flexural test setup; and (b) multi-mode of failure in the vicinity of the mid span

The applied force versus crosshead displacement and midspan deflection are shown in Figures 7.9 and 7.10 respectively.

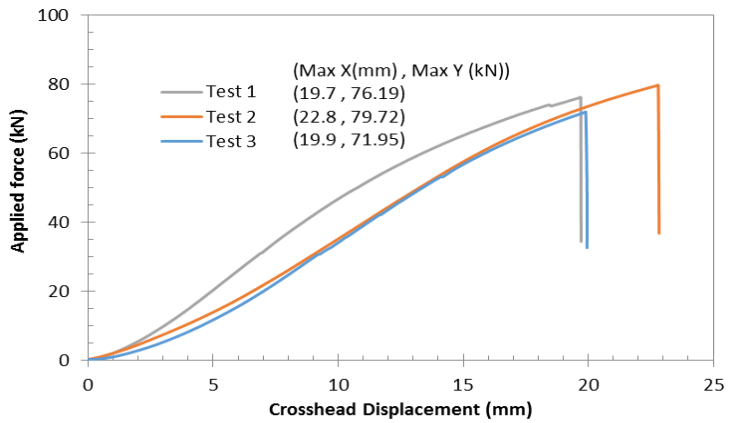

Figure 7.9: The applied force versus crosshead displacement for four-point quarter-span loading test

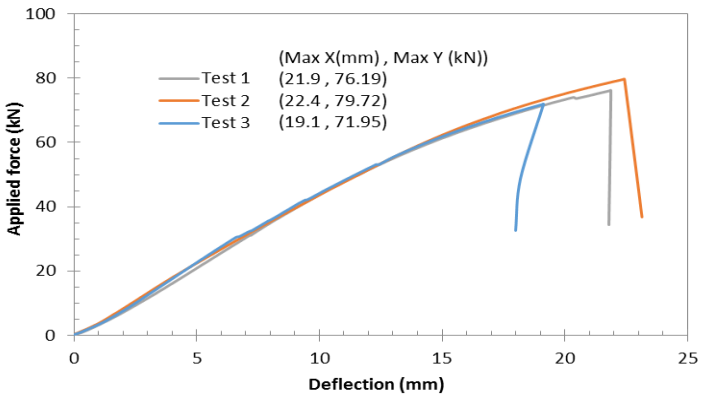

Figure 7.10: The applied force VS mid span deflection for four-point quarter-span loading flexural test

7.4 Calculation of Core Shear Ultimate Stress and Facing Bending Stress

In this section, shear ultimate stress (F_s^{ult}) and facing bending stress (σ) of innovated sandwich panel are calculated using the typical cross section shown in Figure 7.11; parameters and formulas based on ASTM C393/C393M.

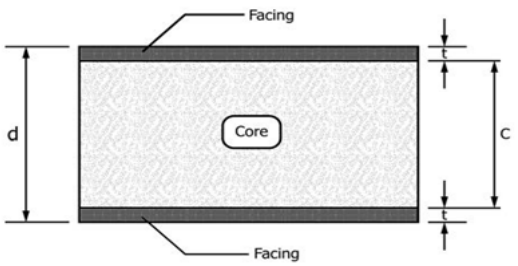

F_s^{ult} = core shear ultimate stress = P_{max} / (d+c)b (MPa)
σ = facing bending stress = PS/[4t(d+c)b] (MPa)

Where:

P_{max} = maximum force carried by test specimen before failure (N)
b = sandwich specimen width (mm)
d = sandwich total thickness (mm)
c = core thickness (mm)
t = facing thickness (mm)

Figure 7.11: Sandwich panel thickness dimensions [59]

The results and calculation of core shear ultimate stress and facing bending stress are summarised in Table 7.4.

Table7.4 Calculation of core shear ultimate stress and facing bending stress of innovated sandwich panel

	P_{max} (kN)	F_s^{ult} (MPa)	σ (MPa)	Failure mode and location*
Specimen 1	76.19	1.9	97.2	(M)(G)(B/C)
Specimen 2	79.72	2	101.7	(M)(G)(B/C)
Specimen 3	71.95	1.8	91.8	(M)(G)(B/C)
Average	75.95	1.9	96.9	(M)(G)(B/C)
Standard deviation	3.89	0.1	5	
CV (%)	5.12	5.2	5.2	

* (M)(G)(B/C): (Multi-mode)/(Gage)/(Bottom facing/Core) [59]

The facing bending stress is calculated as a reference value at the maximum applied force. Since this test method is restricted to the core or core-to-facing shear failures, the facing stress does not represent the facing ultimate strength. To obtain the facing ultimate strength, the test method ASTM D7249/D7249M can be used [156].. The results show that the foam core in composite section, withstand twice shear stress as the bare foam material.

7.5 Calculation of Transverse Shear Rigidity and Core Shear Modulus

Transverse shear rigidity (U) and core shear modulus (G) of innovated sandwich panel can be calculated based on the results of the four-point quarter-span loading tests and a series of similar three-point midspan loading supplementary tests based on ASTM D7250/D7250M. The formulations for calculating are presented in Table 7.5. According to ASTM D7250/D7250M transverse shear rigidity are calculated based on ten load-deflection selective steps of the least maximum applied force regarding both loading configurations (Tables 7.6 and Figure 7.12).

Table 7.5 Transverse shear rigidity and core shear modulus based on ASTM standards [60]

Loading Configuration	U (Transverse shear rigidity)	G (Core shear modulus)
One D7249/D7249M Standard 4-Point Loading and One 3-Point Mid-Span Loading	$9P_1S_1(141S_1^2/S_2^2-121)$ $/4\Delta_1(1269(P_1S_1^3\Delta_2/P_2S_2^3\Delta_1)-1331)$	$U(d-2t)/[(d-t)^2b]$
One D7249/D7249M Standard 4-Point Loading and One 4-Point Third-Span Loading	$9P_1S_1(2538S_1^2/S_2^2-2783)$ $/4\Delta_1(34263(P_1S_1^3\Delta_2/P_2S_2^3\Delta_1)-30613)$	$U(d-2t)/[(d-t)^2b]$
One D7249/D7249M Standard 4-Point Loading and One 4-Point Quarter-Span Loading	$9P_1S_1(1128S_1^2/S_2^2-1331)$ $/4\Delta_1(20304(P_1S_1^3\Delta_2/P_2S_2^3\Delta_1)-14641)$	$U(d-2t)/[(d-t)^2b]$
One 3-Point Mid-Span Loading and One 4-Point Quarter-Span Loading	$P_1S_1(8S_1^2/11S_2^2-1)$ $/4\Delta_1((16P_1S_1^3\Delta_2/11P_2S_2^3\Delta_1)-1)$	$U(d-2t)/[(d-t)^2b]$
One 3-Point Mid-Span Loading and One 4-Point Third-Span Loading	$P_1S_1(18S_1^2/23S_2^2-1)$ $/4\Delta_1((27P_1S_1^3\Delta_2/23P_2S_2^3\Delta_1)-1)$	$U(d-2t)/[(d-t)^2b]$
One 4-Point Quarter-Span Loading and One 4-Point Third-Span Loading	$P_1S_1(99S_1^2/92S_2^2-1)$ $/2\Delta_1((297P_1S_1^3\Delta_2/368P_2S_2^3\Delta_1)-1)$	$U(d-2t)/[(d-t)^2b]$
Two 3-Point Mid-Span Loading	$P_1S_1(S_1^2/S_2^2-1)/4\Delta_1((P_1S_1^3\Delta_2/P_2S_2^3\Delta_1)-1)$	$U(d-2t)/[(d-t)^2b]$
U = transverse shear rigidity (N) G = core shear modulus (MPa) Δ_1 = beam mid-span deflection for configuration #1 corresponding to force P1 (mm) Δ_2 = beam mid-span deflection for configuration #2 corresponding to force P2 (mm)	P_1 = applied force for configuration #1 N) P_2 = applied force for configuration #2 N) S_1 = length of support span for configuration #1 (mm) S_2 = length of support span for configuration #2 (mm)	

Table 7.6 The least maximum applied forces and their related mid-span deflections

	4-Point Quarter Span Loading		3-Point Mid Span Loading	
	P_{max} (kN)	$\Delta_{midspan}$ (mm)	P_{max} (kN)	$\Delta_{midspan}$ (mm)
Specimen 1	76.19	21.9	56.23	24.9
Specimen 2	79.72	22.4	52.54 (minimum)	23.8
Specimen 3	71.95 (minimum)	19.1	53.98	24.2
Average	75.95	21.1	54.25	24.3
Standard deviation	3.89	1.8	1.86	0.56
CV (%)	5.12	8.42	3.5	2.3

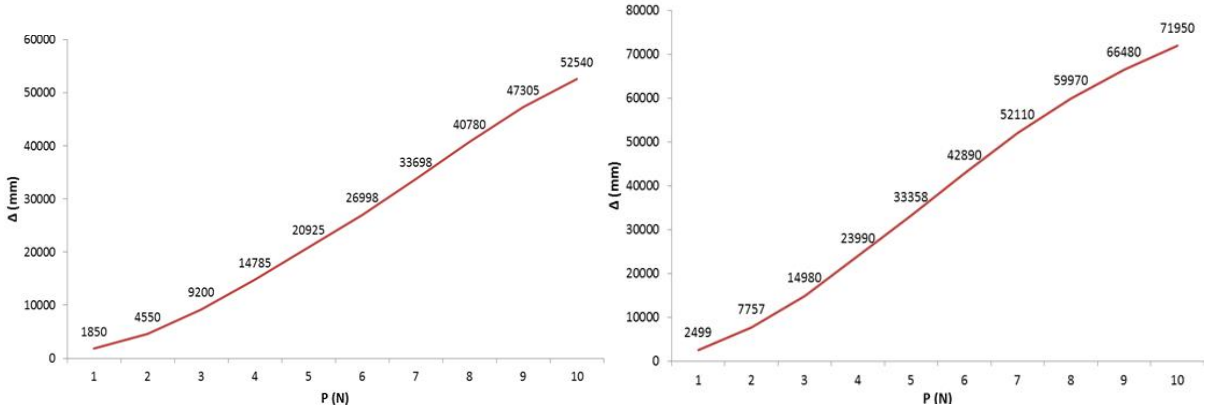

Figure 7.12: Selected load-displacement levels of four-point quarter (right) and three-point mid span (left) loading configurations

The results and calculation of transverse shear rigidity and core shear modulus are summarised in Table 7.7.

Table 7.7 Transverse shear rigidity (U) and core shear modulus calculations (G)

	3-Point Mid Span Loading			4-Point Quarter Span Loading				
	P_1 (N)	Δ_1 (mm)	S_1 (mm)	P_2 (N)	Δ_2 (mm)	S_2 (mm)	U_{STEP} (N)	G_{STEP} (MPa)
Step 1 (adjusting)	1850	1.2	400	2499	0.8	400	adjusting	adjusting
Step 2	4550	2.5	400	7757	2	400	88500	4.4
Step 3	9200	4.6	400	14980	3.5	400	98000	4.9
Step 4	14785	6.9	400	23990	5.3	400	147600	7.4
Step 5	19925	9.1	400	33358	7.4	400	205300	10.3
Step 6	25648	11.9	400	42890	9.7	400	203900	10.2
Step 7	31698	14.5	400	52110	12	400	225000	11.2
Step 8	37180	16.9	400	59970	14.4	400	262300	13.1
Step 9	44305	20.1	400	66480	16.7	400	383500	19.2
Step 10 (main)	52540	23.8	400	71950	19.1	400	417000	20.8
Average over time							225700	11.3

7.6 Numerical Investigation

Numerical simulations were carried out to find the non-linear behaviour of the sandwich panel and compare with the experimental measurements of the flexural behaviour of the composite sandwich beams. The simulations of the four-point static bending test of the composite sandwich, the FE modelling was performed using ANSYS R15 where a quasi-static three-dimensional model has been developed to simulate and predict the mechanical performance of the composite sandwich panel under bending. For FE modelling, the same dimensions, and the same loading rate (6 mm/min) were considered as for the experimental program. The PU foam was meshed using Hexahedral dominant, Quadrilateral and Triangular meshing. The HDPE sheets were meshed using Multizone Hexahedral/prism with Quadrilateral and Triangular elements while the studs meshed using hexahedral elements. The mechanical properties of the PU foam and the HDPE sheets, obtained from experiments, were used for calibrating the inputs.

7.6.1 Flexural Behaviour

The FE results show equivalent (Von-Mises) stress of foam has been concentrated at two strips between loading effect points and supports and other areas are under very low stress. The first yielding symptom of foam occurs when the equivalent (Von-Mises) stress of foam reaches to manufacture minimum identified yielding stress (2.8 MPa). However, the real yielding stress occurs at 3.51 MPa. Figure 7.13 shows Von-Mises stress-strain diagram of foam.

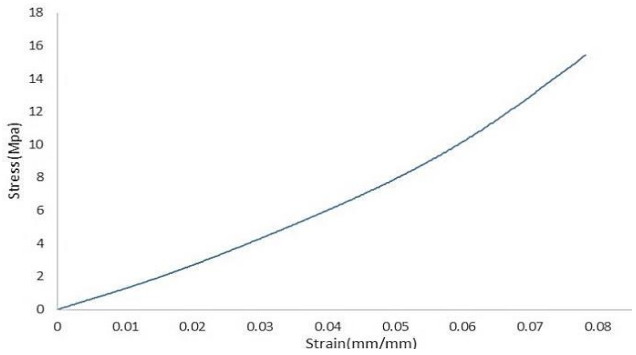

Figure 7.13: Equivalent (Von-Mises) stress – strain diagram of foam

With regard to the skins, by applying more pressure, equivalent (Von-Mises) stress of Studliner reaches to yielding stress, where the maximum strain of Studliner is 0.048 mm/mm. Maximum equivalent stress appears at the edges of Studliner. In addition, shear stress at studs

keeps increasing as the applied load continues increasing. Figure 7.14 shows Von-Mises stress-strain diagram of the skins.

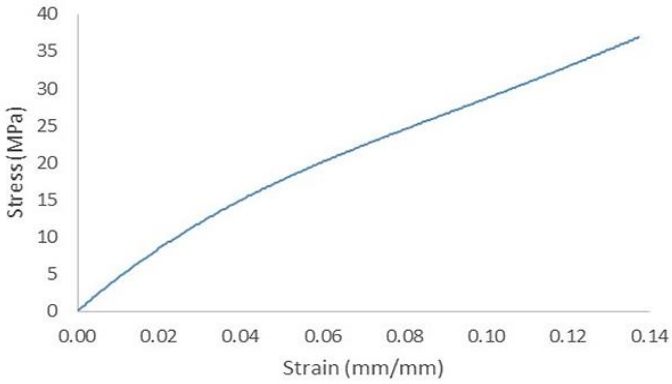

Figure 7.14: Equivalent (Von-Mises) stress – strain diagram of Studliner

Then, as similar as experimental tests, at 60th second the model start to collapse and large deformation, debonding and demolition between foam and skins appear on the loading point until 70th second (Figures 7.15 through 7.18).

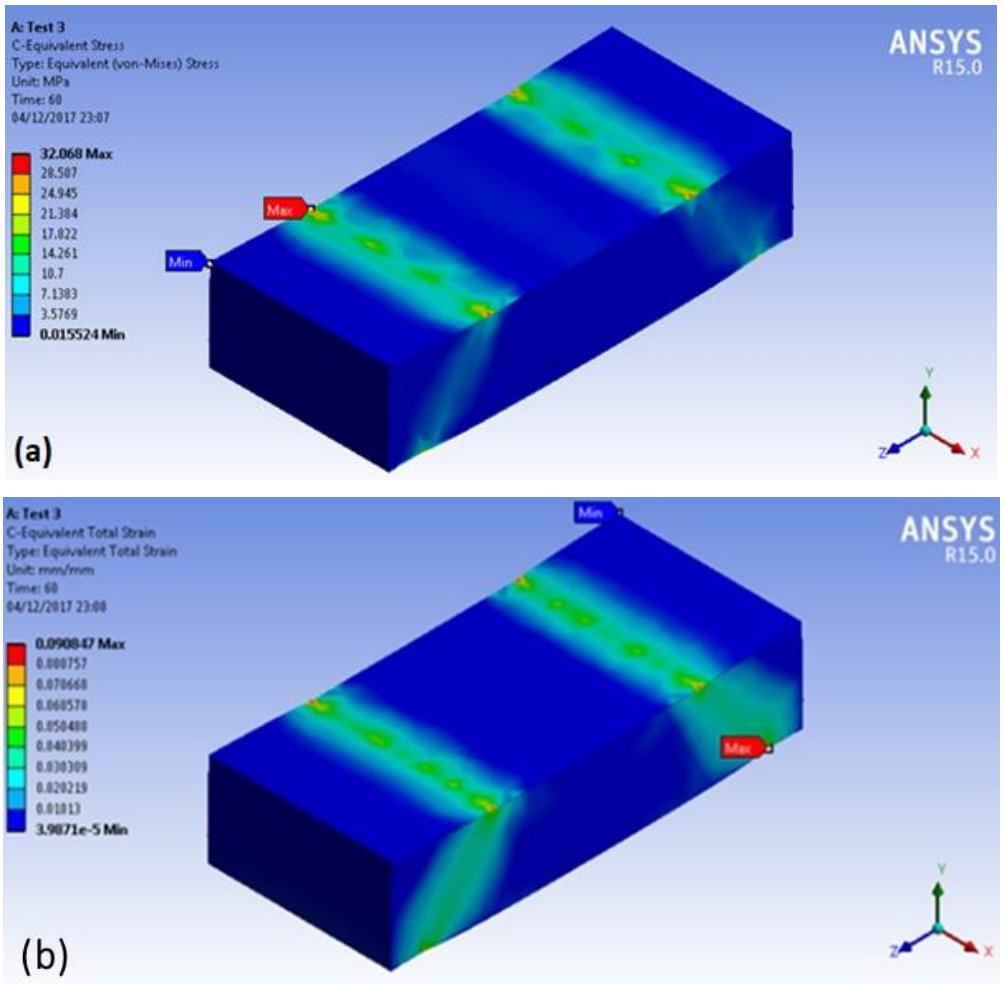

Figure 7.15: (a) Stress and (b) strain of composite panel at collapsing mode

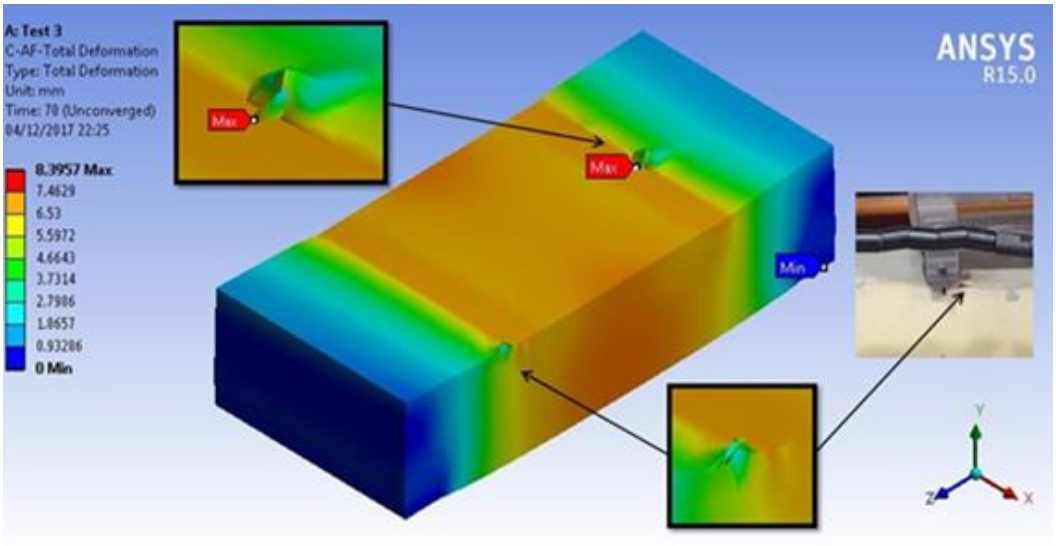

Figure 7.16: large deformation and debonding between the skin and foam core at collapsing mode

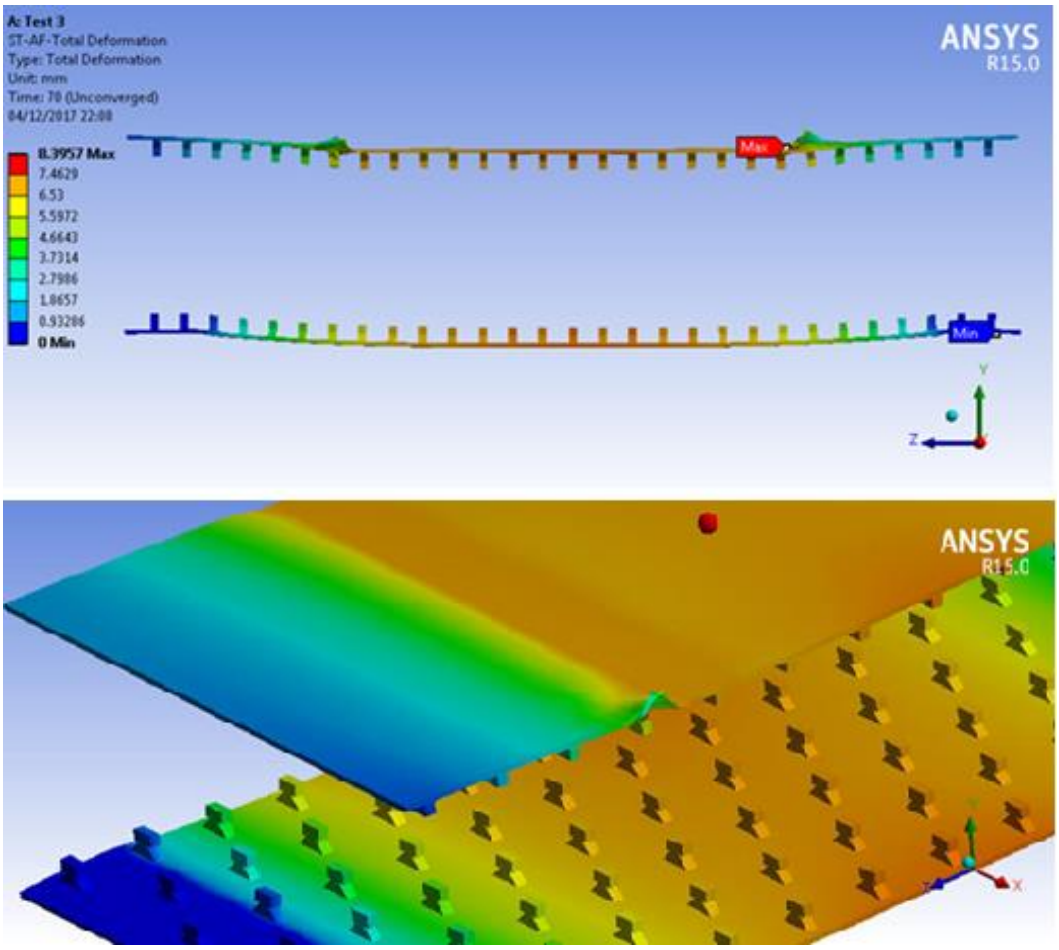

Figure 7.17: Large deformation and debonding of Studliner at collapsing mode

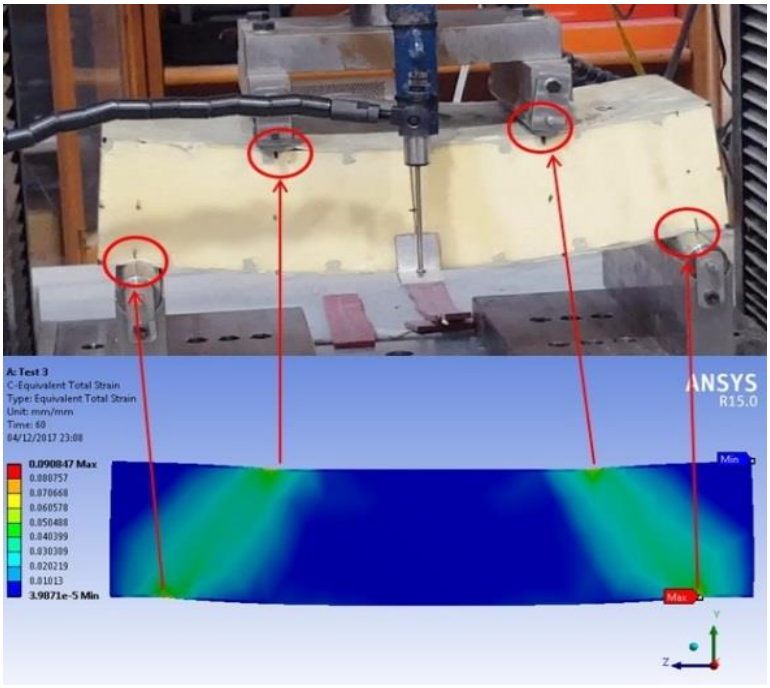

Figure 7.18: Large deformation and maximum strain of composite panel just before collapse

By applying more pressure to the specimens, the ultimate fracture occurs on the midspan at the maximum deflection point. The fracture profile is shown in Figure 7.19.

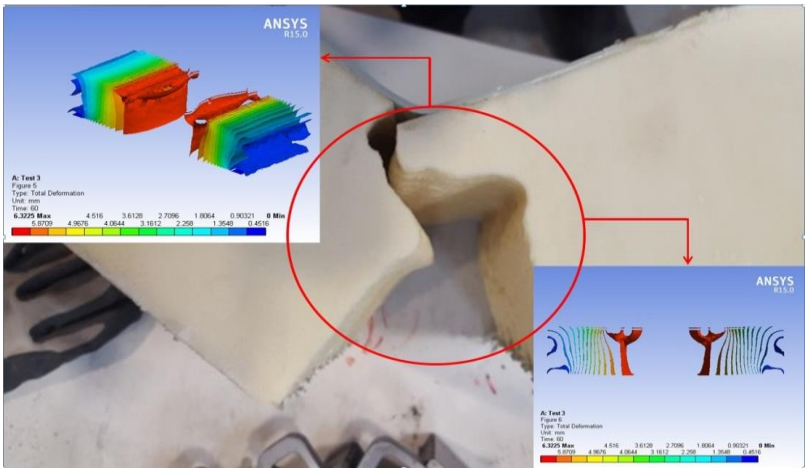

Figure 7.19: The fracture profile and maximum deflection at midspan of composite panel

Figure 7.20 shows maximum Von-Mises stress-strain diagram of the composite panel. As it can be seen, in elastic range (as strain < 2%) the composite panel has a semi linear demeanour but, after yielding point shows a hyper elastic behaviour.

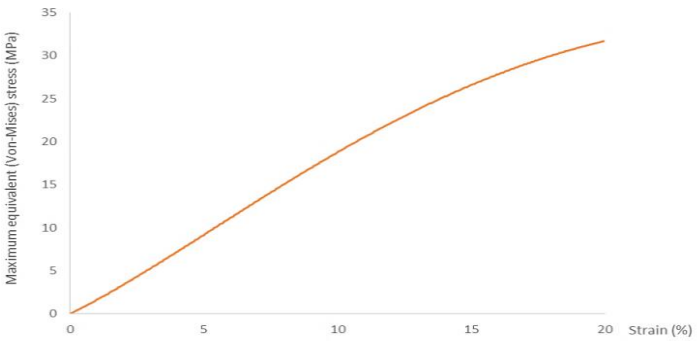

Figure 7.20: Equivalent (Von-Mises) maximum stress – strain diagram of composite panel

Results indicate that under flexure, the foam core and skins displacement are in sync, which demonstrate well integrated behaviour of the introduced composite panel, as shown in Figures 7.21 and 7.22.

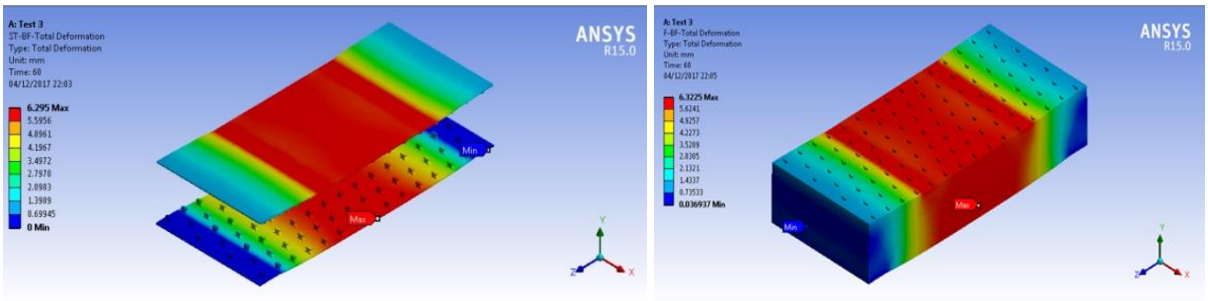

Figure 7.21: Homologous deflection of Studliner skins and foam core

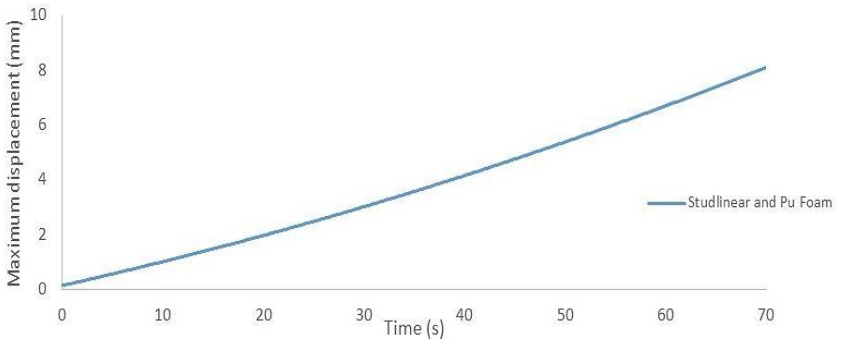

Figure 7.22: Sync behaviour of maximum mid-span displacement of the skin and foam in time

7.6.2 Shear Behaviour

XY component of shear stress has a uniform distribution on the skin and core, which demonstrates the good performance of skin studs in shear transfer. When the XY component of shear stress reaches to yielding point at both of core and skin, maximum XY shear component occurs at edges of the skin and core, under loading point. In addition, there is not any shear concentration in the skin studs on XY plane. YZ component of shear stress has a

uniform distribution on the skin and core. This component has a strip of concentration at the loading line on the surface of the core as well as surface and body of the foam core. These strips continue toward supports in foam core. The YZ component of shear stress reaches to yielding point at both the core and skin, where there is not any shear concentration at studs of skin on the YZ plane. The distribution of XZ component of shear stress on the skin is as similar as XY component. The distribution of this component on studs is completely uniform. Maximum XZ shear component occurs at the edges of skin. The XZ component of shear stress on the core has some local concentration and at other areas has a very low intensity. The XZ component of shear stress reaches to yielding point at both of foam and the skin. These distributions are illustrated in Figure 7.23.

As shown in Figure 7.24, results indicate that the XY component of shear stress show relatively linear behaviour at low strains (< 2%) and nonlinear behaviour at higher amounts. The diagram of YZ component of shear stress-strain is linear. In addition, the XY component of shear stress show nonlinearity with a positive slope until collapsing mode.

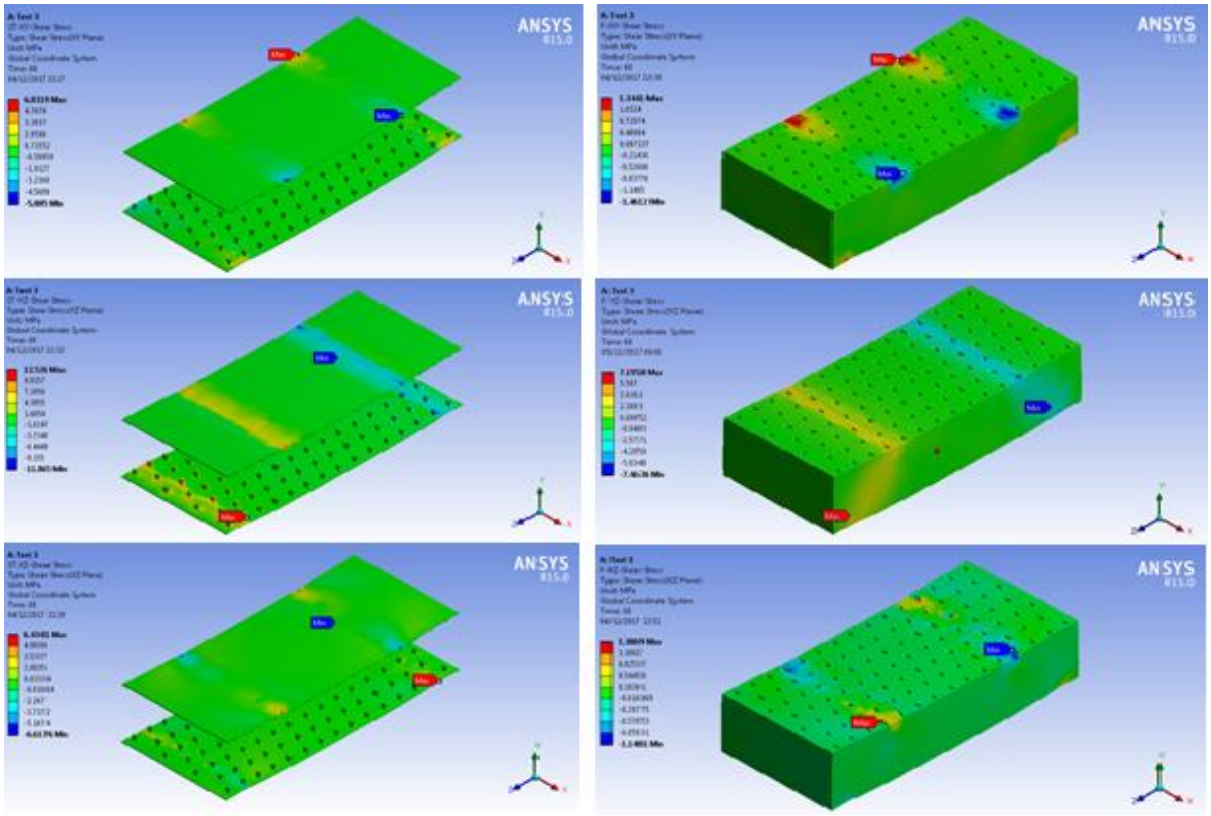

Figure 7.23: Distribution of component of shear stress on the skin and foam core at collapsing mode

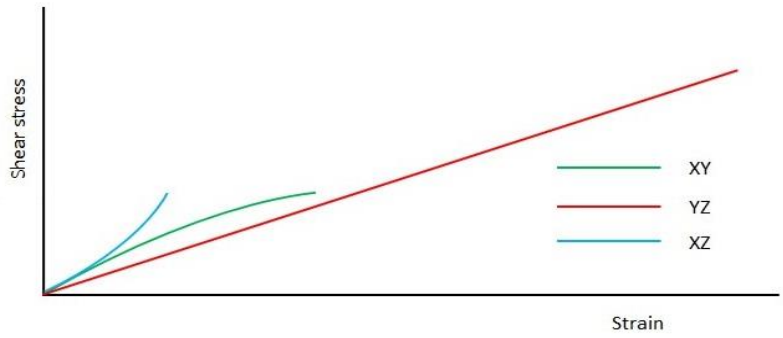

Figure 7.24: Schematic stress-strain diagrams of XY, YZ and XZ component of shear at composite panel

7.7 Conclusion

Foam filled sandwich panels are one of the most popular and widely investigated types of composite structures. In this study an innovative sandwich panel comprising 3D-HDPE skin layers and a high-density foam core was proposed and the flexural and shear behaviour was investigated by experimental and numerical research. The results showed that using 3D skins with 1200 studs per square meter, the composite sandwich panels resulted in a strong and stable composite section than individual sandwich sections alone. Results of the quasi-static three-dimensional model and the material nonlinear simulations of the sandwich panels also indicate that under flexure, the foam core and skins displacement are in sync, which demonstrate well integrated and ductile behaviour of the introduced composite panel.

Chapter 8

Bending behaviour of seamed foam made structural sandwich panels

The contents of this chapter have been accepted to publish in the form of a journal paper as follows:

Saeed Nemati (Full contribution), Pezhman Sharafi (Scientific supervision) and Bijan Samali (Scientific supervision), “Effects of Cold Joints on the Structural Behaviour of Polyurethane Rigid Foam Panels”. Engineering Solid Mechanics (ESM), 2018, Canada.

8.1 Introduction

Light weight structural panels are one of the most popular types of mobile and rapidly assembled structures. Rapidly assembled panels are a form of modular construction, commonly used in residential buildings, as well as industrial structures [33-35]. Some advantages of this system are: (1) They can sit on each other as plate, so substantially reduce the transportation cost per unit; (2) Can be made in any sizes and consequently cut the construction time; (3) Can be connected to each other quickly for quick assembly construction; (4) Can play the role of structural elements, partitions and/or insulators at the same time. Such advantages make structural panels an attractive alternative to the traditional construction systems in the recent years. A wide range of these panels are made from new lightweight components such as foams. Many types of foams are on the market and the Polyurethane (PU) foams are the most popular types [20]. The lightweight penalised foam made products are popular because they are light, easy to install and have good thermal and acoustic properties. However, the effects of construction accuracy, technology and methods on the mechanical behaviour of structural panels are significant. One of the most important construction problems of foam made panels is cold joints, which is also known as seams. When the placing of foam in the panels is delayed or interrupted for some reasons, the foam that has already been placed starts to condense, producing a kind of construction joint (seam) called a cold joint between it and newly placed foam. Seam is a plane under mixed material, or a fold that is developed within the rising foam mass, which appears as a line on the foam surface or section, as shown in Figure 8.1. Such joints between new and old portions of foam that are formed when new foam is placed adjacent to the foam that has hardened or has started to harden, may have negative effects on the strength of rigid foam panel. Hence, attention must be paid to the position and direction of the joints, and the effects on the structural behaviour

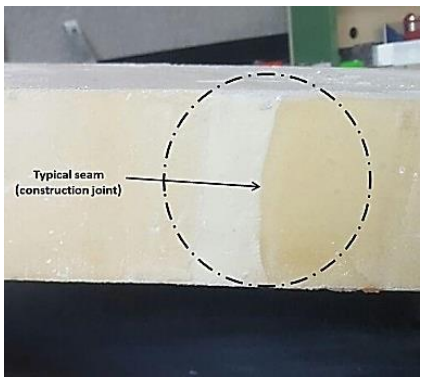

Figure 8.1: Typical studied seams

There are some research studies on the structural applications of foams. Zenkert et al. [157] studied tension, compression and shear fatigue of a closed cell polymer foam, where the foam is tested quasi-statically in tension, compression and shear. Fatigue crack propagation in a closed-cell foam is experimentally investigated by Fan et al. [158]. They conducted series of fatigue tests to obtain crack length vs loading cycle number and fatigue crack propagation rate vs stress intensity. In a similar work, Zhao et al. [159] carried out tension–tension fatigue tests to investigate the fatigue of closed-cell foam. Noble et al. [160] studied the fatigue crack growth in rigid polyurethane foam under conditions of constant load-amplitude cycling. Shipsha et al. [161] carried out an experimental study of fatigue crack propagation in polymeric cellular foam cores for sandwich structures. In a similar work, Poapongsakorn et al. [162] investigated the applicability of linear-elastic fracture mechanics, elastic–plastic fracture mechanics and time-dependent fracture mechanics parameter to characterise fatigue crack growth rate of closed-cell polyvinyl chloride. Kanny et al. [163] ran some dynamic mechanical analyses and flexural fatigue of PVC foams of densities in the range from 75 to 300 kg/m^3. In which the fatigue behaviour was found to be similar to structural materials with a fatigue strength that increased with foam density. Huang et al. [164] analysed the fatigue of cellular materials using dimensional arguments. They found out that the fatigue of cellular materials depends on the cyclic stress intensity range, cell size, relative density and the fatigue parameters of used material. Wang et al. [165] focused on the influence of pores on crack initiation in monotonic and cyclic tensile loadings. Pores were shown to have an important influence on strain localization zones for crack initiation both in monotonic tensile and cyclic loadings. Toubia et al. [166] studied the effects of core joints in sandwich composites under in-plane static and fatigue loads. Their research confirmed that despite the face sheets' primary in-plane load carrying mechanisms, core junction substantially influence the axial fatigue life of the structure. In this study, the effect of seams on the structural behaviour of PU rigid foam panels will be studied through some experiments on the seamed and seamless samples, under monotonic and cyclic loads. The results will be compared with each other in order to investigate the impact of presence of seams on the bending strength of samples.

8.2 Material Properties

To evaluate the basic material properties, in addition to using the manufacturers' data, some experimental tests were carried out. In this regard, PU high-density rigid foam with the

density of 192 kg/m^3 was chosen. Table 8.1 shows the used foam's manufacturing and mechanical properties, provided by the manufacturer and validated in the laboratory using the ASTM 1730 standard specification for rigid foam [22]. Three 50mm×50mm×50mm cubic specimens were tested by a uniaxial load machine, at a loading rate of 5 mm/min in order to identify the structural properties of the rigid PU foam. The results show that this type of PU foam, which is made of a 100:110 weight ratio mixture of AUSTHANE POLYOL AUW763 and AUSTHANE MDI ISOCYANATE (Figure 8.2), can undertake considerable deformation before the failure. In addition, the elastic modulus of foam has been calculated as 135.5 MPa [42, 58, 167].

Table 8.1 Mechanical and manufacturing properties of the selected PU rigid foam

Mechanical Properties of the PU foam			
Density (kg/m^3)	Compressive yield strength (MPa)	Tensile yield strength (MPa)	Shear yield strength (MPa)
192	3.51	1.896	1.034
Manufacturing Properties			
Cream time[1]	Gel time[2]	Tack free time[3]	
35-40 sec	94 ± 4 sec	115 ± 5 sec	

[1]A measure of the beginning of the foam reaction. Usually characterised by a change in the liquids color as it begins to rise.
[2]The time when the foam has developed enough gel strength to be dimensionally stable.
[3]The time between the beginning of the foam pour and the point at which the outer skin of the foam loses its stickiness.

8.3 Description of Specimens and Test Setup

In this study, three series of bending tests were carried out on two types of panelised specimens. Two types of 1500*1000*100 mm^3 rigid polyurethane panels were used: Type S (seamless) and type TS (with transverse seams) specimens. The expansion rate of this type of foam is 3.0, and the average weight of both types of panels is 29.0 kg. In order to make seamless samples, "one shot pouring system" was employed. To that end, 50 litres of mix liquid material is casted in the wooden formworks with a filling rate of 1.25 litres per second.

The TS panels were casted with five cold joints H1 to H5, as shown in Figure 8.2. In fact, TS specimens were made during six pouring steps, using 8.3 litres of mix liquid material for each step and with the same filling rate. Figure 8.3 illustrates the casting schedule for each step.

Figure 8.2:. Locations of transverse seams (H1-H5)

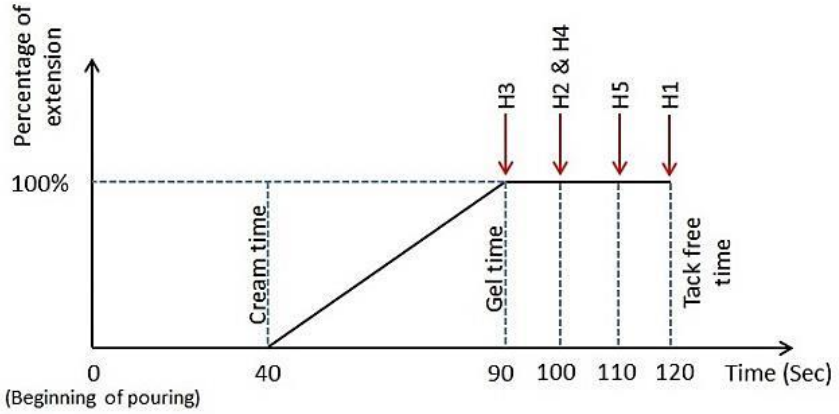

Figure 8.3: Casting schedule of seams at TS specimens

8.3.1 Test Setup

The tests were undertaken using an automated vacuum rig at the Centre for Infrastructure Engineering (CIE) at Western Sydney University. The rig allows for undertaking loading test on panels of heights up to 6m under a vacuum suction of up to 10 kPa. The panels were horizontally loaded into the test chamber, fixed and sealed; the chamber is pulled up by an electric winch until it stands vertically before the suction is applied. The loading regime can be change according to the requirements. In order to adhere to an appropriate regime of loading, the rig enjoys a fully automatic controller, which utilises powerful software developed within the LabView Environment (NI, 2016). Figure 8.4 shows the vacuum test rig setup, and Figure 8.5 illustrates the locations of automatic electrical potentiometers.

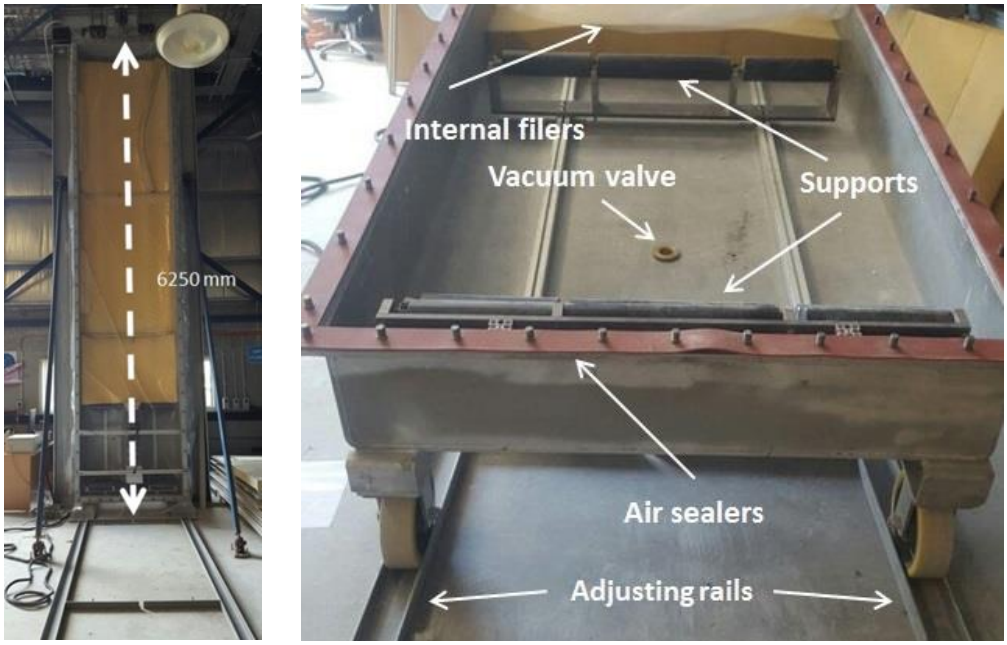

Figure 8.4: Details of vacuum testing rig

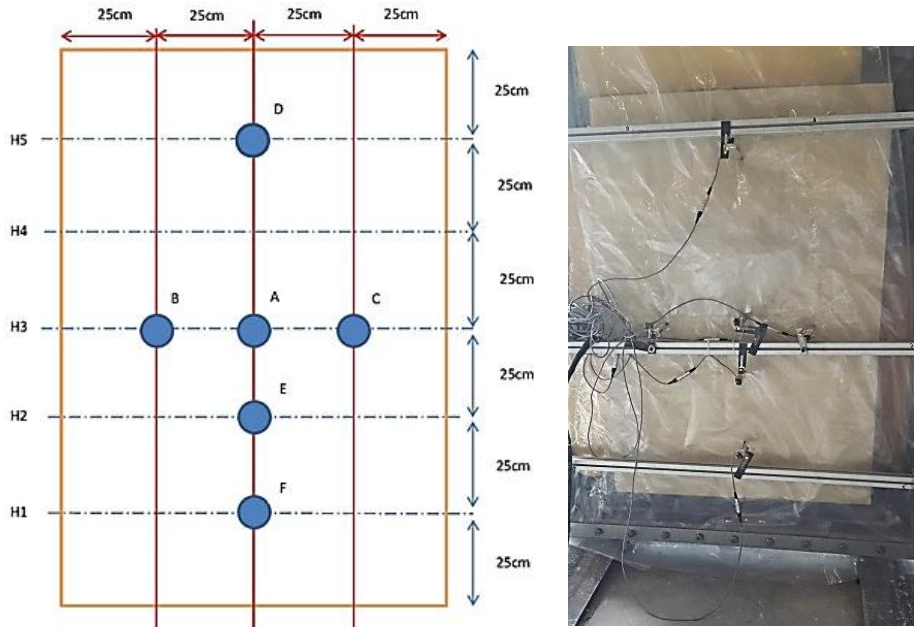

Figure 8.5: Arrangement of potentiometers on panels (for all tests)

8.3.2 Testing Program

Three monotonic tests were conducted on the S and TS specimens, together with three cyclic tests on the TS specimens. Table 8.2 shows the summary of the test arrangement. First series of bending tests carried out on the S panels using a uniform monotonic under about 1 atm air pressure (Load Regime #1) with a rate of 0.1 atm/min. The second series of bending tests were carried out on the TS panels using the same loading regime (Load Regime #1).The third series of bending tests were conducted on the TS panels, using a predicted cyclic air

pressure (Load Regime #2) with a rate of 0.1 atm/min, as shown in Figure 8.6.

Table 8.2 Test arrangement matrix

Test series	Specimen	Number of specimens	Load configuration
1	S	3	Monotonic
2	TS	3	Monotonic
3	TS	3	Cyclic

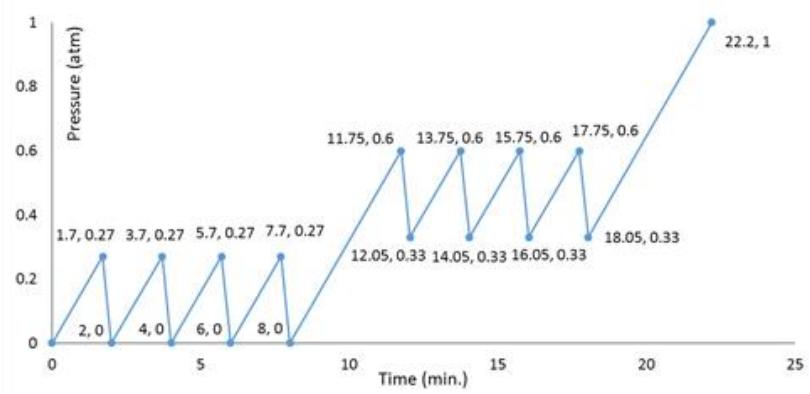

Figure 8.6: Cyclic regime of loading, used at second series of bending tests

8.3.3 Test Results

For the test series #1, all three seamless panels resisted a maximum of 0.77 atm. Figure 8.7 and Table 8.3 show the pressure-deflection diagram and the deflections measured by potentiometer, respectively. Up to a pressure of about 0.23 atm, where shows a large primary deflection, the system is in the adjusting phase, and the pressure is not directly resisted by the panels. Afterwards, the PU foam panels exhibits a relatively linear behaviour up to about 0.77 atm. In addition, the seamless panel showed a symmetric curvature under the applied monotonic load. Figure 8.8 depicts this curvature for longitudinal and transverse direction.

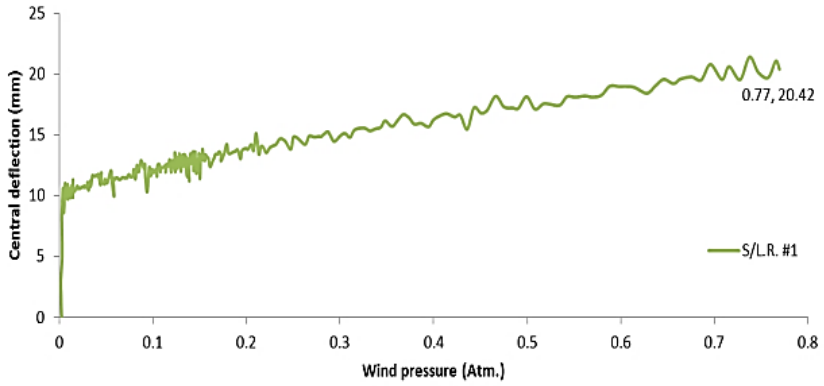

Figure 8.7: Vacuum pressure vs average central deflection (point A) for test series #1

Table 8.3 Deflection at points A to F for test series 1

S panels L.R. #1	Direction	First monotonic test (mm)	Second monotonic test (mm)	Third monotonic test (mm)	Average (mm)	Standard Deviation	CV%
D	longitudinal	14.2	15.1	16	15.1	0.9	6
A	longitudinal	19.7	20.8	20.7	20.4	0.61	3
E	longitudinal	18.3	17.3	18.1	17.9	0.53	3
F	longitudinal	14.7	16.2	16.2	15.7	0.87	5.5
B	transverse	12.2	13	14	13.1	0.9	6.9
C	transverse	12.9	14.1	13.8	13.6	0.63	4.6

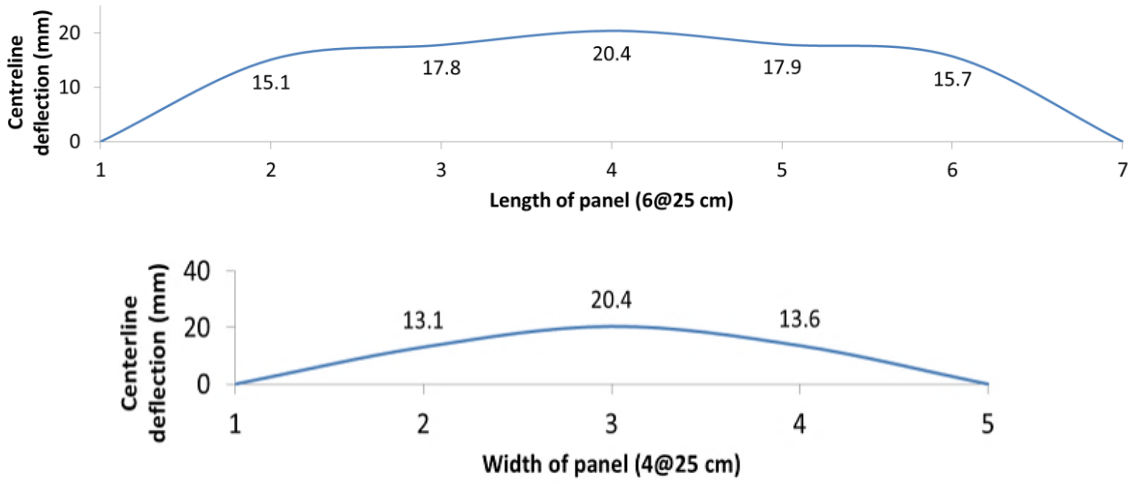

Figure 8.8: Symmetric distribution of deflection at the longitudinal & transverse direction (test series 1)

A comparison between measured deflections, shown in Figure 8.9, point A is at the maximum deflection in all tests.

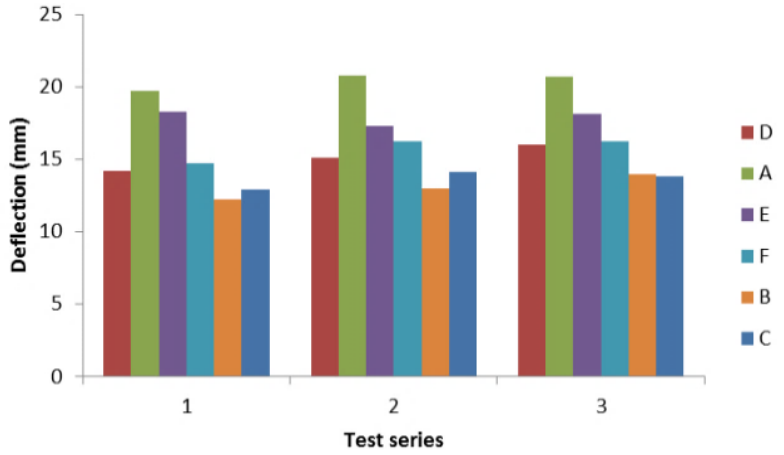

Figure 8.9: Comparison between measured deflections (test series 1)

According to these results, the minimum tensile strength of foam can be calculated by Eq. (1), in which $\sigma_{\min,foam}$ is the minimum tensile strength of foam; M is the maximum bending moment (at point A); y is half of the panel thickness (5cm); I is the section's moment

of inertia; q is the load equivalent linear intensity; and L is the span [55, 56]. Accordingly, this rigid foam panel exhibits a minimum of 13.00 MPa tensile strength.

$$\sigma_{\min,foam} = My / I = qL^2y/(8I) \qquad (1)$$

8.3.4 Test Series 2

In these series of tests, three TS panels were tested under monotonic loading. For all of these panels, similar to test series 1, the maximum deflection appeared at the point A with an average amount of 17.02 mm. Nevertheless, all of these panels collapsed at an average pressure of 0.46 atm at the seam H1 as shown in Figure 8.10. Therefore, the main mode of collapse is assumed tensile at the seam.

Figure 8.10: Typical collapse mode of TS panels at seam H1 under monotonic loading (test series 2)

Similar top the previous case, as shown in Figure 8.11, up to about 0.23 atm, the system is at adjusting phase and exhibits a large primary deflection. Then, TS panels have a semi-linear behaviour before it reaches a pressure of about 0.46 atm. The deflections of pre-identified points of TS panels were measured by potentiometer on the surface. Results shown in Table 8.4 demonstrate very similar behaviours with those for TS panels under monotonic loading.

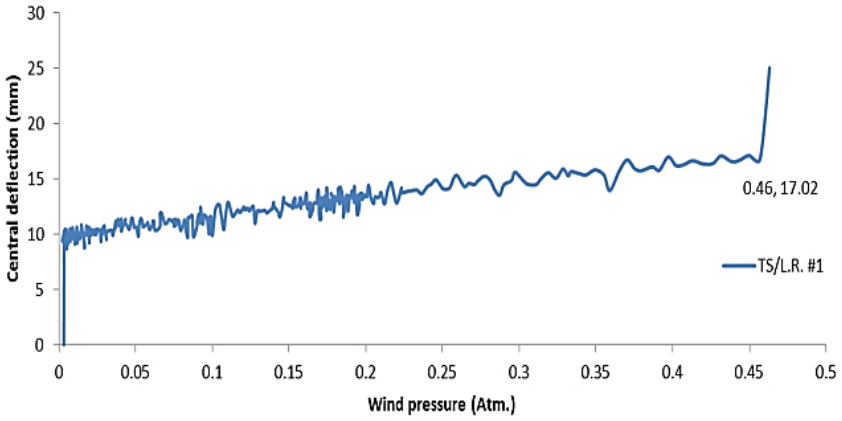

Figure 8.11: Wind pressure vs average central deflection in test series 2

Table 8.4 Deflection at points A to F for test series 2

TS panels L.R. #1	Direction	First monotonic test (mm)	Second monotonic test (mm)	Third monotonic test (mm)	Average (mm)	Standard Deviation	CV%
D	longitudinal	11.8	10.6	11.5	11.3	0.63	5.6
A	longitudinal	16.76	16.9	17.4	17.02	0.34	2
E	longitudinal	15.5	13.6	14.4	14.5	0.95	6.6
F	longitudinal	10.6	12.2	12.3	11.7	0.95	8.1
B	transverse	8	9.6	9.1	8.9	0.82	9.2
C	transverse	7.7	9.1	9.3	8.7	0.87	10

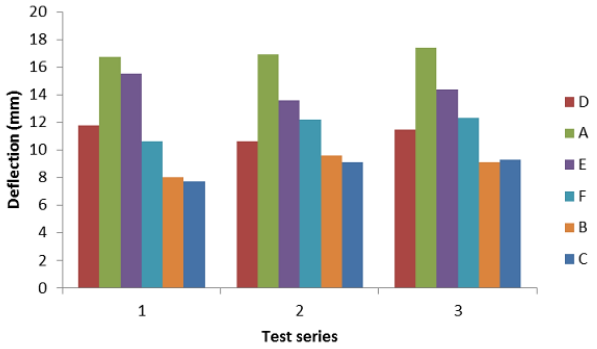

Figure 8.12: Comparison between measured deflections of points A to F (test series 2)

Figure 8.12 shows a comparison between the measured deflections. Based on the results, in all of the tests, point A (the intersection of centrelines) shows the maximum deflection. In addition, as depicted in Figure 8.13 the TS panels exhibit symmetric curvature under monotonic loading in both directions. Figure 8.14 illustrates the model used for the analytical analysis of test series 2. The maximum tensile strength of seams under monotonic loading, therefore is calculated by Equation (2), in which σ_{max} is the maximum tensile strength of the seams. Other parameters are the same as those for Eq (1). Accordingly, this rigid foam panel exhibits a maximum of 4.3 MPa tensile strength.

$$\sigma_{max,seam} = My / I = \text{qxy(L-x)/(2I)} \qquad (2)$$

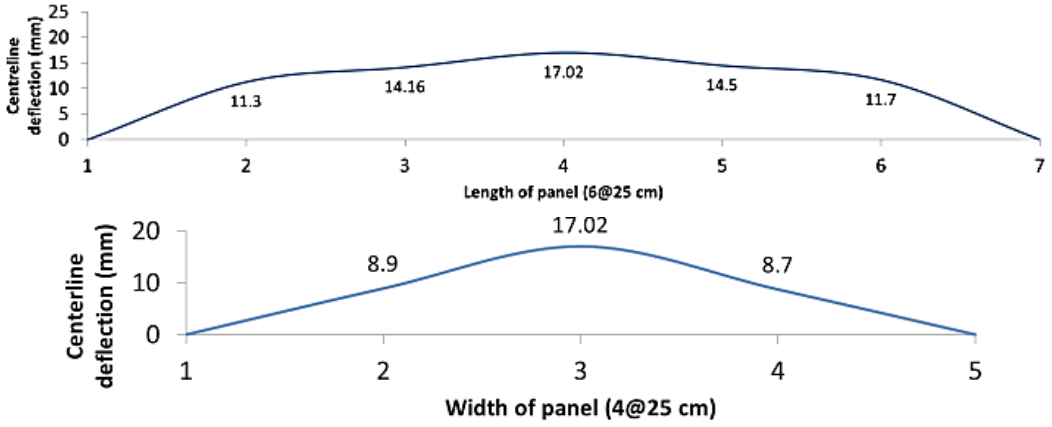

Figure 8.13: Distribution of deflection in longitudinal and transverse direction in test series 2

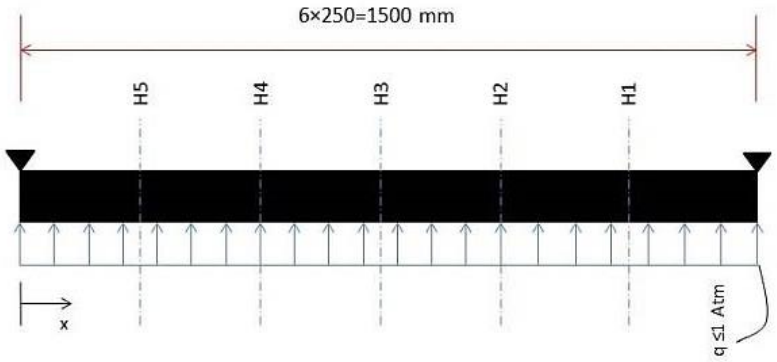

Figure 8.14: Analytical model of test series 2

A comparison between results from Figure 8.7 and 8.11 shows that under monotonic loading, the seamless panels have a larger deflection capacity of about 20% compared to the TS panels (Figure 8.15).

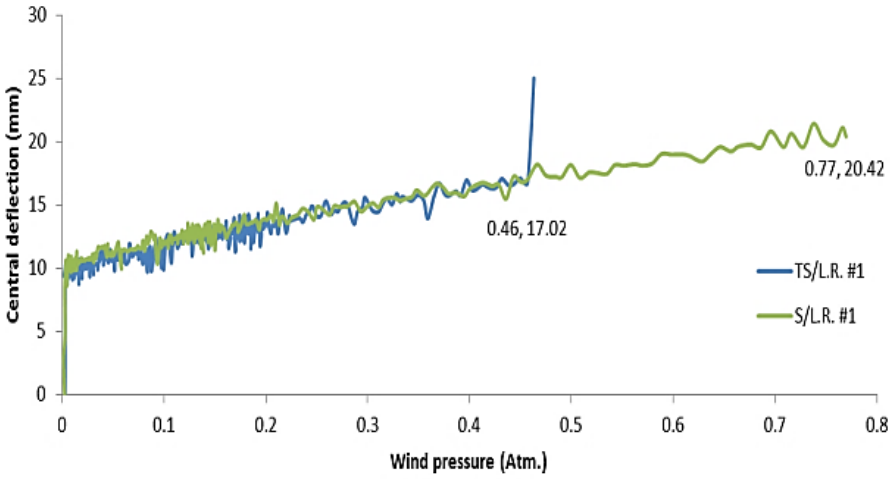

Figure 8.15: Comparison between bending behaviours of S and TS panels under monotonic loading

8.3.5 Test Series 3

Three TS panels were tested under cyclic loading, where the results showed all the panels resisted up to a maximum pressure of about 0.33 atm. The deflections of points A to F have been measured by electrical automatic potentiometers, as shown in Table 8.5. All three panels collapsed at the seam H1 under an average deflection of 8.9 mm. Figure 8.16 shows a comparison between the deflections of points A to F. The minimum deflection occurred at Point F, while the maximum deflection of longitudinal centreline of the panel appeared at point A with an average amount of 17.02 mm. It can be seen that the tensile weakness of the seam is the main reason of failure.

Table 8.5 Deflection at points A to F for test series 3

TS panels L.R. #2	Direction	First cyclic test (mm)	Second cyclic test (mm)	Third cyclic test (mm)	Average (mm)	Standard Deviation	CV%
D	longitudinal	9.9	9.1	9.8	9.6	0.44	4.6
A	longitudinal	11.5	11.4	11.6	11.5	0.1	0.9
E	longitudinal	9.7	9.8	10.2	9.9	0.27	2.7
F	longitudinal	9.4	8.6	8.7	8.9	0.44	4.9
B	transverse	14.1	13.4	13.6	13.7	0.36	2.6
C	transverse	13.8	14.1	13.8	13.9	0.17	1.2

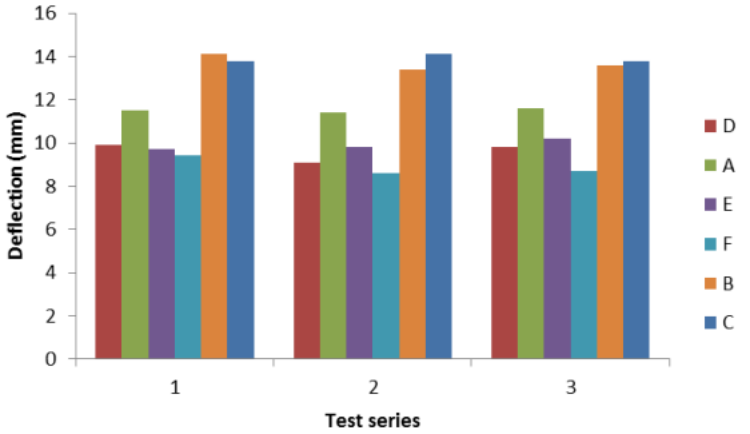

Figure 8.16: Comparison between deflections of points A to F in test series 3

Figure 8.17 depicts the symmetric distribution of deflection at the longitudinal and transverse centrelines of TS panels. In addition, deflections of the transverse distortion can be seen in this Figure 8.18. Using Eq. (2), the maximum tensile strength of seams under cyclic loading is calculated as 3.1 MPa.

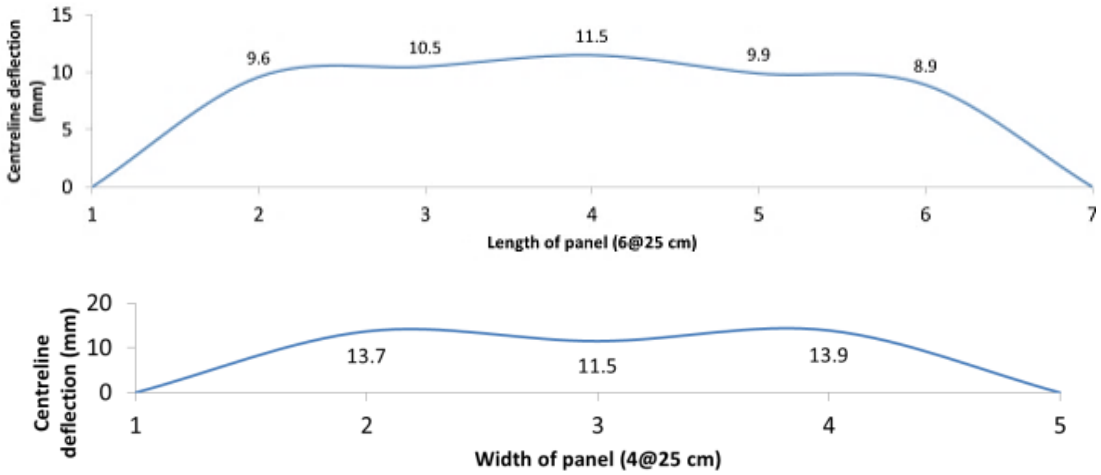

Figure 8.17: Distribution of deflection at length (top) and width (down) of panels in test series 3

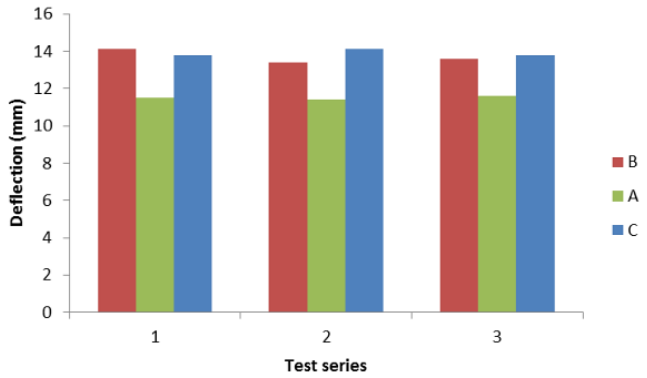

Figure 8.18: Comparison between deflections of transverse points A to C for test series 3

8.3.6 Hysteresis Behaviour

Figure 8.19 shows the applied pressure vs max deflection of points A, B and C in the test series 3. Based on this figure, point A has the most regular and narrowest hysteresis diagram, with the minimum capacity for energy absorption. However, points B and C showed better and relatively more similar hysteresis behaviour that demonstrates that the TS panels exhibit rather symmetric hysteresis behaviour in transverse direction under cyclic loads.

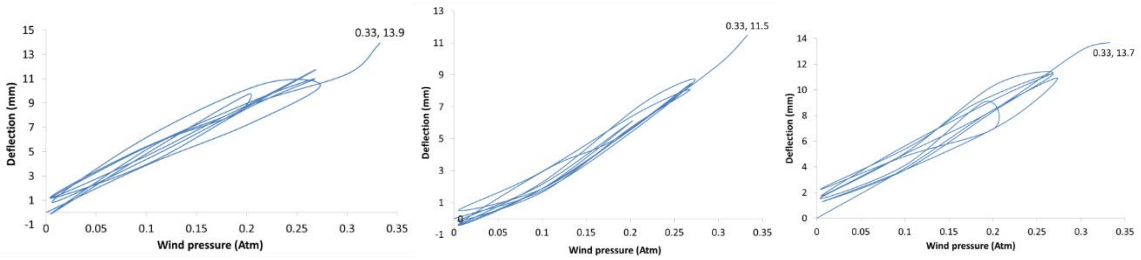

Figure 8.19: Applied pressure vs deflection of point B, A and C in test series 3 (left to right) in test series 3

The applied cyclic pressure vs max deflection of points D, A and F in the test series 3 are shown in Figure 8.20. It reveals that points D and F exhibit two different hysteresis behaviours: Point D has a relative wide and irregular hysteresis diagram in comparison with the point F. The different internal structure of seams at these points can be assumed as the main reason of such difference.

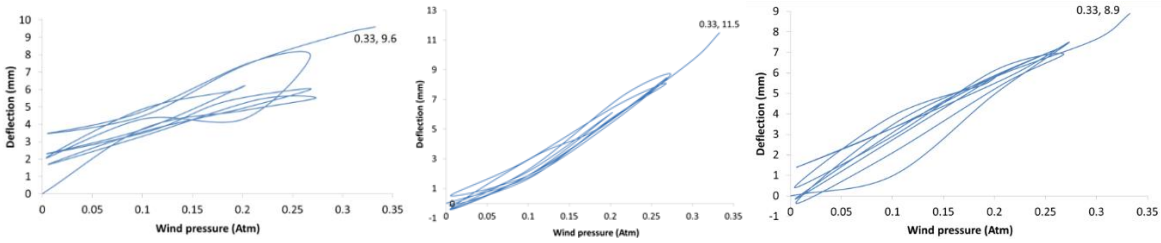

Figure 8.20: Applied pressure vs deflection of points D (left), A (middle) and F (right) in test series 3

The deflection time history of points A to F in test series 3 are shown in Figures 8.21 and 8.22. The relative areas of these graphs addressing the relative energy absorption capacity of seams H1 to H5 under cyclic loading are calculated and presented in Table 8.6.

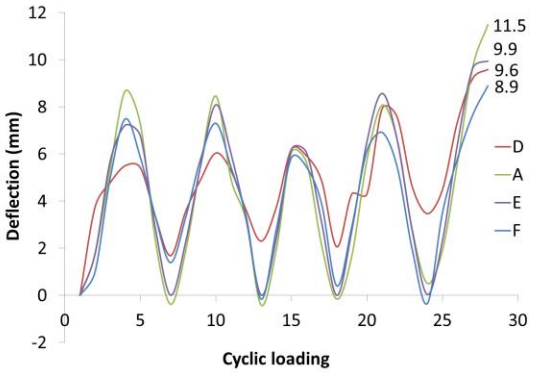

Figure 8.21: Deflection time history for longitudinal centreline in the test series 3

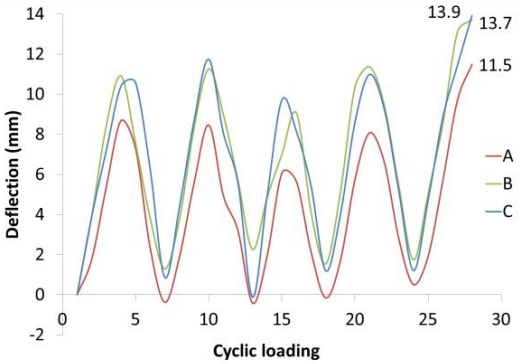

Figure 8.22: Deflection time history for transverse centreline in the test series 3

Table 8.6 Comparison between relative absorbed energy at seams H1 to H5 under cyclic loading

Seam	H1	H2	H3	H4	H5
Relative absorbed energy	1	1.02	1.53	1.02	1.21

Comparison between Table 8.6 and Figure 8.5 indicates that making the seams at end of the gel time (H3) can increase the energy absorption capacity by 53%, compared to the end of take free time (H1).

8.4 Concluding Remarks

A comparison between the results of the monotonic tests shows that:

- ✓ Casting at the end of gel time instead the end of tack free time, resulted in an %80 increase in the tensile strength of the seams ($[X_{H1}(L-X_{H1})] / [X_{H3}(L-X_{H3})]$).
- ✓ Casting at about 20 sec before of the end of tack free time (120^{th} sec), increased the tensile strength of the seams by %60 ($[X_{H1}(L-X_{H1})] / [X_{H4}(L-X_{H4})]$).
- ✓ The seamed section exhibited about 33.1% of the maximum tensile strength of an intact section.
- ✓ Under monotonic loading, the seamless panels showed a larger deflection capacity, as 20% more than that of TS panels.

A comparison between the results of the cyclic tests shows that:

- ✓ Casting at the end of tack free time (120^{th} sec) instead of 110^{th} sec resulted in a significant positive effect on the tensile strength of seams.
- ✓ The tensile strength of a seamed section was under cyclic loading about 72.1% of the strength under monotonic loading.
- ✓ Making the seams at the end of the gel time increased the energy absorption capacity of panels by 53% in comparison with the end of take free time.

Chapter 9

Integrated connections between foam filled modular sandwich panels

The contents of this chapter have been published in the form of a journal paper as follows:

P. Sharafi (Scientific supervision), S. Nemati (Full contribution), B. Samali (Scientific supervision), A. Bahmani (General advising) and S. Khakpour (English language editing), “Behaviour of Integrated Connections Between Adjacent Foam Filled Modular Sandwich Panels”. Engineering Solid Mechanics (ESM), June, 2018 Vol.6, Issue 4, online, DOI: 10.5267/j.esm.2018.6.001, Volume 6 Issue 4 pp. 361-370, 2018, Canada.

9.1 Introduction

Composite lightweight sandwich panels are an effective solution for building construction due to their high strength to weight ratio and adequate levels of acoustic and thermal insulation. Building systems made of composite sandwich panels can be quickly assembled on site, allowing for considerable time savings in fabrication and assembly. Sandwich panels are being increasingly used in civil engineering structural applications, and have already been successfully applied in the construction of walls, roofs and building envelope [168]. There are several types of sandwich panels with different facing or core materials, as well as various geometric designs. Polyurethane (PU) foam filled sandwich panels are one of the most popular kind of them. In addition to non-structural applications of polyurethane foam filled sandwich panels, they can be parts of the structure of buildings [140]. Low self-weight and relatively high stiffness and durability have increased the demand for this type of composite structures. In fact, foam-filled sandwich construction, characterised by two relatively thin and stiff faces and a relatively thick and lightweight foam core, is becoming an interesting solution for building wall and floor systems. Many studies in the Literature indicate that the stiffness and strength of a majority of conventional foam-filled sandwich panels and connections hardly meet the structural requirements for use in building floors or walls, at least for standard spans and loads, mainly due to some different failure modes such as delamination of the skins from the core, buckling or wrinkling of the compression skin, flatwise crushing of the core or rupture of the tension skin. The main deficiencies of this type of composite panels are their low load carrying capacity and susceptibility to the occurrence of local and global failure modes, compared those made by traditional materials, like concrete and steel [169]. In addition, when designing structures by sandwich panels, they must be efficiently interconnected upon assembly, in order to provide an integrated system [33, 35, 36], i.e. appropriate connection systems between composite sandwich panels must be provided. The design of such connection is not an easy task. That is why, although different solutions for the connections between adjacent sandwich panels have been considered in the construction industry, a large majority of them have been developed for non-structural or secondary structural sandwich panels. The rigidity and flexibility of innovative composite connections in buildings design, have been widely investigated in the literature. Kempf and Feldhusen [170] has focused exclusively on finding about 850 solutions to mechanically connect sandwich panels. In another study, Garrido et al. [168]. studied the connections

between adjacent composite sandwich panels for use in building floor rehabilitation, and proposed an adhesively bounded connection system. Mohan et al. [171] studied the moment–rotation behaviour and the joint stiffness of a series of beam–column connections using a single cantilever test set-up. Kujawa et al. [172] investigated rotational resistant stiffness of the zed-purlins connection with sandwich panels. A new foam-filled sandwich panel was developed by Sharafi at al. [42, 58, 173], which is composed of 3-D high density Polyethylene (HDPE) sheets, as the skins with a thickness as 2 mm, and high-density PU foam core with a total thickness as 100 mm. This paper investigates the performance of the integrated connections for the newly developed composite panel, and experimentally and numerically assesses their structural performance under monotonic loading. The integrated connection system between adjacent sandwich panels for use in rapid assembly construction for post-disaster housing is studied. Experimental and numerical investigations are conducted to study the connections' behaviour under actual loading conditions, the overall mechanical response, and the stress distributions. To that end, the panel-to-panel joints are tested to evaluate failure modes, moment resistance, initial rotational stiffness and rotational capacity of the connections. These connections are experimentally tested under vertical loads in a cantilever configuration. Then, using finite element (FE) analysis and the obtained moment–rotation relationships, the stress distributions in the connection components are investigated.

9.2 Description of the Panels and Integrated Connections

In order to enhance the properties of the foam-filled sandwich panels, a new sandwich panel was proposed, with 3-D HDPE skins HD-PU foam core, as shown in Figure . The HDPE sheets manufactured with approximately 1200 studs per square meter, provide higher pull-out and delamination strength, as well as better stress distribution, and buckling performance [42, 58, 173]. The studs also improve the resistance of the face sheets and foam-core from debonding and increasing the interface strength between the foam-core and the face sheets. Table 9.1 presents some physical and mechanical properties of HDPE sheets and PU high-density rigid foam.

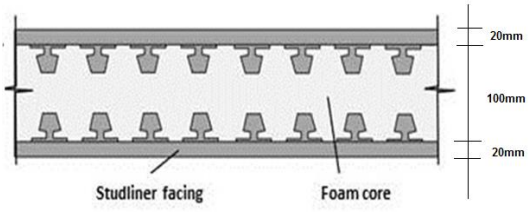

Figure 9.1: Sandwich sections with 3D-HDPE skins and HD-PU foam core

Table 9.1 Physical and mechanical properties of the HDPE skins and PU core

		HDPE sheets		
Density (kg/m^3)	Thickness (mm)	Tensile yield trength (MPa)	Shear yield strength (MPa)	Modulus of elasticity (Mpa)
940	2	20.2	5.2	159
		PU foam		
Density (kg/m^3)	Compressive yield strength (MPa)	Tensile yield trength (MPa)	Shear yield strength (MPa)	Modulus of elasticity (Mpa)
192	3.51	1.9	1.03	135.5

The fabrication of these sandwich panels takes place in one step. Therefore, the face sheets and foam core are integrated into one element. This innovative sandwich panel was developed to be used as modular walls and floors in rapid assembly buildings, in a recent research project on the semi-permanent post disaster housing at the centre for infrastructure engineering in Sydney. The connections between the panels are constructed by continues foam casting to achieve better integrity.

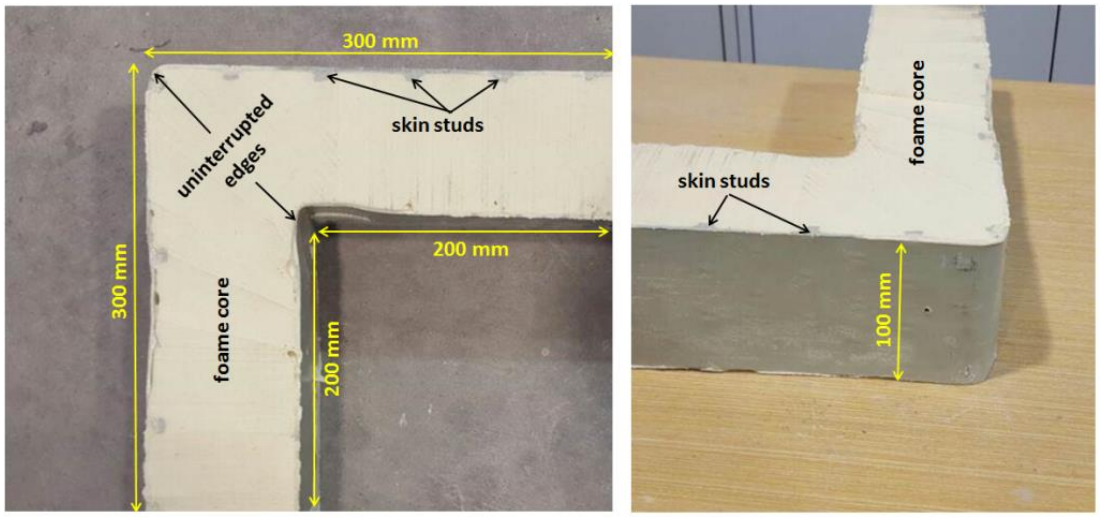

Figure 9.2: Integrated connection with HDPE skins and PU foam core

The primary function of these connections is to guarantee the transfer of lateral (seismic and wind) loads between the composite panels, as well as between panels and roof in rapid assembly post disaster buildings. In addition, this connection accounts for restricting the rotation, i.e. the maximum deflections along the span. This is a significant factor because in practice, the maximum allowable deformation is usually the governing factor in the design of lightweight composite sandwich panels [58].

9.3 Experimental Investigation

The structural behaviour of a connection depends, for a given type of load, on the stress distribution within the connection, which in turn depends on the joint geometry and the mechanical properties.

9.3.1 Test Setup

Six L shape specimens, representing the connections between adjacent sandwich panels, are tested. In order to better study the composite performance and compare the results with non-composite behaviour, three of the specimens were made of composite sections, while here of them were foam-only sections; all of them were manufactured by one shot casting method in wooden formworks and were cut out of actual adjacent sandwich panels. The composite connections comprised of 2 mm thick 3-D HDPE face sheets enclosing a 96 mm thick core of rigid PU foam. A summary of the most relevant properties of the constituent materials used in the connection, obtained from material characterisation tests ASTM E1730, ASTM D1621 [149], ASTM D5199 , ASTM D1505 and ASTM D6693 [49], are shown in Table 9.1. The test specimens were supported in a cantilever configuration test rig, and a point load was applied at 40 mm of the free edge, as illustrated in Figure . The vertical angle that supported the cantilever angle was connected to a steel frame comprised of fixed profiles by a bolted steel strip with a width of 50 mm. The vertical displacement was measured at the top face of the cantilever angle at the load application point by a displacement transducer automatically and with a stroke of 700 mm and precision of 10e-5 mm. Load was applied by a 300 ton hydraulic jack with a displacement rate of 5 mm/min according to literature. A load distribution steel plate (15 mm thick, 100 mm long and 80 mm wide) and a roller were positioned between the test specimen and the hydraulic jack. Additionally, as shown in Figure the local rotations of specimens were measured at four points of cross-section by electrical inclinometers with a precision of 10e-6 degree. Using these inclinometers the relative rotation of any two points can be calculated as difference of related inclinometers rotations [174]. To study the behaviour, the specimens were monotonically loaded up to failure.

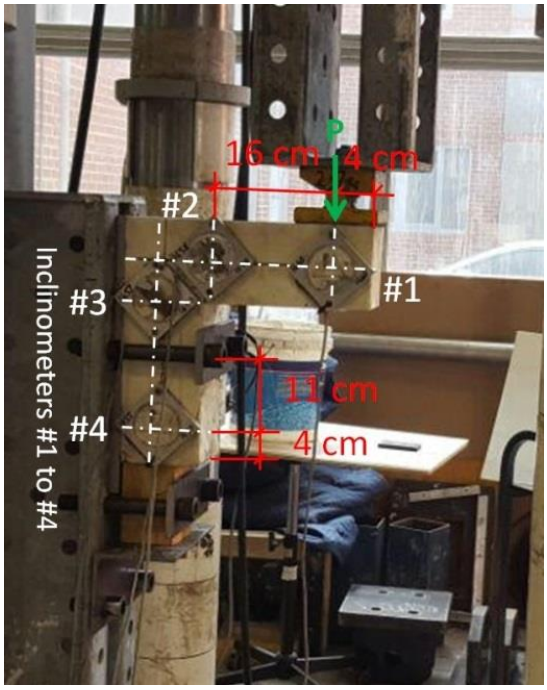

Figure 9.3: Cantilever configuration of experimental tests

9.3.2 Test Results

The results obtained from the experimental tests are illustrated in Figures 9.4 through 9.7. Figure 9.4, and Figure 9.5 illustrate the load-displacement curves obtained for foam-only and composite connection systems respectively; and Figures 9.6 and 9.7 illustrate the load vs. connection angle (Δ) obtained for simple and composite connection systems respectively. Table 9.2 presents a summary of the ultimate (or failure) loads, ultimate connection angle and ultimate displacement for both simple and composite systems. Detailed discussion is provided in the following sections for each type of connection.

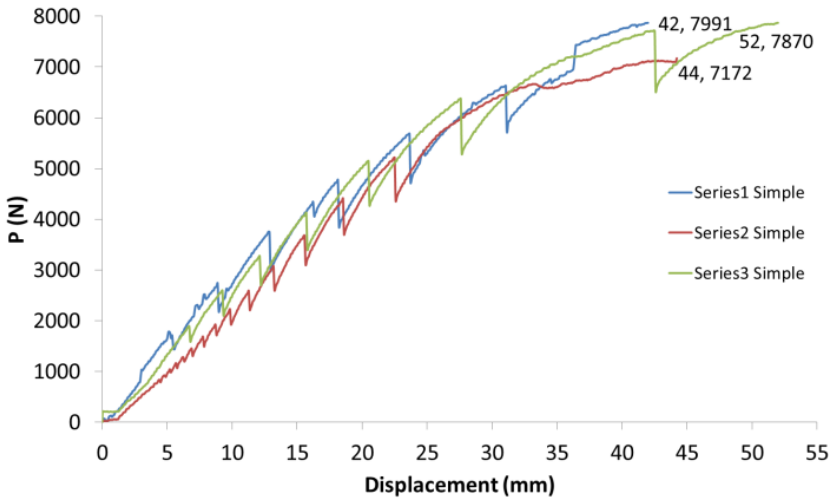

Figure 9.4: Load vs displacement for foam-only specimens at loading point

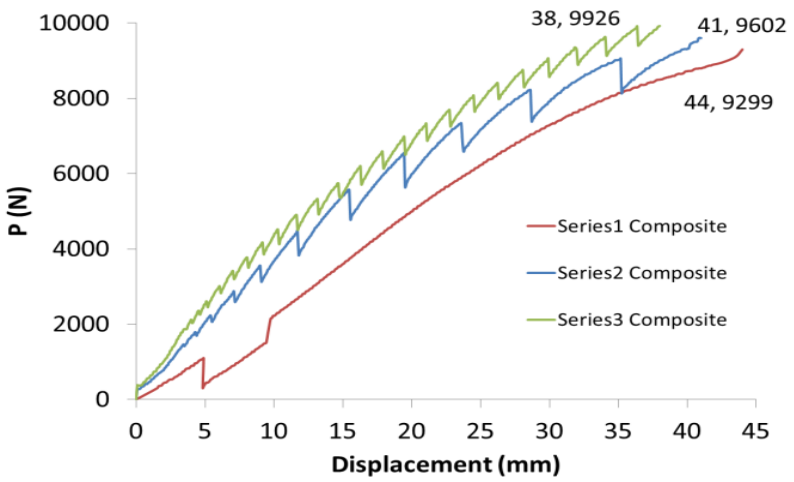

Figure 9.5: Load vs displacement for composite specimens at loading point

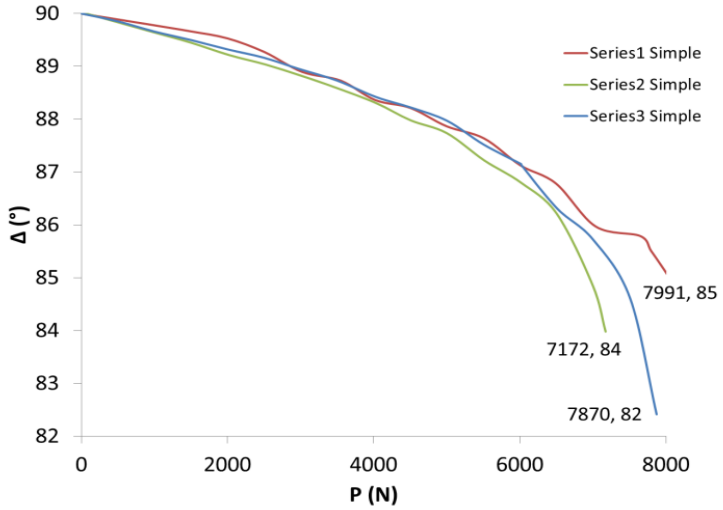

Figure 9.6: Load vs connection angle (Δ) curves for foam-only specimens

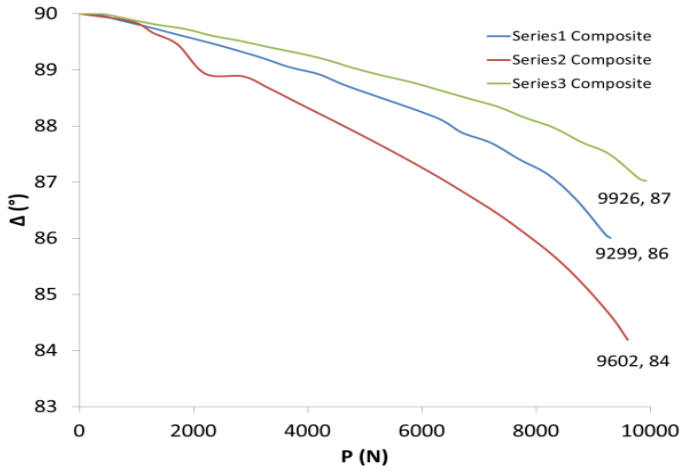

Figure 9.7: Load vs connection angle (Δ) for composite specimens

Table 9.2 Summary of the experimental carried tests for both simple and composite systems

Test Details		Ultimate Load (N)	Ultimate Displacement (mm)	Ultimate Rotation (Degree)
Foam-only Tests	Specimen 1	7991	42.0	5.0
	Specimen 2	7172	44.0	6.0
	Specimen 3	7870	52.0	8.0
	Average	7678	46.0	6.3
	CV (%)	5.8	11.5	1.8
Composite Tests	Specimen 1	9299	44.0	4.0
	Specimen 2	9602	41.0	6.0
	Specimen 3	9926	38.0	3.0
	Average	9609	41.0	4.3
	CV (%)	3.3	7.3	1.8

9.4 Discussion

9.4.1 Behaviour of Foam-Only Connections

As the diagram indicates, all the foam-only connection specimens presented similar behaviours with regard to both rotation and displacement. They also show relatively full elasto-plastic behaviour up to failure with regard to both displacement and rotation. Accordingly, Table 9.3 shows the bending ultimate strength, connection rigidity, connection rotational stiffness, as well as relative ultimate cantilever deflection of simple connections.

Table 9.3 The foam-only connections' structural properties

Bending ultimate strength (kN.m)	Rigidity (%)	Rotational stiffness (kN.m/Rad)	Relative ultimate cantilever deflection (%)
1.612	93	14.532	18.4

The failure modes observed in these series of tests are shown in

Figure 9.8. The first failure mode was a shear crack occurred at the vertical side of internal edge. By applying more pressure to the specimens, connections collapsed in a brittle manner at vertical arm and approximately at the level of bottom surface of horizontal arm. Development of shear stress and consequently the tensile stresses at the edges were the reason of brittle fracture which caused by a sudden reduction of foam tensile area.

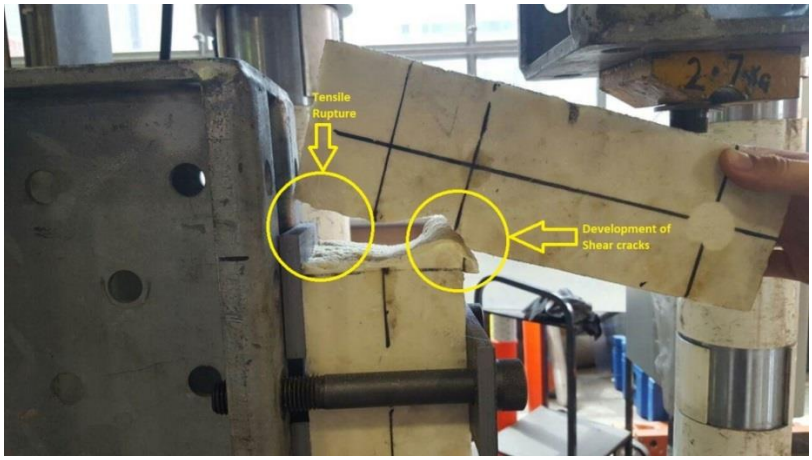

Figure 9.8: The failure modes and brittle fracture of foam-only connections

9.4.2 Behaviour of Composite Connections

The composite connection specimens showed relatively similar behaviour as those for the foam-only specimens, with respect to rotation. Meaning that the composite action and the effect of skins are relatively negligible in rotation, and the major rotational stiffness is provided by foam. Table shows the structural properties of the composite connection, calculated based on the experiment results.

Table 9.4 The composite connections' structural properties

Bending ultimate strength (kN.m)	Rigidity (%)	Rotational stiffness (kN.m/Rad)	Relative ultimate cantilever deflection (%)
2.018	95	26.901	16.4

Composite connections had the same failure modes as simple connections. The failure modes and collapse mechanism observed in these series of tests are shown in Figure . The first sign of failure occurred at the vertical side of internal edge. Bearing stresses were the reason of this matter. The connections were still able to carry some load yet but, lower than the failure load. Although collapse had still not occurred, specimens exhibited very large deformations at this stage (Figure 9.9(a)). Then, by applying more pressure to the specimens, connections collapsed in a gradual manner at the external side of vertical arm and approximately at the level of bottom surface of horizontal arm. Therefore, the tensile strength of external HDPE sheet was the reason of gradual fracture despite caused by a sudden reduction of foam tensile area. In addition, remained internal facing sheet prevents the connection from falling (Figure 9.9(b)).

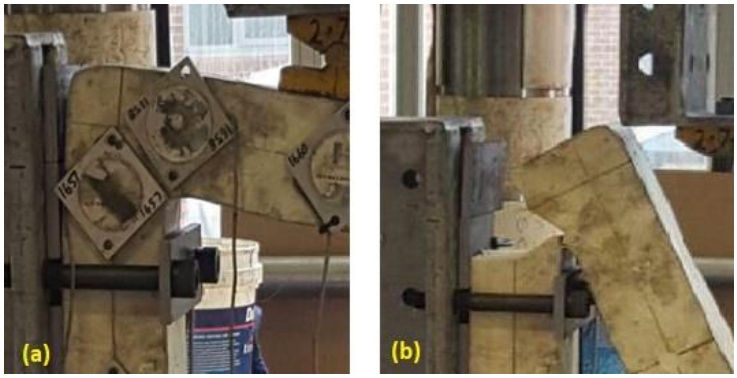

Figure 9.9: The composite connection behaviour. (a) the ultimate deflection (b) the mechanism of collapse

9.4.3 Comparison of Results

A comparison between the results indicates that in composite sections the bending ultimate strength increases by 25% compared to simple connections. The composite connections also show 2.2% greater rigidity. More importantly, the composite action resulted from HDPE facing sheets increases connection rotational stiffness by 85%. With regard to the relative ultimate cantilever deflection, composite connections presented better performance by 12% in comparison with foam-only connections. In the other words, the bending stiffness of composite connections is 12% greater than that of foam-only connections. Figure 9.10 compares the performance and failure mechanisms. Both simple and composite connections showed very similar failure modes and the fracture surface of them are fairly similar to each other. The most important difference therefore was their ductility; i.e. the foam-only connections show a relatively brittle sudden failure, while composite connections managed to undergo rather larger deformations before collapse.

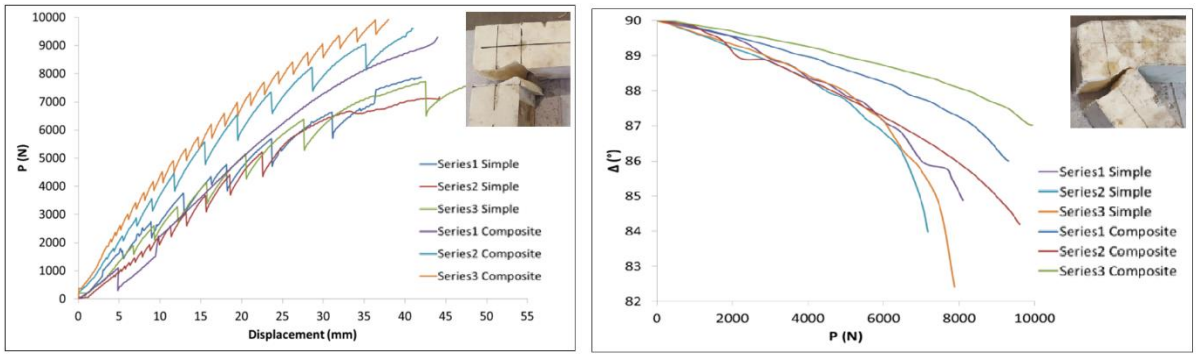

Figure 9.10: A comparison between behaviour, ultimate loads and collapse for two connections

9.5 Numerical Simulation

The integrated connection system in this study, were numerically modelled using a nonlinear FE modelling approach in order to simulate the stress distributions within the connection. In

addition, the maximum deflections of connections components estimated while they were to be supported in a perfect cantilever (clamped) configuration, and the experimentally observed failure modes were compared with those of numeric results. Three-dimensional (3D) FE models were developed using the commercial package ANSYS R15.0 to simulate the foam-only and composite connection systems. The HDPE sheets and PU foam were modelled using hyperelastic isotropic material (Mooney-Rivlin) properties [67, 68]. The PU foam and HDPE properties were obtained from strain energy density function, confirmed from results of material characterisation tests which carried out in Centre for Infrastructure Engineering of Western Sydney University as well as manufacturing specifications. The contacts between all contact surfaces with different material properties were modelled using the ‘‘Bonded” boundary condition in ANSYS 15. This method can be defined as surfaces which are fixed or glued together [55, 175]. Quadratic ten-node tetrahedral solid elements were used to model the different components of the panels and connections. Sensitivity checks were performed regarding the influence of the mesh density/refinement on the results obtained with the FE models, leading to the selection of the adopted meshes. In the foam-only connections, the stress concentration causes the foam reaches to tensile yield under the loading point. When the tensile stress is ١,٨٩٦ MPa, the compressive stress is lower than the ultimate 3.51MPa. Figure 9.11 and Figure 9.12 show the Von-Mises strain and stress distribution, as well as shear stress and strain distribution, at the ultimate stage, respectively. By applying more load, the connection collapse occurs, which is shown in Figure .

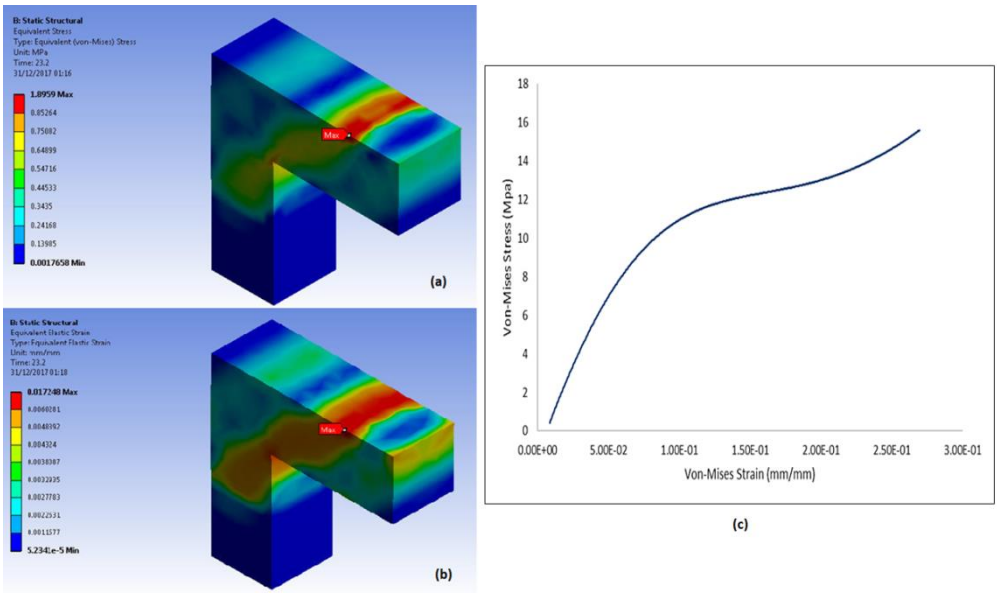

Figure 9.11: Von-Mises (a) stress, (b) strain distribution, and (c) their relation, in the foam-only connections

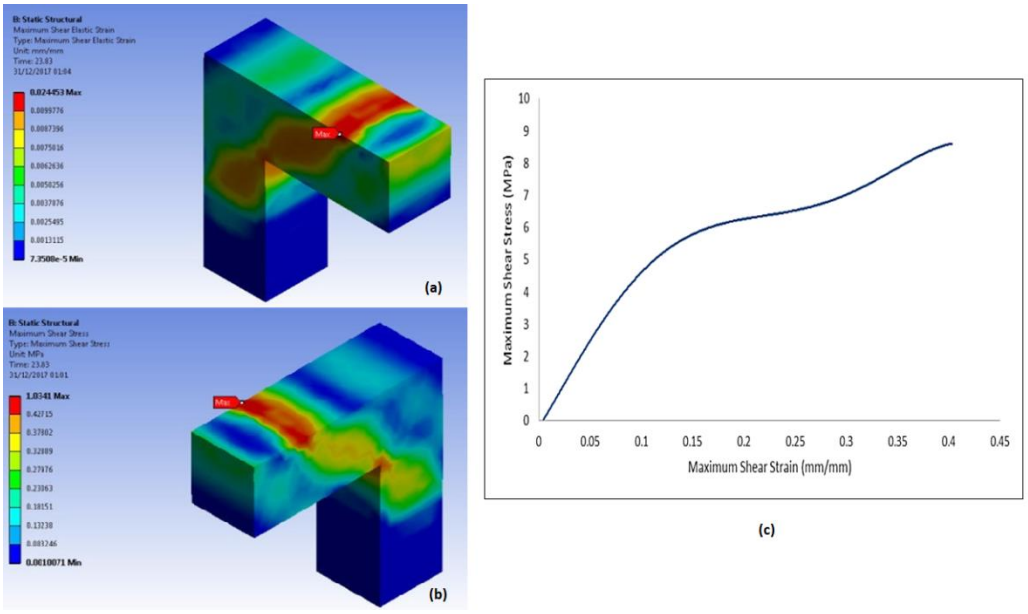

Figure 9.12: Ultimate shear (a) stress, and (b) strain distribution in foam-only connections

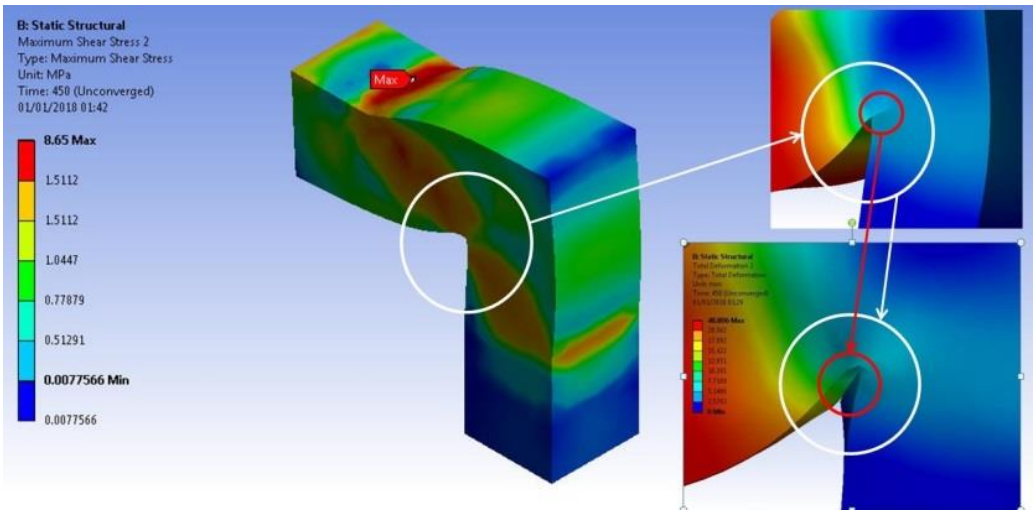

Figure 9.13: Shear stress distribution on the foam-only connection at failure

Unlike the foam-only connections, no early tensile yielding occurs under loading point in the composite sections. At the ultimate state, as shown in Figure 9.14, foam reaches to its shear yield point at the edge of supporters, and it develops through the foam towards the edges. By applying more loads, shear yielding occurs at the inner corner of the lower HDPE sheet, as shown in Figure . Before failure, the top layers of HDPE sheets reaches tensile yield point at the edge of loading surface, and the inner side of lower HDPE sheet enters a local high compressive stress zone. FEM results confirm that the failure happens at the inner corner of connection, similar to the experimental results. The maximum displacement at loading point is 40 mm, which has good agreement with experimental results. The equivalent stress

distribution in the connection components (core and facings) at collapse are shown in Figures 9.16 and 9.17.

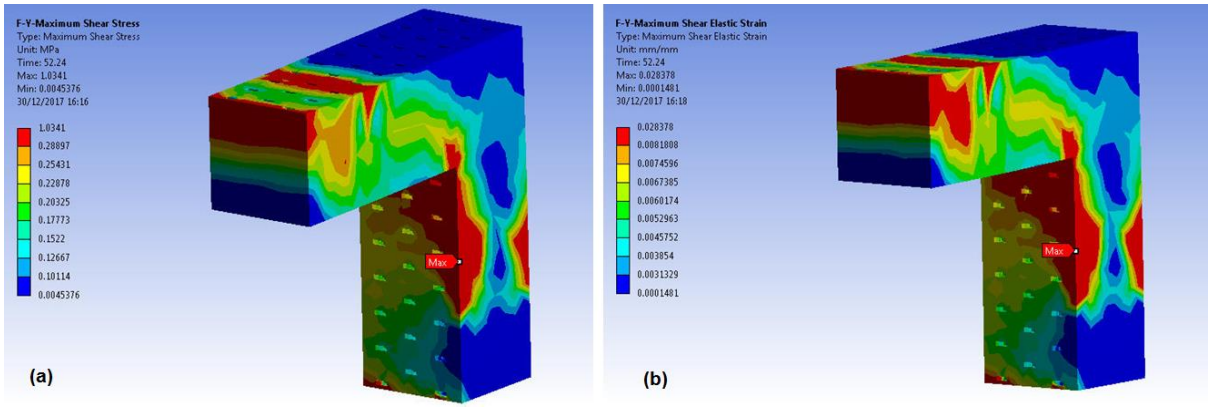

Figure 9.14: Ultimate shear (a) stress, and (b) strain distribution in foam in the composite connection

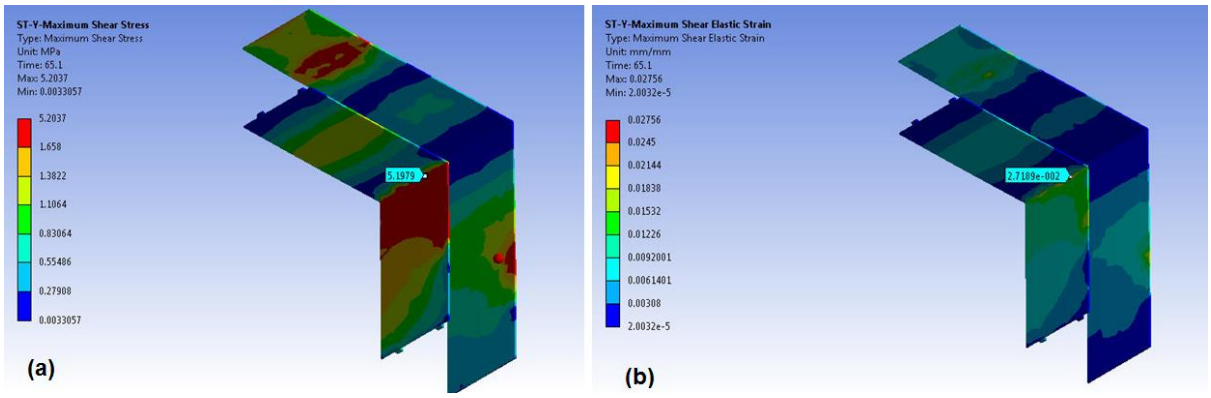

Figure 9.15: Shear stress (left) and strain (right) contours at shear yielding time, 65.1th second

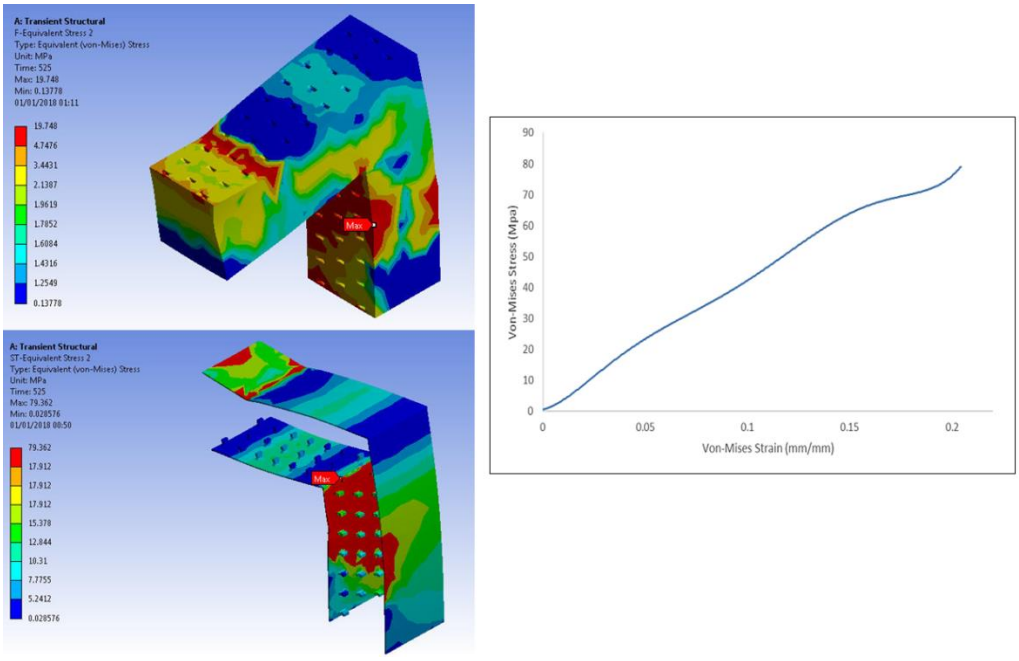

Figure 9.16: Von-Mises stress distribution, and stress-strain relation in the composite connections' components

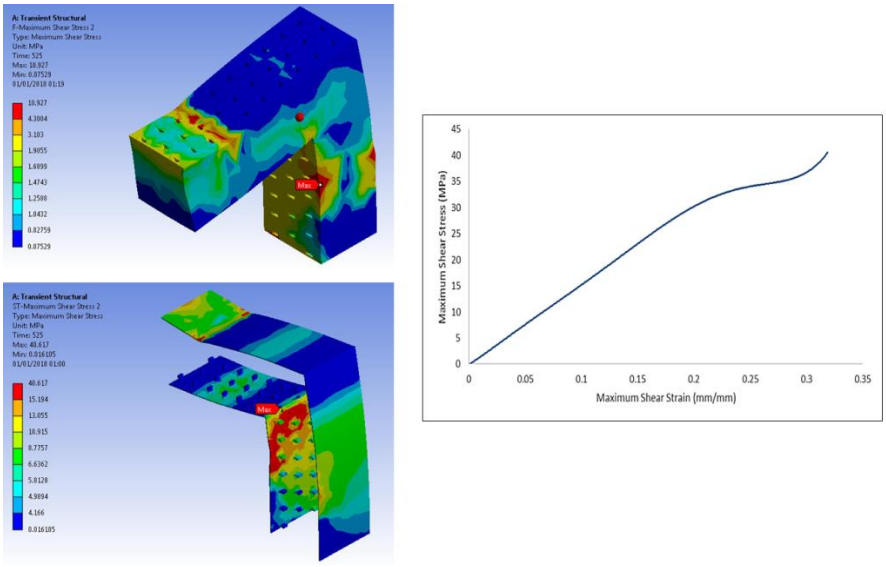

Figure 9.17: Shear stress distribution, and stress-strain relation in the composite connections' components

9.10 Conclusions

Experimental and numerical investigations were conducted on an integrated connection between adjacent foam-filled sandwich panels composed of 3-D high density Polyethylene skins and high-density Polyurethane foam core. The overall mechanical response, and the stress distributions, and failure modes, moment resistance, initial rotational stiffness and rotational capacity of the connections were studied. The experimental test results indicated that in composite sections the bending ultimate strength increases by 25% compared to foam-only connections. The composite connections also show 2.2% greater rigidity, and increased rotational stiffness of 85%. With regard to the relative ultimate cantilever deflection, i.e. bending stiffness, composite connections presented better performance by 12% in comparison with foam-only connections. Both simple and composite connections showed very similar failure modes and the fracture surface of them are fairly similar to each other. The first failure mode was a shear crack occurred at the vertical side of internal edge. By applying more pressure to the specimens, connections collapsed due to the development of shear stress and consequently the tensile stresses at the edges. The most important difference therefore was their ductility; i.e. the foam-only connections show a relatively brittle sudden failure, while composite connections managed to undergo rather larger deformations before collapse. Comparison of finite element model and experimental results of all specimens showed that the load versus displacement were similar. Furthermore, the failure modes, ultimate load and ductility capacities correlated well with experimental observations.

Chapter 10

Foam filled 3D modules for rapidly assembled post disaster housing

The contents of this chapter have been published in the form of a journal paper as follows:

Saeed Nemati (Full contribution), Pezhman Sharafi (Scientific supervision), Bijan Samali (Scientific supervision), Yahya Aliabadizadeh (Contributed in numerical phase) and Shahrokh Saadati (Partial contributed in numerical phase) "Non-Reinforced Foam Filled Modules for Rapidly Assembled Post Disaster Housing", International Journal of GEOMATE, May, 2018 Vol.14, Issue 45, pp.151-161, DOI: 10.21660/2018.45.73573, ISSN: 2186-2982 (Print), 2186-2990 (Online), Japan.

10.1 Introduction

Crisis management after natural and non-natural disasters such as earthquake, flood, drought, bushfire, flood of refugees, raid and war can be a serious concern of governments. In the event of such crises, fast decision making is an essential element of an effective crisis management system [176]. From the civil engineering point of view, Post Disaster Housing (PDH) is a big challenge in the crisis management field. Every year, due to natural and man-made catastrophes worldwide, millions of people have to be accommodated in temporary housing. In the USA alone, such disasters happen over 60 times per year [177]. Experts estimate that on average, it can take 5 [23] to 10 [24] years for communities to recover from the effects of a disaster, which highlights the severity of the disaster and the importance of Rapidly Assembled Buildings (RABs) as an effective PDH system [23]. Rapidly assembled panels are used commonly in residential buildings as well as industrial structures [178]. In addition to residential accommodation, RABs can be employed in several other applications such as, field hospitals, storehouses and other temporary and semi-permanent facilities [179]. Some rapidly assembled systems have the potential to be used as temporary structures as well as providing long term serviceability. Temporary accommodation buildings can only remain on-site for a maximum of two years, unless the local government approves a longer timeframe before the two year period expires [180]. Nevertheless, sometimes, the term of "temporary" returns to several years, especially in developing countries [181-185] that can have significant social and economic effects [186-188]. Mobile and rapidly assembled structures play a major role in post-disaster management through building temporary accommodation and shelters. Wise selection of RAB systems has an impact on their performance in an effective crisis management system. For instance, use of large precast units is adopted by most existing PDH systems. Yet, as the dimension of precast elements increases, some significant construction problems appear in transportation, installation and erection phases. Air-liftable origami-inspired deployable systems, pliable structural systems with rigid couplings for parallel leaf-springs, scissor systems[30], elastic grid shell system [3], and structural panels are some popular types of mobile and rapidly assembled structures [31, 32]. Most of these rapidly assembled structural systems suffer from low tolerance in the fabrication and erection phases. They also need skilled labours for installation that will result in an increase in the total costs, and some other constructional problems. For example, air-liftable origami-inspired deployable systems do not have a reliable architectural form and are

mostly uncomfortable for a long stay. The control of heat exchange in such systems is also very difficult. Pliable structural systems with rigid couplings for parallel leaf-springs have similar problems, in addition to a relative complex design procedure. In addition, in most cases, the elastic grid shell system is limited to non-residential temporary applications. High rate energy loss and expensive construction equipment are some of other downsides of this system. To respond to such shortcomings, in this study, using pneumatic foam filled panels first, an effective rapidly assembled modular system is presented as a PDH that can be used for post disaster management as a temporary and semi-permanent housing system. The modules are made of light weight composite sandwiches fitted in pneumatic formwork that greatly facilitate transportation and installation process. Then, numerical and experimental analyses are performed to investigate the structural performance of this system under severe loading conditions, as a structural feasibility analysis.

10.2 Temporary Housing

A temporary accommodation building can be any class of building as defined under the National Construction Code (NCC). However they are usually a class 1b (boarding house, guest house, hostel or the like), class 2 (residential units) or class 3 (motel) building, depending on its configuration [29]. The Federal Emergency Management Agency (FEMA)'s recent policy change to discontinue using the mobile homes as a temporary housing alternative will result in a significant increase in the cost of the temporary housing program [189]. In addition, studies have shown that innovative prefabricated housings have 25.1 and 29.7% lower life cycle energy and cost requirements respectively [34, 35, 190, 191]. Use of rapidly assembled panelised systems, especially rapidly assembled lightweight panels, is becoming very popular for cutting the construction time, as well as skilled labour and transportation costs that make them suitable options for PDH projects.

Regarding the structural performance of light weight panels, the use of foam materials have been a good choice for filling material. While, many types of foams are available in the market, Polyurethane (PUR) based foams are the most popular types, first introduced into the market in the 1950s. Foams are available in three main categories: flexible (the most popular), semi-rigid and rigid foams [20]. Polyether-based PUR foams are used widely for applications such as furniture, bedding, pillows, padding, and carpet underlay. Polyester-based PUR foams are used for textiles, shoulder pads, noise reduction and other applications. Both are used in automotive, aircraft, household, and footwear industries, too. Nevertheless,

showing some good level of structural strength and durability, these foams have a great potential to be widely used in structural engineering. Structural studies on post disaster housing are mostly limited to some post-disaster shelter design, architectural guidelines or Multi-Criteria Decision Making (MCDM) models for selecting the PDH systems [192-198]. In some research study, new temporary housing planning framework is proposed to offer customised housing plans tailored to the specific social, economic, and psychological needs of displaced families while controlling expenditures [199, 200]. Maximizing temporary housing safety after natural disasters has been studied in other research studies [201]. FEMA has explored a pilot program to evaluate the possibility of providing quickly deployable, affordable housing that can serve both as temporary and permanent housing [186]. In early 2009, FEMA released the first-ever National Disaster Housing Strategy which calls for improved planning and outlines the key principles and policies guiding disaster sheltering, interim housing, and restoration of permanent housing [202]. For disaster relief housing, rapidly deployable shelters must be lightweight, be packaged in a small volume for transportability, and be erected without heavy lifting equipment. In addition, a critical design criterion is also energy efficiency in heating and cooling. To meet these priorities, an optimised solution is found for a thermally insulated rigid wall deployable shelter by Quaglia et al. [203]. Although such rigid wall counterparts provide enhanced insulation, they have high self-weights, limited deploy-ability, and require heavy lifting equipment for placement. To address this downside, United States Army Natick Soldier Research, Development & Engineering Center presented a novel erection strategy for origami-inspired shelters based on the principle of counterweighting as Bascule shelters [204, 205]. Also, some researches proposed a modular box systems for post-earthquake homeless disaster victims in line with the standard sustainability criteria [36, 55, 65, 206]. The design and methodology of construction of a shelter for the victims of the typhoon Haiyan in the Philippines was presented by Ravina and Shih [207].

10.3 Flexible Formwork

An efficient construction system that can be used in rapidly assembled buildings is flexible formwork systems. The most applicable types of flexible formworks are fabric formworks made of synthetic textile sheets of fibres; typically nylon, Polyesters/Polyethylene Terephthalate, Polyolefin or Polypropylene. In casted structural systems, in which a considerable portion of the project budget is allocated to formwork cost, innovative

construction systems can play an important part in PDH programs. Using fabric formwork is one of these solutions. The development of some innovative ideas such as pneumatic formwork has complemented the applications of fabric formwork. The main concept of pneumatic formwork application is ramified from membrane behaviour. A common method of pre-tensioning a membrane is to pressurize the interior with air. Sufficient pressure is applied to counteract dead loads, so that the membrane actually floats in space. Slight additional pressurisation is also used to offset wind and other anticipated loads. Pressure differentials used in practice are not large. They often range between 0.02 and 0.04 psi (3 and 5 psf). A good example is air-inflated dual wall structures. Air-inflated dual wall structures is one of most popular air stabilised structures. Up to now however, this system scarcely applied as a structural pneumatic formwork. The general application of this technique is mostly limited to the erection and setup of domes and arches [47]. Employing the PUR and a pneumatic formwork, this study develops an effective post disaster housing system that can significantly contribute to PDH management (Figure 10.1). In this System, after inflating the fabric formwork, PUR foam is injected between internal and external fabric layers. Therefore, an integrated volumetric structural system including floor, walls and roof will be built. Figure 10.2 shows a schematic perspective of the unit and a cross section of integrated connections between walls.

Figure 10.1: Pneumatic formwork installation steps of introduced system

The remainder of this paper investigates the structural performance of this foam-filled structural panel with fabric formwork (which can be erected by pneumatic force) as an innovative rapidly assembled construction system. Rapid assembly, low maintenance, high structural quality, and ease of transportation are some key aspects of this system that make it a suitable construction system for temporary and semi-permanent housing.

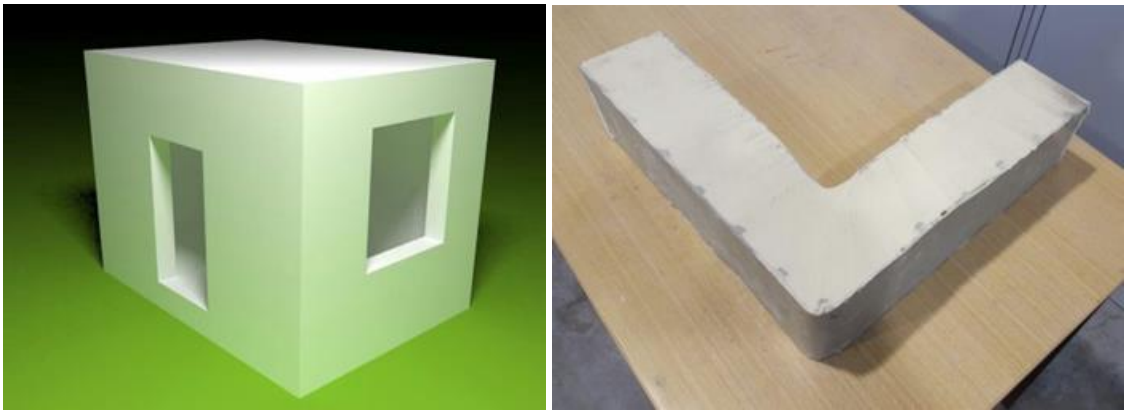

Figure 10.2: Schematic perspective (left) and real cross section of introduced system (right)

10.4 Material Properties

The system fabric pneumatic formwork and PUR foam are the main main materials used for the system. A research study has been done in the Centre for Infrastructure Engineering (CIE) of Western Sydney University in order to identify the best pneumatic formwork textile [47]. Results showed the Barrateen is the best candidate for being used as fabric formwork. Barrateen is a high density polyethylene or polypropylene (HDPE) coated by unbalance woven textile. The coating material is low density polyethylene and well inflatable, whose tensile strengths in the warp and weft directions are not the same. The result of tensile tests according to ASTM D1980-89 is shown in Figure 10.3. Also, Polyurethane high-density rigid foam with a density of 192 kg/m^3 was used for the core material. Table 10.1 shows the PU foam's manufacturing and mechanical properties, provided by the manufacturer, and validated in the laboratory according to the ASTM 1730 standard .

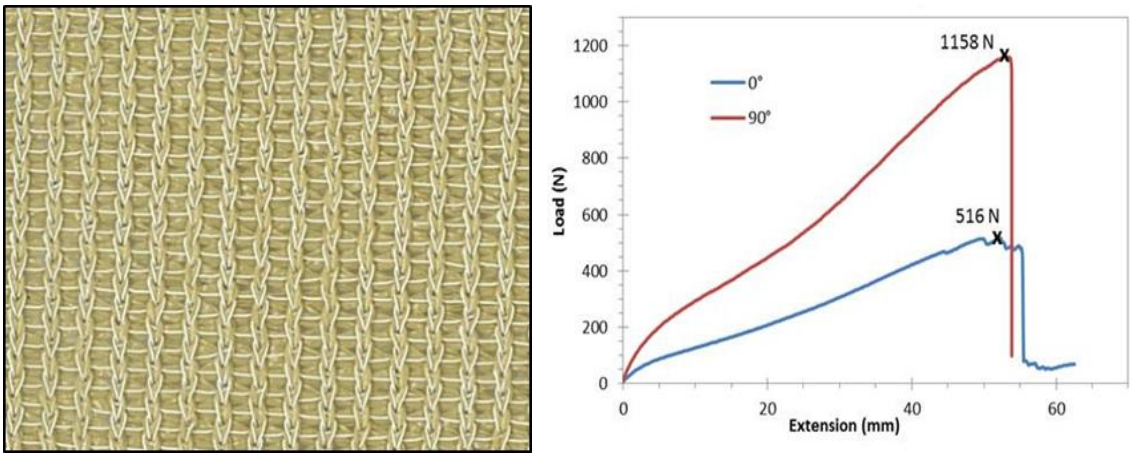

Figure 10.3: Barrateen fabric tensile behaviour in main (90º) and transverse (0º) directions

Table 10.1 Mechanical and manufacturing properties of the selected PU rigid foam

Mechanical properties of the PU foam			
Density (kg/m3)	Compressive yield strength (MPa)	Tensile strength (MPa)	Shear strength (MPa)
192	2.81	1.896	1.034
Manufacturing Properties			
Cream time	Gel time	Tack free time	Free rise cup density
35-40 sec	94 ± 4 sec	115 ± 5 sec	280 – 300 kg/m^3

Using uniaxial load machine, three cubic specimens (dimensions: 50 mm × 50 mm × 50 mm) were tested based on the ASTM E1730 at a loading rate of 5 mm/min in order to identify the structural properties of the rigid PU foam. Figure 10.4 illustrates the stress-strain curves in the elastic region and failure graph respectively. The curves show that this type of PU foam, which is made of a 100:110 weight ratio mixture of AUSTHANE POLYOL AUW763 and AUSTHANE MDI, can undertake considerable deformation before the failure. These stress-strain curves are relatively linear in the elastic region, with a yield region at an average stress of 3.51 MPa, and the average elastic modulus of 135.5 MPa.

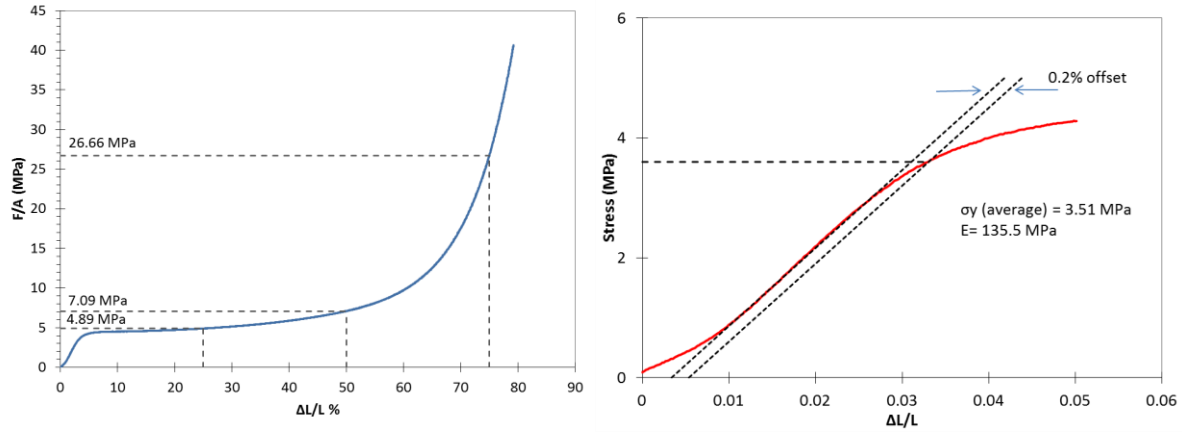

Figure 10.4: Results of the uniaxial load test on selected PU foam

10.5 Loading Analysis and Design

The introduced system is designed to be capable of being used for post disaster housing in severe weather conditions. Therefore, in this study a combination of severe loading scenarios is considered to check the performance of the shelter. In the other hand, because the system is

light in weight, with regard to the lateral loads, the numerical studies showed that wind loads will govern the design, rather than earthquake. The International Building Code (IBC-2015) [208] is used for determining the loads as well as the design. In this regard a 3000 mm x 3000 mm x 3000 mm cubic shelter with 100 mm thick PU foam walls, floor and roof has been analysed and designed. In fact, this cube is a simulation of temporary shelter that can be used in emergency situations. The door and windows are not shown in the model. The computer model is created in ANSYS workbench. For the wind load calculations, the American Society of Civil Engineers ASCE7-10 "Minimum Design Loads for Buildings and other Structures" [209], which is adopted by IBC 2015 is used. To analyze the cube for most extreme wind load, the Cube is subject to calculated wind load induced by an 80 mps wind speed, which is the highest speed for such structures. Also, the studied cubic shelter is categorised as risk category II based on Table 1.5-1 in ACSE 7-10 (Figure 10.5), which is neither a low risk nor a high risk structure. The cube is considered enclosed, so there will be a minimum internal pressure acting perpendicular to the surface. The Exposure category is assumed to be "C" which indicates open terrain with scattered obstruction having height less than 10000 mm or flat open countryside and grassland, which assumed to accommodate temporary shelters at the time of disasters and emergencies. The topography of the site is assumed to be relatively flat with maximum 5000 mm escarpment height.

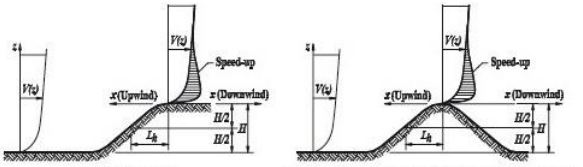

ESCARPMENT 2-D RIDGE OR 3-D AXISYMMETRICAL HILL

Topographic Multipliers for Exposure C

H/L_h	K_1 Multiplier			x/L_h	K_2 Multiplier		z/L_h	K_3 Multiplier		
	2-D Ridge	2-D Escarp.	3-D Axisym. Hill		2-D Escarp.	All Other Cases		2-D Ridge	2-D Escarp.	3-D Axisym. Hill
0.20	0.29	0.17	0.21	0.00	1.00	1.00	0.00	1.00	1.00	1.00
0.25	0.36	0.21	0.26	0.50	0.88	0.67	0.10	0.74	0.78	0.67
0.30	0.43	0.26	0.32	1.00	0.75	0.33	0.20	0.55	0.61	0.45
0.35	0.51	0.30	0.37	1.50	0.63	0.00	0.30	0.41	0.47	0.30
0.40	0.58	0.34	0.42	2.00	0.50	0.00	0.40	0.30	0.37	0.20
0.45	0.65	0.38	0.47	2.50	0.38	0.00	0.50	0.22	0.29	0.14
0.50	0.72	0.43	0.53	3.00	0.25	0.00	0.60	0.17	0.22	0.09
				3.50	0.13	0.00	0.70	0.12	0.17	0.06
				4.00	0.00	0.00	0.80	0.09	0.14	0.04
							0.90	0.07	0.11	0.03
							1.00	0.05	0.08	0.02
							1.50	0.01	0.02	0.00
							2.00	0.00	0.00	0.00

Notes:

1. For values of H/L_h, x/L_h and z/L_h other than those shown, linear interpolation is permitted.
2. For $H/L_h > 0.5$, assume $H/L_h = 0.5$ for evaluating K_1 and substitute $2H$ for L_h for evaluating K_2 and K_3.
3. Multipliers are based on the assumption that wind approaches the hill or escarpment along the direction of maximum slope.
4. Notation:
   - H: Height of hill or escarpment relative to the upwind terrain, in feet (meters).
   - L_h: Distance upwind of crest to where the difference in ground elevation is half the height of hill or escarpment, in feet (meters).
   - K_1: Factor to account for shape of topographic feature and maximum speed-up effect.
   - K_2: Factor to account for reduction in speed-up with distance upwind or downwind of crest.
   - K_3: Factor to account for reduction in speed-up with height above local terrain.
   - x: Distance (upwind or downwind) from the crest to the building site, in feet (meters).
   - z: Height above ground surface at building site, in feet (meters).
   - μ: Horizontal attenuation factor.
   - γ: Height attenuation factor.

Figure 10.5: ASEC 7-10 topographic factor, Kzt [51]

Table 10.2 shows the calculation of wind load and maximum applied pressures on walls and roof of shelter based on Table 27.2-1, ASCE7-10 [209]. For gravity loads, the structure is assumed to be subjected to 4788 Pa ground snow load as the maximum possible for outside Alaskan locations in the United States (4788 Pa) [209]. In this study conservatively the ground snow load is assumed to be applied on the top of the roof.

Table 10.2 Applied wind load calculation

Parameter	Based on	Amount
Risk category	Table 1.5-1 ASCE 7-10	II
Max nominal design wind speed for risk	Fig. 26.5-1A ASCE 7-10	V_{LRFD} = 180 mph
Structure type	Main concept	Flat ground
Wind directionality factor	Table 26.6-1 ASCE 7-10	K_d = 0.85
Exposure category	Fig. 26.6 ASCE 7-10	C
K_1	Figure 8	0.775
K_2	Figure 8	0.815
K_3	Figure 8	0.22
Kzt = (1+K1.K2.K3)**2	Eq. 26.8-1 ASCE 7-10	1.297
Gust effect factor (G)	Eq. 26.9 ASCE 7-10	0.85
Approximate natural frequency (na)	Eq. 26.9-4 ASCE 7-10	7.5 Hz
Nominal height of the atmospheric boundry layer (Zg)	Table 26.9-1 ASCE 7-10	330 m
pressure acting away from internal surface (GCpi_toward)	Table 26.11-1 ASCE 7-10	0.18
pressure acting away from internal surface (GCpi_away)	Table 26.11-1 ASCE 7-10	-0.18
Windward pressure on the wall (P_{wall})		2528 Pa
Leeward pressure on the wall (P_{wall})		–1580 Pa (suction)
Max roof upward pressure (P_{rf})		–4108 Pa (suction)
Max internal upward pressure (P_{int})		669 Pa

The shelter is designed according to Allowable Stress Design (ASD) method. According to IBC2015[208], the reasonable load combinations for this case study are as followings: D; D + L; D + S; D + 0.75L + 0.75S; D + (0.6w or 0.7E); D + 0.75(0.6W) + 0.75L + 0.75S; D+0.75(0.7E)+0.75L+0.75S; 0.6D+0.6W ; 0.6D+0.7E [66-68]. In which D is dead load, E is earthquake load, L is live load due to occupancy, Lr is roof live load, S is snow load and finally W is wind load. In this study, since the dead load and earthquake load are considerably lower than the wind load and snow load, the wind and snow loads are conservatively analysed separately. The shelter therefore, is analysed using ANSYS work bench assuming the global Y axis as perpendicular to the ground (The self-weight of the material is applied in –Y direction, and he roof upward force is applied in +Y direction). The wind load is applied in X direction, and the side pressures are applied in the Z directions. The internal pressure is applied to all faces perpendicular to the surface. The supports of the cube are assumed to be fixed supports at the edges of the walls. The results show under wind loading, both of maximum shear stress and maximum stress intensity are created at the connection of side walls to roof. It is observed that the structure can resist against the

maximum tensile stress caused by wind load with a safety facture of 1.896/1.0166 = 1.87. In addition, the used material can resist against the maximum created shear stress with a safety facture of 1.034/0.5083 = 2.03 (Figure 10.6).

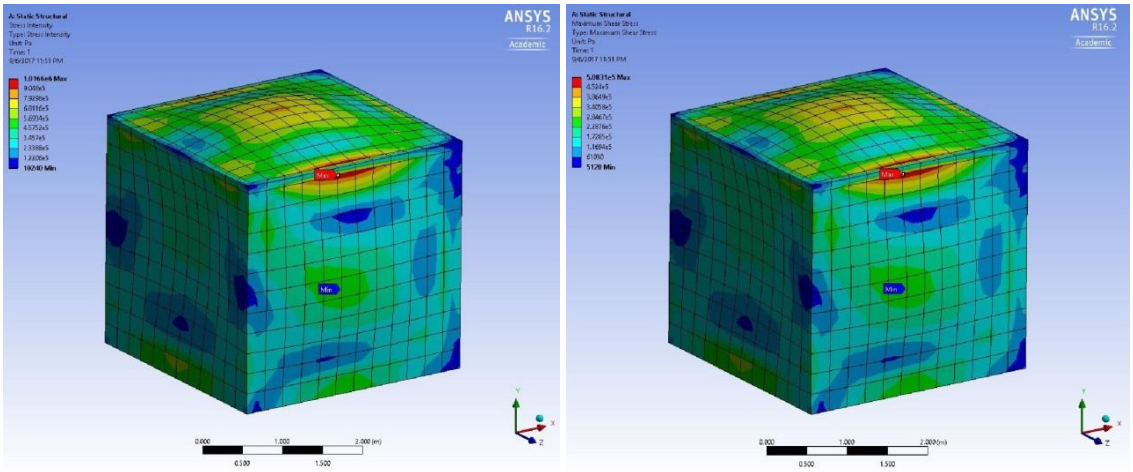

Figure 10.6: Wind load max stress intensity 1.0166 MPa (left) and max shear stress 0.50831 MPa (right)

The maximum deformation under wind load is also equal to 60 mm upward, and is located at the mid centre of the roof. This deformation has been compared with the snow's maximum deflection, which is equal to 75 mm downward (Figure 10.7).

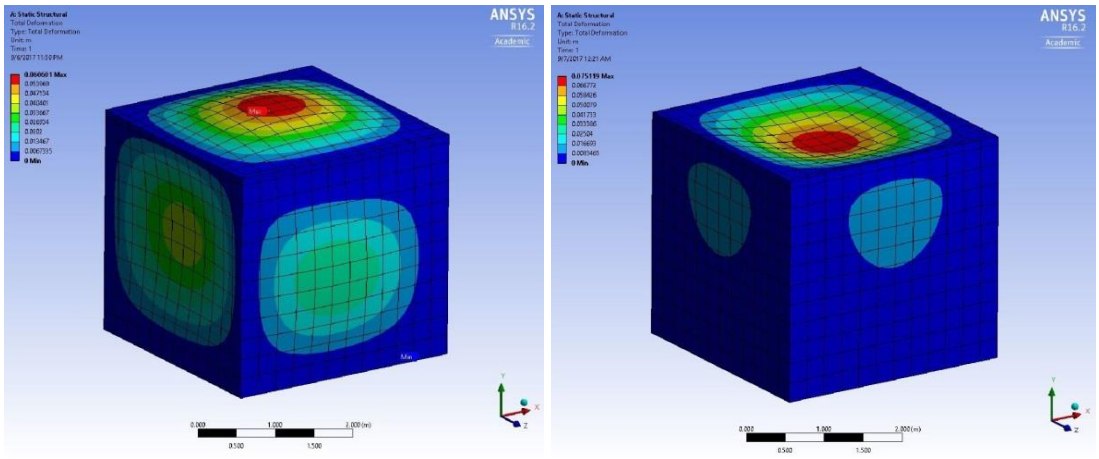

Figure 10.7: Wind load max deformation, 60 mm (left) vs snow maximum deflection, 75 mm (right)

Nonetheless, the results indicate the structure can tolerate these deformations without any fracture. Because, the used material can resist the maximum tensile stress under snow loading with a safety facture about 1.896/0.8662 = 2.19 (Figure 10.8).

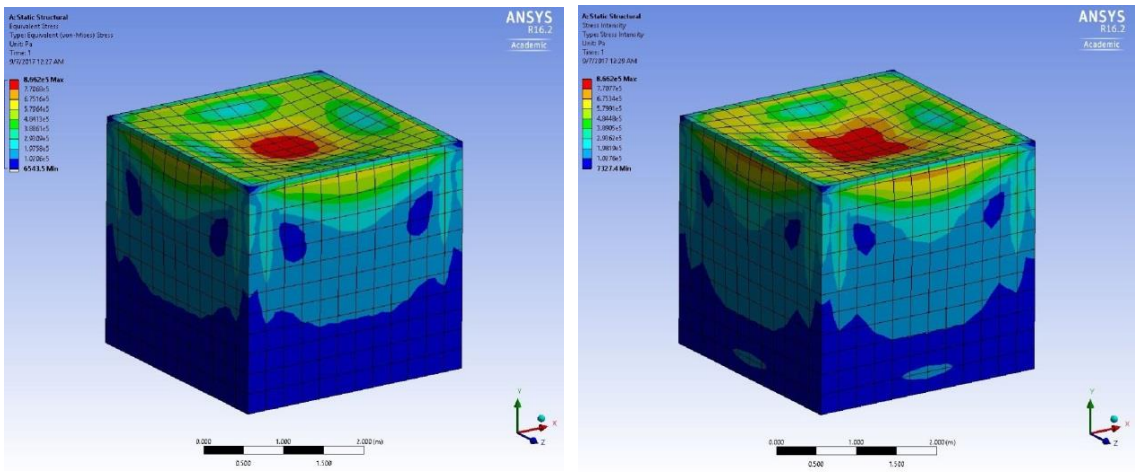

Figure 10.8: Equivalent (Von Miss) stress (left) and stress intensity (right) caused by snow loading

In addition, the location of the maximum shear stress under snow loading is exactly at the middle of span of the roof. The structure can resist the maximum shear stress caused by snow loading with a safety facture about 1.034/0.4331 = 2.39 (Figure 10.9). Therefore, the unit can conservatively withstand highest wind and snow loads.

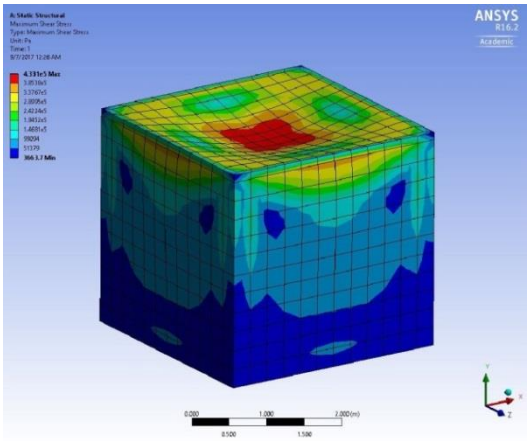

Figure 10.9: Shear stress distribution caused by snow loading

The reaction forces under snow and wind loading are calculated and shown in Table 10.3. The shelter needs to support the above-mentioned loads in its base. For soft ground areas, the system needs to a weight around 40207 N. The perimeter of the unit is 4 x 3 m =12 m therefore the minimum weight of unit length of the foundation is equal to 40207N/12m = 3350 N/m. If the weight is provided by concrete, knowing that the density of concrete is 2.5e4 N/m3, the area of cross section will be calculated as follows: A = 3350/25000 = 0.134 m^2. A 30 cm x 50 cm foundation has area of 0.15 cm^2. Figure 10.10 shows a typical foundation for this system.

Table 10.3 Applied wind load on shelter

Loading	Direction X (N)	Direction Y (N)	Direction Z (N)
Wind Load	- 39437	- 40207	0
Snow Load	0	57728	0

In harder soils the shelter can be supported with an alternative method using anchoring rods (Figure 10.11). As shown in Figure 10.11, the anchoring rods will provide required horizontal and vertical reaction forces. The lateral 39437 N will be distributed on 0.10 m x 3 m = 0.3 m^2 area of angle. The bearing stress is equal to 39437 N / 0.3 m^2 = 0.131 MPa, which is lower than allowable stress of 2.81 MPa.

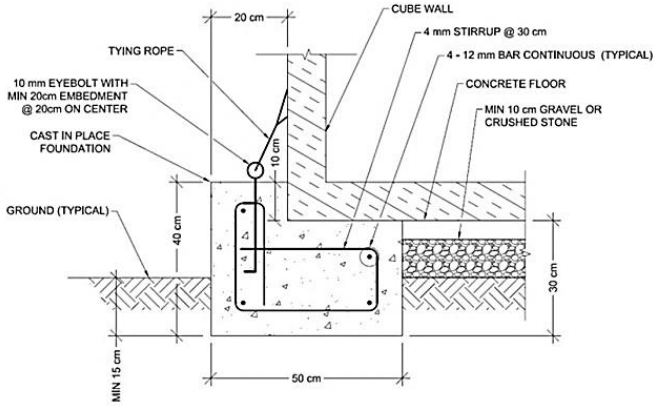

Figure 10.10: Precast or cast in place foundation detail

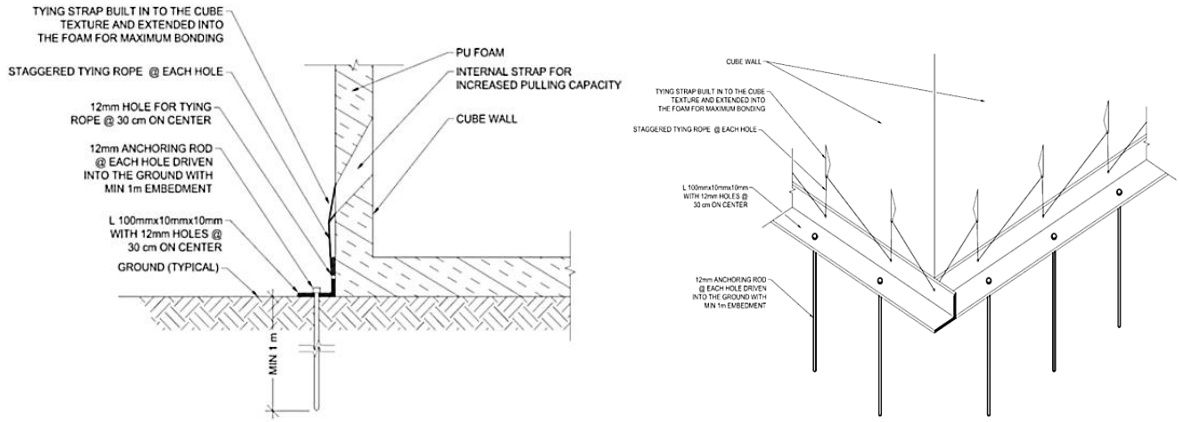

Figure 10.11: Ground anchoring detail

According to the above calculations, the 3m x 3m x 3m structure can withstand most sever wind and snow as well as other applicable loads as per the Internarial Building Code. Analysis and design of some similar structures with various dimensions (from 3 m to 8 m) showed if both of length and wide increase from 4 m simultaneously, the system will increase the risk of collapse with a safety factor bellow 1 (Figures 10.12 and 10.13 and Table 10.4).

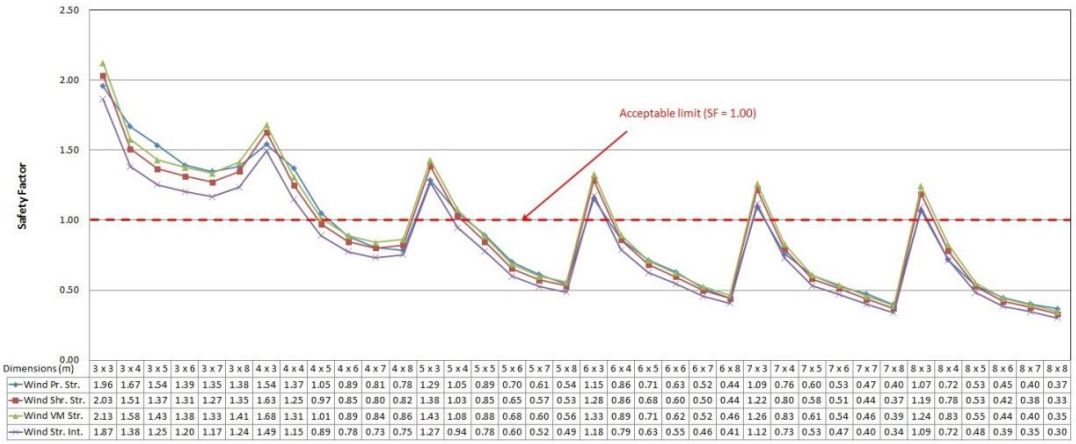

Dimensions (m)	3 x 3	3 x 4	3 x 5	3 x 6	3 x 7	3 x 8	4 x 3	4 x 4	4 x 5	4 x 6	4 x 7	4 x 8	5 x 3	5 x 4	5 x 5	5 x 6	5 x 7	5 x 8	6 x 3	6 x 4	6 x 5	6 x 6	6 x 7	6 x 8	7 x 3	7 x 4	7 x 5	7 x 6	7 x 7	7 x 8	8 x 3	8 x 4	8 x 5	8 x 6	8 x 7	8 x 8
Wind Pr. Str.	1.96	1.67	1.54	1.39	1.35	1.38	1.54	1.37	1.05	0.89	0.81	0.78	1.29	1.05	0.89	0.70	0.61	0.54	1.15	0.86	0.71	0.63	0.52	0.44	1.09	0.76	0.60	0.53	0.47	0.40	1.07	0.72	0.53	0.45	0.40	0.37
Wind Shr. Str.	2.03	1.51	1.37	1.31	1.27	1.35	1.63	1.25	0.97	0.85	0.80	0.82	1.38	1.03	0.85	0.65	0.57	0.53	1.28	0.86	0.68	0.60	0.50	0.44	1.22	0.80	0.58	0.51	0.44	0.37	1.19	0.78	0.53	0.42	0.38	0.33
Wind VM Str.	2.13	1.58	1.43	1.38	1.33	1.41	1.68	1.31	1.01	0.89	0.84	0.86	1.43	1.08	0.88	0.68	0.60	0.56	1.33	0.89	0.71	0.62	0.52	0.46	1.26	0.83	0.61	0.54	0.46	0.39	1.24	0.83	0.55	0.44	0.40	0.35
Wind Str. Int.	1.87	1.38	1.25	1.20	1.17	1.24	1.49	1.15	0.89	0.78	0.73	0.75	1.27	0.94	0.78	0.60	0.52	0.49	1.18	0.79	0.63	0.55	0.46	0.41	1.12	0.73	0.53	0.47	0.40	0.34	1.09	0.72	0.48	0.39	0.35	0.30

Figure 10.12: Variation in Safety Factor for different room dimensions - Wind load

For results confirmation, another series of analyses and designs have been conducted on the introduced system (3m x 3m x 3m) based on the Australian Standards [55, 56]. In this regard, wind load of cyclonic area (88 m/s for region D) with annual probability return of 500 years is applied on the shelter. In this regards the shelter is analysed using a professional loading, analyzing and design software, ROBOT 2016. Also, the most conservative identified load combination (0.9G + W) was used [56]. Based on the Australian standards, the wind is applied on the shelter with both angles of 90° and 45° separately (Figure 10.14). However, since the wind speed with respect to IBC and AS1170.2 are almost the same, only the oblique wind is used for confirmation. The results show all of the maximum amounts of deformation, main stress and shear stress caused by the oblique wind are lower than design limits. As an example, Figure 10.15 shows the Maximum deformation of shelter caused by oblique wind is only 42mm, which is less than the related amount of IBC (60 mm). In addition the results indicates that the maximum uplift force under wind loading 45º is equal to 35300 kN, which is less than the amount used for design (40207 kN).

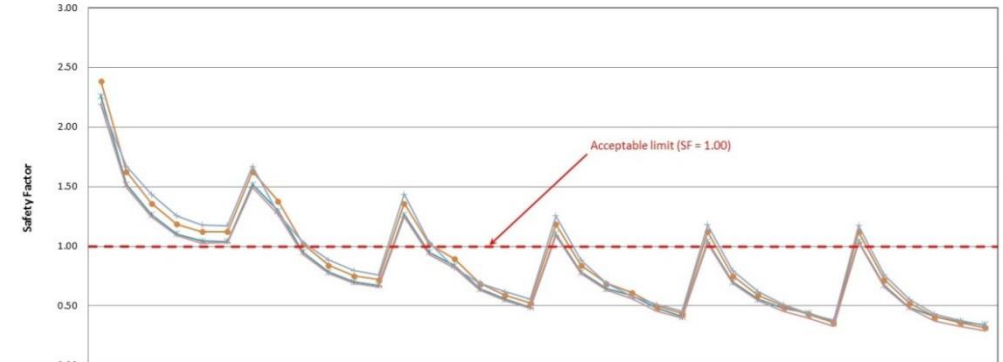

Dimensions (m)	3 x 3	3 x 4	3 x 5	3 x 6	3 x 7	3 x 8	4 x 3	4 x 4	4 x 5	4 x 6	4 x 7	4 x 8	5 x 3	5 x 4	5 x 5	5 x 6	5 x 7	5 x 8	6 x 3	6 x 4	6 x 5	6 x 6	6 x 7	6 x 8	7 x 3	7 x 4	7 x 5	7 x 6	7 x 7	7 x 8	8 x 3	8 x 4	8 x 5	8 x 6	8 x 7	8 x 8
Snow Pr. Str.	2.26	1.52	1.27	1.10	1.04	1.04	1.52	1.30	0.95	0.78	0.70	0.67	1.27	0.95	0.84	0.64	0.56	0.49	1.10	0.78	0.64	0.59	0.48	0.41	1.04	0.70	0.56	0.48	0.44	0.37	1.04	0.67	0.49	0.41	0.37	0.34
Snow Shr. Str.	2.39	1.63	1.36	1.19	1.12	1.12	1.63	1.38	1.02	0.84	0.75	0.72	1.36	1.02	0.89	0.69	0.59	0.52	1.19	0.84	0.69	0.61	0.50	0.44	1.12	0.75	0.59	0.50	0.43	0.36	1.12	0.72	0.52	0.41	0.36	0.32
Snow VM Str.	2.19	1.67	1.44	1.25	1.18	1.17	1.67	1.27	1.03	0.88	0.80	0.76	1.44	1.03	0.82	0.69	0.62	0.55	1.25	0.88	0.69	0.58	0.51	0.45	1.18	0.80	0.62	0.51	0.43	0.38	1.17	0.76	0.55	0.43	0.38	0.33
Snow Str. Int.	2.19	1.49	1.25	1.09	1.03	1.03	1.49	1.26	0.93	0.77	0.69	0.66	1.25	0.93	0.82	0.63	0.54	0.48	1.09	0.77	0.63	0.56	0.46	0.40	1.03	0.69	0.54	0.46	0.40	0.33	1.03	0.66	0.48	0.38	0.33	0.29

Figure 10.13: Variation in Safety Factor for different room dimensions - Snow load

Table 10.4 Safe dimensions of the shelter

	Wind (IBC)				Snow (IBC)				
Dimentions (m)	Principle stress	Shear Stress	VM Stress	Stress intencity	Principle stress	Shear Stress	VM Stress	Stress intencity	Restricting load
3x3	O.K.	O.K.	O.K.	O.K.	O.K.	O.K.	O.K.	O.K.	
3x4	O.K.	O.K.	O.K.	O.K.	O.K.	O.K.	O.K.	O.K.	
3x5	O.K.	O.K.	O.K.	O.K.	O.K.	O.K.	O.K.	O.K.	
3x6	O.K.	O.K.	O.K.	O.K.	O.K.	O.K.	O.K.	O.K.	
3x7	O.K.	O.K.	O.K.	O.K.	O.K.	O.K.	O.K.	O.K.	
3x8	O.K.	O.K.	O.K.	O.K.	O.K.	O.K.	O.K.	O.K.	
4x4	O.K.	O.K.	O.K.	O.K.	O.K.	O.K.	O.K.	O.K.	
4x5	O.K.	N.G.	O.K.	N.G.	N.G.	O.K.	O.K.	N.G.	Wind and Snow
4x6	N.G.	N.G.	N.G.	N.G.	N.G.	N.G.	N.G.	N.G.	Wind and Snow
4x7	N.G.	N.G.	N.G.	N.G.	N.G.	N.G.	N.G.	N.G.	Wind and Snow
4x8	N.G.	N.G.	N.G.	N.G.	N.G.	N.G.	N.G.	N.G.	Wind and Snow
5x5	N.G.	N.G.	N.G.	N.G.	N.G.	N.G.	N.G.	N.G.	Wind and Snow
5x6	N.G.	N.G.	N.G.	N.G.	N.G.	N.G.	N.G.	N.G.	Wind and Snow
5x7	N.G.	N.G.	N.G.	N.G.	N.G.	N.G.	N.G.	N.G.	Wind and Snow
5x8	N.G.	N.G.	N.G.	N.G.	N.G.	N.G.	N.G.	N.G.	Wind and Snow
6x6	N.G.	N.G.	N.G.	N.G.	N.G.	N.G.	N.G.	N.G.	Wind and Snow
6x7	N.G.	N.G.	N.G.	N.G.	N.G.	N.G.	N.G.	N.G.	Wind and Snow
6x8	N.G.	N.G.	N.G.	N.G.	N.G.	N.G.	N.G.	N.G.	Wind and Snow
7x7	N.G.	N.G.	N.G.	N.G.	N.G.	N.G.	N.G.	N.G.	Wind and Snow
7x8	N.G.	N.G.	N.G.	N.G.	N.G.	N.G.	N.G.	N.G.	Wind and Snow
8x8	N.G.	N.G.	N.G.	N.G.	N.G.	N.G.	N.G.	N.G.	Wind and Snow

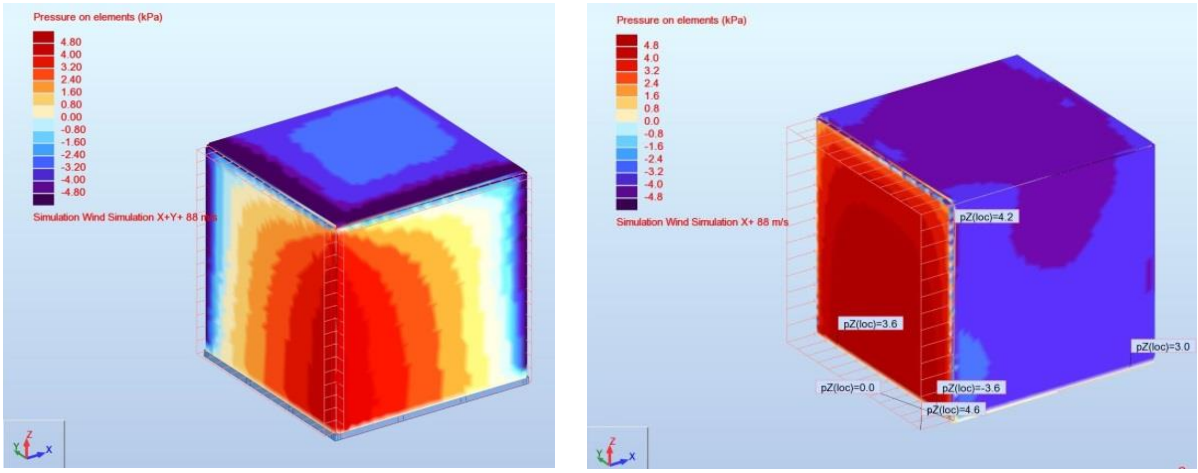

Figure 10.14: Applied wind loading on the shelter based on AS1170.2 with angles of 45º and 90º

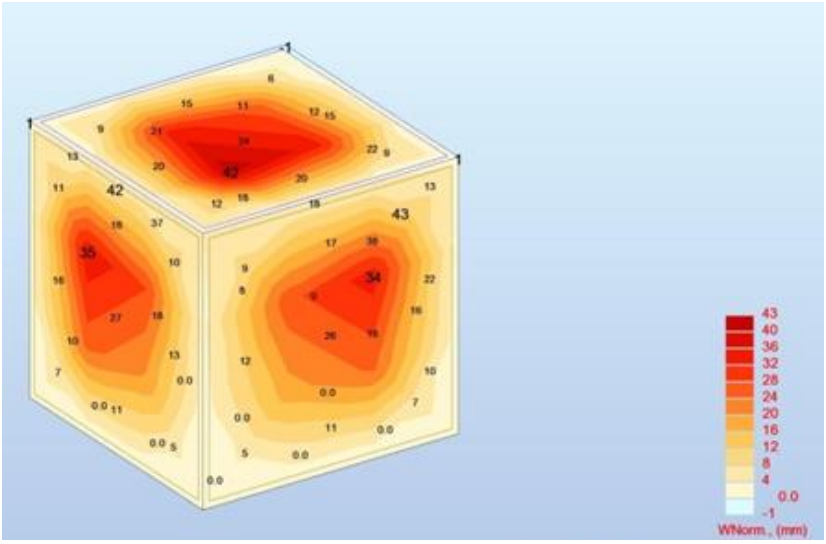

Figure 10.15: Maximum deformation of shelter caused by oblique wind

10.6 Conclusion

An innovative rapidly assembled system, mainly developed for quick assembly of modular post-disaster housing, was studied. The material properties as well as the entire structure of the units we investigated experimentally and by finite element modelling, respectively. Each unit is composed of panels made of a high density polyethylene or polypropylene (HDPE) coated by unbalance woven textile as the skins, filled with high-density Polyurethane (PU) foam as the core. Material characterization tests and finite element modelling were performed in accordance with some international building codes to evaluate the performance of the modular units in severe weather conditions. Results demonstrate that the developed rapidly assembled building units exhibits very good structural performance, and can meet the standards' requirements.

Chapter 11

Conclusions and recommended future work

11.1 Conclusions

In this thesis, the development process of a deployable modular sandwich system for rapid assembly building was studied, and the system's structural performance under some different action effects was investigated. The system is composed of 3-D high-density Polyethylene (HDPE) sheets, as the skins with a thickness of 2 mm, high-density PU foam core with a total thickness of 100 mm, in a pneumatic fabric formwork. The material properties, as well as the entire structure of the units were investigated through experiments and finite element modelling. Results demonstrate that the rapidly assembled building unit developed in this project exhibits very good structural performance, and can meet the standards' requirements. In this regard, the following conclusions can be drawn:

➢ *Conclusions with respect to use of high-density PU foam core:*

Results of carried out tests on the high-density PU foam (AUW763), used for the panels, show that it meets the ASTM requirements and specifications as follows:

- The used rigid foam is in accordance with ASTM E1730 Type 4.
- For introduced foam, carrying out thermal conductivity test is not required.
- Dimensional stability visual test results show minor darkening of specimens at 72 °C and after 836 hours. In addition, the average of the maximum linear change in specimens was only -0.81% which is less than the allowable amount of +/-1.5%. Also, the average of the maximum volumetric change in specimens was only -2.4% which is less than the allowable amount of +/-2.5%.
- The results of carried out flame resistance test as well as heat and smoke release rate show the accordance of the introduced foam with ASTM E1730-15 provisions.
- Based on energy-dispersive X-ray spectroscopy, no toxic components can be observed in investigated foam subsequently in burnt oxides.
- The results of impact resistance test show the maximum crushing areas of skin was less than the allowable amount of 76.2 mm.

Therefore, the investigated foam is certainly suitable for use in structural sandwich panel cores.

➢ *Conclusions with respect to the selection of fabric formwork:*

- The six most effective criteria for a suitable fabric formwork are permeability, strength, relative cost, durability, sew-ability, and aesthetics.
- Seven types of fabrics that meet the above mentioned criteria, are Lockram, Hydrophobic Polyester Fabric, Laminated Chamois, Vinyl Crystal Clear, Rubber fabric, Herculon Fabric, and Barrateen.
- Using a value matrix for mentioned factors as well as Analytical Hierarchy Process (AHP), which has been defined and calculated, Barrateen was selected from the mentioned list of seven potential candidates as the best pneumatic formwork candidate for foam-filled structural composite panels.

➢ *Conclusions with respect to lateral pressure on fabric formwork:*

- The type of lateral pressure of foam on the panelised fabric formwork with thickness of 100 mm is hydrostatic.
- The thickness of panelised fabric formworks does not have any effect on the location of maximum deflection.
- The location of maximum deflection lies at the intersection of primary level of the liquid foam and the vertical centre line of fabric formwork.
- Increasing the foam filled fabric formwork thickness from 100 mm to 200 mm will increase the lateral deformation by 8.75%.
- Increasing the foam filled fabric formwork thickness from 200 mm to 300 mm will increase the lateral deformation by only 3.45%.
- Increasing the foam filled fabric formwork thickness from 100 mm to 300 will decrease the total raised height of foam by 16.7%.
- Increasing in the foam filled fabric formwork thickness shows a relatively liner relationship with the decrease in the total raised height of foam.
- Using facing HDPE sheets and internal ties of 0.7 mm diameter spacing at 20 cm vertical and 20 cm horizontal intervals, the lateral deformation will be reduced to almost zero; i.e. fully prevented.
- The horizontal and vertical deformation curves of panelised fabric formwork with thickness of 100 mm follow second-order and quadratic equations, respectively.

- ***Conclusions with respect to edgewise / flatwise compressive behaviour and flexural and shear performance of foam-filled sandwich panel:***

  - The failure behaviour, the test values and the FE modelling results suggest very good bond strength between PU foam-core and the 3-D HDPE skins in compression that offers interesting capabilities in terms of flatwise compression and edgewise loading.
  - The failure mode of specimens under the edgewise compression was local buckling (wrinkling) of the HDPE sheets between two edge studs, resulting in a local delamination and de-bonding between the face and core.
  - The results of the flatwise compression test indicate that the flatwise compressive behaviour of the specimens is governed by the rigid foam behaviour.
  - Despite some minor discrepancy between the FE model and experimental tests, the results suggest that the FE model well agrees with the experimental test results, and could be used as a design tool to evaluate the compression performance of the sandwich panels.
  - Using 3D skins with 1200 studs per square meter, the composite sandwich panels resulted in a strong and stable composite section than individual sandwich sections alone.
  - Results of the quasi-static three-dimensional model and the material nonlinear simulations of the sandwich panels also indicate that under flexure, the foam core and skins displacement are in sync, which demonstrate well integrated and ductile behaviour of the introduced composite panel.

- ***Conclusions with respect to bending behaviour of seamed foam made sandwich panels:***

  - Casting at the end of gel time instead of the end of tack free time, resulted in a 80 % increase in the tensile strength of the seams.
  - Casting at about 20 seconds before of the end of tack free time (120th sec), increased the tensile strength of the seams by 60 %.
  - The seamed section exhibited about 33.1% of the maximum tensile strength of an intact section.

- Under monotonic loading, the seamless panels showed a larger deflection capacity, about 20% more than that of TS (with transverse seams) panels.
- Casting at the end of tack free time (120th sec) instead of 110th sec resulted in a significant positive effect on the tensile strength of seams.
- The tensile strength of a seamed section under cyclic loading was about 72.1% of the strength under monotonic loading.
- Making the seams at the end of the gel time increased the energy absorption capacity of panels by 53% in comparison with the end of tack free time.

➢ *Conclusions with respect to integrated connections between foam filled modular sandwich panels:*

Experimental and numerical investigations were conducted on an integrated connection between adjacent foam-filled sandwich panels composed of 3-D high density Polyethylene skins and high-density Polyurethane foam core. The overall mechanical response, and the stress distributions, and failure modes, moment resistance, initial rotational stiffness and rotational capacity of the connections were studied. In this regard:

- The experimental test results indicated that in composite sections the bending ultimate strength increases by 25% compared to foam-only connections.
- The composite connections show 2.2% greater rigidity, and increased rotational stiffness of 85%.
- With regard to the relative ultimate cantilever deflection, i.e. bending stiffness, composite connections presented better performance by about 12% in comparison with foam-only connections.
- Both simple and composite connections showed very similar failure modes and the fracture surface of them are fairly similar to each other.
- The first failure mode was a shear crack occurring at the vertical side of internal edge. By applying more pressure to the specimens, connections collapsed due to the development of shear stress and consequently the tensile stresses at the edges.
- The foam-only connections showed a relatively brittle sudden failure, while composite connections managed to undergo rather larger deformations before collapse.

- Comparison of finite element model and experimental results of all specimens showed that the load versus displacement were similar. Furthermore, the failure modes, ultimate load and ductility capacities correlated well with experimental observations.

➢ ***Conclusions with respect to the use of foam filled 3D modules in rapidly assembled buildings:***

- According to the calculations, the 3m x 3m x 3m structure can withstand most severe wind and snow as well as other sustained loads as per the Internarial Building Codes as well as Australian Standards.
- Wind loads with cyclonic strength (88 m/s for region D) with return period of 500 years was applied on the shelter. In this regard, the wind speed with respect to IBC and AS1170.2 are almost the same.
- The results demonstrate that the foam-filled modular units successfully meet the standards' requirements for semi-permanent housing even in cyclonic prone areas based on Standards Australia (AS1170.2), International Building Code (IBC-2015) and an American Standard as Minimum Design Loads for Buildings and Other Structures (ASCE7-10). For example, all maximum deformations, main stress and shear stress caused by wind are lower than design limits. As an example, the Maximum deformation of shelter caused by oblique wind is only 42 mm, which is less than the allowable limit in IBC (60mm).
- Analysis and design of some similar structures with various dimensions (from 3 m to 8 m) showed that if both of the length and width increase beyond 4 m simultaneously, the system will experience an increased risk of collapse with a safety factor bellow 1.

11.2 Recommended Future Work

The panelised system developed in this project was investigated with respect to a number of structural and constructional aspects that was critical to develop a new post disaster rapid assembly system. This thesis has mainly focused on the use of rigid foam and a particular skin for the design of temporary housing applications based on the scope of study. Some future research studies may help better improvement of the system:

- Evaluation of mechanical behaviour of softer and/or semi-rigid foams to be used as the core material of the panels.
- Investigation of real behaviour of full-scale one storey housing samples in wind tunnel. The preliminary results of numerical tests seem to be satisfactory, but further experimental study can provide better understanding of the real behaviour of this system, and probably the effects of different geometric designs.
- Optimizing of geometrical shapes and dimensional ratios of houses based on the result of wind tunnel tests, together with the optimum design of panels for foam rigidity, thickness, and other dimensions, based on structural and constructional constraints.
- Applications in multi-story buildings and the evaluation of seismic performance, using shaking table tests.
- Durability evaluation and use of other types of skins in order to use the proposed panels in semi-permanent or even permanent applications.
- Application of different connecting systems and fasteners (screws, bolts, zipper, et.) for connecting panels to different designs.
- The study of top casting method for in fill foam with different purring rates, and applications of other in filling methods such as injection from bottom.
- The panels may be advantageous in terms of multi-functionality due to the foam-filled sandwich configuration e.g. energy absorption and acoustic impedance is highly beneficial to multi-storey buildings. The study of these topics is recommended.

References

1. *Goodyear, R., Housing in greater Christchurch after the earthquakes: Trends in housing from the Census of Population and Dwellings 1991–2013. Statistics New Zealand. 2014.*
2. *De Temmerman, N. and C. Brebbia, Mobile and Rapidly Assembled Structures IV. Vol. 136. 2014: WIT Press.*
3. *Bouhaya, L., O. Baverel, and J.-F. Caron, Optimization of gridshell bar orientation using a simplified genetic approach. Structural and Multidisciplinary Optimization, 2014. 50(5): p. 839-848.*
4. *See, T. and C. Peter, Work Health and Safety Hazard Identification and Risk Management.*
5. *West, M., Fabric-formed Concrete columns. Concr. Int., 2004. 26(6): p. 42-45.*
6. *West, M., Prestressed fabric formwork for precast concrete panels. CONCRETE INTERNATIONAL-DETROIT-, 2004. 26(4): p. 60-63.*
7. *West, M. and R. Araya. Fabric formwork for concrete structures and architecture. in Int. Conf. Textile Composites and Inflatable Structures, Barcelona, Spain. 2009.*
8. *Abdelgader, H., M. West, and J. Górski. State-of-the-art report on fabric formwork. in Proceedings of the International Conference on Construction and Building Technology, Kuala Lumpur, Malaysia. 2008.*
9. *D.W., J., Formwork for Concrete. SP-4 (14), ed. E. edition. 2014: American Concrete Institute (ACI).*
10. *R.W., I., "Fabric forms for concrete". New Zealand Concrete Construction, 1981: p. 19-22.*
11. *Ghaib, M.A.A. and J. Górski, Mechanical properties of concrete cast in fabric formworks. Cement and concrete research, 2001. 31(10): p. 1459-1465.*
12. *Schipper, H. and J. Vambersky, A flexible mold for double curved precast concrete elements. BFT International,(8), 2010, 2010.*
13. *Orr, J.J., et al., Fabric formwork for ultra high performance fibre reinforced concrete structures. 2012.*
14. *Orr, J.J., et al., Concrete structures using fabric formwork. 2011.*
15. *D., T.G., "Materials in Construction: Principles, Practice and Performance". 2013: Longman.*
16. *KATAYAMA, K. and S. KOBAYASHI, STUDY ON CONCRETE SURFACE MICRO CRACKS WHEN USING PERMEABLE FORMS. Doboku Gakkai Ronbunshu, 1991. 1991(433): p. 119-128.*
17. *Cook, R.J. Forming economical concrete buildings: proceedings of the third international conference. 1988. American Concrete Institute.*
18. *Merritt, F.S. and J.T. Ricketts, Building design and construction handbook. Vol. 13. 2001: Citeseer.*
19. *Kromoser, B. and J. Kollegger, Pneumatic forming of hardened concrete–building shells in the 21st century. Structural Concrete, 2015. 16(2): p. 161-171.*
20. *Defonseka, C., Practical guide to flexible polyurethane foams. 2013: Smithers Rapra.*
21. *ABCB, B., Building Code of Australia. 2014, Class.*
22. *ASTM-E1730, Standard Specification for Rigid Foam for Use in Structural Sandwich Panel Core, in ASTM International. 2015: West Conshohocken, PA.*
23. *Goodyear, R.K. and A. Fabian, Housing in Auckland: Trends in housing from the Census of Population and Dwellings 1991 to 2013. 2014: Statistics New Zealand.*
24. *Goodyear, R., Housing in greater Christchurch after the earthquakes:Trends in housing from the Census of Population and Dwellings 1991–2013. 2014, New Zealand: Statistics New Zealand, Tatauranga Aotearoa.*
25. *Abulnour, A.H., The post-disaster temporary dwelling: Fundamentals of provision, design and construction. HBRC Journal, 2014. 10(1): p. 10-24.*
26. *De Temmerman, N. and C.A. Brebbia, Mobile and Rapidly Assembled Structures IV. 2014: WIT Press.*

27. *Preston, S.J. and L.C. Bank, Portals to an Architecture: Design of a temporary structure with paper tube arches. Construction and Building Materials, 2012. 30: p. 657-666.*
28. *Australian Building Codes, B., National Construction Code series / Australian Building Codes Board. 2011.*
29. *(ABCB), A.B.C.B., TEMPORARY STRUCTURES STANDARD. 2015, Australian Government and States and Territories of Australia: Australia.*
30. *Mira, L.A., A.P. Thrall, and N. De Temmerman, Deployable scissor arch for transitional shelters. Automation in Construction, 2014. 43: p. 123-131.*
31. *C.A., T.N.D.a.B., Mobile and Rapidly Assembled Structures. Vol. IV. 2014: WIT press.*
32. *Thrall, A. and C. Quaglia, Accordion shelters: A historical review of origami-like deployable shelters developed by the US military. Engineering structures, 2014. 59: p. 686-692.*
33. *Sharafi, P., et al., Interlocking system for enhancing the integrity of multi-storey modular buildings. Automation in Construction, 2018. 85: p. 263-272.*
34. *Sharafi, P., et al., Identification of Factors and Multi-Criteria Decision Analysis of the Level of Modularization in Building Construction. ASCE Journal of Architectural Engineering-Special Collection on Housing and Residential Building Construction, 2018. 24(2).*
35. *Sharafi, P., et al., Automated spatial design of multi-story modular buildings using a unified matrix method. Automation in Construction, 2017. 82: p. 31-42.*
36. *Sharafi, P., L.H. Teh, and M.N.S. Hadi, Conceptual design optimization of rectilinear building frames: A knapsack problem approach. Engineering Optimization, 2015. 47(10): p. 1303-1323.*
37. *Allen, H.G. and B.G. Neal, Analysis and Design of Structural Sandwich Panels: The Commonwealth and International Library: Structures and Solid Body Mechanics Division. 2013, London: Elsevier Science.*
38. *Correia, J.R., et al., GFRP sandwich panels with PU foam and PP honeycomb cores for civil engineering structural applications: Effects of introducing strengthening ribs. International Journal of Structural Integrity, 2012. 3(2): p. 127-147.*
39. *Potluri, P., E. Kusak, and T.Y. Reddy, Novel stitch-bonded sandwich composite structures. Composite Structures, 2003. 59(2): p. 251-259.*
40. *Dawood, M., E. Taylor, and S. Rizkalla, Two-way bending behavior of 3-D GFRP sandwich panels with through-thickness fiber insertions. Composite Structures, 2010. 92(4): p. 950-963.*
41. *Company, D.P., How to Reduce Energy Costs in Your Building. 1983: Diane Publishing Company.*
42. *Nemati, S., et al., Non-reinforced foam filled modules for rapidly assembled post disaster housing. International Journal of GEOMATE, 2018. 14(45): p. 151-161.*
43. *Veenendaal, D., M. West, and P. Block, History and overview of fabric formwork: using fabrics for concrete casting. Structural Concrete, 2011. 12(3): p. 164-177.*
44. *Orr, M.J., et al. Fabric formwork for ultra high performance fibre reinforced concrete structures. in fib symposium: Concrete structures for Sustainable Community. 2012.*
45. *Orr, J.J., et al., Concrete structures using fabric formwork. The Structural Engineer, 2011. 89(8): p. 20-26.*
46. *West, M., The Fabric Formwork Book: Methods for Building New Architectural and Structural Forms in Concrete. 2016: Routledge.*
47. *Nemati, S., M. Rashidi, and B. Samali, Decision making on the optimised choice of pneumatic formwork textile for foam-filled structural composite panels. International Journal, 2017. 13(39): p. 220-228.*
48. *McCarthy, M.J., et al., Influence of self-compacting concrete on the lateral pressure on formwork. Proceedings of the Institution of Civil Engineers-Structures and Buildings, 2012. 165(3): p. 127-138.*
49. *ASTM-D6693, Standard Test Method for Determining Tensile Properties of Nonreinforced Polyethylene and Nonreinforced Flexible Polypropylene Geomembranes, in ASTM International. 2015: West Conshohocken, PA.*
50. *ASTM-C364, Standard Test Method for Edgewise Compressive Strength of Sandwich Constructions, in ASTM International. 2016: West Conshohocken, PA.*

51. *Abdi, B., et al., Flatwise compression and flexural behavior of foam core and polymer pin-reinforced foam core composite sandwich panels. International Journal of Mechanical Sciences, 2014. 88: p. 138-144.*
52. *Norouzi, H. and Y. Rostamiyan, Experimental and numerical study of flatwise compression behavior of carbon fiber composite sandwich panels with new lattice cores. Construction and Building Materials, 2015. 100: p. 22-30.*
53. *Carlsson, L.A. and G.A. Kardomateas, Structural and failure mechanics of sandwich composites. Vol. 121. 2011: Springer Science & Business Media.*
54. *Kaveh, A. and P. Sharafi, Nodal ordering for bandwidth reduction using ant system algorithm. Engineering Computations, 2009. 26(3): p. 313-323.*
55. *Kaveh, A. and P. Sharafi, A simple ant algorithm for profile optimization of sparse matrices. Asian Journal of Civil Engineering (Building and Housing), 2007. 9(1): p. 35-46.*
56. *Kaveh, A. and P. Sharafi, Charged System Search Algorithm for Minimax and Minisum Facility Layout Problems. Asian Journal of Civil Engineering, 2011. 12(6): p. 703-718*
57. *Hayes, M.D., Structural analysis of a pultruded composite beam: shear stiffness determination and strength and fatigue life predictions. 2003.*
58. *Sharafi, P., et al., Flexural and shear performance of an innovative foam-filled sandwich panel with 3-D high density polyethylene skins. Engineering Solid Mechanics, 2018. 6(2): p. 113-128.*
59. *ASTM-C393/C393M, Standard Test Method for Core Shear Properties of Sandwich Constructions by Beam Flexure. 2011.*
60. *ASTM-D7250/D7250M, Standard Practice for Determining Sandwich Beam Flexural and Shear Stiffness. 2011.*
61. *Quinn, G. and C. Gengnagel, A review of elastic grid shells, their erection methods and the potential use of pneumatic formwork. Mobile and Rapidly Assembled Structures IV, 2014. 136: p. 129.*
62. *Hanna, A.S. and A.B. Senouci, Material cost minimization of concrete wall forms. Building and environment, 1997. 32(1): p. 57-67.*
63. *Lamberton, B.A., Fabric forms for concrete. Concrete international, 1989. 11(12): p. 58-67.*
64. *Rankilor, P.R., Textiles in civil engineering. Part 1-geotextiles. Handbook of technical textiles, 2000. 12: p. 358.*
65. *Sharafi, P., L.H. Teh, and M.N.S. Hadi, Shape optimization of thin-walled steel sections using graph theory and ACO algorithm. Journal of Constructional Steel Research, 2014. 101: p. 331-341.*
66. *Sharafi, P., M.N.S. Hadi, and L.H. Teh, Geometric Design Optimization for Dynamic Response Problems of Continuous Reinforced Concrete Beams. Journal of Computing in Civil Engineering, 2014. 28(2): p. 202-209.*
67. *Sharafi, P., M.N.S. Hadi, and L.H. Teh, Optimum Spans' Lengths of Multi-span Reinforced Concrete Beams Under Dynamic Loading, in Topics on the Dynamics of Civil Structures, Volume 1: Proceedings of the 30th IMAC, A Conference on Structural Dynamics, 2012, J.M. Caicedo, et al., Editors. 2012, Springer New York: New York, NY. p. 353-361.*
68. *Sharafi, P., M.N.S. Hadi, and L.H. Teh, Optimum Column Layout Design of Reinforced Concrete Frames Under Wind Loading, in Topics on the Dynamics of Civil Structures, Volume 1: Proceedings of the 30th IMAC, A Conference on Structural Dynamics, 2012, J.M. Caicedo, et al., Editors. 2012, Springer New York: New York, NY. p. 327-340.*
69. *Shin, Y., et al. Decision support model using the adaboost algorithm to select formwork systems in high‐rise building construction. in Proceeding of the 25th International Symposium on Automation and Robotics in Construction. 2008.*
70. *Orr, J., et al. Optimisation and durability in fabric cast'Double T'beams. in Second International Conference on Flexible Formwork (icff2012). 2012. University of Bath.*
71. *Proverbs, D.G., Holt, G. D., & Olomolaiye, P. O., Factors in formwork selection: A comparative investigation. Building Research and Information, 1999. 27(2): p. 109-119.*
72. *Nemati, S. and A. Rahai, Reinforced Concrete Construction. 2013: Fadak. 756.*
73. *Domone, P. and S.A. Jefferis, Structural grouts. 2002: CRC Press.*

74. *Lee, S.H., Study of construction methodology and structural behaviour of fabric-formed form-efficient reinforced concrete beam. 2011.*
75. *Chandler, A. and R. Pedreschi, Fabric formwork. 2007: Riba Publishing.*
76. *Rashidi, M., B. Samali, and P. Sharafi, A new model for bridge management: Part A: condition assessment and priority ranking of bridges. Australian Journal of Civil Engineering, 2016. 14(1): p. 35-45.*
77. *Rashidi, M. and B.P. Lemass, A decision support methodology for remediation planning of concrete bridges. 2011.*
78. *Linkov, I., et al., From comparative risk assessment to multi-criteria decision analysis and adaptive management: Recent developments and applications. Environment International, 2006. 32(8): p. 1072-1093.*
79. *Rashidi, M., et al., Remedial modelling of steel bridges through application of analytical hierarchy process (AHP). Applied Sciences, 2017. 7(2): p. 168.*
80. *Saaty, T.L., A scaling method for priorities in hierarchical structures. Journal of mathematical psychology, 1977. 15(3): p. 234-281.*
81. *Cheng, S.-C., et al., Semantic-based facial expression recognition using analytical hierarchy process. Expert Systems with Applications, 2007. 33(1): p. 86-95.*
82. *Saaty, T.L., Response to Holder's comments on the analytic hierarchy process. The Journal of the Operational Research Society, 1991. 42(10): p. 909-914.*
83. *Bello-Dambatta, A., et al., The Analytical Hierarchy Process for contaminated land management. Advanced Engineering Informatics, 2009. 23(4): p. 433-441.*
84. *Saaty, T.L., Decision making—the analytic hierarchy and network processes (AHP/ANP). Journal of systems science and systems engineering, 2004. 13(1): p. 1-35.*
85. *Kim, S.-K. and O. Song, A MAUT approach for selecting a dismantling scenario for the thermal column in KRR-1. Annals of Nuclear Energy, 2009. 36(2): p. 145-150.*
86. *Rashidi, M., B. Samali, and P. Sharafi, A new model for bridge management: Part B: decision support system for remediation planning. Australian Journal of Civil Engineering, 2016. 14(1): p. 46-53.*
87. *Norris, G.A. and H.E. Marshall, Multiattribute decision analysis method for evaluating buildings and building systems. 1995: Building and Fire Research Laboratory, National Institute of Standards and Technology.*
88. *Ishizaka, A., Development of an intelligent tutoring system for AHP (Analytic Hierarchy Process). 2004, WWZ Forschungsbericht.*
89. *Kim, G.-H., et al., Improved productivity using a modified table formwork system for high-rise building in Korea. Building and environment, 2005. 40(11): p. 1472-1478.*
90. *Yip, R. and C.S. Poon. Comparison of timber and metal formwork systems. in Proceedings of the Institution of Civil Engineers-Waste and Resource Management. 2008. Thomas Telford Ltd.*
91. *Hurd, M.K., Formwork for concrete. 1995.*
92. *ACI, I., 347-Guide to Formwork for Concrete. American Concrete Institute International, 2004.*
93. *Hanna, A.S., Concrete formwork systems. 1998: CRC Press.*
94. *Hurd, M.K. and A.C.-.-F.f. Concrete, Formwork for Concrete. 2005: American Concrete Institute.*
95. *Schmitz, R.P., Fabric Forms for Architectural Concrete: A State-of-the-Art Report, in AEI 2015. p. 259-268.*
96. *Khayat, K.H. and J.J. Assaad, Effect of w/cm and high-range water-reducing admixture on formwork pressure and thixotropy of self-consolidating concrete. Materials Journal, 2006. 103(3): p. 186-193.*
97. *Teixeira, S., A. Santilli, and I. Puente, Analysis of casting rate for the validation of models developed to predict the maximum lateral pressure exerted by self-compacting concrete on vertical formwork. Journal of Building Engineering, 2016. 6: p. 215-224.*
98. *Zhang, W., et al., An experimental study on the lateral pressure of fresh concrete in formwork. Construction and Building Materials, 2016. 111: p. 450-460.*

99. *Brameshuber, W. and S. Uebachs. Investigations on the formwork pressure using self-compacting concrete. in Self compacting concrete", Proceedings of the 3rd International RILEM Symposium, PRO33, RILEM, Paris. 2003.*
100. *Assaad, J.J. and K.H. Khayat, Effect of casting rate and concrete temperature on formwork pressure of self-consolidating concrete. Materials and structures, 2006. 39(3): p. 333-341.*
101. *Khayat, K., et al., SCC formwork pressure–task 1: capturing existing knowledge on formwork pressure exerted by SCC. National Ready-Mix Concrete Research Foundation–American Concrete Institute, 2007.*
102. *Khayat, K., et al., Effect of section width and casting rate on variations of formwork pressure of self-consolidating concrete. Materials and structures, 2005. 38(1): p. 73-78.*
103. *Rodin, S., PRESSURE OF CONCRETE ON FORMWORK. Proceedings of the Institution of Civil Engineers, 1952. 1(6): p. 709-746.*
104. *Gardner, N. Pressure of concrete against formwork. in Journal Proceedings. 1980.*
105. *Omran, A.F. and K.H. Khayat, Effect of formwork characteristics on SCC lateral pressure. Journal of Materials in Civil Engineering, 2016. 29(5): p. 04016293.*
106. *Ashby, M.F. and L.J. Gibson, Cellular solids: structure and properties. Press Syndicate of the University of Cambridge, Cambridge, UK, 1997: p. 183e231.*
107. *Goods, S., et al., Mechanical properties of CRETE, a polyurethane foam. Journal of Applied Polymer Science, 1998. 68(7): p. 1045-1055.*
108. *Niyogi, D., R. Kumar, and K. Gandhi, Water blown free rise polyurethane foams. Polymer Engineering & Science, 1999. 39(1): p. 199-209.*
109. *Seo, W., et al., Mechanical, morphological, and thermal properties of rigid polyurethane foams blown by distilled water. Journal of applied polymer science, 2003. 90(1): p. 12-21.*
110. *Mondal, P. and D. Khakhar, Hydraulic resistance of rigid polyurethane foams. II. Effect of variation of surfactant, water, and nucleating agent concentrations on foam structure and properties. Journal of applied polymer science, 2004. 93(6): p. 2830-2837.*
111. *Xu, J., et al., Generalization and modelling of rigid polyisocyanurate foam reaction kinetics, structural units effect, and cell configuration mechanism. Cellular Polymers, 2017. 36(6): p. 285-312.*
112. *ASTM, Standard Test Method for Breaking Strength and Elongation of Textile Fabrics. 2017.*
113. *Bijan Samali, S.N., Phezhman Sharafi, Farzad Yaghmaei, Feasibility study on use of rigid Polyurethane foam (PU) in structural sandwich panel cores of modular rapid assembly buildings. International Journal of Geomate, 2018.*
114. *ASTM-D5199, Standard Test Method for Measuring the Nominal Thickness of Geosynthetics, in ASTM International. 2012: West Conshohocken, PA.*
115. *ASTM-D1505, Standard Test Method for Density of Plastics by the Density-Gradient Technique, in ASTM International. 2010: West Conshohocken, PA.*
116. *Yan, R., et al., Quasi-static and dynamic mechanical responses of hybrid laminated composites based on high-density flexible polyurethane foam. Composites Part B: Engineering, 2015. 83: p. 253-263.*
117. *Wu, Z., et al., Theoretical and experimental study of foam-filled lattice composite panels under quasi-static compression loading. Composites Part B: Engineering, 2014. 60: p. 329-340.*
118. *Nasirzadeh, R. and A.R. Sabet, Study of foam density variations in composite sandwich panels under high velocity impact loading. International Journal of Impact Engineering, 2014. 63: p. 129-139.*
119. *Sharma, R.S. and V. Raghupathy, Influence of core density, core thickness, and rigid inserts on dynamic characteristics of sandwich panels with polyurethane foam as core. Journal of Reinforced Plastics and Composites, 2010. 29(21): p. 3226-3236.*
120. *He, Y., et al., Dynamic mechanical behavior of foam-core composite sandwich structures subjected to low-velocity impact. Archive of Applied Mechanics, 2016. 86(9): p. 1605-1619.*
121. *Wang, J., A.M. Waas, and H. Wang. Experimental study on the low-velocity impact behavior of foam-core sandwich panels. in 53rd AIAA/ASME/ASCE/AHS/ASC Structures, Structural Dynamics and Materials Conference 20th AIAA/ASME/AHS Adaptive Structures Conference 14th AIAA. 2012.*

122. *Feli, S. and M. Mahdipour Jalilian, Three-dimensional solution of low-velocity impact on sandwich panels with hybrid nanocomposite face sheets. Mechanics of Advanced Materials and Structures, 2017: p. 1-13.*
123. *Mirzapour, A., M.H. Beheshty, and M. Vafayan, The response of sandwich panels with rigid polyurethane foam cores under flexural loading. Iranian polymer journal, 2005. 14(12): p. 1082-1088.*
124. *Sharaf, T., W. Shawkat, and A. Fam, Structural performance of sandwich wall panels with different foam core densities in one-way bending. Journal of Composite Materials, 2010. 44(19): p. 2249-2263.*
125. *SHARAF, T., Flexural behaviour of sandwich panels Composed of polyurethane core and GFRP skins and ribs. 2010.*
126. *Sharaf, T. and A. Fam, Experimental investigation of large-scale cladding sandwich panels under out-of-plane transverse loading for building applications. Journal of Composites for Construction, 2010. 15(3): p. 422-430.*
127. *Sharaf, T. and A. Fam, Numerical modelling of sandwich panels with soft core and different rib configurations. Journal of Reinforced Plastics and Composites, 2012. 31(11): p. 771-784.*
128. *Mostafa, A., K. Shankar, and E. Morozov, Behaviour of PU-foam/glass-fibre composite sandwich panels under flexural static load. Materials and Structures, 2015. 48(5): p. 1545-1559.*
129. *Berggreen, C., B.C. Simonsen, and K.K. Borum, Experimental and numerical study of interface crack propagation in foam-cored sandwich beams. Journal of composite materials, 2007. 41(4): p. 493-520.*
130. *Tuwair, H., et al., Evaluation of sandwich panels with various polyurethane foam-cores and ribs. Composites Part B: Engineering, 2015. 79: p. 262-276.*
131. *Kakroodi, A.R., et al., Soy-based polyurethane spray foam insulations for light weight wall panels and their performances under monotonic and static cyclic shear forces. Industrial Crops and Products, 2015. 74: p. 1-8.*
132. *Garrido, M., J.R. Correia, and T. Keller, Effects of elevated temperature on the shear response of PET and PUR foams used in composite sandwich panels. Construction and Building Materials, 2015. 76: p. 150-157.*
133. *Garrido, M., et al., Creep of Sandwich Panels with Longitudinal Reinforcement Ribs for Civil Engineering Applications: Experiments and Composite Creep Modeling. Journal of Composites for Construction, 2016: p. 04016074.*
134. *Garrido, M., J.R. Correia, and T. Keller, Effect of service temperature on the shear creep response of rigid polyurethane foam used in composite sandwich floor panels. Construction and Building Materials, 2016. 118: p. 235-244.*
135. *George, T., et al., Hybrid core carbon fiber composite sandwich panels: Fabrication and mechanical response. Composite structures, 2014. 108: p. 696-710.*
136. *Mohamed, M., et al., Manufacturing and characterization of polyurethane based sandwich composite structures. Composite Structures, 2015. 123: p. 169-179.*
137. *Mostafa, A., K. Shankar, and E. Morozov, Effect of shear keys diameter on the shear performance of composite sandwich panel with PVC and PU foam core: FE study. Composite Structures, 2013. 102: p. 90-100.*
138. *P Sharafi, et al., Identification of Factors and Multi-Criteria Decision Analysis of the Level of Modularization in Building Construction. ASCE Journal of Architectural Engineering-Special Collection on Housing and Residential Building Construction, 2018. (accepted).*
139. *ASTM, Standard Test Method for Response of Rigid Cellular Plastics to Thermal and Humid Aging. Test Method D2126, 2015.*
140. *Thomsen, O.T., E. Bozhevolnaya, and A. Lyckegaard, Sandwich Structures 7: Advancing with Sandwich Structures and Materials: Proceedings of the 7th International Conference on Sandwich Structures, Aalborg University, Aalborg, Denmark, 29-31 August 2005. 2006: Springer Netherlands.*
141. *Fang, H., et al., Mechanical performance of innovative GFRP-bamboo-wood sandwich beams: Experimental and modelling investigation. Composites Part B: Engineering, 2015. 79: p. 182-196.*

142. *Hou, Y., et al., Graded conventional-auxetic Kirigami sandwich structures: Flatwise compression and edgewise loading. Composites Part B: Engineering, 2014. 59: p. 33-42.*
143. *Reis, E.M. and S.H. Rizkalla, Material characteristics of 3-D FRP sandwich panels. Construction and Building Materials, 2008. 22(6): p. 1009-1018.*
144. *Lameiras, R., et al., Development of sandwich panels combining fibre reinforced concrete layers and fibre reinforced polymer connectors. Part I: Conception and pull-out tests. Composite Structures, 2013. 105: p. 446-459.*
145. *Lameiras, R., et al., Development of sandwich panels combining fibre reinforced concrete layers and fibre reinforced polymer connectors. Part II: Evaluation of mechanical behaviour. Composite Structures, 2013. 105: p. 460-470.*
146. *Ferreira, A.J., ICCS19 19th International Conference on Composite Structures. 2016: Società Editrice Esculapio.*
147. *CoDyre, L. and A. Fam, The effect of foam core density at various slenderness ratios on axial strength of sandwich panels with glass-FRP skins. Composites Part B: Engineering, 2016. 106: p. 129-138.*
148. *Fam, A. and T. Sharaf, Flexural performance of sandwich panels comprising polyurethane core and GFRP skins and ribs of various configurations. Composite Structures, 2010. 92(12): p. 2927-2935.*
149. *ASTM, D., 1621-00. Standard Test Method for Compressive Properties of Rigid Cellular Plastics.*
150. *Allen, H.G., Analysis and design of structural sandwich panels: the commonwealth and international library: structures and solid body mechanics division. 2013: Elsevier.*
151. *Manalo, A., Structural behaviour of a prefabricated composite wall system made from rigid polyurethane foam and Magnesium Oxide board. Construction and Building Materials, 2013. 41: p. 642-653.*
152. *Wang, L., et al., Mechanical performance of foam-filled lattice composite panels in four-point bending: Experimental investigation and analytical modeling. Composites part b: engineering, 2014. 67: p. 270-279.*
153. *Kumar, M.V. and B. Soragaon, Fabrication and evaluation of multilayered polyurethane foam core sandwich panels for static flexural stiffness. Procedia Engineering, 2014. 97: p. 1227-1236.*
154. *Lv, L., et al., Bending properties of three-dimensional honeycomb sandwich structure composites: experiment and Finite Element Method simulation. Textile Research Journal, 2017: p. 0040517517703602.*
155. *Mostafa, A., Numerical analysis on the effect of shear keys pitch on the shear performance of foamed sandwich panels. Engineering Structures, 2015. 101: p. 216-232.*
156. *ASTM, D7249/D7249M, Standard Test Method for Facing Properties of Sandwich Constructions by Long Beam Flexure. 2017.*
157. *Zenkert, D. and M. Burman, Tension, compression and shear fatigue of a closed cell polymer foam. Composites Science and Technology, 2009. 69(6): p. 785-792.*
158. *Fan, X., M. Zhao, and T. Wang, Experimental investigation of the fatigue crack propagation in a closed-cell aluminum alloy foam. Materials Science and Engineering: A, 2017.*
159. *Zhao, M., et al., Experimental investigation of the fatigue of closed-cell aluminum alloy foam. Materials Letters, 2015. 160: p. 68-71.*
160. *Noble, F. and J. Lilley, Fatigue crack growth in polyurethane foam. Journal of Materials Science, 1981. 16(7): p. 1801-1808.*
161. *Shipsha, A., M. Burman, and D. Zenkert, On mode I fatigue crack growth in foam core materials for sandwich structures. Journal of Sandwich Structures & Materials, 2000. 2(2): p. 103-116.*
162. *Poapongsakorn, P. and C. Kanchanomai, Fatigue crack growth behavior and mechanism of closed‐cell PVC foam. Polymer Engineering & Science, 2013. 53(8): p. 1719-1727.*
163. *Kanny, K., et al., Dynamic mechanical analyses and flexural fatigue of PVC foams. Composite Structures, 2002. 58(2): p. 175-183.*
164. *Huang, J. and J. Lin, Fatigue of cellular materials. Acta materialia, 1996. 44(1): p. 289-296.*

165. *Wang, L., et al., Influence of pores on crack initiation in monotonic tensile and cyclic loadings in lost foam casting A319 alloy by using 3D in-situ analysis. Materials Science and Engineering: A, 2016. 673: p. 362-372.*
166. *Toubia, E.A. and A. Elmushyakhi, Influence of core joints in sandwich composites under in-plane static and fatigue loads. Materials & Design, 2017.*
167. *Sharafi, P., et al., Behaviour of Integrated Connections Between Adjacent Foam-Filled Modular Sandwich Panels. Engineering Solid Mechanics, 2018. 6(3): p. 214-226.*
168. *Garrido, M., et al., Connection systems between composite sandwich floor panels and load-bearing walls for building rehabilitation. Engineering Structures, 2016. 106: p. 209-221.*
169. *Mastali, M., I.B. Valente, and J.A.O. Barros, Flexural performance of innovative hybrid sandwich panels with special focus on the shear connection behavior. Composite Structures, 2017. 160: p. 100-117.*
170. *Kempf, A. and J. Feldhusen, Entwicklung einer mechanischen Verbindungstechnik für Sandwichwerkstoffe. 2004, Fakultät für Maschinenwesen.*
171. *Mohan, V., et al., Cold-formed steel pallet rack connection: an experimental study. International Journal of Advanced Structural Engineering (IJASE), 2015. 7(1): p. 55-68.*
172. *Kujawa, M. and C. Szymczak, Numerical and experimental investigation of rotational stiffness of zed-purlins connection with sandwich panels. Thin-walled structures, 2014. 75: p. 43-52.*
173. *Sharafi, P., et al., Edgewise and Flatwise Compressive Behaviour of Foam-Filled Sandwich Panels with 3-D High Density Polyethylene Skins. Engineering Solid Mechanics, 2018. 7(1).*
174. *Shek, P., et al., Experimental Evaluation of Flush End—Plate Connection with Built-up Hybrid Beam Section. Advances in Structural Engineering, 2012. 15(2): p. 331-341.*
175. *Kataoka, M.N. and A.L.H.C. El Debs, Parametric study of composite beam-column connections using 3D finite element modelling. Journal of Constructional Steel Research, 2014. 102: p. 136-149.*
176. *Tsai, M.-K., Designing Postdisaster Temporary Housing Facilities: Case Study in Indonesia. Natural Hazards Review, 2014. 16(3): p. 05014007.*
177. *Patel, S. and M. Hastak, A framework to construct post-disaster housing. International Journal of Disaster Resilience in the Built Environment, 2013. 4(1): p. 95-114.*
178. *Development, U.S.D.o.H.a.U., ESG Minimum Habitability Standards for Emergency Shelters and Permanent Housing. 2014: USA.*
179. *HUD, ESG Minimum Habitability Standards for Emergency Shelters and Permanent Housing. 2014: p. 1-15.*
180. *Department of Housing and Public Works, Temporary accommodation buildings, Minimum building standards. 2013, Department of Housing and Public Works: Queensland. p. 1-3.*
181. *Fallahi, A., TECHNICAL REPORT-SHELTERING, FROM RELIEF TO RECONSTRUCTION: One Year after the 2010 East Azerbaijan Province Earthquake. ArchNet-IJAR, 2013. 7(3).*
182. *Tas, M., N. Tas, and N. Cosgun, Study on permanent housing production after 1999 earthquake in Kocaeli (Turkey). Disaster Prevention and Management: An International Journal, 2010. 19(1): p. 6-19.*
183. *Song, Y., N. Mithraratne, and H. Zhang, Life-time performance of post-disaster temporary housing: A case study in Nanjing. Energy and Buildings, 2016. 128: p. 394-404.*
184. *Atmaca, N., Life-cycle assessment of post-disaster temporary housing. Building Research & Information, 2017. 45(5): p. 524-538.*
185. *Gunawardena, T., et al., Time-Efficient Post-Disaster Housing Reconstruction with Prefabricated Modular Structures. open house international, 2014. 39(3): p. 59-66.*
186. *Co-ordinator, O.o.t.U.N.D.R., Shelter after disaster: Guidelines for assistance. 1982: New York: United Nations.*
187. *Arlikatti, S., et al., Temporary Sheltering, Psychological Stress Symptoms, and Perceptions of Recovery. Natural Hazards Review, 2014. 16(3): p. 04014028.*
188. *Kuroda, M., Healthcare ICT for Temporary Housing Community in Disaster-Stricken Area. IEICE transactions on communications, 2012. 95(10): p. 3062-3066.*

189. *Nimmich, J., Unless Modified, FEMA's Temporary Housing Plans Will Increase Costs by an Estimated $76 Million Annually, ed. OIG-13-102. 2013, USA: Department of Homeland Security Office of Insprctor General.*
190. *Atmaca, A. and N. Atmaca, Comparative life cycle energy and cost analysis of post-disaster temporary housings. Applied Energy, 2016. 171: p. 429-443.*
191. *P Sharafi, et al., Identification of Factors and Multi-Criteria Decision Analysis of the Level of Modularization in Building Construction. ASCE Journal of Architectural Engineering-Special Collection on Housing and Residential Building Construction. (Accepted for publication in July 2017), 2017.*
192. *Torus, B. and S.M. Şener, Post-disaster shelter design and CPoDS.*
193. *Societies, I.F.o.R.C.a.R.C., Post-disaster shelter: Ten designs. 2013: Geneva.*
194. *(ESG), T.E.S.G., ESG Minimum Habitability Standards for Emergency Shelters and Permanent Housing: Checklists. 2015. p. 1-5.*
195. *Boehm, S., et al., Interior design as a post-disaster team partner. International Journal of Disaster Resilience in the Built Environment, 2016. 7(3): p. 276-289.*
196. *(HUD), U.S.D.o.H.a.U.D., Housing Quality Standards (HQS) For Section 8 Housing Choice Voucher Properties. 2016, Prepared by the National Center for Healthy Housing. p. 1-6.*
197. *Bauer, R., Oxfam GB"s Guidelines for Post Disaster Housing Reconstruction. 2003.*
198. *government, N., Temporary uses and structures, ed. p.a. infrastructures. 2013.*
199. *El-Anwar, O. and L. Chen, Automated Community-Based Housing Response: Offering Temporary Housing Solutions Tailored to Displaced Populations Needs. Journal of Computing in Civil Engineering, 2016. 30(6): p. 04016019.*
200. *El-Anwar, O. and L. Chen, Maximizing the computational efficiency of temporary housing decision support following disasters. Journal of Computing in Civil Engineering, 2012. 28(1): p. 113-123.*
201. *El-Anwar, O., K. El-Rayes, and A. Elnashai, Maximizing temporary housing safety after natural disasters. Journal of Infrastructure Systems, 2009. 16(2): p. 138-148.*
202. *(FEMA), F.E.M.A., National Disaster Housing Strategy. 2009, USA.*
203. *Quaglia, C., et al., Balancing energy efficiency and structural performance through multi-objective shape optimization: Case study of a rapidly deployable origami-inspired shelter. Energy and Buildings, 2014. 82: p. 733-745.*
204. *Quaglia, C., A. Dascanio, and A. Thrall, Bascule shelters: A novel erection strategy for origami-inspired deployable structures. Engineering Structures, 2014. 75: p. 276-287.*
205. *Quagli, C., Z. Ballard, and A. Thrall, Parametric modelling of an air-liftable origami-inspired deployable shelter with a novel erection strategy. Mobile and Rapidly Assembled Structures IV, 2014. 136: p. 23.*
206. *Ozlem, E., A proposal for sustainable temporary housing applications in earthquake zones in turkey: Modular box system applications. Gazi University Journal of Science, 2012. 25(1): p. 269-288.*
207. *Ravina, D. and R.R. Shih, A shelter for the victims of the Typhoon Haiyan in the Philippines: The design and methodology of construction. Pollack Periodica, 2017. 12(2): p. 129-139.*
208. *Council, I.C., International building code (IBC). 2015: USA.*
209. *(ASCE), A.S.o.C.E., Minimum Design Loads for Buildings and other Structures. ASCE7-10. 2010: USA.*

Appendix A

1) Decision Making on the Optimised Choice of Pneumatic Formwork Textile for Foam-Filled Structural Composite Panels.

International Journal of GEOMATE, Nov., 2017, Vol.13, Issue 39, pp. 220-228 Geotec., Const. Mat. & Env., ISSN:2186-2990, DOI: https://doi.org/10.21660/2017.39.7350, Japan.

2) Effects of Cold Joints on the Structural Behaviour of Polyurethane Rigid Foam Panels.

Engineering Solid Mechanics, 2019, 7(1), pp. 1-12. ISSN 2291-8752 (Online) - ISSN 2291-8744 (Print). DOI: 10.5267/j.esm.2018.12.003, Canada.

3) Non-Reinforced Foam Filled Modules for Rapidly Assembled Post Disaster Housing.

International Journal of GEOMATE, May, 2018 Vol.14, Issue 45, pp.151-161 Geotec., Const. Mat. & Env., DOI: https://doi.org/10.21660/2018.45.73573 ISSN: 2186-2982 (Print), 2186-2990 (Online), Japan.

International Journal of GEOMATE, Nov., 2017, Vol.13, Issue 39, pp.220-228
Geotec., Const. Mat. & Env., ISSN:2186-2990, Japan, DOI: https://doi.org/10.21660/2017.39.7350

DECISION MAKING ON THE OPTIMISED CHOICE OF PNEUMATIC FORMWORK TEXTILE FOR FOAM-FILLED STRUCTURAL COMPOSITE PANELS

*Saeed Nemati[1], Maria Rashidi[1] and Bijan Samali[1]

[1]Centre for Infrastructure Engineering, Western Sydney University, Australia

*Corresponding Author, Received: 14 July 2017, Revised: 21 Aug. 2017, Accepted: 5 Sept. 2017

ABSTRACT: The selection of an appropriate formwork system not only affects the entire construction duration and cost, but also affects subsequent construction activities such as electrical, mechanical, and finishing work. The current intuitive judgment approach in the selection of fabric formwork systems cannot assure an optimal and consistent result. This paper introduces a decision-making method for selection of the most appropriate pneumatic fabric formwork for foam-filled structural panels in rapidly assembled buildings (RABs) that will be used in semi-permanent housing such as post disaster sheltering. First, using a questionnaire survey, six most effective criteria for a suitable pneumatic fabric formwork; permeability, strength, relative cost, durability, sew-ability, and aesthetics are identified. Some experimental tests were conducted to determine the selection indicators for the criteria like durability and strength for each candidate. Then a value matrix for these factors has been defined and calculated, and the best pneumatic formwork candidate for foam-filled structural composite panels is selected from a list of seven potential candidates, using Analytical Hierarchy Process (AHP).

Keywords: Fabric formwork, Pneumatic formwork, Foam-filled panels, Rapid assembly buildings, Decision making, Analytical hierarchy process

1. INTRODUCTION

Fabric formwork is a method for construction of a wide range of architectural and structural components. Fabric formwork is made of textile sheets of synthetic fibres such as nylon, polyesters, polypropylene that are fabricated into containers to contain various type of fillers such as concrete. Fabric formworks can be used to form columns, walls, beams, trusses, slabs, panels, and thin-shell structures in both precast and in-situ construction. Using fabric formwork as a mould in concrete structures, it is possible to cast architecturally interesting, structurally optimized non-prismatic structures that use up to 40% less concrete in comparison with an equivalent prismatic section [1], offering potentially significant embodied energy savings [2] and subsequently, a striking reduction in the CO_2 emissions [3] can be achieved. In a recent ongoing research project at the Centre for Infrastructure Engineering of Western Sydney University, fabric formwork has been used for an innovative foam-filled structural panels in order to be employed for rapidly assembled buildings as a semi-permanent housing system. This study will focus on the pneumatic fabric formworks, in which pneumatic force is used for the erection of the flexible fabric formwork [4]. This system is going to tackle the problems with the existing semi-permanent housing systems' low tolerance in construction, transportation, erection and maintenance phases, as well as their relatively costly materials [5], installation and fabrication methods and labour works. The critical aspect of fabric formwork for achieving desirable performance is the selection of the fabric itself. Although a wide range of woven fabrics can be used as formwork for fabric formwork, tensile strengths in both warp and weft directions must be sufficient to hold the infill material (which is polyurethane [6] in this research) and a low creep modulus is desirable to limit formwork deformations during casting and curing/hardening. In the literature, to date, there is no known study based on systematic decision making methods for fabric formwork selection. This paper identifies the factors influencing the selection of an appropriate fabric, and develops a decision-making system for selecting the best fabric formwork textile for the newly developed foam filled panels, which will be used as a rapidly assembled building system for semi-permanent housing.

2. BACKGROUND OF THE STUDY

There are not many studies on the structural applications of fabric formworks. The work of Lamberton in 1968 in the field of Geotextiles led to the first commercial use of fabric formwork for concrete structures [7]. In the early 1990s, Rob Wheen from the University of Sydney and

Asaddoah Redjvani, developed a flexible formwork wall system for both the Persian Gulf and Caspian sea marine and land construction projects using PVC coated polyester fabric internal ties [8]. Ghaib et al. [9] showed that the mechanical characteristics of fabric formwork affect its filled material. Appropriate selection of a formwork system can considerably affect the cost and speed of many construction projects [10-14]. Shin et al. [15] proposed a decision support model to select a formwork system suitable for the construction site conditions. Optimisation and durability in fabric cast double T-beams have been studied by Orr et al. [16]. Proverbs et al. [17] identified nine formwork selection factors including quality of concrete, relative costs, speed of production, availability of plant and equipment, availability of labour, company practice, building form and location, degree of repetition and on-site transport system and ranked them in terms of importance for each international group of contractors. The formwork systems can be selected based on some construction considerations including easy and economical transportation from factory to construction site, easy and economical assembly and disassembly, maximum rate of construction speed to formwork weight, minimum number of construction joints, minimum waste generation in formwork production process, safety, ease of storage, applicability to high rise structures, reasonable potential for preconstruction, the potential to make non-prismatic sections and complex shapes, not reliant on highly-trained and skilled work force, compatibility with the core material in order to minimize the environmental effects, appropriate specific heat capacity and thermal conductivity, reusability and finally fast connectors applicability [18].

3. FABRIC FORMWORKS

3.1 Fabrics Properties

There are two general types of fabric formworks: slack-sheet mould and energized (tensioned) formwork sheets [19]. Fabrics can be categorised as woven/non-woven fabrics, balanced/unbalanced fabrics, knit fabrics, plastic films and coated/uncoated fabrics. There are many different weaving patterns but the basic pattern called a “plain weave” consists of warp threads (running along the long direction of the roll) and weft threads (filling transversely across the width of the roll) [19]. If a woven textile has the same amount of materials in both the wrap and weft directions, it is referred to as a “balanced” weave. An “unbalanced” weave will have more material in one direction that in the other, and so will have unequal strength and stiffness as well. Because the threads are kept straight, plain woven structures do not allow much stretching at all along the two axes of the weave. Nevertheless, a balanced plain woven fabric will always be slightly less stretchy (i.e. have greater stiffness in tension) in the warp, or machine direction [19]. Non-woven fabric such as felt generally refers to a fabric composed of short fibres, matted and compressed together in what might be described as a structural tangle. Non-woven textiles are not generally used structurally, as they are inherently weaker than woven fabrics, due to their randomized and non-continuous fibres. Knit fabrics are made with a looped thread running in a long meandering course, forming an interlinked mesh. Because the yarns are looped and not straight, a knitted structure allows a good deal of stretch. Plastic films are flexible sheets of plastic, such as a polyethylene vapour barrier film can also be used as a formwork sheet or as a formwork liner. Woven or even knit fabrics can have a waterproof coating applied to one or both sides. Such a coating affects the permeability of the fabric, for example, by making it impervious to water and air. Coating can also inhibit or prevent the threads from fraying at the edges of the cloth, and inhibit or prevent the fabric’s fibres from “shearing” on the bias. When a coating is applied to a woven textile, it binds the woven tapes or threads together, fixing the weave’s 90° geometry in place. Since the coating prevents, or inhibits, the threads from shearing, the fabric behaves less like a woven structure and more like an isotropic sheet such as a sheet of plastic or a piece of paper [19].

3.2 Fabrics for Flexible Formwork

Generally speaking, the viscosity of the fill material, the internal construction details, the hydrostatic pressure action on the outer skin, the internal restraints on the grout level, the size and shape of flexible formwork and its methods of placing and handling, the effects of buoyancy and currents, the sequence of injection, the position of bleed points or overfill prevention and finally, the provision of overfill compartments to compensate for the settlement of grout resulting from excessive bleed are the major factors to be considered when selecting fabric formwork [20]. Current construction practice in this field generally uses woven polyolefin textiles. Polyester, Polyamide, Polypropylene (PP) and Polyethylene (PE), which are not true elastic materials, are the main synthetic polymers used as raw materials to manufacture formwork fabrics [21]. Woven Polyolefin Geotextiles (PP and PE) are a common choice for fabric formwork. PE and PP textiles (that are made from woven high density polyethylene or polypropylene (HDPE or HDPP) threads or tapes) are among the least expensive

options, while they are stronger and more robust than the burlap/hessian fabrics. PP fabrics don't tear easily and are relatively lighter than PE. PE fabrics are resistant to strong acids or strong bases and relatively weaker in strength compared to PP. These materials can be manufactured with varying degrees of quality. Even the lowest quality PP and PE fabrics, such as woven textiles used for sandbags or packaging, will work well as fabric moulds, if used conservatively. There is also a wide range of PE and PP "geotextiles" manufactured for use in landscape construction and road building. These are made of woven high density polyethylene or polypropylene threads or taps and are specifically designed for combinations of strength and permeability to water. PE and PP are so similar in their appearance, handling and performance as formworks, that user will not be able to tell them apart. One weakness of PP and PP fabrics is that they will eventually degrade from exposure to ultraviolet radiation (sunlight), although they can be manufactured with anti-UV stabilizers that do a good job of resisting this degradation. The woven PE and PP fabrics are quite strong and will usually have plenty of reserve strength. Their behaviour is non-linear, with a rough service strain of above 2%. Linear, elastic behaviour may be maintained to 5% strain, or more. PP or PE woven fabrics will not propagate a tear, which makes them safe to use, and allows them to be connected using staples, screws or nails. PP and PE are also thermoplastics.

4. STUDIED FABRICS

The textile industry is developing various types of suitable fabrics for applications in construction [22]. In order to be used as a fabric formwork for structural panels, the most important properties of fabrics are strength, stiffness, failure mode (slow/plastic failure are more desirable than sudden/elastic failure), permeability, weldability (coated PE or PP fabric can be heat-welded together and uncoated fabrics cannot), reusability, easy sewing , and stress distribution ability. Accordingly, in this study seven types of fabrics that meet the abovementioned criteria, and are widely used for similar purposes have been selected and then evaluated as potential options for fabric formwork of foam filled panels. The selected fabrics were: Lockram, Hydrophobic Polyester Fabric, Laminated Chamois, Vinyl Crystal Clear, Rubber fabric, Herculon Fabric, and Barrateen (left to right in Fig.1).

Lockram is made from a semi-industrial type of cotton, and produced in 145 cm wide rolls. The common applications are household applications. This fabric is a balanced woven fabric, and has the identical tensile strength in both the warp and weft directions and is well inflatable too. The result of tensile tests according to ASTM D1980-89 in warp direction is shown in Fig.2. The applied width of specimens is 10cm and mechanism of failure is sudden/brittle rupture. The failure strain has been measured as 15%.

Fig.1 Studied fabrics

Hydrophobic Polyester Fabric is made from pure polyester and is 100% washable and mould resistant, and produced in 260 cm wide rolls. Its common applications are household applications such as curtains.

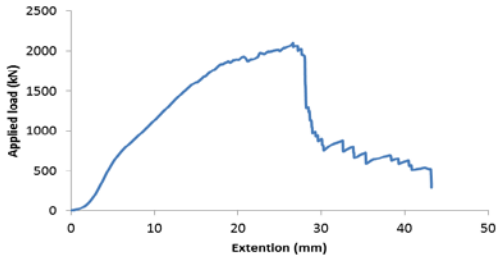

Fig.2 Lockram tensile behaviour

This fabric is a balanced woven fabric. It has the same tensile strength in both the warp and weft directions, and is well inflatable. The result of tensile tests on 10cm wide specimens according to ASTM D1980-89 in warp direction is shown in Fig.3. The failure strain has been measured as 17%, and the mechanism of failure is a sudden/brittle rupture. Laminated Chamois is composed of a plastic film and a layer of non-woven compressed to each other. It is used for household applications and produced in 135 cm wide rolls. By using as internal fabric formwork layer, the cost of finishing and maybe painting can be reduced. The result of tensile tests on 10cm wide specimens according to ASTM D1980-89 is shown in Fig.4, which shows that its failure strain is about 110%. Laminated Chamois is crimped during the tensile test, but at rupture point, only its plastic layer was ruptured and its un-woven layer kept deforming. The mechanism of failure is a ductile rupture. Vinyl Crystal Clear is an un-dyed polymeric fabric, used for household and produced in 135cm wide

rolls. Because of its tensile behaviour and high failure strain (350%) and good stress distribution ability, as shown in Fig.5, it can be suitable for mechanical connections.

Rubber fabric does not display any plastic behaviour during tensile tests. Its fracture mode is very brittle (Fig.6) but, the failure strain has been measured as 90%. This brittle behaviour can create some structural problems when used for mechanical connections. It is produced in 100 cm wide rolls. Herculon fabric is a woven polyolefin textile, used as window shades, children's sandbox cover, pergola, veranda and patio cover, and produced in 185 cm wide rolls. It possesses relatively high strength and durability, and as a lead-free material has 100% UV-stabilised yarn and can reduce the UV flow by 90%. It is classified as mould and mildew resistant and non-shrink heat fabric and is not inflatable.

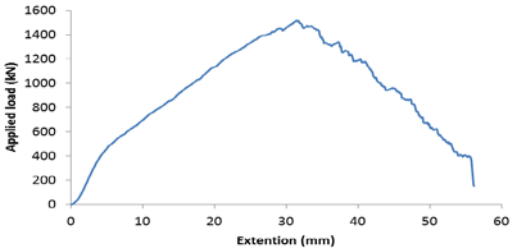

Fig.3 Tearing of Hydrophobic Polyester Fabric and its tensile behavior

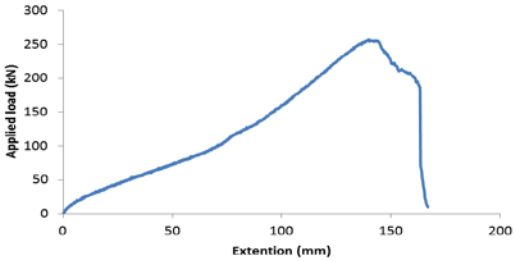

Fig.4 Laminated Chamois tensile behaviour

This fabric is an unbalance plain woven fabric. Therefore its tensile strengths in two directions perpendicular to each other (the warp and weft directions) are not the same. The result of tensile tests according to ASTM D1980-89, is shown in Fig.7. As Shown in Fig.9, before strain reaches 75%, Herculon fabric has similar behaviour in the two directions. Then, before reaching 225% strain, it has elastic behaviour in both directions. Under strains between 75% and 225%, the modulus of elasticity of the principal direction is higher, but, under the strain of 225% the harder specimen had a sudden rupture, whiles the softer specimen continues its deformation to about 250% strain.

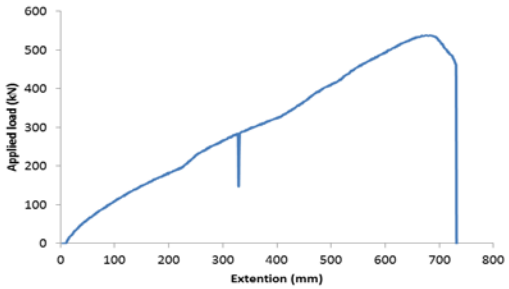

Fig.5 Vinyl Crystal clear tensile behavior

Barrateen is a HDPE coated unbalance woven textile. It is produced in 184 cm wide rolls. The coating material is low density polyethylene and well inflatable. In addition, its tensile strengths in the warp and weft directions are not the same. The result of tensile tests according to ASTM D1980-89 is shown in Fig.10. As can be seen in Fig.8, the modulus of elasticity of the principal direction is higher, but, under the strain of about 270%, both specimens had a sudden brittle rupture. As maintained before, weldability is one of the main benefits of the coated fabric. A series of weldability tests was also conducted on the fabrics (Fig.9).

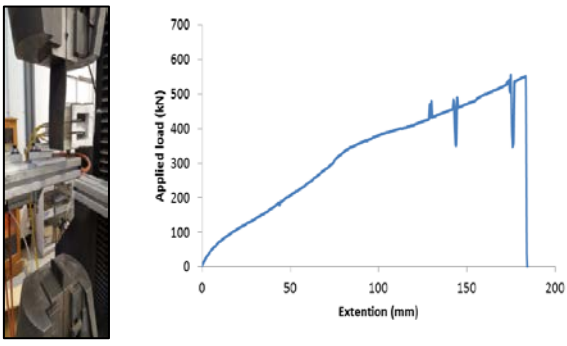

Fig.6 Brittle behaviour of Rubber fabric specimens

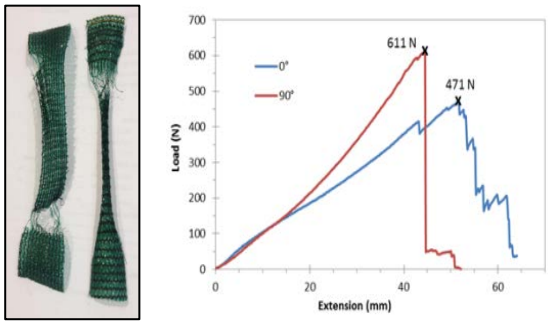

Fig.7 Herculon fabric tensile behaviour in main (90º) and transverse (0º) directions

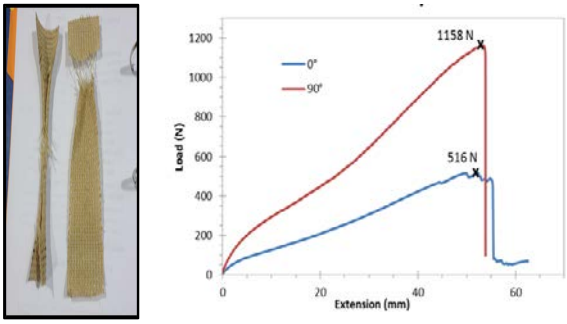

Fig.8 Herculon fabric tensile behaviour in main (90º) and transverse (0º) directions

The results of tensile tests of heat-welded parts showed that this kind of connections has no reliable structural performance (Fig.10). According to the results, the tensile bearing capacity of heat-welded connections can reach up to 13% of the average strength of the material. In addition, the maximum strain was measured as 90% at the failure point.

Fig.9 Heat-welded specimens of Barrateen fabric

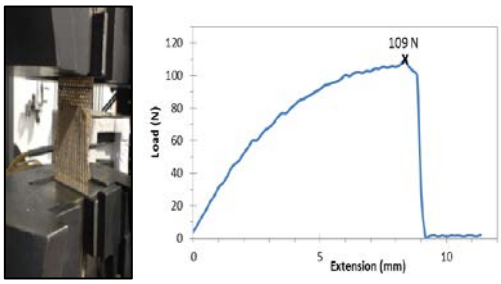

Fig.10 Tensile behaviour of heat-welded Barrateen fabric specimens

5. DECISION MAKING

Most real-world decisions are not limited to unique and single solutions. The decisions are typically less than optimal and are drawn from a set of reasonable alternatives that have been known as 'satisficing' solutions [23-25]. Therefore, the potential range of rational alternatives should be identified and classified [26]. In this case, selection of the most suitable fabric involves a case-by-case assessment to determine the potential risks associated with any given alternative. Potential users and decision makers have various criteria and constraints that must be coped with when endeavouring to suggest the best possible alternative. The main idea of using criteria is to quantify the performance of alternatives in relation to the objectives of the decision maker based on a numerical scale [27, 28].

5.1 Decision Criteria

The selection of an appropriate formwork system is mainly dependent on the intuitive and subjective opinion of practitioners with limited experience. In this study a survey and semi-structured interview with 30 potential users and specialists have been conducted. Based on this survey, the following six constraints/criteria for a suitable pneumatic fabric formwork are selected: permeability, strength, relative cost, durability, sew-ability, and finally aesthetics (Table 1). For scoring of durability, fabrics' resistance was examined against freezing and thawing. Three samples have been tested for different weather conditions. The process has been conducted three times within the interval of two days. At the next step, tensile strength tests were conducted on the specimens and the ratio of rupture force to tensile strength of the fabrics were measured. The average of the above-mentioned ratios was used as an indicator of the overall durability (Table 2).

5.2 Application of Analytical Hierarchy Process (AHP) for Decision Making

AHP is a multi-attribute decision making method which belongs to a broader class, known as "additive weighting methods". The AHP was proposed by Saaty (1977) [29] and uses an objective function to aggregate the different features of a decision problem [28, 32] where the main aim is to select the action item that has the highest value of the objective function. The AHP is based on four axioms[30].

Table 1 Rating of the decision alternatives against the major criteria (7 = best rank)

	Lockram	Hydrophobic Polyester	Laminated Chamois	Vinyl Crystal Clear	Rubber Fabric	Herculon	Barrateen
Aesthetics	5	6	7	2	1	3	4
Permeability	2	3	5	6	6	1	4
Sew-Ability	6	7	5	2	1	3	4
Relative Cost	1	1	1	1	1	2	2
Durability	2	3	1	4	4	4	4
Strength	6	5	1	2	2	3	4

Table 2 The ratio of after freezing-thawing tensile strength to natural tensile strength (F_f/ F_n)

FABRIC	(%) F_f/F_n*
Lockram	90
Hydrophobic Polyester	94
Laminated Chamois	86
Vinyl Crystal Clear	99
Rubber fabric	99
Herculon	99
Barrateen	99

Similar to MAU/VT and SMART, the AHP is classified as a compensatory method, where criteria with low scores are compensated by higher scores in other criteria, but contrasting the utilitarian systems, the AHP uses pairwise comparisons of criteria rather than value functions or utility where all individual criteria are paired with all other constraints and the end results accumulated into a decision matrix[31]. The process of AHP includes three phases: decomposition, comparative judgments, and synthesis of priority. Through the AHP process, decision problems are decomposed into a hierarchical structure, and both qualitative and quantitative data can be used to derive ratio scales between the decision elements at each hierarchical level by means of pair wise comparisons. The top level of hierarchy characterises overall objectives and the lower levels correspond to criteria, sub-criteria, and alternatives. With comparative judgments, decision makers are requested to set up a comparison matrix at each hierarchy by pairwise comparison of criteria or sub-criteria. A scale of values, ranging from 1 (indifference) to 9 (extreme preference) is employed to express the users' priority.

Finally, in the synthesis of priority stage, each matrix is then solved by an eigenvector method for defining the criteria importance and alternative performance [32]. The comparisons are normally documented in a comparative matrix A, which must be both transitive such that if, i > j and j > k then i > k where i, j, and k are alternatives; for all j > k > i and reciprocal, $a_{ij}=1/a_{ji}$. Priorities are then estimated from the comparison matrix by normalising each column of the matrix, to develop the normalised primary right eigenvector, the priority vector, by $A.W=\lambda_{max}.W$; where A is the comparison matrix; W is the principal Eigen vector and λ_{max} is the maximal Eigen value of matrix A [31, 33]. Through the AHP process, decision-makers' inconsistency can be estimated via consistency index (CI) which is employed to determine whether decisions break the transitivity rule, and to what extent. A threshold value of 0.10 is acceptable, but if it is more than that then the CI is calculated by using the consistency ratio CR= CI/RI where RI is the ratio index. CI is further defined as $CI=((\lambda_{max}-n))/((n-1))$; where λ_{max} is as above; n is the dimension [31]. The average consistencies of RI from random matrices are shown in Table 3. The advantages of the AHP method are that it has a systematic approach (through a hierarchy) and presents an objectivity and reliability for quantifying weighting factors for criteria [34]. It can also deliver a well-tested method which allows analysts to include multiple, conflicting, non-monetary features of alternatives into their decision making[35].

On the other hand, the disadvantages are that the estimation of a pair-wise comparison matrix for each attribute is complicated and as the number of criteria and/or alternatives increases, the complexity of the estimations increases considerably. Moreover if a new alternative is added after finishing an evaluation, it is very difficult because all the calculation processes have to be restarted again [34]. The shortcomings of AHP are of a more theoretical nature, and have been the subject of some debate in the technical literature. Many analysts have pointed out that, the attribute weighting questions must be answered considering the average performance levels of the alternatives. Others have noted the possibility for ranking reversal among remaining action items after one is deleted from consideration. Finally, some theorists go so far as to state that as currently practiced, "the rankings of AHP are arbitrary". Defenders of AHP, such as Saaty himself, justified that rank reversal is not a fault because real-world decision-making shows this characteristic as well [36].

Table 3 Random Inconsistency Index, Adapted from[37]

N	1	2	3	4	5	6	7	8	9	10
RI	0	0	0.58	0.9	1.12	1.24	1.32	1.41	1.45	1.49

5.3 Strategy Selection Using AHP

Through the AHP process, the problem under consideration is broken down into a hierarchy, including at least three major levels: goal, criteria (objectives) and alternatives. The criteria might be general and are required to be broken down into

more specific sub-criteria introduced as attributes in another level of hierarchy. AHP deals with identifying the overall goal and proceeding downward until the measure of value is included. Fig.11 shows a four-level hierarchy structure considering the general features of the problem. The first level of the structure is the overall goal of the ranking (Fabric Selection). The second level contains the identified objectives (criteria) to achieve the main goal. The third level holds the sub criteria to be used for assessing the objectives. The final level is added for the alternatives [35]. Each criterion/constraint has a weighting indicating its significance and reflecting the organizational policy. These weightings are defined by the users/decision makers employing the pair wise comparison approach embedded in the AHP and will vary for different problems with different decision makers [29, 30]. The AHP has the major advantage of allowing the decision makers to conduct a consistency check for the developed judgment in regard to its relative importance among the decision making components. Therefore, the decision maker(s) can modify their evaluations to improve the consistency and to supply more informed judgments under consideration.

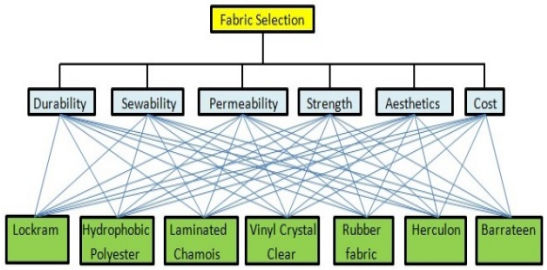

Fig.11 Multi Criteria Decision Hierarchy for Fabric Selection

The procedure is also able to provide flexibility in selecting the criteria to evaluate the alternatives (different types of fabric) and even increasing or decreasing the number of levels (associated with the criteria) in the hierarchy. The overall ranking value of each alternative for a four level hierarchy (as shown in Equation 1) X_j is expressed as follows:

$$X_j = \sum_{i=1}^{n} W_k W_{ki} a_{ij} \quad (1)$$

-W_k is the weighting of criterion k

-W_{ki} is the weighting of the i^{th} sub-criterion in the category of criterion k

-a_{ij} is the importance level of j^{th} alternative with respect to the i^{th} sub criterion and kth criterion.

Table 4 presents the developed comparison matrix for the criteria identified for fabric selection.

Vector of priorities (the Eigen vector of the developed matrix) addressing the weight of criteria has been identified and presented in Equation (2):

$$\text{VOP}=\begin{bmatrix}\mathbf{0.1376}\\ \mathbf{0.4581}\\ \mathbf{0.2627}\\ \mathbf{0.0453}\\ \mathbf{0.0663}\\ \mathbf{0.0299}\end{bmatrix}=\begin{bmatrix}\mathbf{Durability}\\ \mathbf{Cost}\\ \mathbf{Permeability}\\ \mathbf{Sewability}\\ \mathbf{Tesnsile\ Strength}\\ \mathbf{Aesthetic}\end{bmatrix} \quad (2)$$

Since the decision makers may be unable to deliver perfectly consistent pairwise comparisons, it is demanded that the comparison matrix should have an adequate consistency, which can be checked by the following consistency ratio (CR):

$$\text{CR}=\frac{(\boldsymbol{\lambda max-n})/(\mathbf{n-1})}{\mathbf{RI}} \quad (3)$$

where, λ_{max} = 9.73(0.1376) + 1.9(0.4581) + 4.79(0.2627) + 25.33(0.0453) + 16.83(0.0663) + 29(0.0299) = 6.59

In calculating λ_{max}, the values in front of brackets are the summations in AHP matrix in Table 4, and the values inside the brackets are the corresponding VOPs. Random inconsistency index (RI) for 6 criteria is extracted from Table 3 provided by Saaty (2004) [27]. The Consistency Ratio (CR) has been calculated based on Equation 3. Since the value of CR is less than 0.1, it can be concluded that the accomplished judgement has consistency.

$$\text{CR}=\frac{(\boldsymbol{\lambda max-n})/(\mathbf{n-1})}{\mathbf{RI}}=0.095<0.1$$

Then the experts were asked to compare the main alternatives with respect to each criterion. Finally, global priorities of the different major options were estimated by multiplying the weightings of the alternative associated with each constraint by the criterion weighting and finding the overall sum. As shown in Table 5, 'Barrateen' has got the highest score in this analysis; hence it has been selected as the most suitable fabric for pneumatic formwork.

Table 4 AHP Matrix- Pairwise comparison of Criteria

	Cost	Permeability	Strength	Sewability	Durability	Aesthetic
Cost	1	1/5	1/3	5	3	5
Permeability	5	1	3	9	7	9
Strength	3	1/3	1	7	5	9
Sewability	1/5	1/9	1/7	1	1/3	3
Durability	1/3	1/7	1/5	3	1	2
Aesthetic	15	1/9	1/9	1/3	1/2	1

Table 5 Fabric Selection using AHP method

		Alternatives													
		Rubber fabric (3mm)		Vinyl Crystal 0.75 mm		Herculon		Lockram		Laminated	Chamois	Hydrophobic	Polyester	Barrateen	
Criteria	Weight of the Criteria	Rating of the alternatives	Overal importance	Rating of the alternatives	Overal importance	Rating of the alternatives	Overal importance	Rating of the alternatives	Overal importance	Rating of the alternatives	Overal importance	Rating of the alternatives	Overal importance	Rating of the alternatives	Overal importance
Durability	0.07	4	0.27	4	0.27	4	0.27	2	0.13	1	0.07	3	0.2	4	0.27
Sewability	0.05	1	0.05	2	0.09	3	0.14	5	0.23	6	0.27	7	0.32	4	0.18
Permeability	0.46	1	0.46	2	0.92	3	1.37	4	1.83	6	2.75	5	2.29	7	3.21
Strength	0.27	4	1.05	3	0.79	2	0.53	7	1.84	1	0.26	6	1.58	5	1.31
Aesthetic	0.03	1	0.03	3	0.09	5	0.15	2	0.06	7	0.21	4	0.12	6	0.18
Cost	0.1	1	0.14	2	0.28	7	0.96	4	0.55	5	0.69	3	0.41	6	0.83
Total Score			1.99		2.4		3.41		4.64		4.25		4.92		5.97

6. CONCLUSIONS

Innovations in formwork solutions and introduction of flexible fabric in place of stiff traditional formwork elements have created new possibilities for a wide range of construction components. Combined with textile formwork, the production of a new range of structural foam-filled panelized systems has become possible without intensive labour for traditional formwork installation. The objective of this study was to select the most appropriate fabric for a pneumatic formwork, which will be used for the newly developed structural foam-filled panels. First, based on the results of a survey, six criteria for a suitable pneumatic fabric formwork were selected such as permeability, strength, relative cost, durability, sew-ability, and aesthetics. Some experimental tests were conducted to determine the selection indicators for the criteria like durability and strength for each candidate. Then, an analytical hierarchy process was employed for decision making on the best pneumatic formwork candidate for foam-filled structural composite panels. The model can be applied on any potential decision alternatives considering the identified constraints and the associated determined weightings.

7. REFERENCES

[1] West, M. and R. Araya. Fabric formwork for concrete structures and architecture. in Inter. Conf. Textile Composites and Inflatable Structures, Barcelona, 2009, pp. 5-7.

[2] Orr, M.J., et al. Fabric formwork for ultra high performance fibre reinforced concrete structures. in fib symposium: Concrete structures for Sustainable Community. 2012.

[3] Orr, J.J., et al., Concrete structures using fabric formwork. The Structural Engineer, 2011. 89(8): p. 20-26.

[4] Quinn, G. and C. Gengnagel, A review of elastic grid shells, their erection methods and the potential use of pneumatic formwork. Mobile and Rapidly Assembled Structures IV, 2014, p. 129.

[5] Hanna, A.S. and A.B. Senouci, Material cost minimization of concrete wall forms. Building and environment, 1997, pp. 57-67.

[6] Defonseka, C., Practical guide to flexible polyurethane foams. Smithers Rapra, 2013.

[7] Lamberton, B.A., Fabric forms for concrete. Concrete international, 1989, pp. 58-67.

[8] Rankilor, P.R., Textiles in civil engineering. Part 1-geotextiles. Handbook of technical textiles, 2000, p. 358.

[9] Ghaib, M.A.A. and J. Górski, Mechanical properties of concrete cast in fabric formworks. Cement and concrete research, 2001. 31(10): p. 1459-1465.

[10] Sharafi, P., L.H. Teh, and M.N.S. Hadi, Conceptual design optimization of rectilinear building frames: A knapsack problem approach. Engineering Optimization, 2015. 47(10), pp.1303-1323.

[11] Sharafi, P., L.H. Teh, and M.N.S. Hadi, Shape optimization of thin-walled steel sections using graph theory and ACO algorithm. Journal of Constructional Steel Research, 2014. 101: p. 331-341.

[12] Sharafi, P., M.N.S. Hadi, and L.H. Teh, Geometric Design Optimization for Dynamic Response Problems of Continuous RC Beams. Journal of Computing in Civil Engineering, 2014. 28(2): p. 202-209.

[13] Sharafi, P., M.N.S. Hadi, and L.H. Teh, Optimum Spans' Lengths of Multi-span Reinforced Concrete Beams Under Dynamic Loading, in Topics on the Dynamics of Civil Structures, Vol.1: Proc. of the 30th IMAC, A Conf. on Structural Dynamics, 2012, J.M. Caicedo, et al., Editors. 2012, pp. 353-361.

[14] Sharafi, P., M.N.S. Hadi, and L.H. Teh, Optimum Column Layout Design of Reinforced Concrete Frames Under Wind Loading, in Topics on the Dynamics of Civil Structures, Vol.1: Proc. of the 30th IMAC, A Conf. on Structural Dyn., 2012, pp. 327-340.

[15] Shin, Y., D. W., Yang, S. W., Cho, H. H., & Kang, K. I., Decision support model using the *adaboost algorithm to select formwork* systems in highrise building construction. in

Proceeding of the 25th International Symposium on Automation and Robotics in Construction. 2008, pp. 26-29.
[16] Orr, J., et al. Optimisation and durability in fabric cast 'Double T' beams. in 2nd Int. Con. on Flexible Formwork. 2012, pp. 268-279.
[17] Proverbs, D.G., Holt, G. D., & Olomolaiye, P. O., Factors in formwork selection: A comparative investigation. Building Research and Information, 1999, pp. 109-119.
[18] Nemati, S. and A. Rahai, Reinforced Concrete Construction. 2013: Fadak. 756.
[19] West, M., The Fabric Formwork Book: Methods for Building New Architectural and Structural Forms in Concrete. 2016: Routledge.
[20] Domone, P. and S.A. Jefferis, Structural grouts. 2002: CRC Press.
[21] Lee, S.H., Study of construction methodology and structural behaviour of fabric-formed form-efficient RC beam. 2011, pp. 1-305.
[22] Chandler, A. and R. Pedreschi, Fabric formwork. 2007: Riba Publishing.
[23] Rashidi, M., B. Samali, and P. Sharafi, A new model for bridge management: Part A: condition assessment and priority ranking of bridges. Australian Journal of Civil Engineering, 2016. 14(1): p. 35-45.
[24] Kaveh, A. and P. Sharafi, Charged System Search Algorithm for Minimax and Minisum Facility Layout Problems. Asian Journal of Civil Engineering, 2011. 12(6): p. 703-718
[25] Kaveh, A. and P. Sharafi, A simple ant algorithm for profile optimization of sparse matrices. Asian Journal of Civil Engineering (Building and Housing), 2007. 9(1): p. 35-46.
[26] Rashidi, M. and B.P. Lemass, A decision support methodology for remediation planning of concrete bridges. 2011.
[27] Linkov, I., et al., From comparative risk assessment to multi-criteria decision analysis and adaptive management: Recent develop. and applications. Envir. International, 2006.
[28] Rashidi, M., et al., Remedial modelling of steel bridges through application of analytical hierarchy process (AHP). Applied Sciences, 2017. 7(2): p. 168.
[29] Saaty, T.L., A scaling method for priorities in hierarchical structures. Journal of mathematical psychology, 1977.
[30] Saaty, T.L., Response to Holder's comments on the analytic hierarchy process. The Journal of the ORS, 1991, pp. 918-924.
[31] Bello-Dambatta, A., et al., The Analytical Hierarchy Process for contaminated land management. Advanced Engineering Informatics, 2009. 23(4): p. 433-441.
[32] Cheng, S.-C., et al., Semantic-based facial expression recognition using analytical hierarchy process. Expert Systems with Applications, 2007, pp. 86-95.
[33] Saaty, T.L., Decision making, the analytic hierarchy and network processes (Journal of sys. science and systems eng. 2004, pp. 1-35.
[34] Kim, S.-K. and O. Song, A MAUT approach for selecting a dismantling scenario for the thermal column in KRR-1. Annals of Nuclear Energy, 2009, pp. 145-150.
[35] Rashidi, M., B. Samali, and P. Sharafi, A new model for bridge management: Part B: decision support system for remediation planning. Australian Journal of Civil Engineering, 2016, pp. 46-53.
[36] Norris, G.A. and H.E. Marshall, Multiattribute decision analysis method for evaluating buildings and building systems. 1995: BFR Laboratory, National Institute of Standards and Technology.
[37] Ishizaka, A., Development of an intelligent tutoring system for Analytic Hierarchy Process. 2004, WWZ Fors., NO. 10/04.

EFFECTS OF COLD JOINTS ON THE STRUCTURAL BEHAVIOUR OF POLYURETHANE RIGID FOAM PANELS

Saeed Nemati*[1], Pezhman Sharafi[1] and Bijan Samali[1]

[1]*Centre for Infrastructure Engineering, Western Sydney University, Australia*

*Corresponding Author

ABSTRACT: Foam made panels as efficient building elements are becoming a major role player in modular construction with a variety of applications worldwide. However, construction accuracy, technology, and method can have serious effects on the panels' behaviour. In this study, using a unique pneumatic pressure testing rig, bending tests are conducted on the two types of rigid polyurethane panels. The panels are categorised based on the existence of construction cold joints (seams) as S (Seamless) type and TS (Transverse Seams) type. The S type panels are tested under monotonic uniform loading with a maximum nominal pressure of about 1 atm as the witness specimens. The TS panels are tested under both monotonic and cyclic uniform loading, and the deflections-pressure behaviour obtained. The results show that S panels could resist up to 0.77 atm under monotonic uniform loading, while the minimum tensile strength of the foam is 13 MPa. In addition, panels with transverse seams collapsed under monotonic and cyclic loads at an average of 0.46 atm and 0.33 atm respectively but at the same position, located on the seamed section, which represent the same failure mode. Based on the results, the seamed section exhibited a maximum tensile strength of about 33.1% of an intact section under monotonic loading; and 27.9% lower results under cyclic loading.

Keywords: *Foam, Panel, Seam, Tensile strength, Cyclic loading.*

1. INTRODUCTION

Light weight structural panels are one of the most popular types of mobile and rapidly assembled structures. Rapidly assembled panels are a form of modular construction, commonly used in residential buildings, as well as industrial structures [1-3]. Some advantages of this system are: (1) They can sit on each other as plate, so substantially reduce the transportation cost per unit; (2) Can be made in any sizes and consequently cut the construction time; (3) Can be connected to each other quickly for quick assembly construction; (4) Can play the role of structural elements, partitions and/or insulators at the same time.

Such advantages make structural panels an attractive alternative to the traditional construction systems in the recent years. A wide range of these panels are made from new lightweight components such as foams. Many types of foams are on the market and the Polyurethane (PU) foams are the most popular types [4]. The lightweight penalized foam

made products are popular because they are light, easy to install and have good thermal and acoustic properties. However, the effects of construction accuracy, technology and methods on the mechanical behaviour of structural panels are significant. One of the most important construction problems of foam made panels is cold joints, which is also known as seams. When the placing of foam in the panels is delayed or interrupted for some reasons, the foam that has already been placed starts to condense, producing a kind of construction joint (seam) called a cold joint between it and newly placed foam. Seam is a plane under mixed material, or a fold that is developed within the rising foam mass, which appears as a line on the foam surface or section, as shown in Figure 1 [5]. Such joints between new and old portions of foam that are formed when new foam is placed adjacent to the foam that has hardened or has started to harden, may have negative effects on the strength of rigid foam panel. Hence, attention must be paid to the position and direction of the joints, and the effects on the structural behaviour

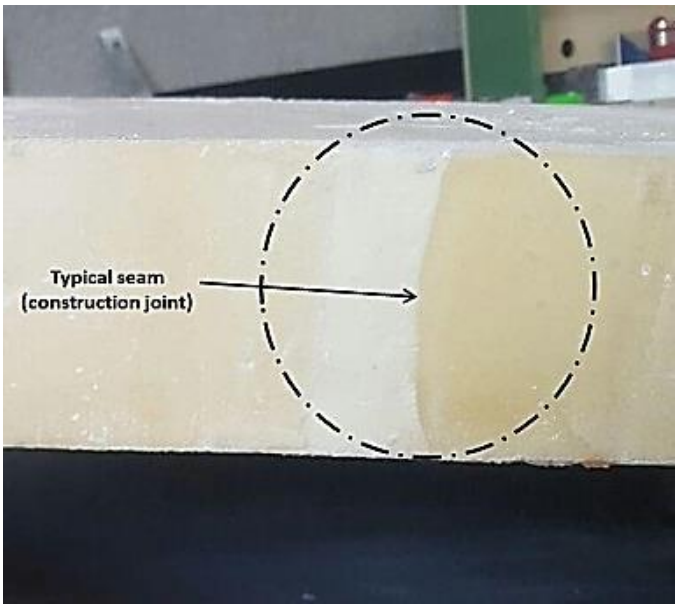

Fig1. Typical studied seams

There are some research studies on the structural applications of foams. Zenkert et al. [6] studied tension, compression and shear fatigue of a closed cell polymer foam, where the foam is tested quasistatically in tension, compression and shear. Fatigue crack propagation in a closed-cell foam is experimentally investigated by Fan et al. [7]. They conducted series of fatigue tests to obtain crack length vs loading cycle number and fatigue crack propagation rate vs stress intensity. In a similar work, Zhao et al. [8] carried out tension–tension fatigue tests to investigate the fatigue of closed-cell foam. Noble et al. [9]

studied the fatigue crack growth in rigid polyurethane foam under conditions of constant load-amplitude cycling. Shipsha et al. [10] carried out an experimental study of fatigue crack propagation in polymeric cellular foam cores for sandwich structures. In a similar work, Poapongsakorn et al. [11] investigated the applicability of linear-elastic fracture mechanics, elastic–plastic fracture mechanics and time-dependent fracture mechanics parameter to characterise fatigue crack growth rate of closed-cell polyvinyl chloride. Kanny et al. [12] ran some dynamic mechanical analyses and flexural fatigue of PVC foams of densities in the range from 75 to 300 kg/m^3. In which the fatigue behaviour was found to be similar to structural materials with a fatigue strength that increased with foam density. Huang et al. [13] analysed the fatigue of cellular materials using dimensional arguments. They found out that the fatigue of cellular materials depends on the cyclic stress intensity range, cell size, relative density and the fatigue parameters of used material. Wang et al. [14] focused on the influence of pores on crack initiation in monotonic and cyclic tensile loadings. Pores were shown to have an important influence on strain localization zones for crack initiation both in monotonic tensile and cyclic loadings. Toubia et al. [15] studied the effects of core joints in sandwich composites under in-plane static and fatigue loads. Their research confirmed that despite the face sheets' primary in-plane load carrying mechanisms, core junction substantially influence the axial fatigue life of the structure.

In this paper, the effect of seams on the structural behaviour of PU rigid foam panels will be studied through some experiments on the seamed and seamless samples, under monotonic and cyclic loads. The results will be compared with each other in order to investigate the impact of presence of seams on the bending strength of samples.

2. MATERIAL PROPERTIES

To evaluate the basic material properties, in addition to using the manufacturers' data, some experimental tests were carried out. In this regard, PU high-density rigid foam with the density of 192 kg/m^3 was chosen. Table 1 shows the used foam's manufacturing and mechanical properties, provided by the manufacturer and validated in the laboratory using the ASTM 1730 standard specification for rigid foam [16]. Three 50mm×50mm×50mm cubic specimens were tested by a uniaxial load machine, at a loading rate of 5 mm/min in order to identify the structural properties of the rigid PU foam. The results show that this type of PU foam, which is made of a 100:110 weight ratio mixture of AUSTHANE

POLYOL AUW763 and AUSTHANE MDI ISOCYANATE (Figure 2), can undertake considerable deformation before the failure. In addition, the elastic modulus of foam has been calculated as 135.5 MPa [17-19].

Table 1. Mechanical and manufacturing properties of the selected PU rigid foam

Mechanical Properties of the PU foam			
Density (kg/m^3)	Compressive yield strength (MPa)	Tensile yield strength (MPa)	Shear yield strength (MPa)
192	3.51	1.896	1.034
Manufacturing Properties			
Cream time[1]	Gel time[2]	Tack free time[3]	
35-40 sec	94 ± 4 sec	115 ± 5 sec	

[1]A measure of the beginning of the foam reaction. Usually characterized by a change in the liquids color as it begins to rise.
[2]The time when the foam has developed enough gel strength to be dimensionally stable.
[3]The time between the beginning of the foam pour and the point at which the outer skin of the foam loses its stickiness.

3. DESCRIPTION OF SPECIMENS AND TEST SETUP

In this study, three series of bending tests were carried out on two types of panelised specimens. Two types of 1500*1000*100 mm^3 rigid polyurethane panels were used: Type S (seamless) and type TS (with transverse seams) specimens. The expansion rate of this type of foam is 3.0, and the average weight of both types of panels is 29.0 kg. In order to make seamless samples, “one shot pouring system” was employed. To that end, 50 litres of mix liquid material is casted in the wooden formworks with a filling rate of 1.25 litres per second.

The TS panels were casted with five cold joints H1 to H5, as shown in Figure 2. In fact, TS specimens were made during six pouring steps, using 8.3 litres of mix liquid material for each step and with the same filling rate. Figure 3 illustrates the casting schedule for each step.

Fig2. Locations of transverse seams (H1-H5)

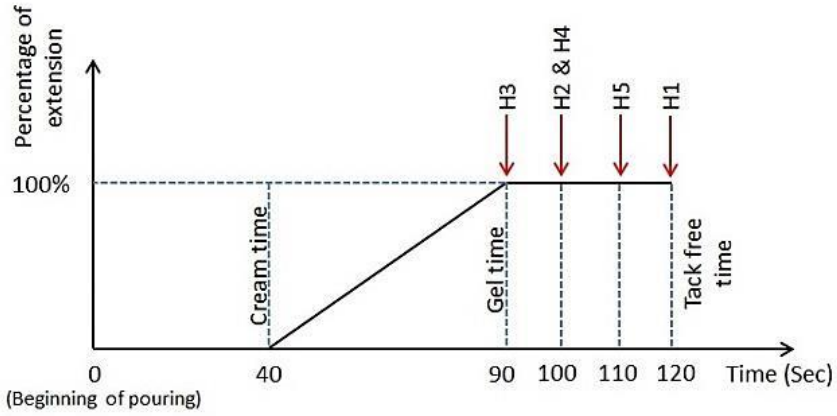

Fig3. Casting schedule of seams at TS specimens

3.1 Test Setup

The tests were undertaken using an automated vacuum rig at the Centre for Infrastructure Engineering (CIE) at Western Sydney University. The rig allows for undertaking loading test on panels of heights up to 6m under a vacuum suction of up to 10 kPa. The panels were horizontally loaded into the test chamber, fixed and sealed; the chamber is pulled up by an electric winch until it stands vertically before the suction is applied. The loading regime can be change according to the requirements. In order to adhere to an appropriate regime of loading, the rig enjoys a fully automatic controller, which utilises powerful software developed within the LabView environment (NI, 2016). Figure 4 shows the vacuum test rig setup, and Figure 5 illustrates the locations of automatic electrical potentiometers.

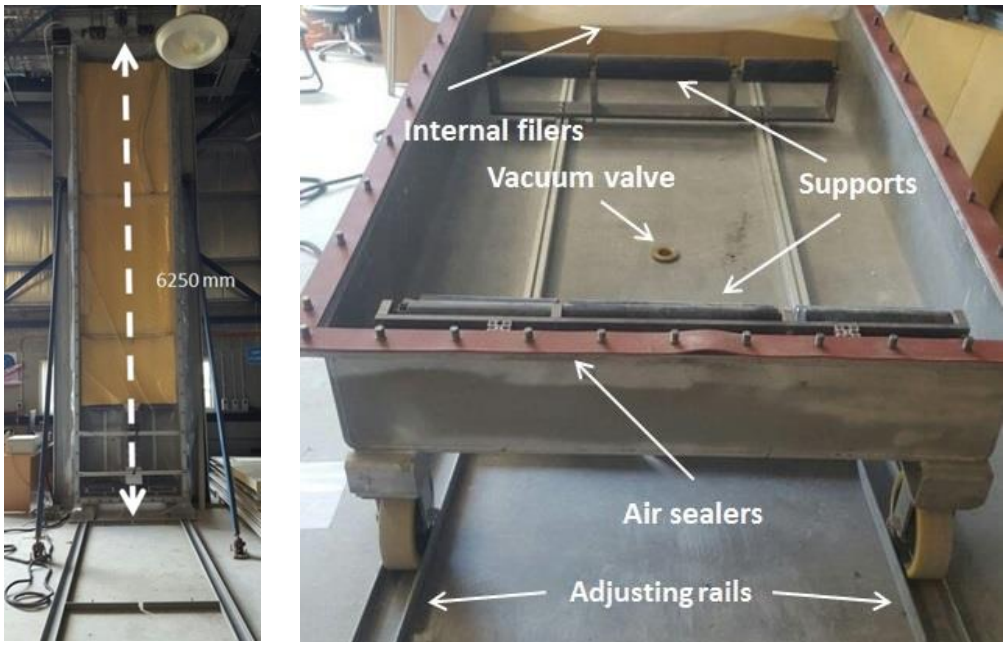

Fig4. Details of vacuum testing rig

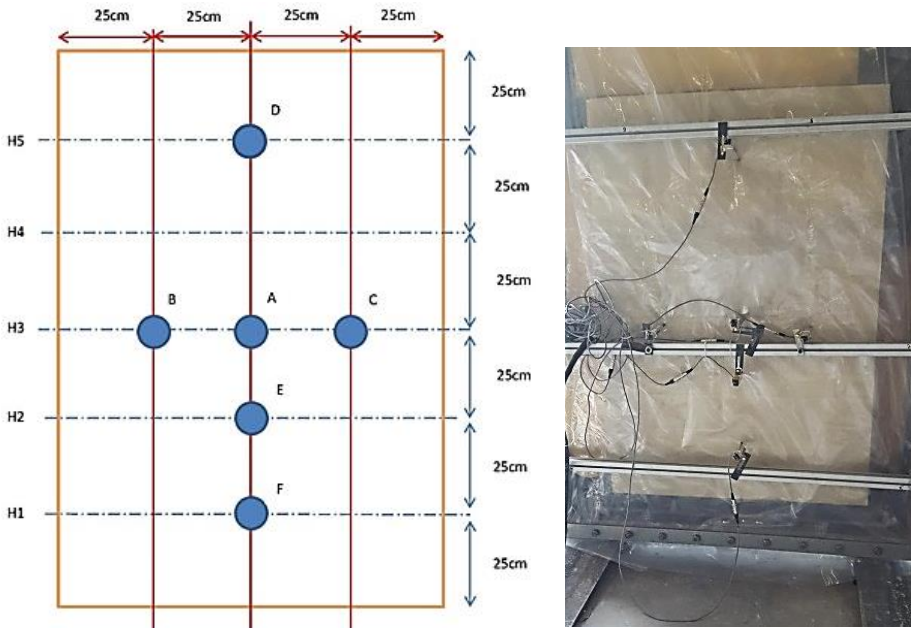

Fig5. Arrangement of potentiometers on panels (for all tests)

3.2 Testing Program

Three monotonic tests were conducted on the S and TS specimens, together with three cyclic tests on the TS specimens. Table 2 shows the summary of the test arrangement. First

series of bending tests carried out on the S panels using a uniform monotonic under about 1 atm air pressure (Load Regime #1) with a rate of 0.1 atm/min. The second series of bending tests were carried out on the TS panels using the same loading regime (Load Regime #1).The third series of bending tests were conducted on the TS panels, using a predicted cyclic air pressure (Load Regime #2) with a rate of 0.1 atm/min, as shown in Figure 6.

Table 2. Test arrangement matrix

Test series	Specimen	Number of specimens	Load configuration
1	S	3	Monotonic
2	TS	3	Monotonic
3	TS	3	Cyclic

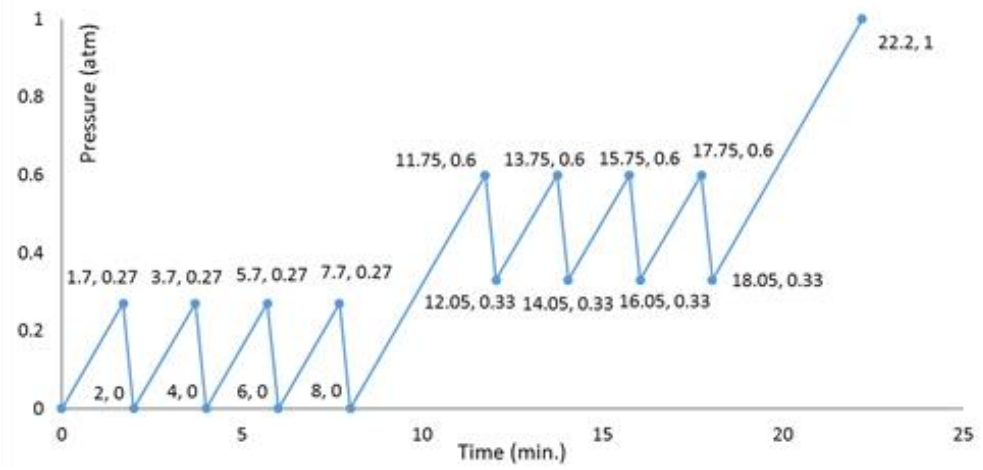

Fig6. Cyclic regime of loading, used at second series of bending tests

4. TEST RESULTS

For the test series #1, all three seamless panels resisted a maximum of 0.77 atm. Figure 7 and Table 2 show the pressure-deflection diagram and the deflections measured by potentiometer, respectively. Up to a pressure of about 0.23 atm, where shows a large primary deflection, the system is in the adjusting phase, and the pressure is not directly resisted by the panels. Afterwards, the PU foam panels exhibits a relatively liner behaviour up to about 0.77 atm. In addition, the seamless panel showed a symmetric curvature under the applied monotonic load. Figure 8 depicts this curvature for longitudinal and transverse

direction.

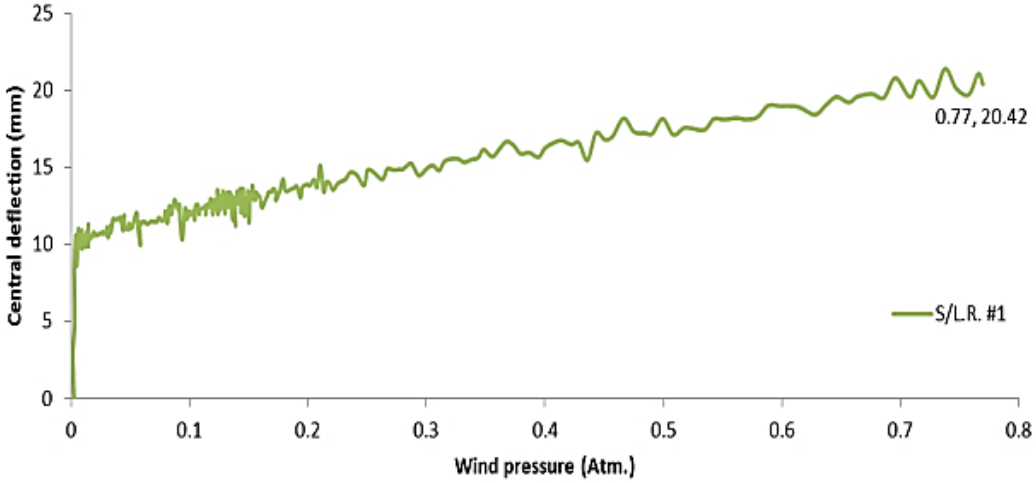

Fig7. Vacuum pressure vs average central deflection (point A) for test series #1

Table 3. Deflection at points A to F for test series 1

S panels L.R. #1	Direction	First monotonic test (mm)	Second monotonic test (mm)	Third monotonic test (mm)	Average (mm)	Standard Deviation	CV%
D	longitudinal	14.2	15.1	16	15.1	0.9	6
A	longitudinal	19.7	20.8	20.7	20.4	0.61	3
E	longitudinal	18.3	17.3	18.1	17.9	0.53	3
F	longitudinal	14.7	16.2	16.2	15.7	0.87	5.5
B	transverse	12.2	13	14	13.1	0.9	6.9
C	transverse	12.9	14.1	13.8	13.6	0.63	4.6

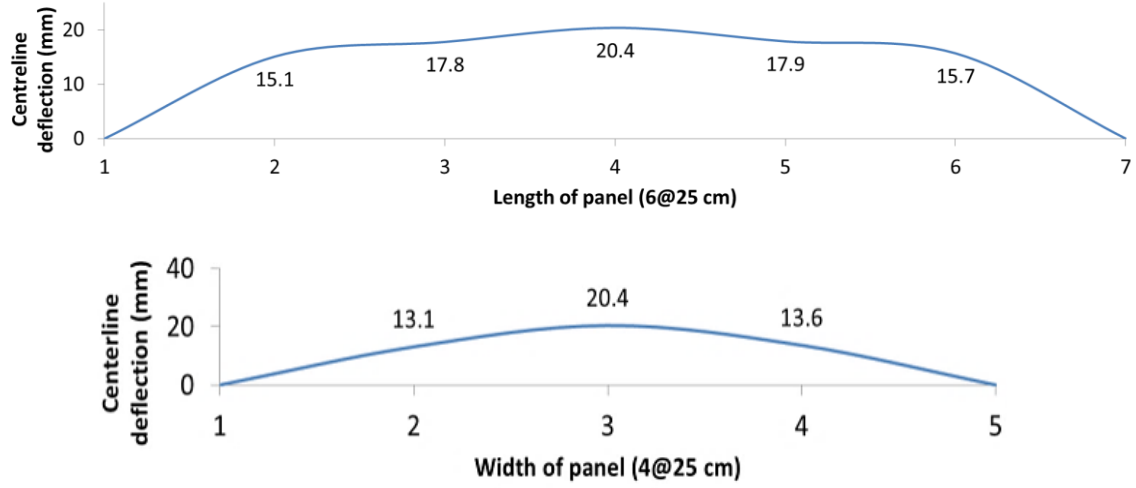

Fig8. Symmetric distribution of deflection at the longitudinal and transverse direction in test series 1

A comparison between measured deflections, shown in Figure 9, point A is at the maximum deflection in all tests.

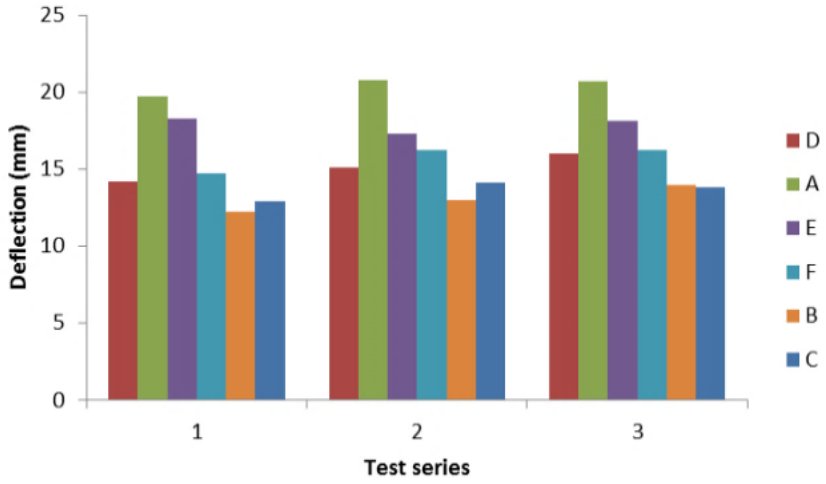

Fig 9. Comparison between measured deflections (test series 1)

According to these results, the minimum tensile strength of foam can be calculated by Eq. (1), in which $\sigma_{\min,foam}$ is the minimum tensile strength of foam; M is the maximum bending moment (at point A); y is half of the panel thickness (5cm); I is the section's moment of inertia; q is the load equivalent linear intensity; and L is the span [20, 21]. Accordingly, this rigid foam panel exhibits a minimum of 13.00 MPa tensile strength.

$$\sigma_{\min,foam} = My / I = qL^2y/(8I) \qquad (1)$$

4.2 Test Series 2

In these series of tests, three TS panels were tested under monotonic loading. For all of these panels, similar to test series 1, the maximum deflection appeared at the point A with an average amount of 17.02 mm. Nevertheless, all of these panels collapsed at an average pressure of 0.46 atm at the seam H1 as shown in Figure 10. Therefore, the main mode of collapse is assumed tensile at the seam.

Fig10. Typical collapse mode of TS panels at seam H1 under monotonic loading (test series 2)

Similar top the previous case, as shown in Figure 11, up to about 0.23 atm, the system is at adjusting phase and exhibits a large primary deflection. Then, TS panels have a semi-liner behavior before it reaches a pressure of about 0.46 atm. The deflections of pre-identified points of TS panels were measured by potentiometer on the surface. Results shown in Table 4 demonstrate very similar behaviours with those for TS panels under monotonic loading.

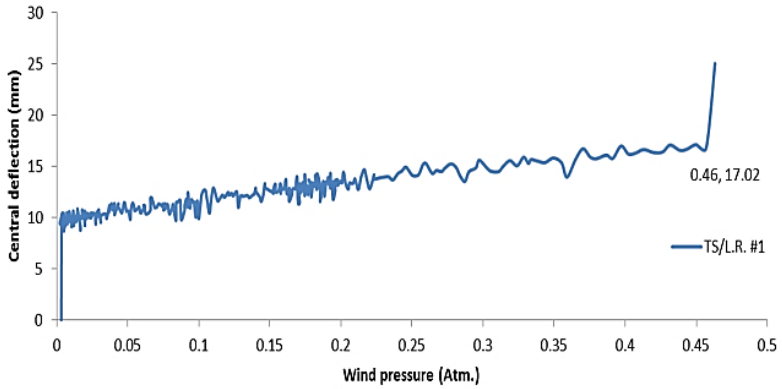

Fig11. Wind pressure vs average central deflection in test series 2

Table 4. Deflection at points A to F for test series 2

TS panels L.R. #1	Direction	First monotonic test (mm)	Second monotonic test (mm)	Third monotonic test (mm)	Average (mm)	Standard Deviation	CV%
D	longitudinal	11.8	10.6	11.5	11.3	0.63	5.6
A	longitudinal	16.76	16.9	17.4	17.02	0.34	2
E	longitudinal	15.5	13.6	14.4	14.5	0.95	6.6
F	longitudinal	10.6	12.2	12.3	11.7	0.95	8.1
B	transverse	8	9.6	9.1	8.9	0.82	9.2
C	transverse	7.7	9.1	9.3	8.7	0.87	10

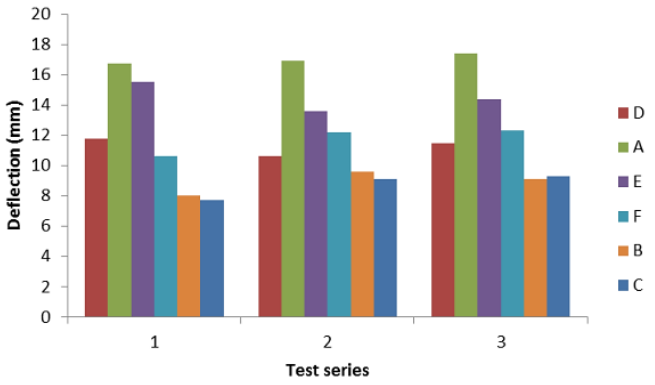

Fig12. Comparison between measured deflections of points A to F (test series 2)

Figure 12 shows a comparison between the measured deflections. Based on the results, in all of the tests, point A (the intersection of centrelines) shows the maximum deflection. In addition, as depicted in Figure 13 the TS panels exhibit symmetric curvature under monotonic loading in both directions. Figure 14 illustrates the model used for the analytical analysis of test series 2. The maximum tensile strength of seams under monotonic loading, therefore is calculated by Equation (2), in which σ_{max} is the maximum tensile strength of the seams. Other parameters are the same as those for Eq (1). Accordingly, this rigid foam panel exhibits a maximum of 4.3 MPa tensile strength.

$$\sigma_{max,seam} = My / I = \text{qxy(L-x)/(2I)} \qquad (2)$$

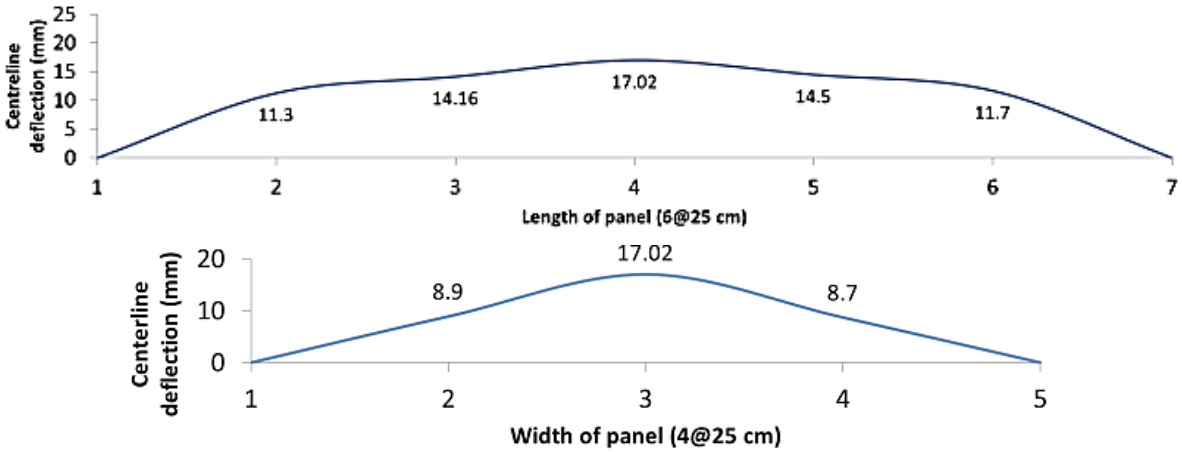

Fig13. Distribution of deflection in longitudinal and transverse direction in test series 2

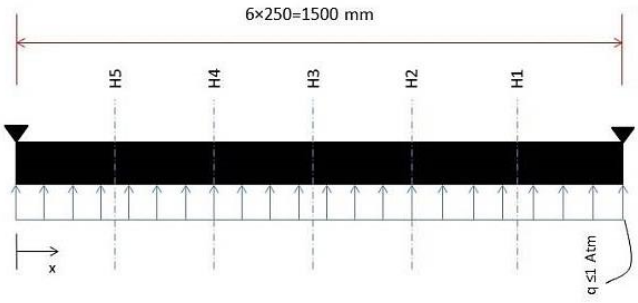

Fig14. Analytical model of test series 2

A comparison between results from Figure 7 and 11 shows that under monotonic loading, the seamless panels have a larger deflection capacity of about 20% compared to the TS panels (Figure 15).

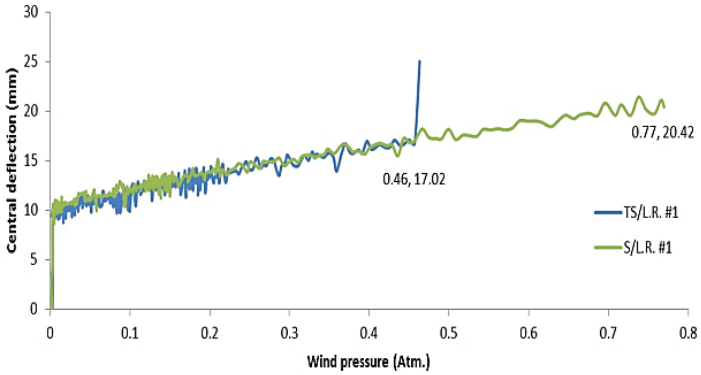

Fig15. Comparison between bending behaviors of S and TS panels under monotonic loading

4.3 Test Series 3

Three TS panels were tested under cyclic loading, where the results showed all the panels resisted up to a maximum pressure of about 0.33 atm. The deflections of points A to F have been measured by electrical automatic potentiometers, as shown in Table 5. All three panels collapsed at the seam H1 under an average deflection of 8.9 mm. Figure 16 shows a comparison between the deflections of points A to F. The minimum deflection occurred at Point F, while the maximum deflection of longitudinal centreline of the panel appeared at point A with an average amount of 17.02 mm. It can be seen that the tensile weakness of the seam is the main reason of failure.

Table 5. Deflection at points A to F for test series 3

TS panels L.R. #2	Direction	First cyclic test (mm)	Second cyclic test (mm)	Third cyclic test (mm)	Average (mm)	Standard Deviation	CV%
D	longitudinal	9.9	9.1	9.8	9.6	0.44	4.6
A	longitudinal	11.5	11.4	11.6	11.5	0.1	0.9
E	longitudinal	9.7	9.8	10.2	9.9	0.27	2.7
F	longitudinal	9.4	8.6	8.7	8.9	0.44	4.9
B	transverse	14.1	13.4	13.6	13.7	0.36	2.6
C	transverse	13.8	14.1	13.8	13.9	0.17	1.2

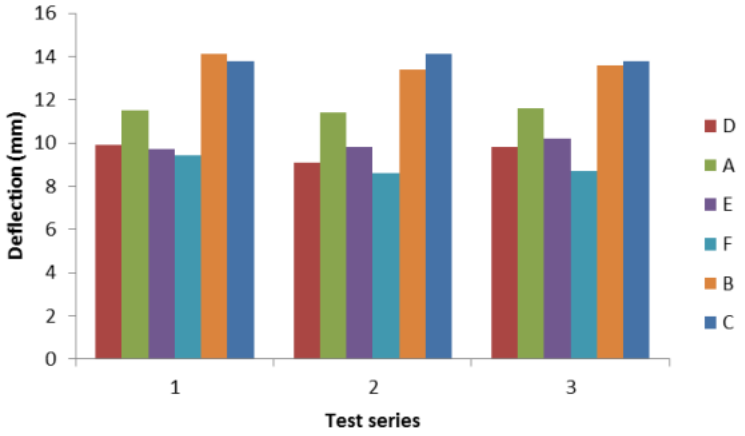

Fig16. Comparison between deflections of points A to F in test series 3

Figure 17 depicts the symmetric distribution of deflection at the longitudinal and transverse centrelines of TS panels. In addition, deflections of the transverse distortion can be seen in this Figure 18. Using Eq. (2), the maximum tensile strength of seams under cyclic loading is calculated as 3.1 Mpa.

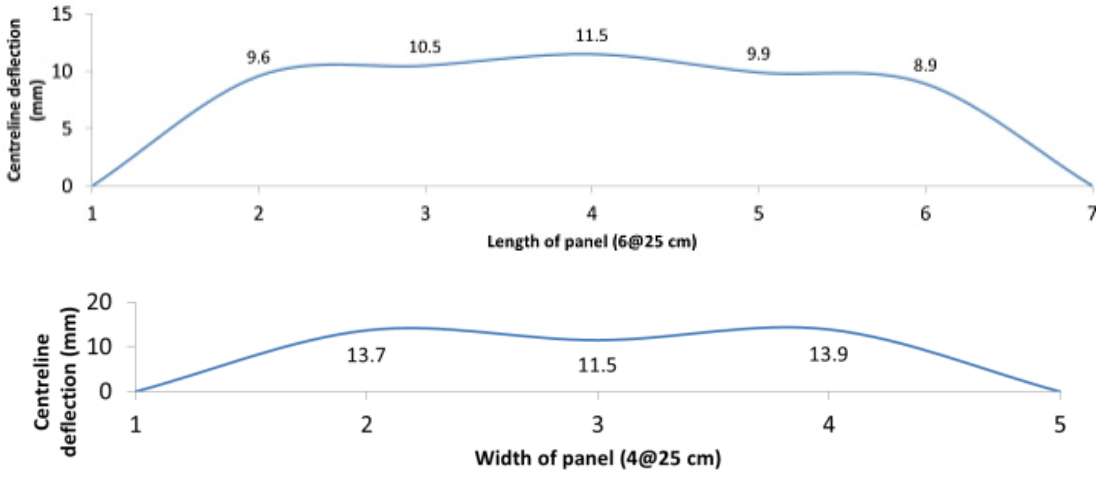

Fig17. Distribution of deflection at length (top) and width (down) of panels in test series 3

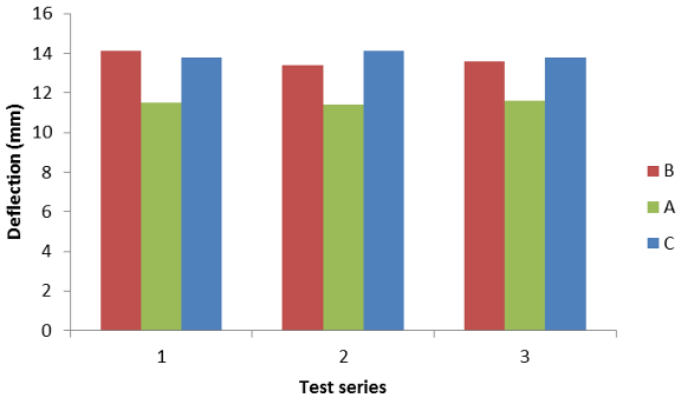

Fig18. Comparison between deflections of transverse points A to C for test series 3

4.4 Hysteresis Behaviour

Figures 19 shows the applied pressure vs max deflection of points A, B and C in the test series 3. Based on these figures, point A has the most regular and narrowest hysteresis diagram, with the minimum capacity for energy absorption. However, points B and C showed better and relatively more similar hysteresis behaviour that demonstrates that the TS panels exhibit rather symmetric hysteresis behaviour in transverse direction under cyclic loads.

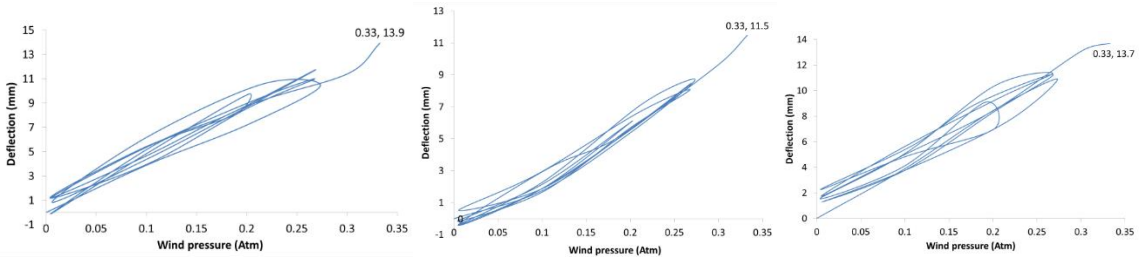

Fig19. Applied pressure vs deflection of point B, A and C in test series 3 (left to right) in test series 3

The applied cyclic pressure vs max deflection of points D, A and F in the test series 3 are shown in Figure 20. It reveals that points D and F exhibit two different hysteresis behaviours: Point D has a relative wide and irregular hysteresis diagram in comparison with the point F. The different internal structure of seams at these points can be assumed as the main reason of such difference.

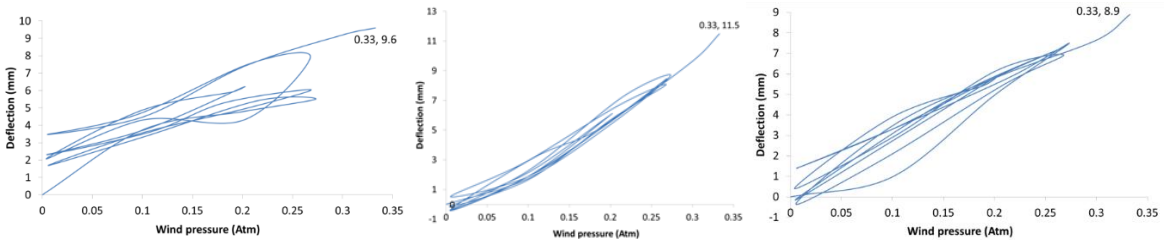

Fig 20. Applied pressure vs deflection of points D (left), A (middle) and F (right) in test series 3

The deflection time history of points A to F in test series 3 are shown in Figures 21 and 22. The relative areas of these graphs addressing the relative energy absorption capacity of seams H1 to H5 under cyclic loading are calculated and presented in Table 6.

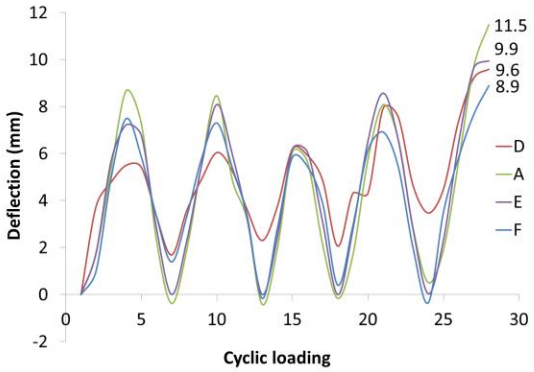

Fig21. Deflection time history for longitudinal centreline in the test series 3

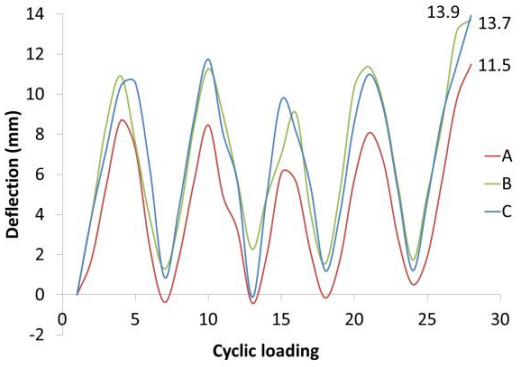

Fig22. Deflection time history for transverse centreline in the test series 3

Table 6. Comparison between relative absorbed energy at seams H1 to H5 under cyclic loading.

Seam	H1	H2	H3	H4	H5
Relative absorbed energy	1	1.02	1.53	1.02	1.21

Comparison between Table 6 and Figure 5 indicates that making the seams at end of the gel time (H3) can increase the energy absorption capacity by 53%, compared to the end of take free time (H1).

5. CONCLUDING REMARKS

A comparison between the results of the monotonic tests shows that:

- ✓ Casting at the end of gel time instead the end of tack free time, resulted in an %80 increase in the tensile strength of the seams ($[X_{H1}(L-X_{H1})] / [X_{H3}(L-X_{H3})]$).
- ✓ Casting at about 20 sec before of the end of tack free time (120^{th} sec), increased the tensile strength of the seams by %60 ($[X_{H1}(L-X_{H1})] / [X_{H4}(L-X_{H4})]$).
- ✓ The seamed section exhibited about 33.1% of the maximum tensile strength of an intact section.
- ✓ Under monotonic loading, the seamless panels showed a larger deflection capacity, as 20% more than that of TS panels.

A comparison between the results of the cyclic tests shows that:

- ✓ Casting at the end of tack free time (120^{th} sec) instead of 110^{th} sec resulted in a significant positive effect on the tensile strength of seams.
- ✓ The tensile strength of a seamed section was under cyclic loading about 72.1% of the strength under monotonic loading.
- ✓ Making the seams at the end of the gel time increased the energy absorption capacity of panels by 53% in comparison with the end of take free time.

6. REFERENCES

1. Sharafi, P., et al., *Interlocking system for enhancing the integrity of multi-storey modular buildings.* Automation in Construction, 2018. 85: p. 263-272.

2. Sharafi, P., et al., *Identification of Factors and Multi-Criteria Decision Analysis of the Level of Modularization in Building Construction.* ASCE Journal of Architectural Engineering- Special Collection on Housing and Residential Building Construction, 2018. 24(2).

3. Sharafi, P., et al., *Automated spatial design of multi-story modular buildings using a unified matrix method.* Automation in Construction, 2017. 82: p. 31-42.

4. Defonseka, C., *Practical guide to flexible polyurethane foams*. 2013: Smithers Rapra.

5. ASTM-E1730, *Standard Specification for Rigid Foam for Use in Structural Sandwich Panel Cores.* 2015.

6. Zenkert, D. and M. Burman, *Tension, compression and shear fatigue of a closed cell polymer foam.* Composites Science and Technology, 2009. 69(6): p. 785-792.

7. Fan, X., M. Zhao, and T. Wang, *Experimental investigation of the fatigue crack propagation in a closed-cell aluminum alloy foam.* Materials Science and Engineering: A, 2017.

8. Zhao, M., et al., *Experimental investigation of the fatigue of closed-cell aluminum alloy foam.* Materials Letters, 2015. 160: p. 68-71.

9. Noble, F. and J. Lilley, *Fatigue crack growth in polyurethane foam.* Journal of Materials Science, 1981. 16(7): p. 1801-1808.

10. Shipsha, A., M. Burman, and D. Zenkert, *On mode I fatigue crack growth in foam core materials for sandwich structures.* Journal of Sandwich Structures & Materials, 2000. 2(2): p. 103-116.

11. Poapongsakorn, P. and C. Kanchanomai, *Fatigue crack growth behavior and mechanism of closed‐cell PVC foam.* Polymer Engineering & Science, 2013. 53(8): p. 1719-1727.

12. Kanny, K., et al., *Dynamic mechanical analyses and flexural fatigue of PVC foams.* Composite Structures, 2002. 58(2): p. 175-183.

13. Huang, J. and J. Lin, *Fatigue of cellular materials.* Acta materialia, 1996. 44(1): p. 289-296.

14. Wang, L., et al., *Influence of pores on crack initiation in monotonic tensile and cyclic loadings in lost foam casting A319 alloy by using 3D in-situ analysis.* Materials Science and Engineering: A, 2016. 673: p. 362-372.

15. Toubia, E.A. and A. Elmushyakhi, *Influence of core joints in sandwich composites under in-plane static and fatigue loads.* Materials & Design, 2017.

16. ASTM-E1730, *Standard Specification for Rigid Foam for Use in Structural Sandwich Panel Core*, in *ASTM International*. 2015: West Conshohocken, PA.

17. Sharafi, P., et al., *Edgewise and flatwise compressive behaviour of foam-filled sandwich panels with 3-D high density polyethylene skins.* Engineering Solid Mechanics, 2018. 6(3): p. 201-213.

18. Sharafi, P., et al., *Flexural and shear performance of an innovative foam-filled sandwich panel with 3-D high density polyethylene skins.* Engineering Solid Mechanics, 2018. 6(2): p. 113-128.

19. Sharafi, P., et al., *Behaviour of Integrated Connections Between Adjacent Foam-Filled Modular Sandwich Panels.* Engineering Solid Mechanics, 2018. 6(3): p. 214-226.

20. Kaveh, A. and P. Sharafi, *Charged System Search Algorithm for Minimax and Minisum Facility Layout Problems.* Asian Journal of Civil Engineering, 2011. 12(6): p. 703-718

21. Kaveh, A. and P. Sharafi, *A simple ant algorithm for profile optimization of sparse matrices.* Asian Journal of Civil Engineering (Building and Housing), 2007. 9(1): p. 35-46.

International Journal of GEOMATE, May, 2018 Vol.14, Issue 45, pp.151-161
Geotec., Const. Mat. & Env., DOI: https://doi.org/10.21660/2018.45.73573
ISSN: 2186-2982 (Print), 2186-2990 (Online), Japan

NON-REINFORCED FOAM FILLED MODULES FOR RAPIDLY ASSEMBLED POST DISASTER HOUSING

*Saeed Nemati[1], Pezhman Sharafi[2], Bijan Samali[3], Yahya Aliabadizadeh[4] and Shahrokh Saadati[5]

[1,2,3]Centre for Infrastructure Engineering, Western Sydney University, Australia
[4]A & A Structures LLC, Maryland, USA, [5]GHD, Sydney, Australia

*Corresponding Author, Received: 18 Dec. 2018, Revised: 19 Jan. 2018, Accepted: 15 Feb. 2018

ABSTRACT: Rapidly assembled structures play an important role in post-disaster housing. This research study introduces a modular non-reinforced foam-filled system for rapidly assembled buildings and studies its structural performance. A novel structural modular construction system using pneumatic formwork is presented and its structural performance as a post-disaster housing system is studied. To that end, this paper presents a numerical analysis using finite element modeling on the foam-filled modular units, together with a set of experimental tests on the elements. Finally, the performance of a real size module made of polyurethane AUW763 against snow and wind loads in critical areas is modeled, using the software ROBOT 2016 and ANSYS. The results demonstrate that the foam-filled modular units successfully meet the standards' requirements for semi-permanent housing even in cyclonic prone areas based on Standards Australia (AS1170.2), International Building Code (IBC-2015) and an American standard as Minimum Design Loads for Buildings and Other Structures (ASCE7-10).

Keywords: Foam filled structures, Rapidly assembled buildings, Post disaster housing, Crisis management, Structural performance

1. INTRODUCTION

Crisis management after natural and non-natural disasters such as earthquake, flood, drought, bushfire, flood of refugees, raid and war can be a serious concern of governments. In the event of such crises, fast decision making is an essential element of an effective crisis management system [1]. From the civil engineering point of view, Post Disaster Housing (PDH) is a big challenge in the crisis management field. Every year, due to natural and man-made catastrophes worldwide, millions of people have to be accommodated in the temporary housing. In the USA alone, such disasters happen over 60 times per year [2]. Experts estimate that on average, it can take 5 [3] to 10 [4] years for communities to recover from the effects of a disaster, which highlights the severity of the disaster and the importance of Rapidly Assembled Buildings (RABs) as an effective PDH system [3]. Rapidly assembled panels are used commonly in residential buildings as well as industrial structures [5]. In addition to residential accommodation, RABs can be employed in several other applications such as field hospitals, storehouses and other temporary and semi-permanent facilities [6]. Some rapidly assembled systems have the potential to be used as temporary structures as well as providing long-term serviceability. Temporary accommodation buildings can only remain on-site for a maximum of two years unless the local government approves a longer timeframe before the two year period expires [7]. Nevertheless, sometimes, the term of "temporary" returns to several years, especially in developing countries [8-12] that can have significant social and economic effects [13-15].

Mobile and rapidly assembled structures play a major role in post-disaster management through building temporary accommodation and shelters. Wise selection of RAB systems has an impact on their performance in an effective crisis management system. For instance, use of large precast units is adopted by most existing PDH systems. Yet, as the dimension of precast elements increases, some significant construction problems appear in transportation, installation and erection phases. Air-liftable origami-inspired deployable systems, pliable structural systems with rigid couplings for parallel leaf-springs, scissor systems[16], elastic grid shell system [17], and structural panels are some popular types of mobile and rapidly assembled structures [18, 19]. Most of these rapidly assembled structural systems suffer from low tolerance in the fabrication and erection phases. They also need skilled labors for installation that will result in an increase in the total costs, and some other constructional problems. For example, air-liftable origami-inspired deployable systems do not have a reliable architectural form and are most uncomfortable for a long stay. The control of heat exchange in such systems is also very difficult. Pliable structural systems with rigid couplings for parallel leaf-

springs have similar problems, in addition to a relative complex design procedure. In addition, in most cases, the elastic grid shell system is limited to non-residential temporary applications. High rate energy loss and expensive construction equipment are some of the other downsides of this system. To respond to such shortcomings, in this study, using pneumatic foam filled panels first, an effective rapidly assembled modular system is presented as a PDH that can be used for post-disaster management as a temporary and semi-permanent housing system. The modules are made of lightweight composite sandwiches fitted in pneumatic formwork that greatly facilitate transportation and installation process. Then, numerical and experimental analyses are performed to investigate the structural performance of this system under severe loading conditions, as a structural feasibility analysis.

2. TEMPORARY HOUSING

A temporary accommodation building can be any class of building as defined under the National Construction Code (NCC). However, they are usually a class 1b (boarding house, guest house, hostel or the like), class 2 (residential units) or class 3 (motel) building, depending on its configuration [20]. The Federal Emergency Management Agency (FEMA)'s recent policy change to discontinue using the mobile homes as a temporary housing alternative will result in a significant increase in the cost of the temporary housing program [21].

In addition, studies have shown that innovative prefabricated housings have 25.1 and 29.7% lower life-cycle energy and cost requirements respectively [22-25]. Use of rapidly assembled panelised systems, especially rapidly assembled lightweight panels, is becoming very popular for cutting the construction time, as well as skilled labor and transportation costs that make them suitable options for PDH projects (Figure 1).

Regarding the structural performance of lightweight panels, the use of foam materials has been a good choice for filling material. While many types of foams are available in the market, Polyurethane (PUR) based foams are the most popular types, first introduced into the market in the 1950s. Foams are available in three main categories: flexible (the most popular), semi-rigid and rigid foams [26]. Polyether-based PUR foams are used widely for applications such as furniture, bedding, pillows, padding, and carpet underlay. Polyester-based PUR foams are used for textiles, shoulder pads, noise reduction and other applications. Both are used in automotive, aircraft, household, and footwear industries, too. Nevertheless, showing some good level of structural strength and durability, these foams have a great potential to be widely used in structural engineering.

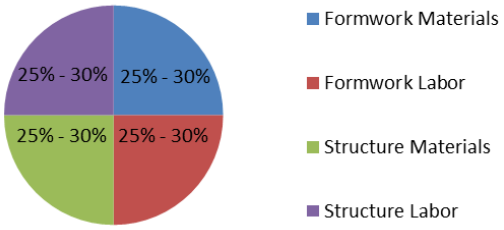

Fig.1 Distribution of costs for usually poured structures [27]

Structural studies on post-disaster housing are mostly limited to some post-disaster shelter design, architectural guidelines or Multi-Criteria Decision Making (MCDM) models for selecting the PDH systems [28-34]. In some research study, new temporary housing planning framework is proposed to offer customized housing plans tailored to the specific social, economic, and psychological needs of displaced families while controlling expenditures [35, 36]. Maximizing temporary housing safety after natural disasters have been studied in other research studies [37].

FEMA has explored a pilot program to evaluate the possibility of providing quickly deployable, affordable housing that can serve both as temporary and permanent housing [13]. In early 2009, FEMA released the first-ever National Disaster Housing Strategy which calls for improved planning and outlines the key principles and policies guiding disaster sheltering, interim housing, and restoration of permanent housing [38].

For disaster relief housing, rapidly deployable shelters must be lightweight, be packaged in a small volume for transportability, and be erected without heavy lifting equipment. In addition, a critical design criterion is also energy efficiency in heating and cooling. To meet these priorities, an optimized solution is found for a thermally insulated rigid wall deployable shelter by Quaglia et al. [39]. Although such rigid wall counterparts provide enhanced insulation, they have high self-weights, limited deploy-ability, and require heavy lifting equipment for placement. To address this downside, United States Army Natick Soldier Research, Development & Engineering Center presented a novel erection strategy for origami-inspired shelters based on the principle of counterweighting as Bascule shelters [40, 41]. Also, some researches proposed modular box systems for post-earthquake homeless disaster victims in line with the standard sustainability criteria [42-45]. The design and methodology of

construction of a shelter for the victims of the typhoon Haiyan in the Philippines were presented by Ravina and Shih [46].

3. FLEXIBLE FORMWORK

An efficient construction system that can be used in rapidly assembled buildings is flexible formwork systems. The most applicable types of flexible formworks are fabric formworks made of synthetic textile sheets of fibers; typically nylon, Polyesters/Polyethylene Terephthalate, Polyolefin or Polypropylene. In casted structural systems, in which a considerable portion of the project budget is allocated to formwork cost, innovative construction systems can play an important part in PDH programs. Using fabric formwork is one of these solutions.

The development of some innovative ideas such as pneumatic formwork has complemented the applications of fabric formwork. The main concept of pneumatic formwork application is ramified from membrane behavior. A common method of pre-tensioning a membrane is to pressurize the interior with air. Sufficient pressure is applied to counteract dead loads so that the membrane actually floats in space. Slight additional pressurization is also used to offset wind and other anticipated loads. Pressure differentials used in practice are not large. They often range between 0.02 and 0.04 psi (3 and 5 psf).

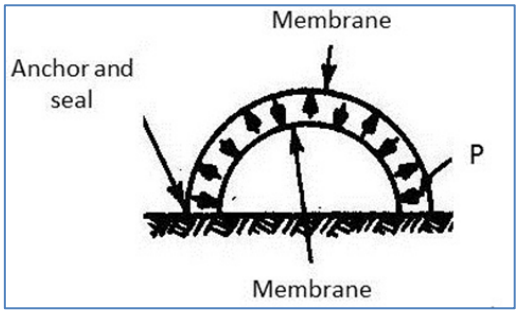

Fig.2 Air-inflated dual wall structures

A good example is air-inflated dual wall structures. Air-inflated dual wall structures (Figure 2) is one of most popular air stabilized structures. Up to now, however, this system scarcely applied as a structural pneumatic formwork. The general application of this technique is mostly limited to the erection and setup of domes and arches[47]. Employing the PUR and a pneumatic formwork, this study develops an effective post-disaster housing system that can significantly contribute to PDH management (Figure 3). In this System, after inflating the fabric formwork, PUR foam is injected between internal and external fabric layers. Therefore, an integrated volumetric structural system including floor, walls, and roof will be built. Figure 4 shows a schematic perspective of the unit and a cross-section of integrated connections between walls.

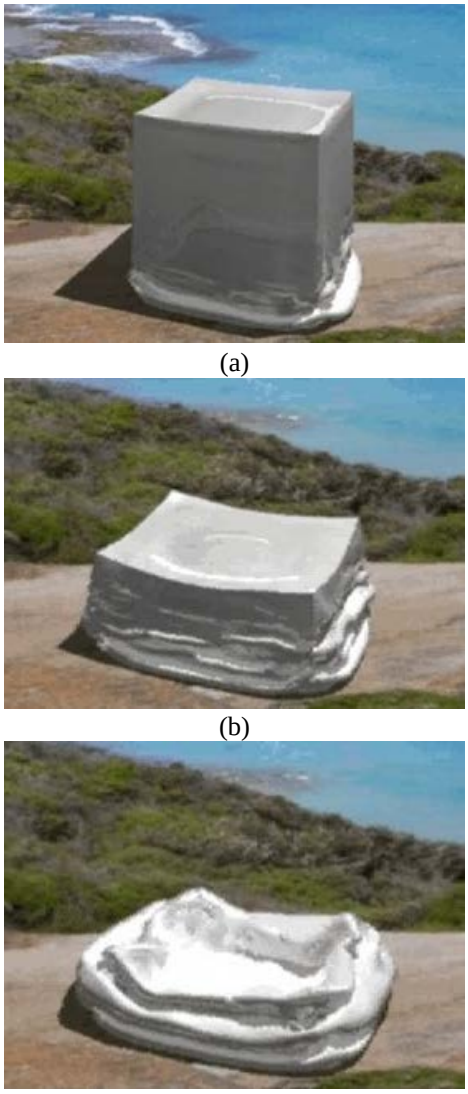

(a)

(b)

(c)

Fig.3 Pneumatic formwork installation steps of introducer system (a-c)

The remainder of this paper investigates the structural performance of this foam-filled structural panel with fabric formwork (which can be erected by pneumatic force) as an innovative rapidly assembled construction system. Rapid assembly, low maintenance, high structural quality, and ease of transportation are some key aspects of this system that make it a suitable construction system for temporary and semi-permanent housing.

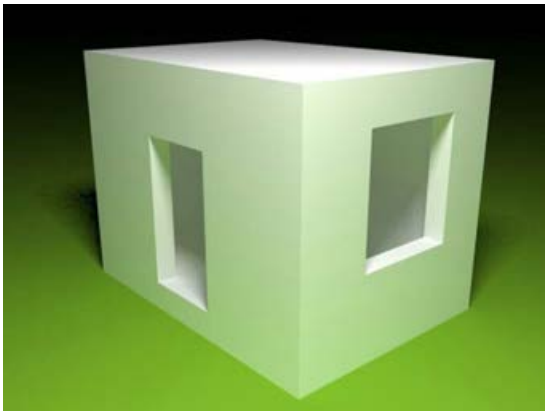

Fig.4a Schematic perspective

Fig.4b Real cross-section of introduced system

4. MATERIAL PROPERTIES

The system fabric pneumatic formwork and PUR foam are the main materials used for the system. A research study has been done in the Centre for Infrastructure Engineering (CIE) of Western Sydney University in order to identify the best pneumatic formwork textile [48]. Results showed the Barrateen is the best candidate for being used as fabric formwork. Barrateen is a high-density polyethylene or polypropylene (HDPE) coated by unbalancing woven textile. The coating material is low-density polyethylene and well inflatable, whose tensile strengths in the warp and weft directions are not the same. The result of tensile tests according to ASTM D1980-89 is shown in Fig.5. Also, Polyurethane high-density rigid foam with a density of 192 kg/m3 was used for the core material. Table 1 shows the PU foam's manufacturing and mechanical properties, provided by the manufacturer and validated in the laboratory according to the ASTM 1730 standard [49].

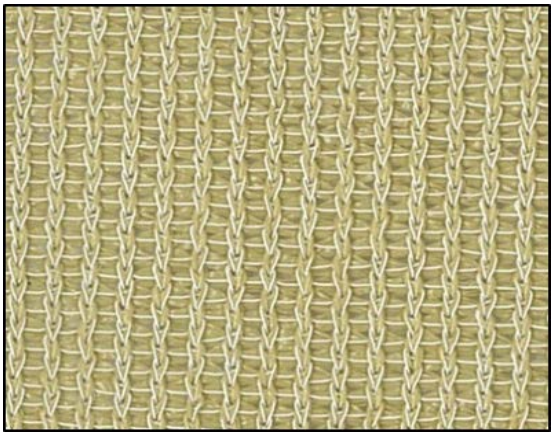

Fig.5a Barrateen fabric

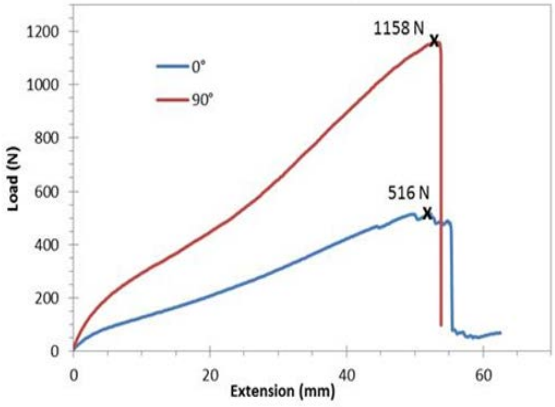

Fig.5b Barrateen fabric tensile behavior in main (90º) and transverse (0º) directions

Table 1 Mechanical and manufacturing properties of the selected PU rigid foam

Mechanical properties of the PU foam			
Density (kg/m3)	Compressive yield strength (MPa)	Tensile strength (MPa)	Shear strength (MPa)
192	2.81	1.896	1.034
Manufacturing Properties			
Cream time	Gel time	Tack free time	Free rise cup density
35-40 sec	94 ± 4 sec	115 ± 5 sec	280 – 300 kg/m^3

Using uniaxial load machine (Figure 2), three cubic specimens (dimensions: 50mm × 50mm × 50mm) were tested based on the ASTM E1730 at a loading rate of 5 mm/min in order to identify the structural properties of the rigid PU foam. Figure 6 illustrates the stress-strain curves in the elastic region and failure graph respectively. The curves show that this type of PU foam, which is made of a

100:110 weight ratio mixture of AUSTHANE POLYOL AUW763 and AUSTHANE MDI, can undertake considerable deformation before the failure. These stress-strain curves are relatively linear in the elastic region, with a yield region at an average stress of 3.51 MPa, and the average elastic modulus of 135.5 MPa.

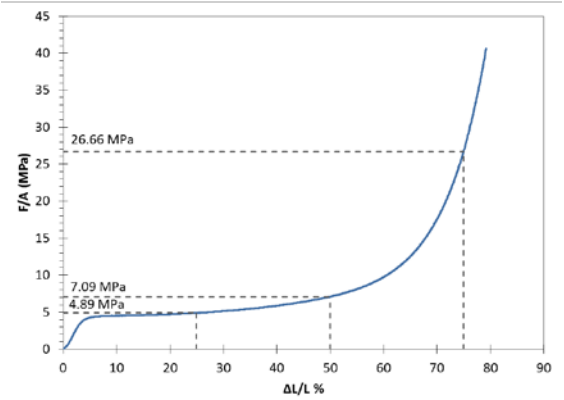

Fig.6a Results of the uniaxial load test on selected PU foam

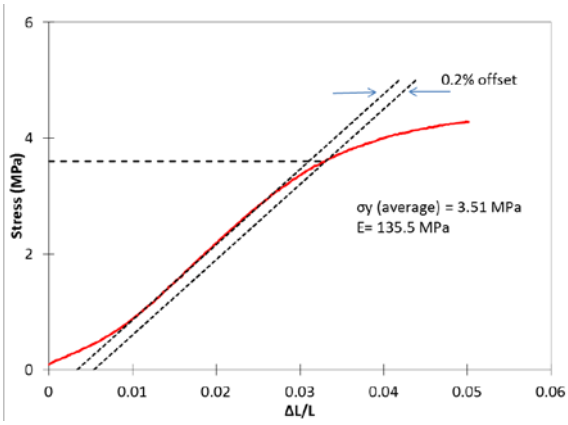

Fig.6b Results of the uniaxial load test on selected PU foam

5. LOADING ANALYSIS AND DESIGN

The introducer system is designed to be capable of being used for post-disaster housing in severe weather conditions. Therefore, in this study, a combination of severe loading scenarios is considered to check the performance of the shelter. On the other hand, because the system is light in weight, with regard to the lateral loads, the numerical studies showed that wind loads will govern the design, rather than an earthquake. The International Building Code (IBC-2015) [50] is used for determining the loads as well as the design. In this regard, a 3000 mm x 3000 mm x 3000 mm cubic shelter with 100 mm thick PU foam walls, floor, and the roof has been analyzed and designed. In fact, this cube is a simulation of temporary shelter that can be used in emergency situations. The door and windows are not shown in the model. The computer model is created in ANSYS workbench. For the wind load calculations, the American Society of Civil Engineers ASCE7-10 “Minimum Design Loads for Buildings and Other Structures” [51], which is adopted by IBC 2015 is used. To analyze the cube for most extreme wind load, the Cube is subject to calculated wind load induced by an 80 mps wind speed, which is the highest speed for such structures. Also, the studied cubic shelter is categorized as risk category II based on Table 1.5-1 in ACSE 7-10, which is neither a low risk nor a high-risk structure. The cube is considered enclosed, so there will be a minimum internal pressure acting perpendicular to the surface. The Exposure category is assumed to be “C” which indicates open terrain with scattered obstruction having a height less than 10000 mm or flat open countryside and grassland, which assumed to accommodate temporary shelters at the time of disasters and emergencies. The topography of the site is assumed to be relatively flat with maximum 5000 mm escarpment height.

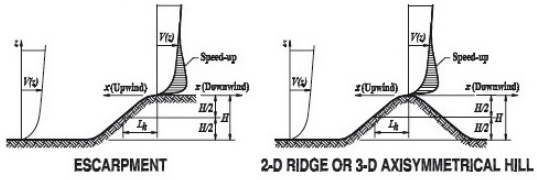

Topographic Multipliers for Exposure C

H/Lh	K1 Multiplier 2-D Ridge	K1 Multiplier 2-D Escarp.	K1 Multiplier 3-D Axisym. Hill	x/Lh	K2 Multiplier 2-D Escarp.	K2 Multiplier All Other Cases	z/Lh	K3 Multiplier 2-D Ridge	K3 Multiplier 2-D Escarp.	K3 Multiplier 3-D Axisym. Hill
0.20	0.29	0.17	0.21	0.00	1.00	1.00	0.00	1.00	1.00	1.00
0.25	0.36	0.21	0.26	0.50	0.88	0.67	0.10	0.74	0.78	0.67
0.30	0.43	0.26	0.32	1.00	0.75	0.33	0.20	0.55	0.61	0.45
0.35	0.51	0.30	0.37	1.50	0.63	0.00	0.30	0.41	0.47	0.30
0.40	0.58	0.34	0.42	2.00	0.50	0.00	0.40	0.30	0.37	0.20
0.45	0.65	0.38	0.47	2.50	0.38	0.00	0.50	0.22	0.29	0.14
0.50	0.72	0.43	0.53	3.00	0.25	0.00	0.60	0.17	0.22	0.09
				3.50	0.13	0.00	0.70	0.12	0.17	0.06
				4.00	0.00	0.00	0.80	0.09	0.14	0.04
							0.90	0.07	0.11	0.03
							1.00	0.05	0.08	0.02
							1.50	0.01	0.02	0.00
							2.00	0.00	0.00	0.00

Notes:

1. For values of H/Lh, x/Lh and z/Lh other than those shown, linear interpolation is permitted.
2. For H/Lh > 0.5, assume H/Lh = 0.5 for evaluating K1 and substitute 2H for Lh for evaluating K2 and K3.
3. Multipliers are based on the assumption that wind approaches the hill or escarpment along the direction of maximum slope.
4. Notation:
   H: Height of hill or escarpment relative to the upwind terrain, in feet (meters).
   Lh: Distance upwind of crest to where the difference in ground elevation is half the height of hill or escarpment, in feet (meters).
   K1: Factor to account for shape of topographic feature and maximum speed-up effect.
   K2: Factor to account for reduction in speed-up with distance upwind or downwind of crest.
   K3: Factor to account for reduction in speed-up with height above local terrain.
   x: Distance (upwind or downwind) from the crest to the building site, in feet (meters).
   z: Height above ground surface at building site, in feet (meters).
   μ: Horizontal attenuation factor.
   γ: Height attenuation factor.

Fig.7 ASEC 7-10 Topographic factor, Kzt [51]

Table 2 shows the calculation of wind load and maximum applied pressures on walls and roof of shelter based on table 27.2-1, ASCE7-10 [51]. For gravity loads, the structure is assumed to be subjected to 4788 Pa ground snow load as the maximum possible for outside Alaskan locations in the United States (4788 Pa) [51]. In this study conservatively the ground snow load is assumed to be applied to the top of the roof.

Table 2 Applied wind load calculation

Parameter	Based on	Amount
Risk category	Table 1.5-1 ASCE 7-10	II
Max nominal design wind speed for risk	Fig. 26.5-1A ASCE 7-10	V_{LRFD} = 180 mph
Structure type	Main concept	Flat ground
Wind directionality factor	Table 26.6-1 ASCE 7-10	K_d = 0.85
Exposure category	Fig. 26.6 ASCE 7-10	C
K_1	Figure 8	0.775
K_2	Figure 8	0.815
K_3	Figure 8	0.22
Kzt = (1+K1.K2.K3)**2	Eq. 26.8-1 ASCE 7-10	1.297
Gust effect factor (G)	Eq. 26.9 ASCE 7-10	0.85
Approximate natural frequency (na)	Eq. 26.9-4 ASCE 7-10	7.5 Hz
Nominal height of the atmospheric boundry layer (Zg)	Table 26.9-1 ASCE 7-10	330 m
pressure acting away from internal surface (GCpi_toward)	Table 26.11-1 ASCE 7-10	0.18
pressure acting away from internal surface (GCpi_away)	Table 26.11-1 ASCE 7-10	-0.18
Windward pressure on the wall (Pwall)		2528 Pa
Leeward pressure on the wall (Pwall)		−1580 Pa (suction)
Max roof upward pressure (Prf)		−4108 Pa (suction)
Max internal upward pressure (Pint)		669 Pa

The shelter is designed according to Allowable Stress Design (ASD) method. According to IBC2015[50], the reasonable load combinations for this case study are as followings:

D; D + L; D + S; D + 0.75L + 0.75S; D + (0.6w or 0.7E); D + 0.75(0.6W) + 0.75L + 0.75S; D+0.75(0.7E)+0.75L+0.75S; 0.6D+0.6W ; 0.6D+0.7E [52-54]. In which D is dead load, E is earthquake load, L is live load due to occupancy, Lr is roof live load, S is snow load and finally, W is wind load. In this study, since the dead load and earthquake load are considerably lower than the wind load and snow load, the wind and snow loads are conservatively analyzed separately. The shelter, therefore, is analyzed using ANSYS workbench assuming the global Y axis as perpendicular to the ground (The self-weight of the material is applied in –Y direction, and the roof upward force is applied in the +Y direction). The wind load is applied in the X direction, and the side pressures are applied in the Z directions. The internal pressure is applied to all faces perpendicular to the surface. The support of the cube is assumed to be fixed supports at the edges of the walls. The results show under wind loading, both of maximum shear stress and maximum stress intensity are created at the connection of side walls to roof. It is observed that the structure can resist against the maximum tensile stress caused by wind load with a safety facture of 1.896/1.0166 = 1.87. In addition, the used material can resist against the maximum created shear stress with a safety facture of 1.034/0.5083 = 2.03 (Figure 8).

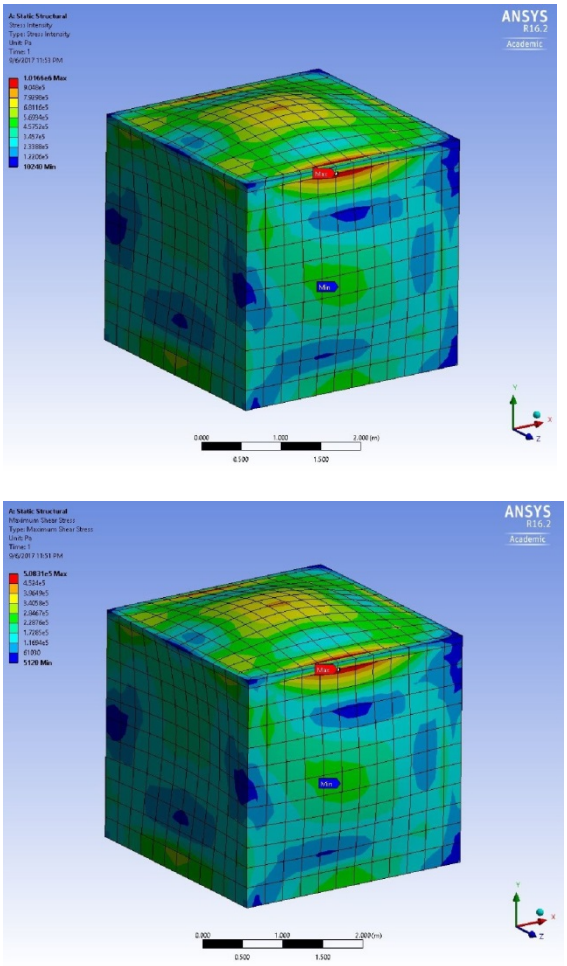

Fig.8 Wind load max stress intensity 1.0166 MPa (up) and max shear stress 0.50831 MPa (down)

The maximum deformation under wind load is also equal to 60 mm upward and is located at the mid center of the roof. This deformation has been compared with the snow's maximum deflection, which is equal to 75 mm downward (Figure 9).

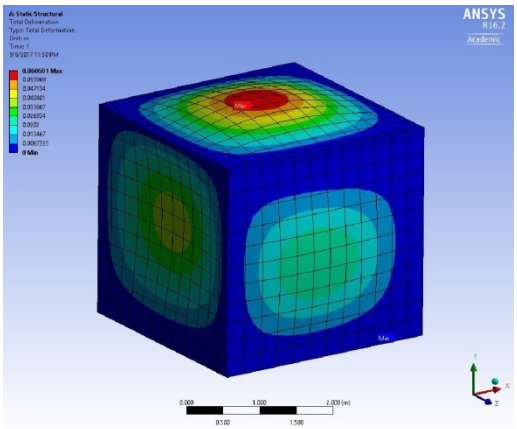

Fig.9a Wind load max deformation, 60 mm (up) vs snow maximum deflection, 75 mm (down)

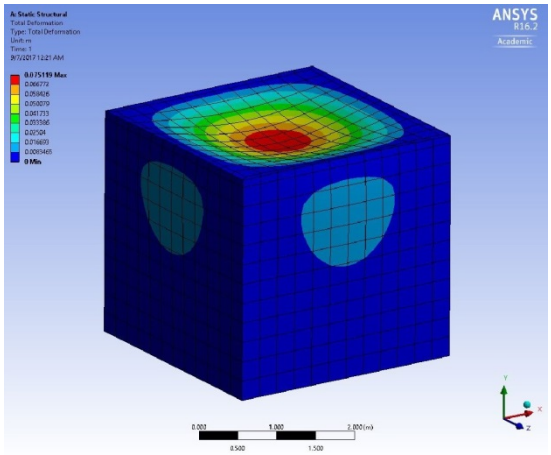

Fig.9b Wind load max deformation, 60 mm (up) vs snow maximum deflection, 75 mm (down)

Nonetheless, the results indicate the structure can tolerate these deformations without any fracture. Because the used material can resist the maximum tensile stress under snow loading with a safety facture about 1.896/0.8662 = 2.19 (Figure 10).

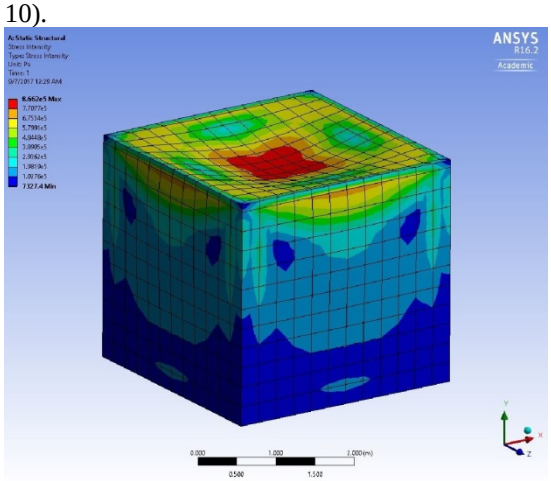

Fig.10a Equivalent (Von Miss) stress (up) and stress intensity (down) caused by snow loading

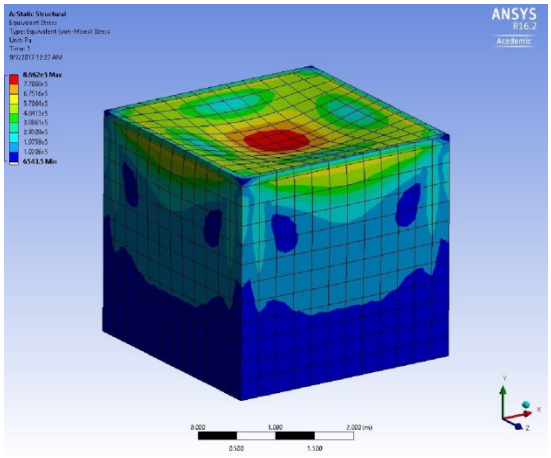

Fig.10b Equivalent (Von Miss) stress (up) and stress intensity (down) caused by snow loading

In addition, the location of the maximum shear stress under snow loading is exactly in the middle of the span of the roof. The structure can resist the maximum shear stress caused by snow loading with a safety facture about 1.034/0.4331 = 2.39 (Figure 11). Therefore, the unit can conservatively withstand highest wind and snow loads.

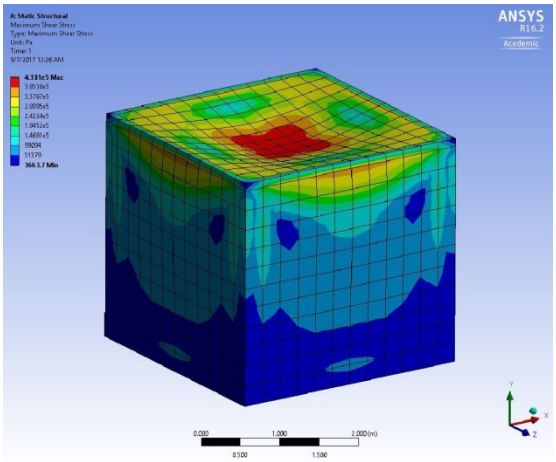

Fig.11 Shear stress distribution caused by snow loading

The reaction forces under snow and wind loading are calculated and shown in Table 3. The shelter needs to support the above-mentioned loads in its base. For soft ground areas, the system needs to a weight around 40207 N. The perimeter of the unit is 4 x 3 m=12 m, therefore, the minimum weight of the unit length of the foundation is equal to 40207N/12m = 3350 N/m. If the weight is provided by concrete, knowing that the density of concrete is 2.5e4 N/m^3, the area of cross section will be calculated as follows: A = 3350/25000 = 0.134 m^2. A 30 cm x 50 cm foundation has area of 0.15 cm^2. Figure 12 shows a typical foundation for this system.

Table 3 Applied wind load on shelter

Loading	Direction X (N)	Direction Y (N)	Direction Z (N)
Wind Load	- 39437	- 40207	0
Snow Load	0	57728	0

In harder soils, the shelter can be supported with an alternative method using anchoring rods (figure 13). As shown in figure 13, the anchoring rods will provide required horizontal and vertical reaction forces. The lateral 39437 N will be distributed on 0.10 m x 3 m = 0.3 m^2 area of angle. The bearing stress is equal to 39437 N / 0.3 m^2 = 0.131 MPa, which is lower than the allowable stress of 2.81 MPa.

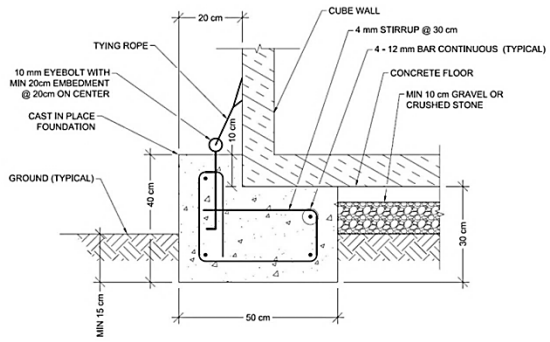

Fig.12 Precast or cast in place foundation detail

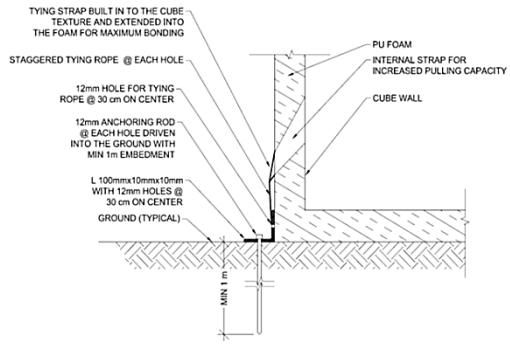

Fig.13a Ground anchoring detail

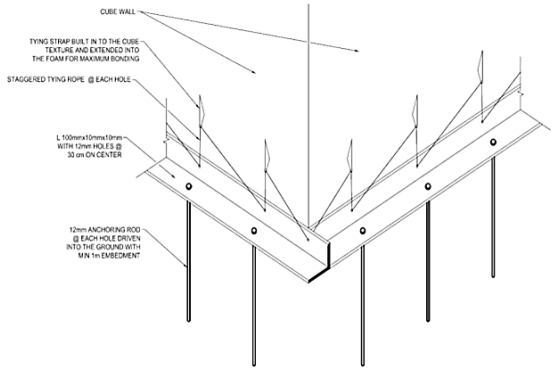

Fig.13b Ground anchoring detail

According to the above calculations, the 3m x 3m x 3m structure can withstand most severe wind and snow as well as other applicable loads as per the Internarial Building Code. Analysis and design of some similar structures with various dimensions (from 3 m to 8 m) showed if both of length and wide increase from 4 m simultaneously, the system will increase the risk of collapse with a safety factor bellow 1(Figures 14 and 15 and table 4).

For results confirmation, another series of analyses and designs have been conducted on the introduced system (3m x 3m x 3m) based on the Australian Standards [55, 56]. In this regard, wind load of the cyclonic area (88 m/s for region D) with annual probability return of 500 years is applied on the shelter. In this regards the shelter is analyzed using a professional loading, analyzing and design software, ROBOT 2016. Also, the most conservative identified load combination (0.9G + W) was used [56].

Based on the Australian standards, the wind is applied to the shelter with both angles of 90° and 45° separately (Figure 16). However, since the wind speed with respect to IBC and AS1170.2 are almost the same, only the oblique wind is used for confirmation. The results show all of the maximum amounts of deformation, main stress and shear stress caused by the oblique wind are lower than design limits. As an example, Figure 17 shows the Maximum deformation of shelter caused by oblique wind is only 42mm, which is less than the related amount of IBC (60mm). In addition, the results indicate that the maximum uplift force under wind loading 45º is equal to 35300 kN, which is less than the amount used for design (40207 kN).

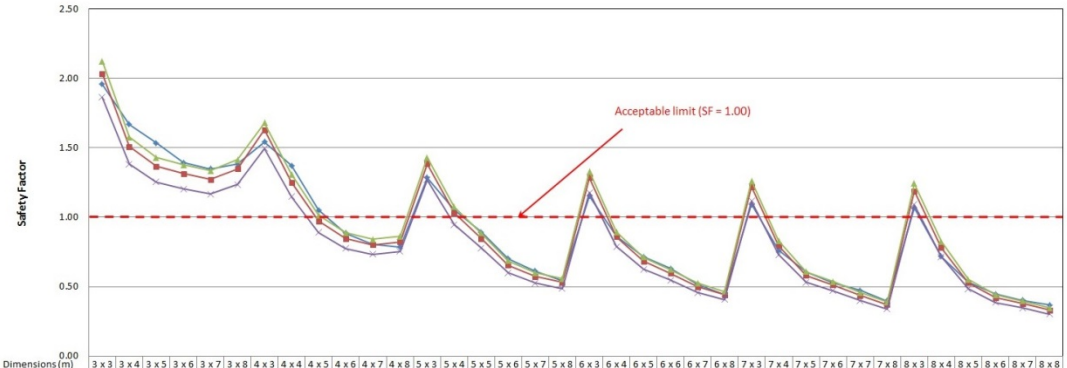

Dimensions (m)	3 x 3	3 x 4	3 x 5	3 x 6	3 x 7	3 x 8	4 x 3	4 x 4	4 x 5	4 x 6	4 x 7	4 x 8	5 x 3	5 x 4	5 x 5	5 x 6	5 x 7	5 x 8	6 x 3	6 x 4	6 x 5	6 x 6	6 x 7	6 x 8	7 x 3	7 x 4	7 x 5	7 x 6	7 x 7	7 x 8	8 x 3	8 x 4	8 x 5	8 x 6	8 x 7	8 x 8
Wind Pr. Str.	1.96	1.67	1.54	1.39	1.35	1.38	1.54	1.37	1.05	0.89	0.81	0.78	1.29	1.05	0.89	0.70	0.61	0.54	1.15	0.86	0.71	0.63	0.52	0.44	1.09	0.76	0.60	0.53	0.47	0.40	1.07	0.72	0.53	0.45	0.40	0.37
Wind Shr. Str.	2.03	1.51	1.37	1.31	1.27	1.35	1.63	1.25	0.97	0.85	0.80	0.82	1.38	1.03	0.85	0.65	0.57	0.53	1.28	0.86	0.68	0.60	0.50	0.44	1.22	0.80	0.58	0.51	0.44	0.37	1.19	0.78	0.53	0.42	0.38	0.33
Wind VM Str.	2.13	1.58	1.43	1.38	1.33	1.41	1.68	1.31	1.01	0.89	0.84	0.86	1.43	1.08	0.88	0.68	0.60	0.56	1.33	0.89	0.71	0.62	0.52	0.46	1.26	0.83	0.61	0.54	0.46	0.39	1.24	0.83	0.55	0.44	0.40	0.35
Wind Str. Int.	1.87	1.38	1.25	1.20	1.17	1.24	1.49	1.15	0.89	0.78	0.73	0.75	1.27	0.94	0.78	0.60	0.52	0.49	1.18	0.79	0.63	0.55	0.46	0.41	1.12	0.73	0.53	0.47	0.40	0.34	1.09	0.72	0.48	0.39	0.35	0.30

Fig.14 Variation in Safety Factor for different room dimensions - Wind load

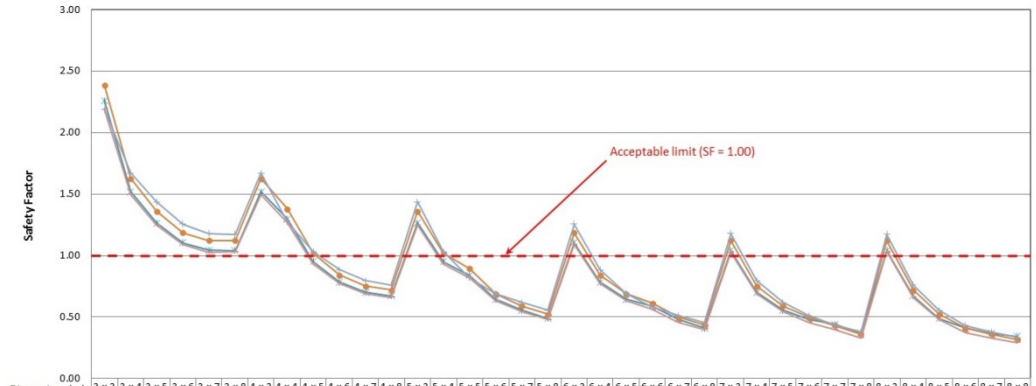

Dimensions (m)	3 x 3	3 x 4	3 x 5	3 x 6	3 x 7	3 x 8	4 x 3	4 x 4	4 x 5	4 x 6	4 x 7	4 x 8	5 x 3	5 x 4	5 x 5	5 x 6	5 x 7	5 x 8	6 x 3	6 x 4	6 x 5	6 x 6	6 x 7	6 x 8	7 x 3	7 x 4	7 x 5	7 x 6	7 x 7	7 x 8	8 x 3	8 x 4	8 x 5	8 x 6	8 x 7	8 x 8
Snow Pr. Str.	2.26	1.52	1.27	1.10	1.04	1.04	1.52	1.30	0.95	0.78	0.70	0.67	1.27	0.95	0.84	0.64	0.56	0.49	1.10	0.78	0.64	0.59	0.48	0.41	1.04	0.70	0.56	0.48	0.44	0.37	1.04	0.67	0.49	0.41	0.37	0.34
Snow Shr. Str.	2.39	1.63	1.36	1.19	1.12	1.12	1.63	1.38	1.02	0.84	0.75	0.72	1.36	1.02	0.89	0.69	0.59	0.52	1.19	0.84	0.69	0.61	0.50	0.44	1.12	0.75	0.59	0.50	0.43	0.36	1.12	0.72	0.52	0.41	0.36	0.32
Snow VM Str.	2.19	1.67	1.44	1.25	1.18	1.17	1.67	1.27	1.03	0.88	0.80	0.76	1.44	1.03	0.82	0.69	0.62	0.55	1.25	0.88	0.69	0.58	0.51	0.45	1.18	0.80	0.62	0.51	0.43	0.38	1.17	0.76	0.55	0.43	0.38	0.33
Snow Str. Int.	2.19	1.49	1.25	1.09	1.03	1.03	1.49	1.26	0.93	0.77	0.69	0.66	1.25	0.93	0.82	0.63	0.54	0.48	1.09	0.77	0.63	0.56	0.46	0.40	1.03	0.69	0.54	0.46	0.40	0.33	1.03	0.66	0.48	0.38	0.33	0.29

Fig.15 Variation in Safety Factor for different room dimensions - Wind load

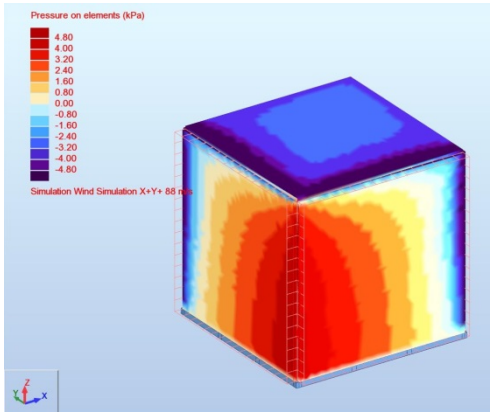

Fig.16a Applied wind loading on the shelter based on AS1170.2 with angles of 45º

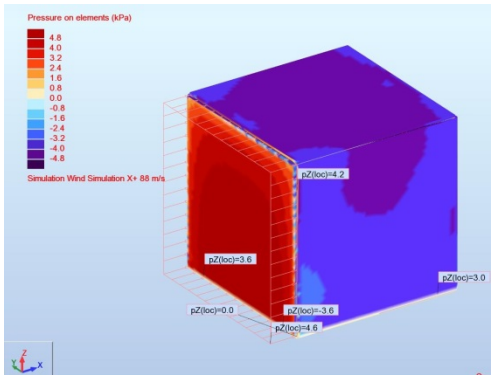

Fig.16b Applied wind loading on the shelter based on AS1170.2 with 90º

6. CONCLUSION

An innovative rapidly assembled system, mainly developed for quick assembly of modular post-disaster housing, was studied. The material properties as well as the entire structure of the units we investigated experimentally and by finite element modeling, respectively.

Table 4 Safe dimensions of the shelter

	Wind (IBC)				Snow (IBC)				
Dimentions (m)	Principle stress	Shear Stress	VM Stress	Stress intencity	Principle stress	Shear Stress	VM Stress	Stress intencity	Restricting load
3 x 3	O.K.	O.K.	O.K.	O.K.	O.K.	O.K.	O.K.	O.K.	
3 x 4	O.K.	O.K.	O.K.	O.K.	O.K.	O.K.	O.K.	O.K.	
3 x 5	O.K.	O.K.	O.K.	O.K.	O.K.	O.K.	O.K.	O.K.	
3 x 6	O.K.	O.K.	O.K.	O.K.	O.K.	O.K.	O.K.	O.K.	
3 x 7	O.K.	O.K.	O.K.	O.K.	O.K.	O.K.	O.K.	O.K.	
3 x 8	O.K.	O.K.	O.K.	O.K.	O.K.	O.K.	O.K.	O.K.	
4 x 4	O.K.	O.K.	O.K.	O.K.	O.K.	O.K.	O.K.	O.K.	
4 x 5	O.K.	N.G.	O.K.	N.G.	N.G.	O.K.	O.K.	N.G.	Wind and Snow
4 x 6	N.G.	N.G.	N.G.	N.G.	N.G.	N.G.	N.G.	N.G.	Wind and Snow
4 x 7	N.G.	N.G.	N.G.	N.G.	N.G.	N.G.	N.G.	N.G.	Wind and Snow
4 x 8	N.G.	N.G.	N.G.	N.G.	N.G.	N.G.	N.G.	N.G.	Wind and Snow
5 x 5	N.G.	N.G.	N.G.	N.G.	N.G.	N.G.	N.G.	N.G.	Wind and Snow
5 x 6	N.G.	N.G.	N.G.	N.G.	N.G.	N.G.	N.G.	N.G.	Wind and Snow
5 x 7	N.G.	N.G.	N.G.	N.G.	N.G.	N.G.	N.G.	N.G.	Wind and Snow
5 x 8	N.G.	N.G.	N.G.	N.G.	N.G.	N.G.	N.G.	N.G.	Wind and Snow
6 x 6	N.G.	N.G.	N.G.	N.G.	N.G.	N.G.	N.G.	N.G.	Wind and Snow
6 x 7	N.G.	N.G.	N.G.	N.G.	N.G.	N.G.	N.G.	N.G.	Wind and Snow
6 x 8	N.G.	N.G.	N.G.	N.G.	N.G.	N.G.	N.G.	N.G.	Wind and Snow
7 x 7	N.G.	N.G.	N.G.	N.G.	N.G.	N.G.	N.G.	N.G.	Wind and Snow
7 x 8	N.G.	N.G.	N.G.	N.G.	N.G.	N.G.	N.G.	N.G.	Wind and Snow
8 x 8	N.G.	N.G.	N.G.	N.G.	N.G.	N.G.	N.G.	N.G.	Wind and Snow

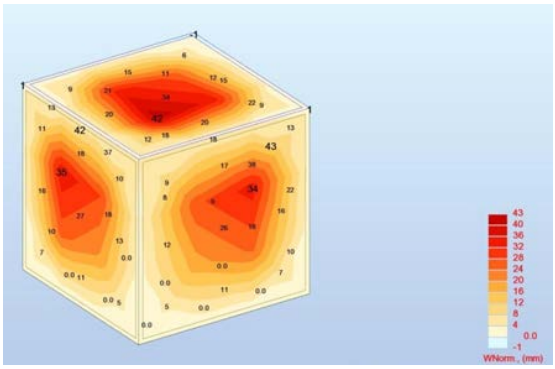

Fig.17 Maximum deformation of shelter caused by oblique wind

Each unit is composed of panels made of a high-density polyethylene or polypropylene (HDPE) coated by unbalancing woven textile as the skins, filled with high-density Polyurethane (PU) foam as the core. Material characterization tests and finite element modeling were performed in accordance with some international building

codes to evaluate the performance of the modular units in severe weather conditions. Results demonstrate that the developed rapidly assembled building unit exhibit very good structural performance, and can meet the standards' requirements.

7. REFERENCES

[1] Tsai, M.-K., Designing Postdisaster Temporary Housing Facilities: Case Study in Indonesia. Natural Hazards Review, 2014. 16(3): p. 05014007.

[2] Patel, S. and M. Hastak, A framework to construct post-disaster housing. International Journal of Disaster Resilience in the Built Environment, 2013. 4(1): p. 95-114.

[3] Goodyear, R.K. and A. Fabian, Housing in Auckland: Trends in housing from the Census of Population and Dwellings 1991 to 2013. 2014: Statistics New Zealand.

[4] Goodyear, R., Housing in greater Christchurch after the earthquakes: Trends in housing from the Census of Population and Dwellings 1991–2013. 2014, New Zealand: Statistics New Zealand, Tatauranga Aotearoa.

[5] Development, U.S.D.o.H.a.U., ESG Minimum Habitability Standards for Emergency Shelters and Permanent Housing. 2014: USA.

[6] HUD, ESG Minimum Habitability Standards for Emergency Shelters and Permanent Housing. 2014: p. 1-15.

[7] Department of Housing and Public Works, Temporary accommodation buildings, Minimum building standards. 2013, Department of Housing and Public Works: Queensland. p. 1-3.

[8] Fallahi, A., TECHNICAL REPORT-SHELTERING, FROM RELIEF TO RECONSTRUCTION: One Year after the 2010 East Azerbaijan Province Earthquake. ArchNet-IJAR, 2013. 7(3).

[9] Tas, M., N. Tas, and N. Cosgun, Study on permanent housing production after 1999 earthquake in Kocaeli (Turkey). Disaster Prevention and Management: An International Journal, 2010. 19(1): p. 6-19.

[10] Song, Y., N. Mithraratne, and H. Zhang, Lifetime performance of post-disaster temporary housing: A case study in Nanjing. Energy and Buildings, 2016. 128: p. 394-404.

[11] Atmaca, N., Life-cycle assessment of post-disaster temporary housing. Building Research & Information, 2017. 45(5): p. 524-538.

[12] Gunawardena, T., et al., Time-Efficient Post-Disaster Housing Reconstruction with Prefabricated Modular Structures. Open house international, 2014. 39(3): p. 59-66.

[13] Co-ordinator, O.o.t.U.N.D.R., Shelter after a disaster: Guidelines for assistance. 1982: New York: United Nations.

[14] Arlikatti, S., et al., Temporary Sheltering, Psychological Stress Symptoms, and Perceptions of Recovery. Natural Hazards Review, 2014. 16(3): p. 04014028.

[15] Kuroda, M., Healthcare ICT for Temporary Housing Community in Disaster-Stricken Area. IEICE transactions on communications, 2012. 95(10): p. 3062-3066.

[16] Mira, L.A., A.P. Thrall, and N. De Temmerman, Deployable scissor arch for transitional shelters. Automation in Construction, 2014. 43: p. 123-131.

[17] Bouhaya, L., O. Baverel, and J.-F. Caron, Optimization of gridshell bar orientation using a simplified genetic approach. Structural and Multidisciplinary Optimization, 2014. 50(5): p. 839-848.

[18] C.A., T.N.D.a.B., Mobile and Rapidly Assembled Structures. Vol. IV. 2014: WIT press.

[19] Thrall, A. and C. Quaglia, Accordion shelters: A historical review of origami-like deployable shelters developed by the US military. Engineering structures, 2014. 59: p. 686-692.

[20] (ABCB), A.B.C.B., TEMPORARY STRUCTURES STANDARD. 2015, Australian Government and States and Territories of Australia: Australia.

[21] Nimmich, J., Unless Modified, FEMA's Temporary Housing Plans Will Increase Costs by an Estimated $76 Million Annually, ed. OIG-13-102. 2013, USA: Department of Homeland Security Office of Inspector General.

[22] Atmaca, A. and N. Atmaca, Comparative life cycle energy and cost analysis of post-disaster temporary housings. Applied Energy, 2016. 171: p. 429-443.

[23] Sharafi, P., et al., an Interlocking system for enhancing the integrity of multi-story modular buildings. Automation in Construction, 2018. 85(Supplement C): p. 263-272.

[24] P Sharafi, et al., Identification of Factors and Multi-Criteria Decision Analysis of the Level of Modularization in Building Construction. ASCE Journal of Architectural Engineering- Special Collection on Housing and Residential Building Construction. (Accepted for publication in July 2017), 2017.

[25] Sharafi, P., et al., the Automated spatial design of multi-story modular buildings using a unified matrix method. Automation in Construction, 2017. 82: p. 31-42.

[26] Defonseka, C., Practical guide to flexible polyurethane foams. 2013: Smithers Rapra.

[27] D.W., J., Formwork for Concrete. SP-4 (14), ed. E. edition. 2014: American Concrete Institute (ACI).

[28] Torus, B. and S.M. Şener, Post-disaster shelter design and CPoDS.

[29] Societies, I.F.o.R.C.a.R.C., Post-disaster shelter: Ten designs. 2013: Geneva.

[30] (ESG), T.E.S.G., ESG Minimum Habitability Standards for Emergency Shelters and Permanent Housing: Checklists. 2015. p. 1-5.

[31] Boehm, S., et al., Interior design as a post-disaster team partner. International Journal of Disaster Resilience in the Built Environment, 2016. 7(3): p. 276-289.

[32] (HUD), U.S.D.o.H.a.U.D., Housing Quality Standards (HQS) For Section 8 Housing Choice Voucher Properties. 2016, Prepared by the National Center for Healthy Housing. p. 1-6.

[33] Bauer, R., Oxfam GB‟s Guidelines for Post Disaster Housing Reconstruction. 2003.

[34] Government, N., Temporary uses and structures, ed. p.a. infrastructures. 2013.

[35] El-Anwar, O. and L. Chen, Automated

Community-Based Housing Response: Offering Temporary Housing Solutions Tailored to Displace Populations Needs. Journal of Computing in Civil Engineering, 2016. 30(6): p. 04016019.
[36] El-Anwar, O. and L. Chen, Maximizing the computational efficiency of temporary housing decision support following disasters. Journal of Computing in Civil Engineering, 2012. 28(1): p. 113-123.
[37] El-Anwar, O., K. El-Rayes, and A. Elnashai, Maximizing temporary housing safety after natural disasters. Journal of Infrastructure Systems, 2009. 16(2): p. 138-148.
[38] (FEMA), F.E.M.A., National Disaster Housing Strategy. 2009, USA.
[39] Quaglia, C., et al., Balancing energy efficiency and structural performance through multi-objective shape optimization: a Case study of a rapidly deployable origami-inspired shelter. Energy and Buildings, 2014. 82: p. 733-745.
[40] Quaglia, C., A. Dascanio, and A. Thrall, Bascule shelters: A novel erection strategy for origami-inspired deployable structures. Engineering Structures, 2014. 75: p. 276-287.
[41] Quagli, C., Z. Ballard, and A. Thrall, Parametric modeling of an air-liftable origami-inspired deployable shelter with a novel erection strategy. Mobile and Rapidly Assembled Structures IV, 2014. 136: p. 23.
[42] Ozlem, E., A proposal for sustainable temporary housing applications in earthquake zones in turkey: Modular box system applications. Gazi University Journal of Science, 2012. 25(1): p. 269-288.
[43] Kaveh, A. and P. Sharafi, A simple ant algorithm for profile optimization of sparse matrices. Asian Journal of Civil Engineering (Building and Housing), 2007. 9(1): p. 35-46.
[44] Sharafi, P., L.H. The, and M.N.S. Hadi, Conceptual design optimization of rectilinear building frames: A knapsack problem approach. Engineering Optimization, 2015. 47(10): p. 1303-1323.
[45] Sharafi, P., L.H. The, and M.N.S. Hadi, Shape optimization of thin-walled steel sections using graph theory and ACO algorithm. Journal of Constructional Steel Research, 2014. 101: p. 331-341.
[46] Ravina, D. and R.R. Shih, A shelter for the victims of the Typhoon Haiyan in the Philippines: The design and methodology of construction. Pollack Periodica, 2017. 12(2): p. 129-139.
[47] Kromoser, B. and J. Kollegger, Pneumatic forming of hardened concrete–building shells in the 21st century. Structural Concrete, 2015. 16(2): p. 161-171.
[48] Saeed Nemati, M.R., Bijan Samali, Decision Making on the Optimised Choice of Pneumatic Formwork Textile for Foam-Filled Structural Composite Panels. International Journal of GEOMATE, 2017.
[49] ASTM, ASTM-E1730, Standard Specification for Rigid Foam for Use in Structural Sandwich Panel Core, in ASTM International. 2015.
[50] Council, I.C., International building code (IBC). 2015: USA.
[51] (ASCE), A.S.o.C.E., Minimum Design Loads for Buildings and other Structures. ASCE7-10. 2010: USA.
[52] Sharafi, P., M.N.S. Hadi, and L.H. The, Optimum Spans' Lengths of Multi-span Reinforced Concrete Beams Under Dynamic Loading, in Topics on the Dynamics of Civil Structures, Volume 1: Proceedings of the 30th IMAC, A Conference on Structural Dynamics, 2012, J.M. Caicedo, et al., Editors. 2012, Springer New York: New York, NY. p. 353-361.
[53] Sharafi, P., M.N.S. Hadi, and L.H. The, Geometric Design Optimization for Dynamic Response Problems of Continuous Reinforced Concrete Beams. Journal of Computing in Civil Engineering, 2014. 28(2): p. 202-209.
[54] Sharafi, P., M.N.S. Hadi, and L.H. The, Optimum Column Layout Design of Reinforced Concrete Frames Under Wind Loading, in Topics on the Dynamics of Civil Structures, Proc. of the 30th IMAC Conf. on Structural Dynamics, 2012, New York, Vol.1, pp. 327-340.
[55] ABCB, B., Building Code of Australia. 2014, Class.
[56] Structural Design Action. Australian/New Zealand Standard (AS/NZS 1170). 2009.